Universidad de Valladolid

Escuela de Doctorado Universidad de Valladolid

PROGRAMA DE DOCTORADO EN FÍSICA

TESIS DOCTORAL:

SYNTHESIS, CHARACTERIZATION, AND STRUCTURE-PROPERTIES RELATIONSHIP OF AEROGELS AND AEROGEL-BASED COMPOSITES

Presentada por Beatriz Merillas Valero para optar al grado de Doctora por la Universidad de Valladolid

Dirigida por:
Prof. Dr. Miguel Ángel Rodríguez Pérez
Prof. Dr. Fernando Villafañe González

“Somewhere inside all of us

is the power to change the world.”

Roald Dahl

Financiación

Se agradece al Ministerio de Ciencia, Innovación y Universidades por el apoyo económico aportado para la realización de esta tesis doctoral a través de un contrato de Formación del Personal Universitario (FPU17/03299) y a la Universidad de Valladolid por su financiación a través de un contrato predoctoral (convocatoria 2018). Se agradece también la financiación recibida por parte de la COST (European Cooperation in Science and Technology) ACTION CA18125- Advanced Engineering and Research of aeroGels for Environment and Life Sciences financiado por la Comisión Europea a través de su programa Short Term Scientific Missions (STSM) con la referencia nº 47454, escuelas de aprendizaje y congresos.

Adicionalmente, quiero agradecer la financiación recibida por el grupo CellMat procedente de los siguientes proyectos de investigación:

- Espumas poliméricas funcionales para el tratamiento de aguas (RTI2018-097367-A- I00). Financiado por Agencia Estatal de Investigación; Fondos FEDER.
- Polímeros nanocelulares transparentes y aislantes térmicos_ fabricación, caracterización y relación proceso-estructura-propiedades (RTI2018-098749-B-I00). Financiado por Proyecto Reto-Plan Nacional.
- Polímeros nanocelulares micronizados: una nueva generación de materiales para el core de aislantes térmicos avanzados basados en paneles de vacío (VIP) (VA202P20). Financiado por Subvenciones del programa de apoyo a proyectos de investigación cofinanciadas por el Fondo Europeo de Desarrollo Regional. Junta de Castilla y León.
- Desarrollo de super aislantes térmicos basados en polímeros nanocelulares y bloqueadores de la radiación infrarroja (PID2021- 127108OB-I00). Financiado por Agencia Estatal de Investigación; Fondos FEDER, Ministerio de Ciencia e Innovación. Unión Europea.
- Hacia la producción industrial de polímeros nanocelulares transparentes (PDC2022-133391- I00). Financiado por Agencia Estatal de Investigación; Ministerio de Ciencia e Innovación; Plan de recuperación, transformación y resiliencia. Unión Europea – Next Generation UE.
- Producción sostenible de super aislantes térmicos basados en polímeros nanocelulares con conductividad térmica reducida a través del incremento de la dispersión de fonones (TED2021-130965B- I00). Financiado por Agencia Estatal de Investigación; Ministerio de Ciencia e Innovación; Plan de recuperación, transformación y resiliencia. Unión Europea – Next Generation UE.

Funding

Financial support from the FPU contract (FPU17/03299) from the Spanish Ministry of Science, Innovation and Universities and the University of Valladolid for a predoctoral contract are gratefully acknowledged. Additionally, I would like to thank the COST-Action “Advanced Engineering of aeroGels for Environment and Life Sciences” (AERoGELS, Ref. CA18125) funded by the European Commission for its Short-Term Scientific Missions workplan (STSM) grant No 47454, training schools and congresses.

In addition, financial assistance by CellMat group provided by the following research projects is also acknowledged:

- Espumas poliméricas funcionales para el tratamiento de aguas (RTI2018-097367-A- I00). Funded by Agencia Estatal de Investigación; Fondos FEDER.
- Polímeros nanocelulares transparentes y aislantes térmicos_ fabricación, caracterización y relación proceso-estructura-propiedades (RTI2018-098749-B-I00). Funded by Proyecto Reto-Plan Nacional.
- Polímeros nanocelulares micronizados: una nueva generación de materiales para el core de aislantes térmicos avanzados basados en paneles de vacío (VIP) (VA202P20). Funded by Subvenciones del programa de apoyo a proyectos de investigación cofinanciadas por el Fondo Europeo de Desarrollo Regional. Junta de Castilla y León.
- Desarrollo de super aislantes térmicos basados en polímeros nanocelulares y bloqueadores de la radiación infrarroja (PID2021- 127108OB-I00). Funded by Agencia Estatal de Investigación; Fondos FEDER, Ministerio de Ciencia e Innovación. Unión Europea.
- Hacia la producción industrial de polímeros nanocelulares transparentes (PDC2022-133391- I00). Funded by Agencia Estatal de Investigación; Ministerio de Ciencia e Innovación; Plan de recuperación, transformación y resiliencia. Unión Europea – Next Generation UE.
- Producción sostenible de super aislantes térmicos basados en polímeros nanocelulares con conductividad térmica reducida a través del incremento de la dispersión de fonones (TED2021-130965B- I00). Funded by Agencia Estatal de Investigación; Ministerio de Ciencia e Innovación; Plan de recuperación, transformación y resiliencia. Unión Europea – Next Generation UE.

CONTENTS

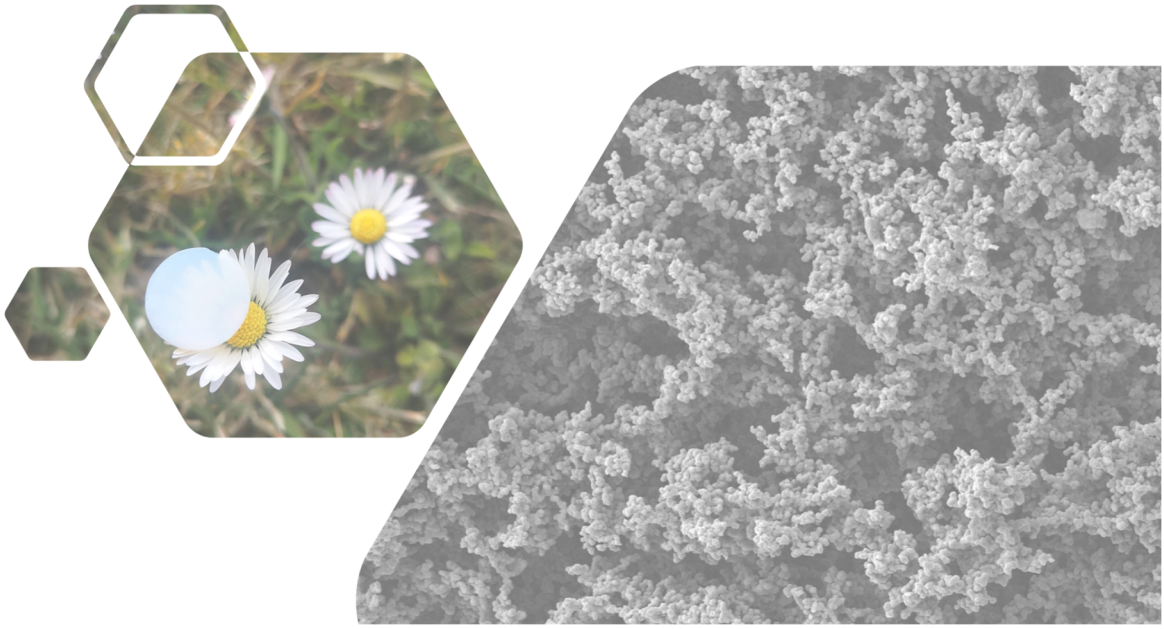

Contents

CHAPTER 0

RESUMEN EN ESPAÑOL

Resumen en español

I Introducción

A principios del siglo XX, concretamente en 1920, se descubrieron los polímeros celulares sintéticos con el objetivo de sustituir a los productos naturales por sus propiedades atractivas [1]. Estos materiales están formados por dos fases; una matriz sólida polimérica y una fase gaseosa dispersa a lo largo del material. La inclusión de la fase gaseosa contribuye a reducir significativamente la densidad del polímero sólido, además de aportar interesantes propiedades a los polímeros celulares, como absorción de energía, absorción de vibraciones, aislamiento acústico y térmico, así como aligeramiento de las estructuras, entre otras. Estas propiedades pueden ser aún más excepcionales cuando el tamaño de los poros que forman la fase gaseosa se reduce hasta alcanzar la escala nanométrica. La reducción del tamaño de los poros a nanómetros conduce a notables cambios en las propiedades ópticas y mecánicas, y también en la conductividad térmica, permitiendo extender su uso a sectores y campos insospechados.

I.a Aerogeles

Fue a principios de los años treinta, en 1931, cuando Kistler reportó un novedoso material nanoporoso en La Universidad del Pacífico en Stockton, California [2], [3]. El nacimiento de esta investigación surgió de la controversia sobre la estructura de los geles. Aunque la mayoría de los químicos coloidales aceptaron que los geles estuvieran formados por una estructura sólido-líquido de dos fases (Nägeli 1855 [4]), no hubo suficiente evidencia experimental para respaldar esta propuesta. Kistler fue pionero en demostrar la independencia entre la fase sólida del gel y el fluído que llena sus poros. Tratando de evitar el posterior colapso de la estructura sólida cuando se produce la evaporación del líquido, se desarrolló una nueva metodología para extraer el fluido. Dado que el colapso del gel se produce por un efecto capilar que la estructura no es capaz de soportar, la sustitución del fluido debe realizarse evitando que el líquido retroceda al interior del gel. Para lograr esto, el gel se colocó en un autoclave y la temperatura y la presión se ajustaron por encima de la temperatura y presión de vapor críticas del líquido, respectivamente, alcanzando el secado completo del gel sin colapso de la estructura. El resultado de este secado es lo que se conoce como **aerogel** y es apodado como el "humo azul" o "humo congelado" debido a su apariencia generalmente nubosa.

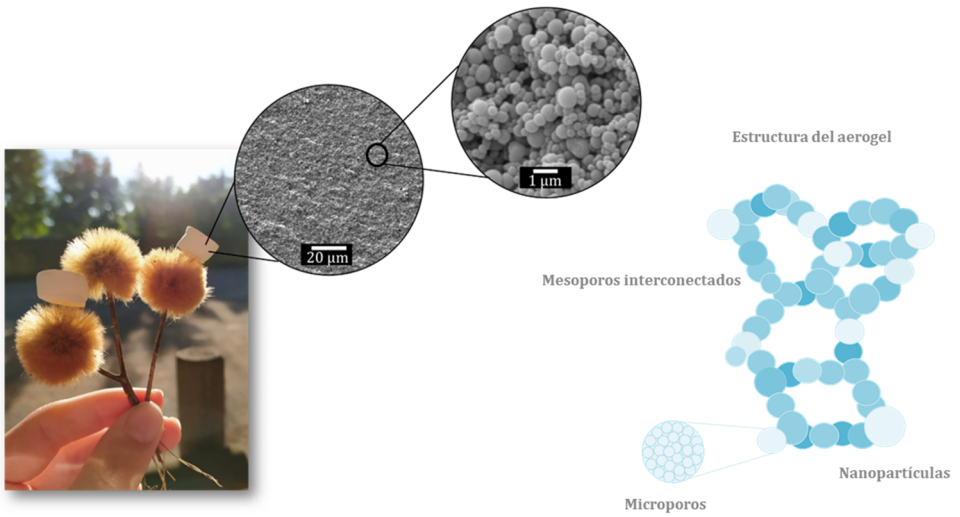

Figura R.1. Micrografías del microscopio electrónico de barrido y esquema de la estructura del aerogel.

Durante esa investigación, el primer aerogel sintetizado fue un aerogel de sílice, utilizando silicato de sodio como precursor. La investigación de Kistler se amplió aún más a la alúmina, dióxido de estaño, el óxido de tungsteno, el tartrato de níquel, el agar, la nitrocelulosa, la celulosa, el caucho y los aerogeles de albúmina de huevo. Los aerogeles obtenidos eran materiales con nuevas propiedades físicas nunca antes observadas.

Como se muestra en la **Figura R.1**, los aerogeles son materiales caracterizados por una estructura altamente porosa formada en más de un 90 % por nanoporos interconectados. El esqueleto sólido, típicamente formado por partículas o fibras, conduce a la presencia de una estructura porosa bimodal; los microporos comprendidos entre las nanopartículas (partículas primarias) y mesoporos entre los agregados de partículas (partículas secundarias). Como se explicó con el trabajo pionero de Kistler, la matriz sólida puede basarse en una gran variedad de materiales. El pequeño tamaño de las características estructurales contribuye a la aparición de propiedades excepcionales.

I.b Evolución de los aerogeles

Aunque las primeras patentes para la producción de aerogeles de sílice a gran escala se obtuvieron en la década de 1950 [5], [6], no fue hasta 1972 cuando Teichner y Nicoloan comercializaron los primeros aerogeles [7]. Estos investigadores sustituyeron el precursor de silicato de sodio empleado por Kistler por tetrametil ortosilicato (TMOS), que se convertiría en uno de los precursores de sílice más utilizados. Desde entonces, investigadores de todo el mundo comenzaron a sintetizar aerogeles con un amplio espectro de materiales, tanto orgánicos como inorgánicos. Los principales hitos alcanzados en este campo se han recogido en la **Figura R.2**.

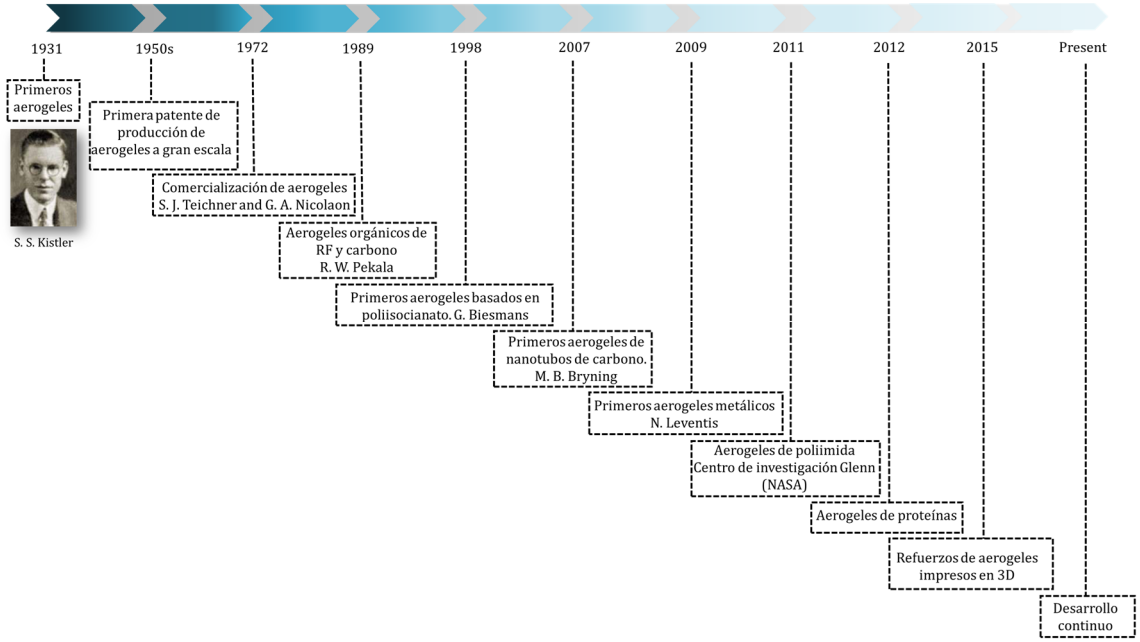

Figura R.2. Principales hitos en la investigación de aerogeles.

Los aerogeles orgánicos fueron profundamente estudiados por Pekala, quien por primera vez a finales de la década de 1980, sintetizó aerogeles de resorcinol-formaldehído y aerogeles de carbono mediante la pirólisis de los mismos [8]–[10]. En 1989, Biesmans et al. produjeron los primeros aerogeles basados en poliisocianato que también fueron transformados en aerogeles de carbono [11], [12]. Posteriormente, en 2001, las empresas Aspen Aerogels y Cabot Corporation comenzaron a comercializar aerogeles en base sílice que se convertirían en los referentes en el comercio de aerogeles. Los aerogeles basados en nanotubos de carbono se describieron por primera vez en 2007 mediante el secado de geles acuosos, consiguiendo una excelente conducción del calor y la electricidad. [13]. Más tarde, en 2009, Leventis et al. fabricaron por primera vez aerogeles metálicos, encontrando nuevas propiedades magnéticas y eléctricas [14]. La mayoría de estos avances en el ámbito del aerogel, hasta 2009, se han recogido en un interesante manual que describe la síntesis, propiedades y aplicaciones de estos materiales [15]. Más recientemente, se sintetizaron por primera vez otros aerogeles poliméricos, como los aerogeles de poliimida en el Centro de Investigación Glenn de la NASA en Ohio en 2011 [16]–[18]. En la última década, diferentes autores han explorado los aerogeles basados en proteínas en busca de materiales nanoporosos biodegradables y biocompatibles para la administración de fármacos y otras aplicaciones farmacéuticas y médicas [19], [20]. En la misma línea, las investigaciones más recientes se centran en la obtención de aerogeles biobasados y aerogeles producidos a partir de residuos de biomasa [21]–[23]. En 2015, Zhu et al. [24], reportaron por primera vez la impresión tridimensional de aerogeles de grafeno, lo que permite una nueva generación de avances tecnológicos para la producción de aerogel. Esta tecnología permite la producción de formas personalizadas y complejas que no están disponibles con los métodos de producción tradicionales.

A partir de estos hitos, se ha llevado a cabo una amplia investigación en aerogeles enfocada en su desarrollo, empleando matrices novedosas y mejorando sus principales propiedades. No hay duda de que, en los próximos años, el campo del aerogel continuará mostrando un rápido desarrollo buscando tanto la reducción de los precios de producción y la mejora de las propiedades físicas como la búsqueda de nuevas aplicaciones prácticas.

I.c Propiedades y aplicaciones de los aerogeles

El interés que han despertado los aerogeles durante su evolución es debido principalmente a sus propiedades excepcionales. Sus bajas densidades están comprendidas entre 0.003 y 0.15 g/m^3 [25], como resultado de su alta porosidad (típicamente por encima de 90 %). Además, el pequeño tamaño de los componentes de su red tridimensional (partículas o fibras) conduce a grandes áreas superficiales (500 – 1000 m^2/g) [26]. Se han definido otras propiedades específicas para estos materiales, todas ellas reunidas en la **Figura R**.3. Entre ellas destacan su baja conductividad térmica y baja velocidad del sonido, así como la baja constante dieléctrica y la alta capacidad de carga que presentan algunos de ellos. La química de estos materiales permite su funcionalización y realización de modificaciones químicas a través de cambios en las formulaciones o procedimientos adicionales.

La combinación de propiedades inusuales los convierte en candidatos únicos para una gran variedad de aplicaciones que no pueden ser cubiertas por otros polímeros celulares como espumas, fibras, materiales impresos en 3D, etc. Las principales aplicaciones de los aerogeles se centran en el sector de la construcción, sector textil, almacenamiento de energía, eliminación de residuos, sector farmacéutico y cosmético, y la industria alimentaria (ver **Figura R.3**).

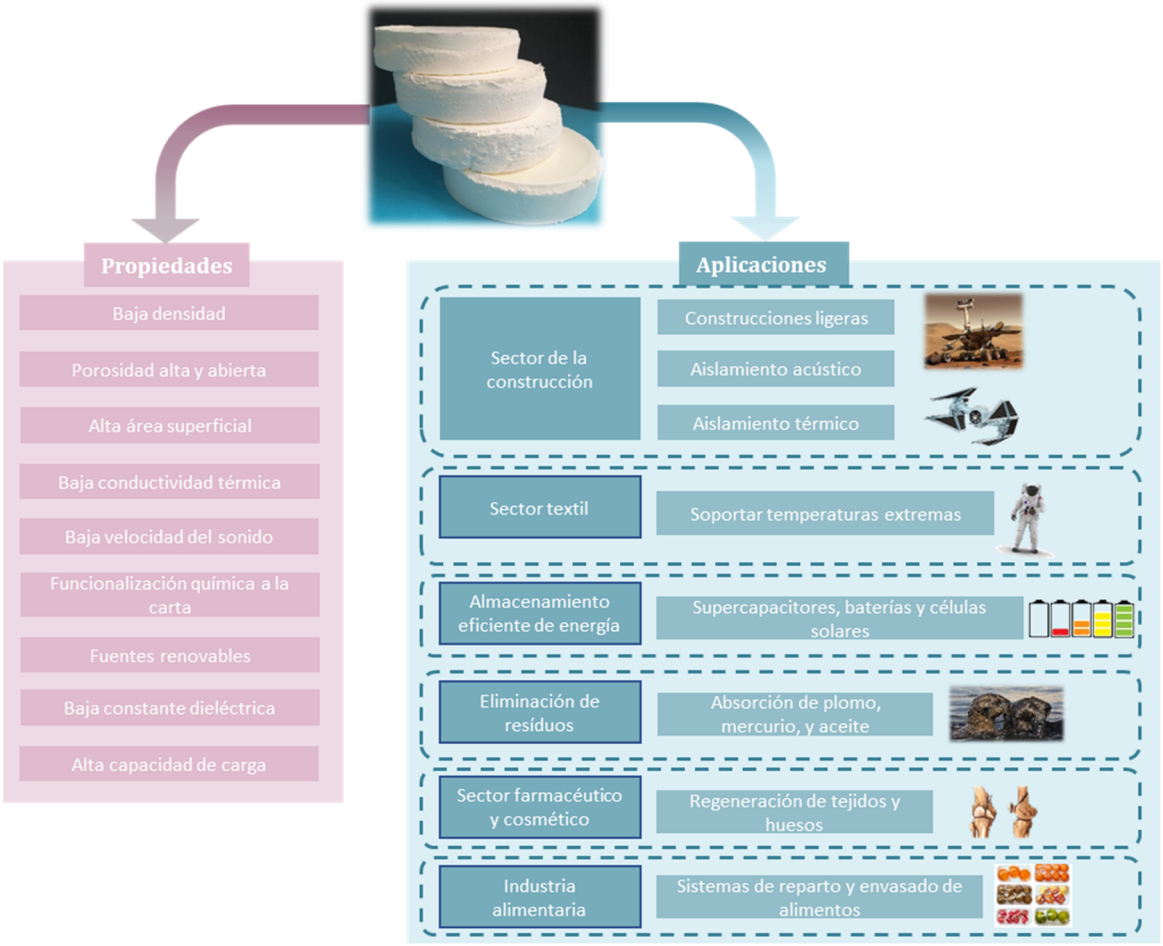

Figura R.3. Propiedades específicas y aplicaciones de los aerogeles.

Los aerogeles se emplean principalmente en el sector de la construcción por su ligereza y también por su aislamiento térmico y acústico. Esto amplía su aplicabilidad a sectores afines como la automoción o la aeronáutica en los que se requieren propiedades similares. Recientemente, el sector textil ha comenzado a incorporar aerogeles en sus prendas, con el objetivo de hacer frente a temperaturas extremas, tanto de calor como de frío. Cada vez son más las industrias que utilizan aerogeles para aplicaciones medioambientales como un almacenamiento de energía eficiente en supercondensadores, baterías o células solares, o para procesos de tratamiento de la contaminación como la absorción de metales pesados, la eliminación de aceites o el tratamiento de aguas. Además, se han llevado a cabo avances prometedores en la industria farmacéutica hacia la regeneración de tejidos y huesos o la administración de fármacos, así como en la industria alimentaria, especialmente para el envasado de alimentos.

I.d Perspectivas de futuro

Hace más de un siglo, ya en 1820, los científicos comenzaron a estudiar la influencia de los gases de efecto invernadero en el clima de la Tierra. Muchos años después, en 1975, apareció el primer término "calentamiento global" en una revista científica. Esta preocupación mundial llevó a adaptaciones humanas y a la implementación de diferentes estrategias y medidas con el objetivo de reducir las emisiones de gases de efecto invernadero. Entre los sectores que contribuyen a los efectos perjudiciales, destaca el sector de la edificación, que representa un tercio de la demanda total de energía y las emisiones de CO_2 asociadas [27], [28]. Por lo tanto, una fuerte disminución del consumo de energía de los edificios constituye un requisito crucial para cumplir con las regulaciones cada vez más estrictas [29]. Los materiales aislantes térmicos son críticos en este contexto. En cuanto al Mercado Global de Aislantes (**Figura R.4 a**), el sector de la construcción es el principal campo en el que se aplican materiales aislantes, constituyendo un 34 % del mercado total de los mismos. Por ello, y debido a que los materiales aislantes de uso común – como las espumas de poliuretano – aportan conductividades térmicas entre 20 – 35 mW/(m·K), insuficientes para cumplir con la futura normativa de aislamiento, destacan los aerogeles como sustitutos muy prometedores [30],[31].

El creciente interés por los aerogeles se ha hecho notar desde hace muchos años, alcanzando un valor de 818.9 millones de USD en el mercado mundial en 2020, y se espera que crezca a una tasa anual del 15,1 % alcanzando los 2.2 billones de USD para 2028 [32], como muestra la **Figura R.4 b**.

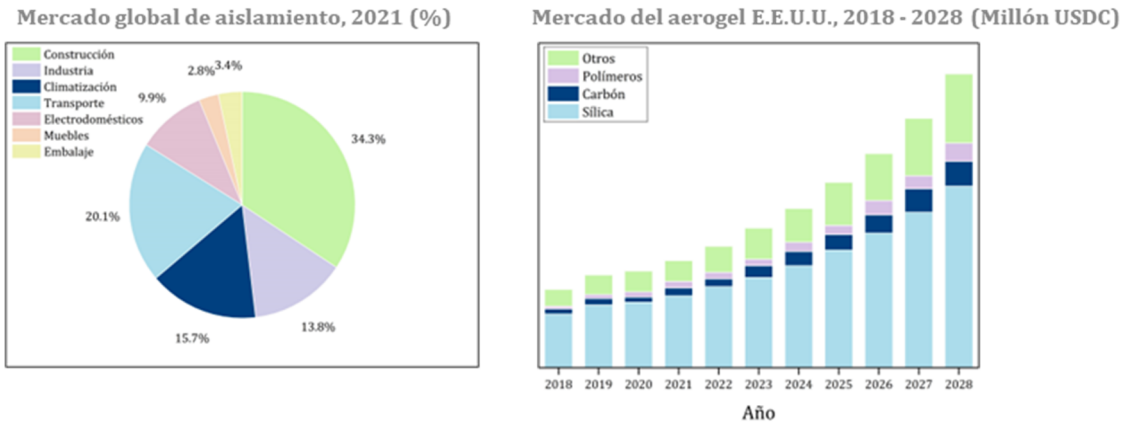

Figura R.4. a) Mercado global de aislamiento durante el año 2021 por sectores, b) Mercado del aerogel en E.E.U.U 2018 a 2028 (de la referencia [32]).

Como se describe en los gráficos anteriores, la matriz de aerogel más utilizada es la sílice. Sin embargo, durante los últimos años se ha observado una tendencia creciente en aerogeles de carbono y aerogeles poliméricos, así como en aerogeles de base biológica de diversos orígenes (celulosa, quitosano, alginato, almidón, agar, entre otros [33], [34]). Una de las razones de esta tendencia creciente podría estar basada en la mejora de las propiedades mecánicas que ofrecen otras matrices en comparación con la sílice, a menudo caracterizada por su fragilidad.

El control de las propiedades finales de estos materiales está íntimamente ligado a la matriz inicial, la formulación química y la estructura porosa. Tanto los procesos como las

estructuras de estos materiales son realmente complejos y poco conocidos, por lo que existe una clara necesidad de seguir investigando sobre estos materiales. Por tanto, el diseño de propiedades específicas solo es posible realizando un control exhaustivo del proceso de producción y de secado del gel, así como profundizando en los parámetros que afectan a la estructura porosa final del aerogel. Además, se debe ampliar la comprensión de la relación entre proceso, estructura porosa, propiedades y, por lo tanto, aplicaciones finales.

Estas afirmaciones han motivado el desarrollo de esta tesis, llevada a cabo en el Laboratorio CellMat, como se explicará en los siguientes apartados, y ha fijado las metas y objetivos principales (**sección III**). Además de este tema de investigación sobre aerogeles, esta tesis también presenta algunas contribuciones en el campo de las espumas de poliuretano, como se explica a continuación.

II Marco de la tesis

Esta tesis, supervisada por el Prof. Dr. Miguel Ángel Rodríguez-Pérez y Prof. Dr. Fernando Villafañe González, ha sido desarrollada en el **laboratorio CellMat** [35], que pertenece al departamento de Física de la Materia Condensada, Cristalografía y Mineralogía de la Universidad de Valladolid, España.

CellMat es un grupo de investigación que fue fundado en 1999 por ambos, el Prof. Dr. José Antonio de Saja y el Prof. Dr. Miguel Angel Rodríguez- Pérez, quien actualmente lidera el grupo.

Desde el inicio, este laboratorio comenzó a caracterizar espumas de poliolefina comerciales [36]–[38] y, dos años después, a producir y caracterizar espumas metálicas [39]–[43]. Posteriormente, se sentaron las bases del laboratorio CellMat, alcanzando un amplio conocimiento en el tetraedro de los materiales celulares (**Figura R.5**) para una gran colección de polímeros celulares (PS, PU, PMMA, cauchos, etc.). Este tetraedro se basa en la comprensión de las relaciones producción-estructura-propiedades y en el análisis de las aplicaciones de los polímeros celulares.

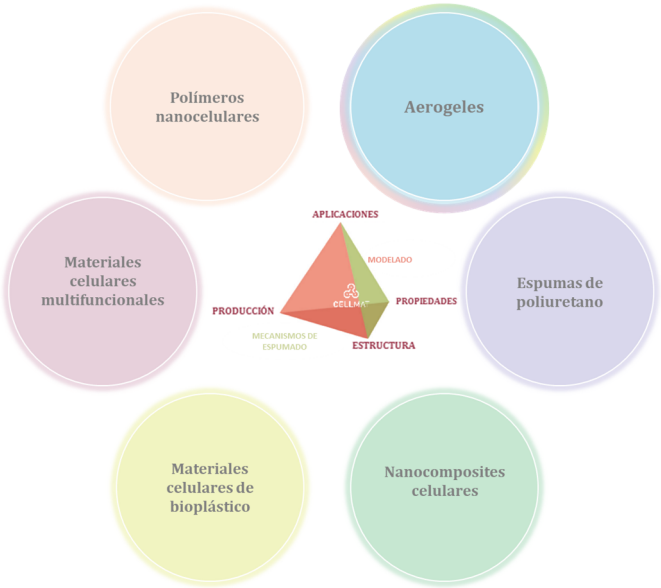

Figura R.5. Tetraedro de los materiales celulares y áreas de investigación de CellMat.

Uno de los principales objetivos de CellMat es desarrollar nuevos conocimientos sobre estos materiales de interés para varios sectores, como la automoción, las energías renovables, la edificación y construcción, la aeronáutica, etc. y realizar investigaciones científicas de interés en el campo de los materiales celulares.

CellMat cubre diferentes áreas de investigación: materiales celulares multifuncionales [44]–[46], materiales celulares de bioplástico [47]–[51], nanocomposites celulares [52]–[55], espumas de poliuretano [56]–[59], y polímeros nanocelulares [60]–[65]. En esta tesis, se ha llevado a cabo una combinación de las dos últimas líneas de investigación, uniendo la versatilidad de la matriz de poliuretano con las interesantes propiedades de los materiales celulares con celdas nanométricas. Esta combinación ha dado lugar a una nueva línea de investigación basada en aerogeles, tema principal de esta tesis, que se beneficia de la experiencia previa del grupo. Además, a lo largo de este trabajo, se han sintetizado nuevos compuestos celulares que amplían nuestro conocimiento en el campo.

El principal objetivo de esta tesis consiste en desarrollar nuevos conocimientos sobre aerogeles, su síntesis, caracterización, y posibles aplicaciones finales. En este grupo se han realizado anteriormente varias tesis dedicadas al estudio de la síntesis, cinética y propiedades físicas de nanocomposites celulares basados en poliuretano rígido. En la del Dr. Sergio Estravís Sastre en 2014 y en la de la Dra. Mercedes Santiago Calvo en 2019, en las que el poliuretano fue el material principal.

El proceso de producción y la estructura porosa de los aerogeles se han estudiado en detalle teniendo en cuenta los posibles factores que afectan a sus propiedades finales, así como la optimización del método de secado. Posteriormente, se ha evaluado la relación estructura-propiedades y se han estudiado diferentes propiedades físicas, como las propiedades texturales, térmicas, mecánicas y ópticas.

Posteriormente, durante una estancia internacional de tres meses en el grupo de investigación Computation and Materials (CeM), se llevó a cabo la producción de composites aerogel de sílice-espuma de PU flexible (Sil-PU) y PU aerogel-espuma de PU flexible (PU_A-PU_F), perteneciente al Centro de Investigación de Ingeniería de Procesos Químicos y Productos Forestales (CIEPQPF) en el Departamento de Ingeniería Química (DEQ) de la Universidad de Coimbra (Portugal), bajo la supervisión de la Prof. Dra. Luisa Maria Rocha Durães. Esta institución fue fundada en 1994 con el objetivo de crear un marco estructurado para las actividades de investigación. La amplia experiencia del grupo CeM en aerogeles de sílice y en sus homólogos modificados/reforzados orgánicamente nos ha proporcionado un conocimiento muy valioso y un marco sólido para empezar a trabajar con estos materiales.

Adicionalmente, la COST (European Cooperation in Science and Technology) CA18125 - Advanced Engineering and Research of aeroGels for Environment and Life Sciences también ha sido importante para el desarrollo de esta tesis. Se realizó un intercambio conocido como Short-Term Scientific Mission (STSM) de un período de tres meses en la misma universidad portuguesa que permitió al doctorando aprender nuevas técnicas y métodos relacionados con los aerogeles. Esta Cost Action a través de su financiación, cursos y conferencias internacionales, reúne a expertos académicos, de la industria y regulaciones; por lo tanto, impulsando las interacciones entre la industria y la academia y capacitar a jóvenes investigadores europeos a través de escuelas técnicas y becas STSM.

III Objetivos

La decisión de investigar sobre aerogeles en nuestro laboratorio se tomó tras de considerar el enorme interés de estos materiales, la necesidad de seguir investigándolos, y la experiencia previa de CellMat sobre polímeros celulares. Una de las principales prioridades era ampliar nuestro conocimiento relacionado con los materiales nanoporosos. Además, la capacidad de aislamiento de las espumas de poliuretano y los polímeros nanocelulares presenta un margen de mejora interesante, solo posible mediante la reducción tanto de la densidad como del tamaño de los poros. Así, una línea de investigación de novedosos materiales nanoporosos fue la principal motivación para comenzar con el desarrollo de esta tesis.

Los diferentes objetivos de esta tesis se centran en la producción de materiales basados en aerogeles y en comprender la relación entre la estructura porosa y las propiedades de los nuevos materiales desarrollados.

A la hora de definir los objetivos de esta tesis se han considerado dos líneas principales de investigación, recogidas en la **Figura R.6**.

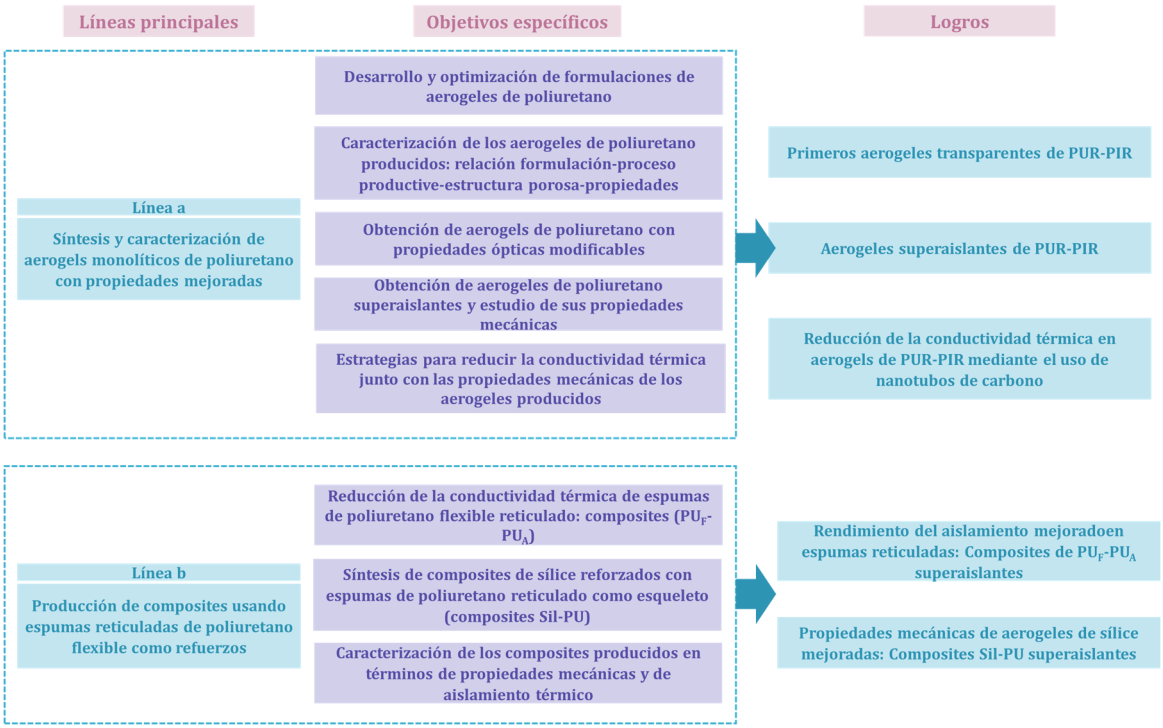

Figura R.6. Principales líneas de investigación, objetivos específicos, y resumen de los principales logros de esta tesis.

a) Síntesis y caracterización de aerogeles de poliuretano monolíticos con propiedades mejoradas

En esta primera línea se definen dos temas principales. Por un lado, sintetizar aerogeles de poliuretano de baja densidad, con una estructura nanoporosa controlada y con excelentes propiedades físicas. Por otro lado, un análisis detallado de la relación estructura-propiedades. Los principales objetivos de esta línea son obtener aerogeles con una gran capacidad de

aislamiento térmico e intentar conseguir un alto grado de transparencia. Este objetivo general se puede dividir en cinco objetivos específicos:

1. Desarrollo y optimización de formulaciones en base poliuretano para la obtención de aerogeles nanoporosos.

Se han desarrollado diferentes formulaciones para seleccionar aquella que condujera a un gel homogéneo con una estructura nanoporosa que no colapse durante el proceso de secado. Para realizar este estudio se llevaron a cabo diferentes estrategias:

- Estudio de diferentes catalizadores
- Estudio de la influencia del contenido de catalizador en la estructura nanoporosa
- Efecto del método de secado en la estructura nanoporosa

2. Caracterización de los aerogeles de poliuretano producidos, con el fin de comprender la relación formulación – proceso de producción – estructura porosa – propiedades.

En primer lugar, se establecieron las técnicas específicas para caracterizar estos materiales. Con el fin de cumplir con este objetivo, se evaluaron diferentes parámetros y propiedades:

- Se determinaron las densidades aparentes (ρ_B) y relativa (ρ_r) de los aerogeles producidos.
- Estudio de la estructura porosa: las fases gaseosa y sólida que constituyen estos materiales se describieron mediante diferentes parámetros. La fase sólida fue descrita mediante el tamaño promedio de partícula (ϕ_{part}), distribución de tamaño de partícula y área superficial específica (S_{BET}), mientras que la fase gaseosa fue definida por el tamaño promedio de poro (ϕ_{pore}) y la porosidad (Π).
- Estudio de las propiedades aislantes: se evaluó la conductividad térmica (λ).
- Estudio de las propiedades mecánicas: el módulo de elasticidad (E), curvas esfuerzo (σ) – deformación (ε), así como el coeficiente de pérdida de energía (ELC).
- Estudio de las propiedades ópticas: se llevaron a cabo medidas de transmitancia de luz (T) para evaluar la transparencia óptica de estos aerogeles. Se emplearon dos procedimientos de medida para obtener este parámetro:
    - Medidas con láseres: se emplearon láseres con diferentes longitudes de onda características (450, 532 and 650 nm).
    - Medidas con UV-vis: se midió un espectro continuo de 400 a 900 nm.

3. Obtención de aerogeles de poliuretano con propiedades ópticas a la carta.

La transparencia es, en combinación con otras características, una de las propiedades más deseadas en los aerogeles. Por lo tanto, controlar la estructura porosa de los aerogeles producidos conduciría a transmitancias de luz modificables. Además, se analizarán en detalle sus propiedades ópticas para comprender los mecanismos de dispersión de la luz que tienen lugar.

4. Obtención de aerogeles de poliuretano superaislantes y estudio de sus propiedades mecánicas.

Se midió la conductividad térmica de los aerogeles producidos y se analizaron las diferentes contribuciones a la conductividad térmica efectiva. Además, se estudiaron las

propiedades mecánicas incluyendo resistencia a la compresión, elasticidad y flexibilidad.

5. Desarrollo de estrategias para reducir la conductividad térmica de los aerogeles producidos y modificación de las propiedades mecánicas.

Con el objetivo de reducir la contribución radiativa, una estrategia bien conocida en el campo de los polímeros celulares consiste en la adición de opacificantes para reducir la radiación infrarroja. Esta aproximación se llevó a cabo en aerogeles de poliuretano mediante la incorporación de nanotubos de carbono (**CNTs**) en la formulación.

Para todos los materiales producidos se ha realizado un análisis detallado de la relación proceso – estructura – propiedades.

b) Producción de composites utilizando espumas de poliuretano flexible reticulado como esqueleto

La segunda línea de investigación tiene como objetivo producir compuestos de espuma de PU-aerogel tratando de mejorar tanto las propiedades iniciales de las espumas (en el caso de los aerogeles de PU) como las propiedades de los aerogeles (en el caso de los aerogeles de sílice). Esto incluye la síntesis y evaluación de sus propiedades mecánicas y de aislamiento térmico. Los objetivos específicos de esta línea de investigación son los siguientes.

1. Reducción de la conductividad térmica de las espumas de poliuretano flexible reticulado mediante la producción de compuestos de espuma de poliuretano – aerogel de poliuretano (**PU_F–PU_A**).

La inclusión de aerogel de poliuretano en los poros de las espumas de PU flexibles contribuye a cambiar significativamente contribución gaseosa en la transferencia de calor sin alterar la cinética de reacción de la espuma de PU, ya que el aerogel se incluye en la espuma ya fabricada. Se utilizaron espumas con diferentes tamaños de poro para analizar la influencia de este parámetro en las propiedades finales de los composites.

2. Síntesis de composites en base aerogel de sílice reforzados con espumas de poliuretano reticulado como esqueleto (composites Sil-PU).

Se ha utilizado la misma estrategia con aerogeles de sílice con el fin de mejorar las propiedades mecánicas de los monolitos, manteniendo su excelente capacidad como aislantes térmicos. Se utilizaron espumas con diferentes tamaños de poro para analizar la influencia de este parámetro en las propiedades finales de los composites.

3. Caracterización de los compuestos producidos en términos de propiedades mecánicas y aislamiento térmico.

Una vez producidos los composites, se evaluaron sus propiedades mecánicas y conductividad térmica, y se analizó el efecto del tamaño de poro de la espuma sobre las propiedades finales de los composites.

Finalmente, se realizó un análisis detallado de la relación proceso – estructura – propiedades.

Los objetivos específicos descritos para cada línea principal de investigación, junto con los parámetros estudiados, se recogen en la **Figura R.7**.

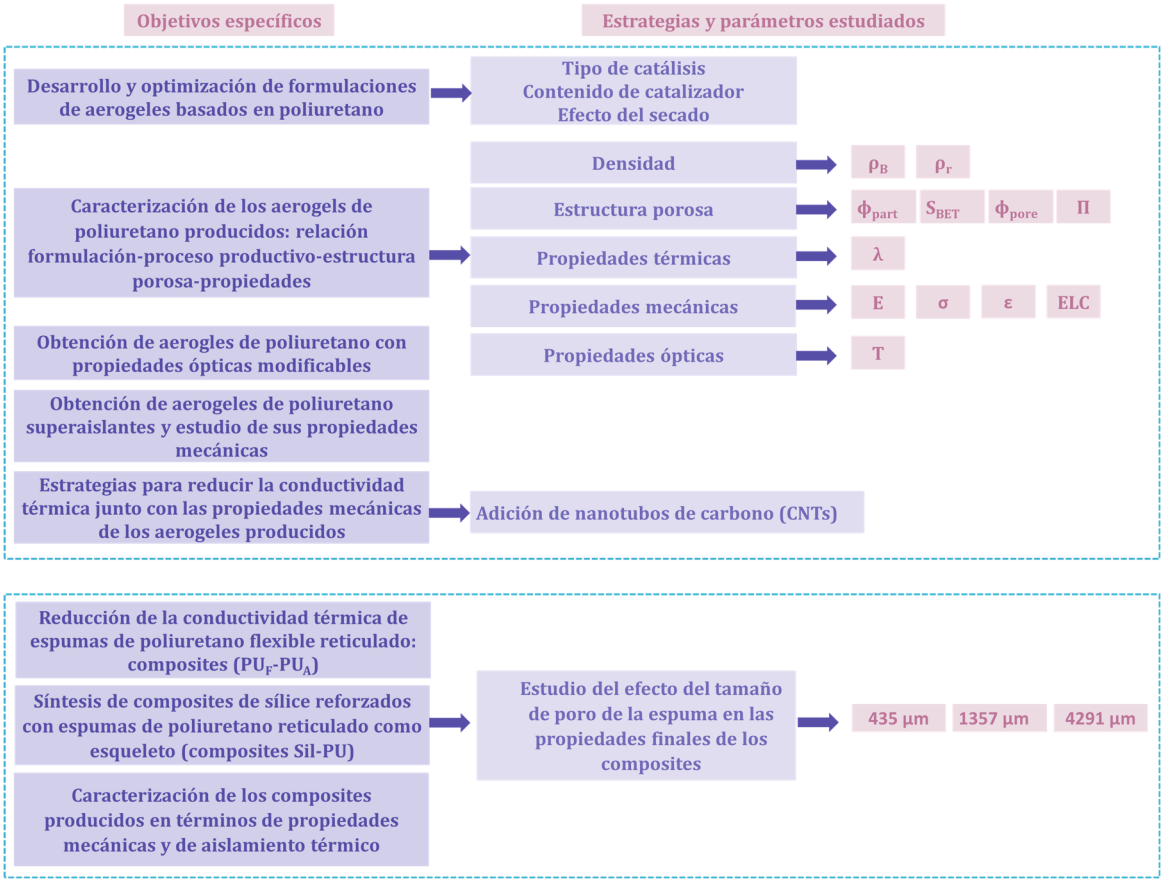

Figura R.7. Objetivos específicos de la tesis y parámetros estudiados.

Mediante el cumplimiento de estos objetivos, nuestro conocimiento en aerogeles se ha ampliado alcanzando la producción de aerogeles bajo demanda en nuestras instalaciones, mediante el control de sus estructuras porosas. Además, la evaluación de las propiedades ópticas, térmicas y mecánicas de los materiales producidos se ha cubierto durante esta investigación.

No obstante, somos conscientes de que varias propiedades interesantes, como las propiedades acústicas, la capilaridad o la cinética de reacción, podrían estudiarse adicionalmente, proporcionando así un trasfondo más completo. Por lo tanto, se espera que, a partir de esta tesis, se origine un extenso trabajo futuro.

Anexo

Durante el período de formación como estudiante de doctorado, también se llevó a cabo una investigación en el campo de las espumas de poliuretano. Aunque este no es el tema principal de la tesis, al final del documento se incluye un anexo que recoge los principales trabajos realizados sobre estos materiales. Los objetivos de la investigación realizada en espumas de PU son los siguientes:

1. Estudiar la influencia de la adición de nanopartículas a la mezcla reactiva de espumas rígidas de poliuretano.

Se evaluó el efecto de la adición de nanopartículas a las formulaciones de PU. Mediante la restricción de la inclusión de aire en la mezcla reactiva mientras se mezclan los componentes, se analizó la influencia del aire atrapado en la nucleación celular.

2. Analizar la influencia de la estructura porosa en el coeficiente de absorción acústica de una colección de espumas semirrígidas en base poliuretano con diferentes estructuras celulares.

Para llevar a cabo este objetivo, se desarrolló una nueva metodología para caracterizar los agujeros de las paredes celulares y características principales de las celdas que forman las espumas de poliuretano.

3. Adsorción de nitratos mediante el uso de espumas de PU hidrofílicas y flexibles.

Se fabricaron nanocompuestos basados en espumas de PU flexibles e hidrofílicas y sepiolitas organomodificadas como relleno. Se emplearon diferentes cantidades de sepiolita y se evaluó la afinidad de los nanocomposites producidos por nitratos disueltos en agua.

IV Novedades

Esta investigación aborda diferentes aspectos de los aerogeles de poliuretano y sílice, así como de las espumas de poliuretano, aportando a la literatura científica algunas novedades, que se indican a continuación.

En primer lugar, se han **sintetizado por primera vez aerogeles en base poliuretano** que presentan **transparencia óptica** a la luz visible. Se incrementó el tamaño de los aerogeles sintetizados mediante la optimización de los procedimientos de producción, lo que permitió medir su conductividad térmica con mayor precisión.

Además, debido a la interesante estructura nanoporosa que presentan estos aerogeles, la conductividad térmica de los monolitos reveló **la mayor capacidad aislante** de esta matriz **alcanzando los valores más bajos de conductividad térmica** conocidos hasta ahora **para aerogeles de PU**.

La inclusión de nanotubos de carbono (CNTs) en las formulaciones de aerogel en base poliuretano condujo a una mayor reducción de la conductividad térmica de estos materiales, así como a modificaciones de las propiedades mecánicas y estructuras porosas.

Adicionalmente, una **estrategia novedosa** basada en la **inclusión de aerogeles a base de poliuretano en los poros de las espumas de poliuretano flexible reticulado**, condujo

a una reducción significativa de la conductividad térmica nunca antes explorada, mostrando un **método simple y directo para mejorar el rendimiento del aislamiento térmico de espumas de poliuretano flexibles** que podría aplicarse a otros materiales celulares en futuras investigaciones. Además, se ha **analizado la influencia del tamaño de poro** de la espuma sobre las propiedades finales de los composites producidos, encontrando que, para todos ellos, **la cohesión entre el aerogel y las aristas de PU es efectiva**, y que las **propiedades finales son similares a las del aerogel monolítico**.

La misma estrategia se aplicó para **reforzar aerogeles de sílice** logrando mejores propiedades mecánicas **mientras que se mantiene su capacidad super-aislante**. Por lo tanto, aquí se presenta un **método innovador de mejorar la resistencia de los aerogeles de sílice** y, por lo tanto, reducir su fragilidad común.

Esta última **estrategia ha sido optimizada mediante el estudio del efecto de diferentes tamaños de poros de la espuma**, lo que lleva a una **inclusión de aerogel más eficiente cuando los poros de espuma son más pequeños**. De esta forma, el aerogel de sílice mantiene su estructura en forma de red 3D sin roturas ni desconexiones con las aristas poliméricas.

Además, tal y como se recoge en el Anexo, se han realizado diferentes estudios sobre espumas de poliuretano:

Se ha estudiado en detalle **el efecto del aire atrapado en espumas rígidas de PU conteniendo nanoarcillas**, llegando a la conclusión de que **el aumento de la viscosidad** que experimenta la mezcla reactiva cuando se añaden las nanopartículas, es el principal factor que **contribuye a un efecto nucleante, en lugar de ser efecto de las propias partículas**. La razón sería la mayor cantidad de gas atrapado al aumentar la viscosidad del poliol cuando se incluyen las nanopartículas.

En el presente documento **se han descrito nuevos parámetros** que describen la estructura porosa de las espumas de PU semirrígidas. Estos parámetros permiten describir la **relación entre la absorción acústica y los parámetros estructurales** de estos materiales.

Finalmente, la **inclusión de nanoarcillas organomodificadas en formulaciones de espumas flexibles de PU hidrofílicas** ha supuesto la mejora de los métodos actuales de **adsorción de nitratos en soluciones acuosas**, actuando como **soporte de estas partículas** y, por tanto, evitando etapas de filtración, así como alcanzando **altas capacidades de adsorción** de nitratos.

V Estructura de la tesis

Esta tesis ha sido escrita por compendio de publicaciones. Se han publicado once artículos científicos en revistas internacionales. Además, hay algunos resultados no publicados que se han incluido para proporcionar información adicional. Esta tesis cumple con los requisitos para solicitar el grado de Doctor en Filosofía (Ph.D.) con Mención Internacional.

Este manuscrito incluye ocho capítulos y un anexo al final del trabajo. Las diferentes secciones incluyen la siguiente información:

- **Capítulo 1: Introducción.** En esta sección se ha incorporado una breve introducción sobre los aerogeles, su nacimiento, evolución, y principales características. A continuación, se incluye el marco de esta tesis, los objetivos

generales y específicos, y las novedades que aporta este trabajo. Finalmente, se presenta una sección que reúne las publicaciones científicas, congresos internacionales y nacionales, proyectos y otra información adicional. También se incluye la estructura de esta tesis.

- **Capítulo 2: Estado del arte.** Este capítulo reúne la información esencial para comprender los conceptos, procesos y mecanismos involucrados en la síntesis de los materiales producidos, la estructura y las propiedades. Las secciones principales de este capítulo contienen las definiciones de aerogel, tipos de aerogeles según la matriz, proceso de síntesis y de secado, y los parámetros estructurales. Después, se describen sus propiedades ópticas, mecánicas y térmicas incluyendo una revisión de la bibliografía existente y datos encontrados en el estado del arte. Al final del capítulo se encuentra un resumen de las principales aplicaciones de estos aerogeles.

- **Capítulo 3: Sección experimental: Materiales y Técnicas.** Los reactivos de partida y las formulaciones desarrolladas para sintetizar los materiales producidos en esta tesis se describen en detalle en este capítulo. Posteriormente, se explican los métodos de producción seguidos durante la fabricación de los materiales, las técnicas de caracterización empleadas para analizar su estructura, propiedades mecánicas y ópticas, así como la conductividad térmica.

- **Capítulo 4: Síntesis y caracterización de aerogeles monolíticos transparentes de poliuretano.** En este capítulo se describe la síntesis y caracterización inicial de aerogeles de poliisocianurato-poliuretano. Se incluye una publicación científica con los primeros resultados de aerogeles en base poliuretano que muestran transparencia. Un análisis más profundo de las propiedades ópticas de estos aerogeles se incluye en la segunda publicación de este capítulo, conduciendo a la comprensión de diferentes parámetros que afectan la transparencia final de los materiales producidos.

- **Capítulo 5: Conductividad térmica y propiedades mecánicas de aerogeles monolíticos transparentes de poliuretano.** En este capítulo se presentan los resultados obtenidos en cuanto a las propiedades mecánicas y conductividad térmica de las formulaciones de aerogeles de poliisocianurato–poliuretano descritas previamente en el capítulo 4. Se incluye una publicación científica que trata sobre la relación formulación – estructura – propiedades mecánicas y conductividad térmica de estos aerogeles. Además, se adjunta una publicación adicional que recoge los resultados obtenidos para conseguir una mayor reducción de la conductividad térmica de los aerogeles de poliuretano mediante la incorporación de bloqueadores de infrarrojos. Este estudio analiza en detalle las contribuciones a la conductividad térmica total para estos aerogeles.

- **Capítulo 6: Mejorando el aislamiento térmico de espumas de poliuretano mediante la inclusión de aerogel en la estructura porosa.** En este capítulo se describe una estrategia novedosa para disminuir drásticamente la conductividad térmica de espumas de poliuretano reticulado. Esta estrategia consiste en llenar los poros de la espuma con aerogel de poliuretano que presenta una capacidad de aislamiento excelente. Se ha incluido una publicación científica con los resultados

de la síntesis y caracterización completa de estos novedosos composites de espuma de poliuretano–aerogel de poliuretano.

- **Capítulo 7: Refuerzo mecánico de Aerogeles de Sílice mediante espumas de Poliuretano como esqueleto.** El capítulo 7 fusiona los resultados del refuerzo de aerogeles de sílice con espumas de poliuretano flexible reticulado para mejorar sus propiedades mecánicas manteniendo su comportamiento aislante. La primera publicación que se encuentra en este capítulo describe la síntesis y caracterización de estos compuestos buscando la mejor ruta de síntesis y formulación. La segunda publicación estudia el efecto del tamaño de poro de la espuma en las propiedades finales de los compuestos espuma de poliuretano– aerogel de sílice para encontrar el refuerzo óptimo.

- **Capítulo 8: Conclusiones y Trabajo Futuro.** En este capítulo se presentan las principales conclusiones de esta investigación. Además, los resultados obtenidos se comparan con los encontrados en la literatura. Finalmente, se incluyen algunas ideas para trabajo futuro al final del capítulo.

- **Anexo:** Al final de esta tesis se incluye un anexo que reúne tres publicaciones relacionadas con espumas de poliuretano y la comprensión de sus diferentes propiedades.

Una visión general de la estructura y la distribución de las publicaciones científicas a lo largo de esta tesis se representan en la **Figura R.8** y la **Figura R.9**, respectivamente.:

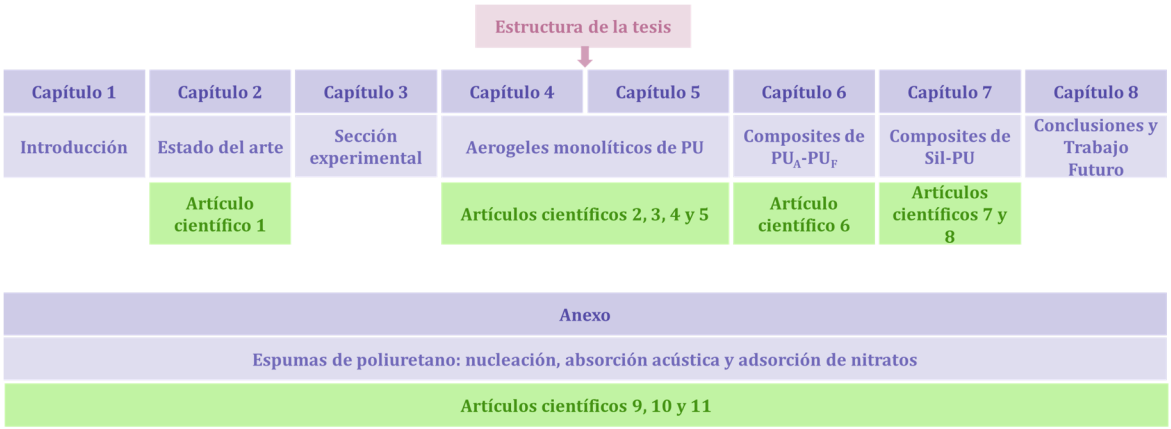

Figura R.8. Estructura de la tesis; capítulos que contiene y tema principal de investigación.

Figura R.9. Publicaciones incluidas en esta tesis.

VI Publicaciones, conferencias, proyectos y cursos

En este apartado se incluyen las publicaciones científicas incluidas en esta tesis (**Tabla R.1**), contribuciones a congresos nacionales e internacionales relacionados con la investigación de esta tesis (**Tabla R.2** y **Tabla** R.3), proyectos industriales y de investigación (**Tabla R.4**), estancias en centros de investigación (**Tabla R.5**), premios (**Tabla R.6**), becas y contratos (**Tabla R.7**), y actividades complementarias como publicaciones y congresos complementarios, actividades de divulgación y cursos de formación (**Tabla R.8**).

Se han publicado un total de 11 artículos científicos en revistas internacionales durante el desarrollo de la presente tesis.

Tabla R.1. Publicaciones científicas incluidas en esta tesis.

Publicaciones científicas indexadas			
Número	**Referencia**	**Q/IF**	**Capítulo**
1	Merillas B.; Vareda J.; Martín-de León J.; Rodríguez-Pérez MÁ.; Durães L. **Thermal Conductivity of Nanoporous Materials: Where Is the Limit?** Polymers, (2022), 14, 2556.	Q1/4.967	2
2	Merillas B.; Martín-de León J.; Villafañe F.; Rodríguez-Pérez MA. **Transparent Polyisocyanurate-Polyurethane-Based Aerogels: Key Aspects on the Synthesis and Their Porous Structures.** ACS Appl. Polym. Mater. (2021), 3, 4607–4615.	Q1/4.855	4
3	Merillas B.; Martín-de León J.; Villafañe F.; Rodríguez-Pérez MÁ. **Optical Properties of Polyisocyanurate – Polyurethane Aerogels: Study of the Scattering Mechanisms**. Nanomaterials, (2022), 12, 1522.	Q1/5.719	4
4	Merillas B.; Villafañe F.; Rodríguez-Pérez MÁ. **Super-insulating transparent polyisocyanurate-polyurethane aerogels: analysis of the thermal conductivity and mechanical properties**. Nanomaterials (2022), 12, 2409.	Q1/5.719	5
5	Merillas B.; Villafañe F.; Rodríguez-Pérez MÁ. **Effect of the addition of carbon nanotubes on the final properties of polyurethane-polyisocyanurate aerogels**. Submitted	-	5
6	Merillas B.; Villafañe F.; Rodríguez-Pérez MÁ. **Improving the Insulating Capacity of Polyurethane Foams through Polyurethane Aerogel Inclusion: From Insulation to Superinsulation**. Nanomaterials, (2022) 12, 2232.	Q1/5.719	6
7	Merillas B.; Lamy-Mendes A.; Villafañe F.; Durães L.; Rodríguez-Pérez MÁ. **Silica-Based Aerogel Composites Reinforced with Reticulated Polyurethane Foams: Thermal and Mechanical Properties**. Gels, (2022), 8, 392.	Q1/4.432	7
8	Merillas B.; Lamy-Mendes A.; Villafañe F.; Durães L.; Rodríguez-Pérez MÁ. **Polyurethane foam scaffold for silica aerogels: effect of the cell size on the mechanical properties and thermal insulation**. Mater. Today Chem., (2022), 26, 101257.	Q1/7.613	7
9	Merillas B.; Villafañe F.; Rodríguez-Pérez MÁ. **Nanoparticles addition in PU foams: The dramatic effect of trapped-air on nucleation**. Polymers, (2021), 13, 1–11.	Q1/4.329	Annex
10	Merillas B.; Villafañe F.; Rodríguez-Pérez MÁ. **A New Methodology Based on Cell-Wall Hole Analysis for the Structure-Acoustic Absorption Correlation on Polyurethane Foams**. Polymers, (2022), 14, 1807.	Q1/4.329	Annex
11	Barroso-Solares S.; Merillas B.; Cimavilla-Roman P.; Rodríguez-Pérez MA.; Pinto J. **Enhanced nitrates-polluted water remediation by polyurethane/sepiolite cellular nanocomposites**. J. Clean. Prod., (2020), 254, 120038.	Q1/9.297	Annex

Publicaciones científicas no-indexadas	
Número	**Referencia**
1	Barroso-Solares S.; Merillas B.; López-González E.; Rodríguez-Pérez MA.; Pinto J. Proceedings paper. EDULEARN18 – 10th International Conference on Education and new Learning Technologies. Page 6196-6206. **Development of a postgraduate training program on surface functionalization of polymers/polymer foams**.
2	Merillas B.; Martín-de León J.; Villafañe F.; Rodríguez-Pérez MÁ. Conference Proceedings. 18th International Conference on Advances in Foam Materials & Technology (FOAMS® 2021). **Highly Transparent Polyurethane-based Aerogels: effect of catalyst on the porous structure and final properties**.
3	Barroso-Solares S.; Vázquez-Corrales L.; Moral-Domingo, R.; Merillas B.; Cuadra-Rodríguez, D.; Rodríguez-Pérez MA.; Pinto J. Conference Proceedings. 18th International Conference on Advances in Foam Materials & Technology (FOAMS® 2021). **Water Pollutants Removal by Nanocomposite foamed Polymers**.

Los resultados de esta tesis se han presentado en varias conferencias internaciones y nacionales, recogidas en las siguientes tablas.

Tabla R.2. Conferencias Internacionales.

Conferencias Internacionales		
Número	**Conferencia**	**Contribución**
1	Barroso-Solares S.; Merillas B.; Cimavilla P.; Rodríguez-Pérez M.A.; Pinto J. **Nitrates and other pollutants removal from water resources using multifunctional polyurethane foams**. 4th International Congress on Water, Waste and Energy Management (WWEM-18), 2018, Madrid, Spain.	Comunicación oral
2	Merillas B.; Barroso-Solares S.; Cimavilla P.; Pinto J.; Rodríguez-Pérez M.A. **Nitrate removal from aqueous solution by adsorption onto polyurethane/sepiolite cellular nanocomposites.** 17th International Conference on Advances in Foam Materials & Technology (FOAMS® 2019), 2019, Valladolid, Spain.	Póster
3	Merillas B.; Villafañe F.; Rodríguez-Pérez MÁ. **Ex-situ analysis of the synthesis of PU aerogels: time evolution of particle size.** International Conference on Aerogels for Biomedical and Environmental Applications, 2020, Santiago de Compostela, Spain.	Póster
4	Merillas B.; Villafañe F.; Rodríguez-Pérez MÁ. **Synthesis of polyurethane aerogels and the effect of the structure on thermal conductivity.** 6th Cellular Materials CellMAT 2020, 2020, Web-Conference (CEST), Germany.	Comunicación oral
5	Merillas B.; Martín-de León J.; Villafañe F.; Rodríguez-Pérez MÁ.	Comunicación oral

	Highly transparent polyurethane-based aerogels: effect of catalyst on the porous structure and final properties. 18th International Conference on Advances in Foam Materials & Technology (FOAMS® 2021), 2021, Online conference.	
6	Barroso-Solares S.; Vázquez-Corrales L.; Moral-Domingo R.; Merillas B.; Cuadra-Rodríguez D.; Rodríguez-Pérez MA.; Pinto J. **Water Pollutants Removal by Nanocomposite foamed Polymers.** 18th International Conference on Advances in Foam Materials & Technology (FOAMS® 2021), 2021, Online conference.	Comunicación oral
7	Merillas B.; Martín-de León J.; Villafañe F.; Rodríguez-Pérez MÁ. **Transparent Polyurethane-based aerogels with tunable optical properties**. Advanced Technologies for the processing and characterization of nanostructured materials. AERoGELS COST ACTION CA18125. AGH University of Science and Technology, 2021, Online conference, Cracow, Poland	Comunicación oral
8	Merillas B.; Lamy-Mendes A.; Duraes L.; Villafañe F.; Rodríguez-Pérez MÁ. **Reinforced silica aerogels by using open cell polyurethane foams as skeleton: thermal and mechanical properties**. Spanish-Portuguese Industry-Academia Aerogel Meeting, 2022, Coimbra, Portugal.	Comunicación oral
9	Merillas B.; Lamy-Mendes A.; Duraes L.; Villafañe F.; Rodríguez-Pérez MÁ. **Polyurethane foam scaffold for silica and polyurethane aerogels: effect of pore size on mechanical properties and thermal insulation**. 2nd International Conference on Aerogels for Biomedical and Environmental Applications, 2022, Athens, Greece.	Comunicación oral
10	Merillas B.; Martín-de León J.; Villafañe F.; Rodríguez-Pérez MA. **Polyurethane aerogels: lightweight, transparency and super-insulation in one material**. 7th International Conference on Cellular Materials, CellMAT 2022, Online conference, Dresden, Germany.	Comunicación oral
11	Barroso-Solares S.; Merillas B.; Cimavilla P **Nitrates and other pollutants removal from water resources using multifunctional porous polymers**. Workshop "Polymers for Environmental Preservation and Remediation". BioEcoUVA Research Institute on Bioeconomy (University of Valladolid) within the project "Functional polymeric FOams for WAter RemeDiation (FORWARD)" (RTI2018-097367-A-I00, founded by MCIN/ AEI /10.13039/501100011033/ and "FEDER Una manera de hacer Europa"). 2022, On-line.	Comunicación oral

Tabla R.3. Conferencias Nacionales.

Conferencias Nacionales		
Número	**Conferencia**	**Contribución**
1	Merillas B.; Arroyo M.; Cuéllar E.; Martín-Álvarez J. M..; Miguel D.; Villafañe F. **Green synthesis of 3-(2-Pyridyl)Pyrazole and its group 6 and 7 metal carbonyl complexes**. XXXVI Reunión Bienal de la Sociedad Española de Química, 2017, Sitges, Spain.	Póster
2	Merillas B.; Villafañe F.; Rodríguez-Pérez M.A. **Synthesis and structural characterization of polyurethane aerogels**. X Congress of Young Researchers in Polymers, 2019, Burgos, Spain.	Comunicación oral

El doctorando participó en las actividades de investigación de los siguientes proyectos con financiación pública y privada.

Tabla R.4. Proyectos industriales y de investigación.

Proyectos de Investigación		
Financiación Pública		
1	**Proyecto**	**Espumas poliméricas funcionales para el tratamiento de aguas.** RTI2018-097367-A- I00
	Financiación	Agencia Estatal de Investigación; Fondos FEDER
	Duración	Enero 2019 – Junio 2022
	Investigador principal	Javier Pinto Sanz
	Presupuesto	72.600,00 €
2	**Proyecto**	**Polímeros nanocelulares transparentes y aislantes térmicos: fabricación, caracterización y relación proceso-estructura-propiedades**. RTI2018-098749-B-I00
	Financiación	Proyecto Reto-Plan Nacional
	Duración	Enero 2019 – Septiembre 2022
	Investigador principal	Miguel Ángel Rodríguez Pérez
	Presupuesto	157.300 €
3	**Proyecto**	**Polímeros nanocelulares micronizados: una nueva generación de materiales para el core de aislantes térmicos avanzados basados en paneles de vacío (VIP)**. VA202P20
	Financiación	Junta de Castilla y León. Subvenciones del programa de apoyo a proyectos de investigación cofinanciadas por el Fondo Europeo de Desarrollo Regional.
	Duración	Noviembre 2020 – Octubre 2023
	Investigador principal	Miguel Ángel Rodríguez Pérez
	Presupuesto	240.000 €
4	**Proyecto**	**Desarrollo de super aislantes térmicos basados en polímeros nanocelulares y bloqueadores de la radiación infrarroja.** PID2021- 127108OB-I00.
	Financiación	Agencia Estatal de Investigación; Fondos FEDER, Ministerio de Ciencia e Innovación. Unión Europea.
	Duración	Septiembre 2022 – Agosto 2025
	Investigador principal	Miguel Ángel Rodríguez Pérez
	Presupuesto	205.700,00 €

5	**Proyecto**	**Hacia la producción industrial de polímeros nanocelulares transparentes.** PDC2022-133391- I00.
	Financiación	Agencia Estatal de Investigación; Ministerio de Ciencia e Innovación; Plan de recuperación, transformación y resiliencia. Unión Europea – Next Generation UE.
	Duración	Diciembre 2022 – Noviembre 2024
	Investigador principal	Miguel Ángel Rodríguez Pérez
	Presupuesto	149.500,00 €
6	**Proyecto**	**Producción sostenible de super aislantes térmicos basados en polímeros nanocelulares con conductividad térmica reducida a través del incremento de la dispersión de fonones.** TED2021-130965B- I00.
	Financiación	Agencia Estatal de Investigación; Ministerio de Ciencia e Innovación; Plan de recuperación, transformación y resiliencia. Unión Europea – Next Generation UE.
	Duración	Diciembre 2022 – Noviembre 2024
	Investigador principal	Miguel Ángel Rodríguez Pérez
	Presupuesto	168.820,00 €
Financiación Privada		
7	**Proyecto**	**Investigación sobre aplicaciones de nanomateriales avanzados de carbono a la mejora de las prestaciones de matrices de poliuretano (PU) con interés en el sector de la automoción**.
	Financiación	Grupo Antolín Ingeniería
	Duración	Abril 2017 – Diciembre 2018
	Investigador principal	Miguel Ángel Rodríguez Pérez
	Presupuesto	60000 €
8	**Proyecto**	**Análisis comparativo de la estructura y cinética de reacción de sistemas en base poliuretano**.
	Financiación	Grupo Antolín Ingeniería
	Duración	Septiembre 2017 – Mayo 2018
	Investigador principal	Miguel Ángel Rodríguez Pérez
	Presupuesto	9000 €
9	**Proyecto**	**Desarrollo y optimización de materiales celulares de celda abierta para aplicaciones de confort y de absorción de líquidos**.
	Financiación	CellMat Technologies SL
	Duración	Diciembre 2016 – Diciembre 2020
	Investigador principal	Miguel Ángel Rodríguez Pérez
	Presupuesto	60000 €
10	**Proyecto**	**Desarrollo y optimización de materiales celulares de elevada resistencia al impacto**.
	Financiación	CellMat Technologies SL
	Duración	Diciembre 2016 – Diciembre 2020
	Investigador principal	Miguel Ángel Rodríguez Pérez
	Presupuesto	40000 €

En la siguiente tabla se resumen las estancias de investigación en otras instituciones durante el desarrollo de esta tesis. Dos estancias de investigación en el Departamento de Ingeniería Química de la Universidad de Coimbra, bajo la supervisión de la Prof. Dra. Luisa Durães, tuvieron una duración de seis meses. Durante este tiempo, se realizaron algunos de

los experimentos incluidos en el **Capítulo 7**, lo que resultó en dos publicaciones y una colaboración (revisión incluida en el **Capítulo 2**).

Tabla R.5. Estancias Internacionales.

Estancias	
1	Estancia Internacional (1) (3 meses). **Computation and Materials (CeM)** Laboratory, Chemical Process Engineering and Forest Products Research Centre (CIEPQPF), Dept. Chemical Engineering, University of Coimbra (11/01/2021 – 12/04/2021)
2	Estancia Internacional (2) (3 meses). **Computation and Materials (CeM)** Laboratory, Chemical Process Engineering and Forest Products Research Centre (CIEPQPF), Dept. Chemical Engineering, University of Coimbra (01/07/2021 – 30/09/2021)

Algunos de los trabajos presentados en congresos y concursos han sido premiados, tal y como se recoge en la siguiente tabla.

Tabla R.6. Premios.

Premios	
1	**Segundo premio: IV Edición "Three-Minute Thesis"**. Doctoral School in the University of Valladolid (2019)
2	**Segundo premio: Best Poster Presentation from Early Career Researchers in International Conference on Aerogels for Biomedical and Environmental Application**. Organized by the AERoGELS COST Action. (2020)
3	**Primer premio: Young researchers'– Best Oral Presentation Award in the Spanish-Portuguese Industry-Academia Aerogel Meeting**. Organized by the AERoGELS COST Action and University of Coimbra. (2022)
4	**Finalista en la I Edición del Concurso de Divulgación #HiloTesis"** organized by the group Divulgación y Cultura Científica (Red Divulga) de la sectorial de I+d+i de Crue. 1-23th April (2021).
5	Certificate of excellence, entrepreneurship and innovation as a member of "3IN-sole". **Finalist team of the IMFAHE´s Idea Competition-Nodal Award/Shark Tank Edition** celebrated during the VIII IMFAHE´s International Conference on May 30th, IMFAHE FOUNDATION, (2022).

La siguiente tabla recoge las principales becas y contratos recibidos durante el desarrollo de esta tesis.

Tabla R.7. Becas y contratos.

Becas y contratos	
1	**Fundación General de la Universidad de Valladolid.** (2017 – 2019)
2	**Contrato Predoctoral de la Universidad de Valladolid**, 2018. (2019)
3	**Contrato Predoctoral de Ministerio de Ciencia, Innovación y Universidades FPU, 2017**. (2019 – 2023)
4	**Short Term Scientific Missions (STSM). AERoGELS COST Action (CA18125 - Advanced Engineering and Research of aeroGels for Environment and Life Sciences)**. Computation and Materials (CeM), Chemical Process Engineering and Forest Products Research Centre (CIEPQPF), Dept. Chemical Engineering, University of Coimbra. (2021).
5	**Ayudas para estancias breves y traslados temporales para beneficiarios del programa FPU. Ministerio de Universidades FPU 2020**, (2021).
6	**Ayudas para la Asistencia a Cursos, Congresos y Jornadas relevantes en el desarrollo de Tesis Doctorales de la Universidad de Valladolid**, (2021).
7	**Ayudas para la Asistencia a Cursos, Congresos y Jornadas relevantes en el desarrollo de Tesis Doctorales de la Universidad de Valladolid**, (2022).

Otras contribuciones a congresos internacionales y nacionales, publicaciones, actividades de divulgación y formación se resumen en la siguiente tabla.

Tabla R.8. Actividades adicionales.

Publicaciones científicas adicionales	
Número	**Referencia**
1	Merillas B.; Cuéllar E.; Diez-Varga A.; Asensio-Bartolomé M.; García-Herbosa G.; Torroba T.; Martín-Álvarez J.M..; Miguel Daniel.; Villafañe Fernando. **Whole microwave syntheses of pyridylpyrazole and of Re and Ru luminescent pyridylpyrazole complexes**. Inorganica Chim Acta. (2019), 484, 1–7.
2	Merillas B.; Cuéllar E.; Diez-Varga A.; Torroba T.; García-Herbosa G.; Fernández S.; Lloret-Fillol Julio.; Martín-Álvarez J.M..; Miguel Daniel.; Villafañe Fernando. **Luminescent Rhenium(I)tricarbonyl Complexes Containing Different Pyrazoles and Their Successive Deprotonation Products: CO_2 Reduction Electrocatalysts**. Inorg Chem. (2020), 59, 15, 11152–65.
3	Linhares T.; Carneiro VH.; Merillas B.; Pessoa De Amorim M.T.; Durães L. **Textile waste-reinforced cotton-silica aerogel composites for moisture regulation and thermal / acoustic barrier**. J Sol-Gel Sci Technol. (2022), 102, 574–588.
4	Sánchez-Calderón I.; Merillas B.; Bernardo V.; Rodríguez-Pérez MÁ. **Methodology for measuring the thermal conductivity of insulating samples with small dimensions by heat flow meter technique**. J. Therm. Anal. Calorim. (2022), 147, 12523–12533.
Conferencias adicionales	
1	Barroso-Solares S.; Merillas B.; López-González E.; Rodríguez-Pérez M.A.; Pinto J. **Development of a postgraduate training program on surface functionalization of polymers/polymer foams.** EDULEARN18: 10th International Conference on Education and New Learning Technologies, 2018, Mallorca, Spain
2	Merillas B.; Cuéllar E.; Diez-Varga A.; Asensio-Bartolomé M.; Torroba T.; Martín-Álvarez J.M..; Miguel Daniel.; Villafañe Fernando. **Tricarbonylrhenium(I) luminescent complexes with mono- and bidentate pyrazoles.** 7th EuCheMS Conference on Nitrogen Ligands, 2018, Lisbon, Portugal.
3	Merillas B.; Cuéllar E.; Diez-Varga A.; Asensio-Bartolomé M.; García-Herbosa G.; Torroba T.; Martín-Álvarez J.M..; Miguel Daniel.; Villafañe Fernando. **Deprotonation studies, luminescent properties and catalytic CO_2 reduction activity of $Re(CO)_3$ complexes with pyrazole and (3-(2pyridyl)pyrazole).** UK-Spain Organometallic Chemistry Symposium (USOCS2019), 2019, Alcalá de Henares, Spain.
Actividades de Divulgación	
1	Cycle of conferences "Women Researchers in the University of Valladolid". Oral contribution: **"Rhenium(I) luminescent complexes with the ligand 3-(2-pyridyl)pyrazole"**. (2017)
2	Theoretical classes for the preparation, supervision and development of laboratory experiments for the students participating in the workshop "Foams in Operation" of the 2018 **Summer Scientific Campus** promoted by the Spanish Foundation for Science and Technology (FECYT) held at the University of Valladolid.
3	**Three-Minute Thesis Contest 2019** organized by the School of Doctoral in the University of Valladolid. Finalist of the contest with the intervention "Air bricks to build the future".
4	**Oral presentation in the National "Pint of Science". 2021** online Edition. Entitled "¿Tienes ya una casa en Marte?" in the "Tech me out" section. Spain

5	Finalist in the I Edition of the **Divulgation Contest #HiloTesis"** organized by the group Divulgación y Cultura Científica (Red Divulga) de la sectorial de I+d+i de Crue. 1-23th April (2021)
6	2021 - **Divulgation Activity #Cuéntame11FUVa**, promoted by the Unidad de Cultura Científica y de la Innovación from the University of Valladolid on social media YouTube, Twitter e Instagram. 7-13th February, (2022)
7	**Scientist Photography Contest (DIL)** organized by the Unidad de Cultura Científica y de la Innovación of the University of Valladolid, (2022)
8	**IX Jornadas de Investigadoras de Castilla y León,** comunicación oral "Aerogeles de poliuretano: superaislantes contra el cambio climático." Promovido por las universidades de Burgos, León, Salamanca y Valladolid, 9-10th February, (2023)
Cursos y otras actividades	
1	Taller de autores. "**Guía práctica para la publicación de trabajos**", University of Valladolid, 2017.
2	**Infrared Thermography with image processing**. Organized by the School of Doctoral in the University of Valladolid, 2018.
3	**Conference "Plastic, Containers, Fundamentals, Regulations and Trends"** organized by LEICAL, 2018
4	**5th International Summer School on Aerogels**. 19th -21st September 2018, Cologne, Germany. Department of Aerogels and Aerogel Composites of the Institute of Materials Research at the **German Aerospace Center (DLR)**.
5	**Introduction to Project Management**. Polytechnic University of Valencia, 2020.
6	**6th International Online Summer School on Aerogels** (IOSSA). 16th September 2021, Online, Department of Aerogels and Aerogel Composites of the Institute of Materials Research at the **German Aerospace Center (DLR)**.
7	**AERoGELS COST Action WG1&5-Virtual Hands-On Trainning School**. Held in Virtual Lab Simulation – LABSTER, 2021.
8	**Workshop: Advices and Regulatory Aspects on Health Risk, LCA and Production Management of Aerogels**. AERoGELS COST ACTION CA18125, 2021, On-line.
9	**Webinar: Sustainable silica-based nanomaterials for thermal protection systems.** 2022. On-Line event, University of Coimbra, Nanofire, Tyre4build Ins, AeroXtreme.
10	IMFAHE´s Online **Quarter Course on "Professional Development"**. IMFAHE FOUNDATION, 2022.
11	IMFAHE´s Online **Quarter Course on "Innovation, Entrepreneurship and Leadership"**. IMFAHE FOUNDATION, 2022.
12	IMFAHE´s Online **Quarter Course on "Careers in Science"**. IMFAHE FOUNDATION, 2022.
13	**Mentee of the International Mentor Program (IMP).** IMFAHE FOUNDATION, 2022.
14	Certificate of excellence, entrepreneurship and innovation as a member of "3IN-sole". Finalist team of the **IMFAHE´s Idea Competition-Nodal Award/Shark Tank Edition** celebrated during the VIII IMFAHE´s International Conference on May 30th, IMFAHE FOUNDATION, 2022.
15	**IMFAHE´s VIII International Conference Innovation Camp "Connecting Talent Worldwide, Promoting Innovation and Excellence in Higher Education"** IMFAHE FOUNDATION, 2022, Online on May 30th.

VII Metodología de trabajo

En este apartado se describe brevemente la metodología que se ha seguido para la realización de este trabajo.

VII.a Materiales y síntesis

Los materiales seleccionados para la síntesis de aerogeles y composites basados en aerogel son los siguientes:

Aerogeles de poliuretano

- Isocianato (IsoPMDI® 92140): es un isocianato polimérico correspondiente a la formulación difenilmetano 4,4'-diisocianato empleado para la formación de los grupos uretano.
- Poliol (pentaeritritol): es un compuesto orgánico caracterizado por contener cuatro grupos alcohol -OH que permiten la reacción de poliadición en presencia de grupos isocianato (**Figura R.10**).
- Catalizador (KOSMOS® 75 MEG): tras un estudio del efecto de diferentes catalizadores en la reacción de poliuretano con los componentes previamente descritos, se seleccionó un catalizador basado en octoato de potasio ya que proporcionó las estructuras más homogéneas y con menores tamaños de poro y partícula.

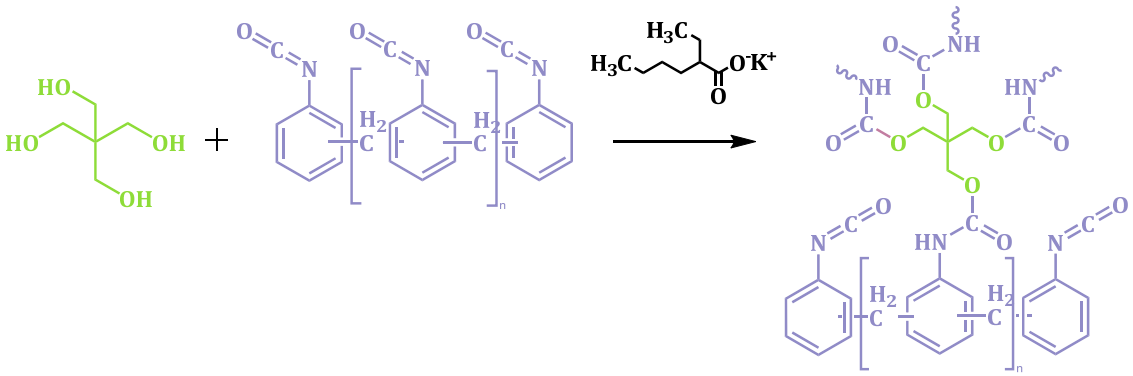

Figura R.10. Reacción de policondensación entre poliol e isocianato polimérico para formar la red de aerogel de poliuretano.

Aerogeles de sílice

- Tetraetoxisilano (TEOS): se empleó un alcóxido de silicio como precursor de los aerogeles de sílice en disolución de etanol. Este compuesto consta de cuatro grupos etóxido que permiten la posterior reacción de hidrólisis y de condensación que da lugar a la estructura macromolecular.
- Ácido oxálico ($C_2H_2O_4$): fue utilizado como catalizador ácido en disolución de agua destilada en las reacciones de hidrólisis de los grupos etóxido (**Figura R.11**).
- Hidróxido de amonio (NH_4OH): se empleó como catalizador básico en una disolución de agua destilada para promover las reacciones de policondensación.

- Hexametildisilazano ($(CH_3)_3SiNHSi(CH_3)_3$): se eligió este compuesto como agente sililante reaccionando con los grupos hidroxilo para evitar que la condensación continúe una vez se ha terminado la síntesis del aerogel.

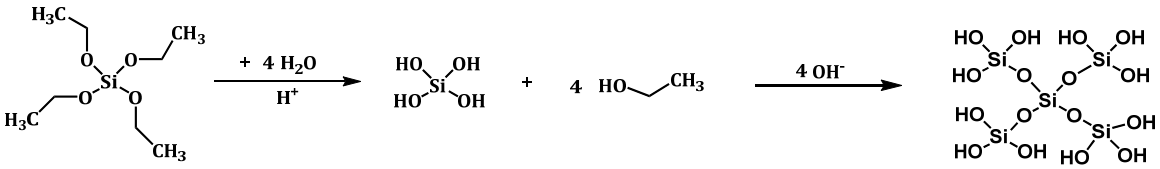

Figura R.11. Reacciones de hidrólisis y condensación del precursor de sílice.

Composites de aerogel (sílice y poliuretano)

- Las formulaciones previamente descritas para la síntesis de aerogeles de sílice y poliuretano se emplearon en la producción de estos composites.
- Espumas de poliuretano reticuladas: la elección de este tipo de espumas se basó en sus características estructurales. Las espumas reticuladas presentan una estructura celular cuyas paredes han sido eliminadas y solamente están presentes las aristas de las celdas. Este rasgo permite la incorporación de aerogel en su estructura interna formando una red continua. Se usaron espumas con tres tamaños de poro diferentes para realizar un análisis de su influencia en el composite final.

Síntesis: proceso sol-gel

El método sol-gel utilizado para la síntesis de aerogeles (**Figura R.12**) consiste en una solución inicial que contiene los precursores y, tras la adición de los correspondientes catalizadores que favorecen las reacciones de polimerización, las partículas coloidales formadas dan lugar a un sol. Tras continuar la polimerización y el crecimiento de estas partículas, un proceso conocido como gelificación genera la aparición de un gel. Este gel es una estructura porosa sólida cuyos poros están llenos del disolvente empleado en la síntesis. Por ello, un proceso de secado es empleado para la eliminación de este disolvente.

Proceso de secado

- Secado supercrítico: este proceso consiste en el empleo de un fluído en estado supercrítico para sustituir, por difusión, el líquido que se encuentra en el interior de los poros del gel. Estas condiciones facilitan la eliminación del sistema bifásico líquido-gas presente si se produce la evaporación, lo que provocaría gradientes de presión en el interior de los poros del gel y, como consecuencia, la estructura se puede ver afectada. El gas que se ha utilizado para este procedimiento es el dióxido de carbono (CO_2).
- Secado a presión ambiente: los aerogeles monolíticos de poliuretano y sílice se secaron a presión ambiente para analizar el efecto de este método en su densidad y contracción. Las muestras de aerogel de poliuretano se dejaron secar a temperatura ambiente durante varios días. Sin embargo, las fuerzas capilares causadas por la evaporación del disolvente provocaron una gran contracción, por lo tanto, este método no se siguió aplicando para estas muestras. Los aerogeles de sílice siguieron

un proceso diferente. Primero, un paso de secado inicial de 5 h a temperatura ambiente para mantener una evaporación lenta, seguido de calentamiento a 60 °C durante 24 h. Finalmente, las muestras se calentaron a 150 °C durante 2 h, con el fin de asegurar un secado completo de las muestras. Estas muestras no pudieron resistir las fuerzas capilares durante el proceso de secado y se rompieron en pedazos pequeños.

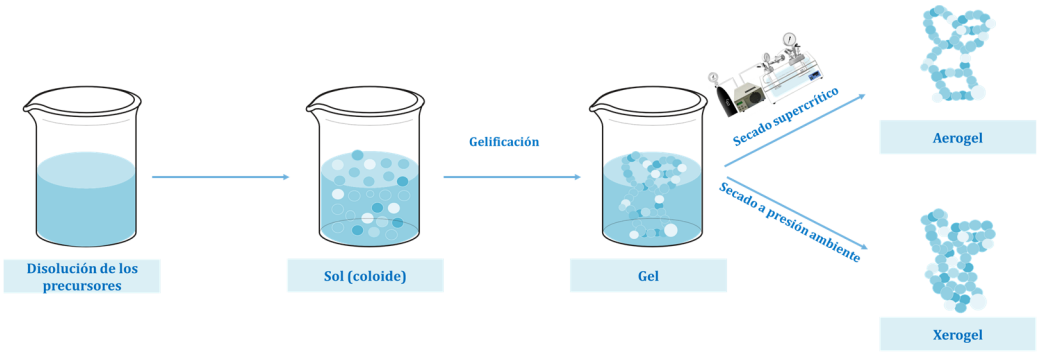

Figura R.12. Método sol-gel empleado para la síntesis de aerogeles y posterior secado.

VII.b Caracterización

En esta tesis, los materiales sintetizados, tanto aerogeles monolíticos como composites de aerogel, se han caracterizado desarrollando una metodología específica. La **Figura R.13** resume de forma esquemática las principales propiedades y parámetros estudiados para cada material, así como las técnicas empleadas para ello.

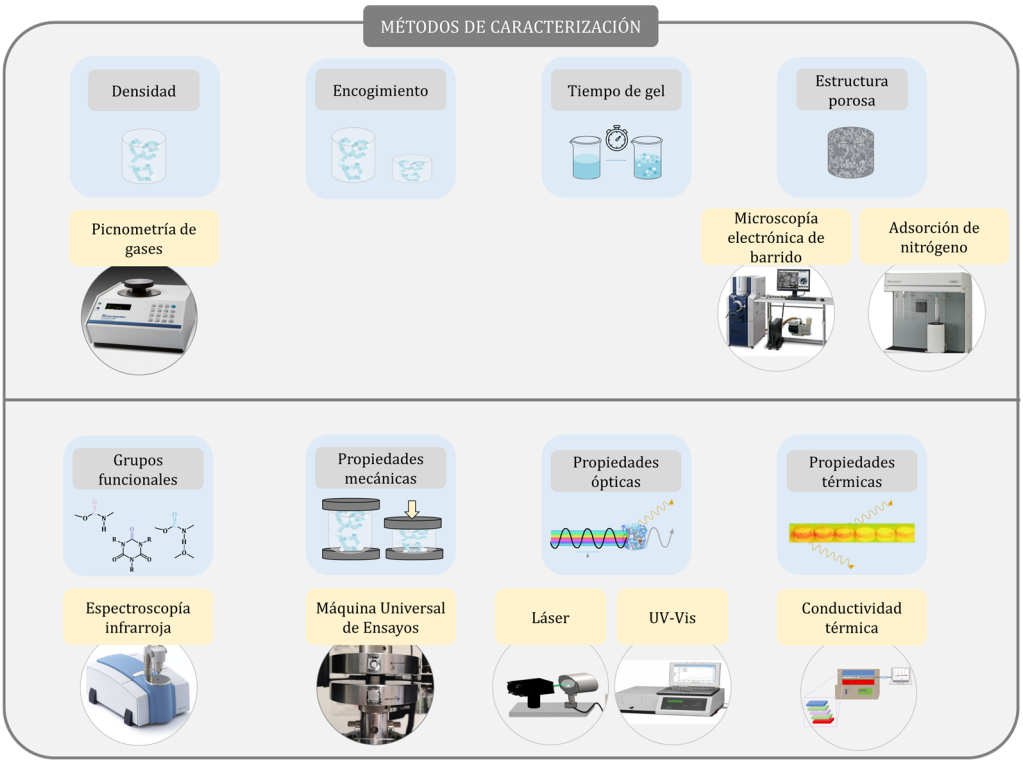

Figura R.13. Esquema de la caracterización realizada (propiedades y técnicas empleadas) para las muestras sintetizadas en esta tesis.

VIII Principales resultados y conclusiones de la tesis

Los resultados obtenidos a lo largo de esta tesis se han reunido del **Capítulo 4** al **Capítulo 7,** y el **Anexo** donde se han incluido un total de once publicaciones científicas. Estos resultados han permitido alcanzar conclusiones relevantes en el campo de los aerogeles y en el de los compuestos basados en aerogeles, completando así los objetivos principales marcados al comienzo de esta tesis.

Línea a: Síntesis y caracterización de aerogeles de poliuretano monolíticos con propiedades mejoradas.

VIII.a Conductividad térmica de los materiales nanoporosos: técnicas y mecanismos de transferencia del calor.

Se ha escrito una revisión científica [66] reuniendo las investigaciones realizadas sobre la conductividad térmica de los materiales nanoporosos, analizando las principales diferencias entre los polímeros nanocelulares y los aerogeles (**Capítulo 2, sección 2.3.3.1.**).

Técnicas de medición

- Se ha realizado una comparativa detallada entre los métodos transitorio y estacionario para medir la conductividad térmica de materiales porosos altamente aislantes tanto teórica como experimentalmente.
- Los resultados experimentales, basados en los compuestos de aerogel producidos para esta tesis y en espumas de PMMA, muestran que las diferencias en las medidas obtenidas con el método de fuente de plano transitorio (TPS) y el método del medidor de flujo de calor (método estacionario) son mayores cuando el rendimiento de aislamiento aumenta (valores por debajo de 20 mW/m K), siendo el método estacionario la técnica más precisa y fiable.

Mecanismos de transferencia de calor en los materiales nanoporosos

- Las principales diferencias en el aislamiento térmico entre los polímeros nanocelulares y los aerogeles radica en sus características estructurales: distinto tamaño de poro (mayor en los polímeros nanocelulares) y distribución del material sólido (continua en los polímeros nanocelulares y con interrupciones en los aerogeles).
- De esta forma, la clave para desarrollar materiales aislantes con una conductividad térmica aún más reducida respecto a los actuales es crear materiales con alta porosidad y poros nanométricos, lo más pequeños posible, para tener un gran efecto Knudsen que reduzca drásticamente la contribución de la conducción de gases.
- Además, una estrategia efectiva para minimizar la conductividad térmica es crear una fase sólida con “interrupciones del sólido” que restringen la transferencia de fonones.

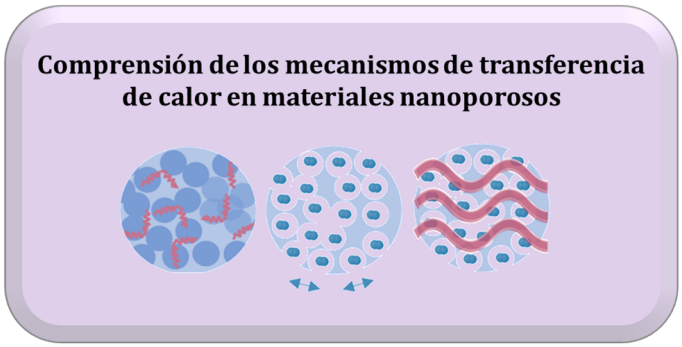

Figura R.14. Conclusión principal de la sección VIII.a.

La producción de materiales de baja densidad con celdas o poros en la escala nanométrica, lo más pequeños posible, y presentando interrupciones en la fase sólida es el punto clave para desarrollar materiales superaislantes.

VIII.b Síntesis de aerogeles de Poliisocianurato-Poliuretano

Se han estudiado diferentes parámetros y propiedades en relación con la síntesis de aerogeles de poliisocianurato-poliuretano [67]–[69]:

Reacciones cinéticas

- La modificación de las cinéticas de reacción durante la reacción de polimerización y el proceso de gelificación produce una clara modificación de la estructura porosa, incluyendo el tamaño de las partículas, su distribución de tamaño, el empaquetamiento (es decir, la densidad aparente), el tamaño de los poros, la superficie específica y el encogimiento. La modificación de la concentración de catalizador en las formulaciones de aerogel de poliuretano se convierte en una estrategia eficaz para obtener estructuras de aerogel modificables (**Capítulo 4, sección 4.2**).
- Reducir la concentración de catalizador lleva a la obtención de aerogeles de poliuretano con menores tamaños de partícula y de poro.
- Adicionalmente, la densidad aparente de los aerogeles aumenta con bajos contenidos de catalizador debido a un efectivo empaquetamiento de las partículas y a un mayor encogimiento.

Transparencia

- En relación con la sección anterior, la disminución del contenido de catalizador en la síntesis de los aerogeles de poliuretano producidos en esta tesis lleva a una fuerte reducción del tamaño de partícula y de poro, obteniendo tamaños de partícula inferiores a 25 nm y tamaños promedio de poro por debajo de 90 nm. Estos tamaños de poro y partícula permiten a estos aerogeles transmitir la luz visible hasta un cierto grado, alcanzando valores de transmitancia por encima del 76 % a 532 nm y mayores del 85 % a 650 nm para aerogeles de 1 mm de espesor.

- Este hecho constituye uno de los principales logros de esta tesis, el cual es producir **por primera vez aerogeles transparentes de poliisocianurato-poliuretano (Capítulo 4, sección 4.2**).
- En comparación con los datos de la bibliografía para aerogeles transparentes producidos con otras matrices orgánicas (**Figura R.15**), se pueden realizar las siguientes observaciones:
  - Los valores de transmitancia (a 550 nm) obtenidos para aerogeles de 1 mm de espesor son comparables a los obtenidos con aerogeles de celulosa y superiores a los obtenidos con matrices de poliimida o quitosano.
  - Al aumentar el espesor de los aerogeles de poliuretano, la transmitancia de la luz se reduce progresivamente, siendo menor que para otras matrices como la melamina-formaldehído o los aerogeles híbridos.

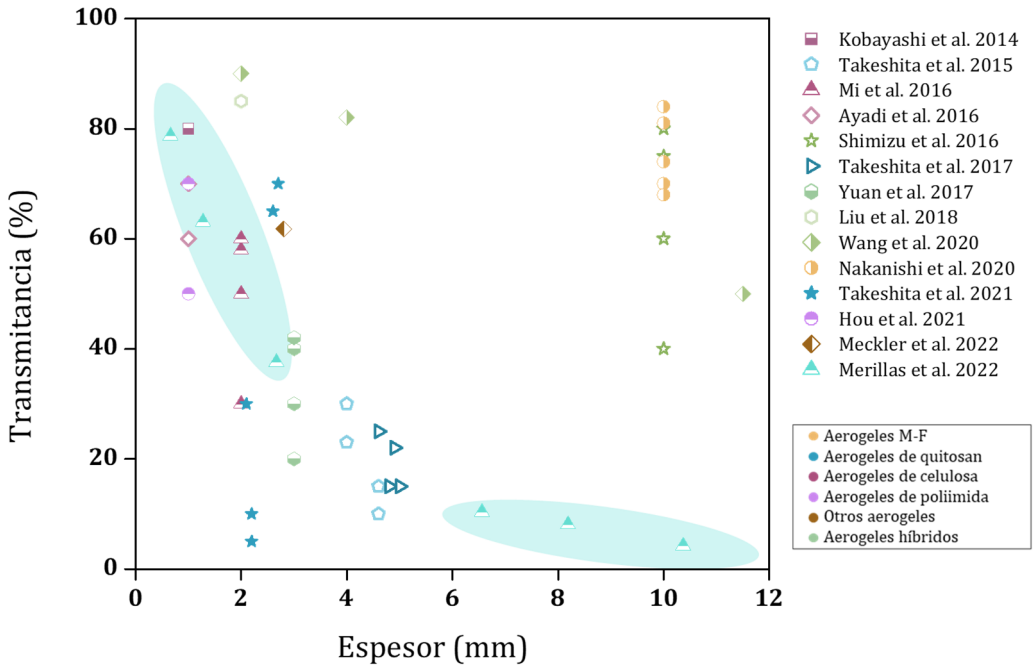

Figura R.15. Transmitancia a 550 nm como función del espesor de la muestra para distintos aerogeles orgánicos y los aerogeles producidos en esta tesis.

Se estudiaron diferentes factores que afectan la transmitancia final, lo que permitió concluir las siguientes afirmaciones (**Capítulo 4, sección 4.3**):

- Las transmitancias más altas se alcanzaron para aerogeles con menor contenido de catalizador, lo que condujo a partículas y poros más pequeños.
- Se demostró el cumplimiento de la ley de Beer-Lambert mediante la variación del espesor de las muestras.
- El coeficiente de atenuación muestra una relación directa con el tamaño de partícula y una tendencia inversa con la longitud de onda.
- Se ha encontrado una fuerte correlación entre el tamaño de partícula y la distribución del tamaño de partícula con la luz transmitida. Se observa una disminución brusca en la transparencia cuando las partículas miden más de 30 nm.

Mecanismos de dispersión

- La dependencia de la transmitancia con la longitud de onda permite determinar el mecanismo de dispersion que actúa en cada muestra.
- Una variación del tamaño de partícula de 23 a 78 nm permite observer la transición de la dispersión Rayleigh (L/λ^4) a la dispersión Mie (L/λ), siendo el primero el mecanismo principal que actúa en los aerogeles con tamaño de partícula por debajo de 32 nm, mientras que el segundo es el mecanismo principal en aerogeles con partículas mayores a este valor.

Propiedades mecánicas

- Los aerogeles de poliisocianurato-poliuretano producidos muestran rigidez modificable a través de la densidad y nanoestructura (ver la sección de cinéticas de reacción) (**Capítulo 5, sección 5.2**).
- El módulo elástico obtenido varía de 0,13 a 6,32 MPa debido a las distintas densidades y conectividad entre las partículas de los aerogeles cuando su estructura porosa se modifica:
  - Se calculó un exponente de 10,2 en el ajuste exponencial del módulo elástico frente a la densidad relativa.
  - No solo la variación de la densidad produce cambios notables en la rigidez de los aerogeles producidos, sino que también la conectividad entre las partículas y los cuellos interpartícula son factores importantes.
- Los aerogeles de poliuretano sintetizados no se rompen a grandes deformaciones, sino que se densifican a partir del 40 % de deformación.
- Mediante ensayos de compresión–descompresión a una deformación del 10 % se ha demostrado la gran elasticidad de los aerogeles de poliuretano. Además, se han observado altos valores de recuperación.
- Los resultados obtenidos se pueden comparar con los encontrados en la bibliografía para aerogeles basados en poliuretano (**Figura R.16** y **Figura R.17**) llegando a las siguientes conclusiones:
  - El módulo de elasticidad de los aerogeles de poliisocianurato-poliuretano producidos es similar a los obtenidos para otros aerogeles con la misma densidad (entre 0,1 y 0,2 g/cm^3).

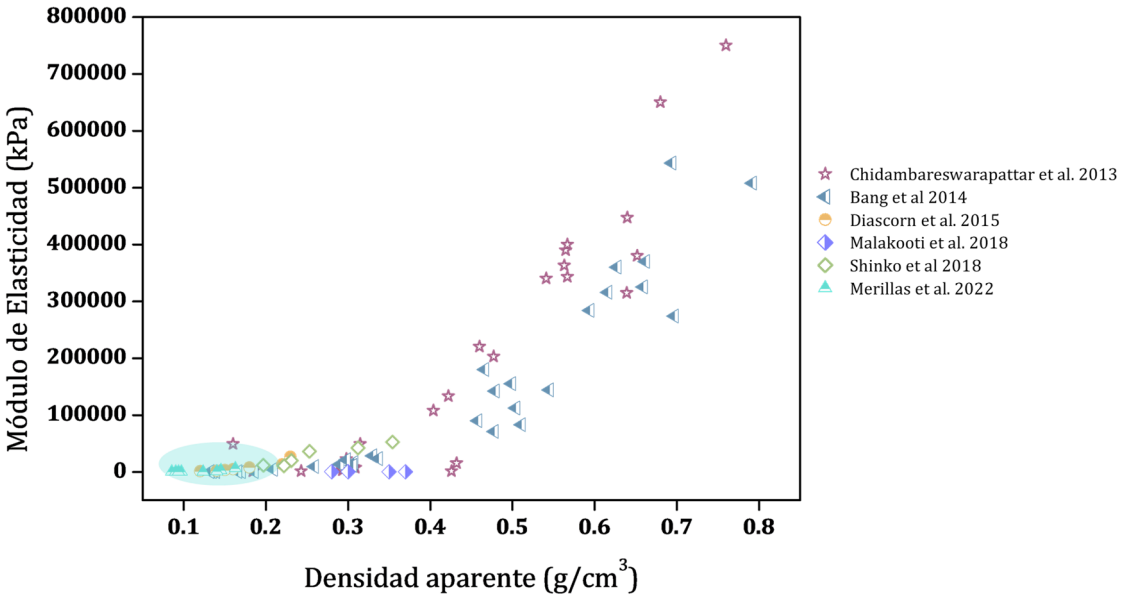

Figura R.16. Módulo elástico en función de la densidad aparente para los aerogeles de poliuretano de la literatura y los producidos en esta tesis.

- El esfuerzo necesario para deformar los aerogeles de poliuretano al 50 % de deformación sigue la misma tendencia que la de otros aerogeles de poliuretano de la literatura, alcanzando valores entre 100 y 1000 kPa para densidades entre 0,1 y 0,2 g/cm^3.

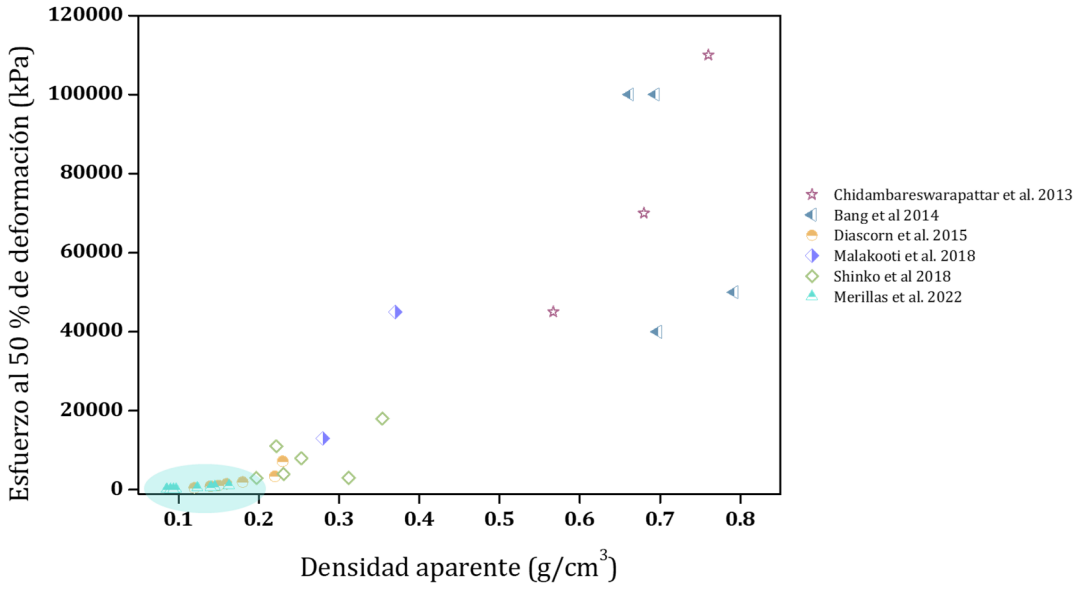

Figura R.17. Deformaciones al 50 % de deformación como función de la densidad aparente de los aerogeles de poliuretano de la bibliografía y los producidos en esta tesis.

Conductividad térmica

- Los aerogeles de poliuretano producidos muestran valores de super aislamiento térmico (desde 12 hasta 24 mW/mK a 10 °C (**Capítulo 5, sección 5.2**)).
- Los cálculos teóricos de los mecanismos de transferencia de calor que actúan en estas muestras sugieren que la reducción de poros y partículas que se produce cuando se reduce la cantidad de catalizador tiene una mayor relevancia que el aumento de la densidad aparente experimentado por estas muestras.
- De este modo, la principal diferencia de la capacidad aislante de los aerogeles producidos con baja cantidad de catalizador se debe a la disminución del tamaño de poro y de partícula, que reducen significativamente las contribuciones del gas y del sólido a través de los efectos Knudsen y efectos de tamaño, respectivamente.
- La contribución radiativa de estas muestras alcanza un valor de en torno a 1 mW/mK, mientras que no se detectan diferencias significativas entre las muestras.
- Comparando las conductividades térmicas obtenidas con los datos encontrados en la literatura para aerogeles de poliuretano, (**Figura R.18)** podemos concluir que:
  - El **valor de 12 mW/mK es el más bajo que se ha obtenido con matrices de poliuretano** independientemente de la densidad aparente.
  - Trifu et al. [70] sintetizó aerogeles de poliuretano con densidades más bajas que los de esta tesis, 0,04 g/cm^3 alcanzando una conductividad térmica de 18 mW/mK.

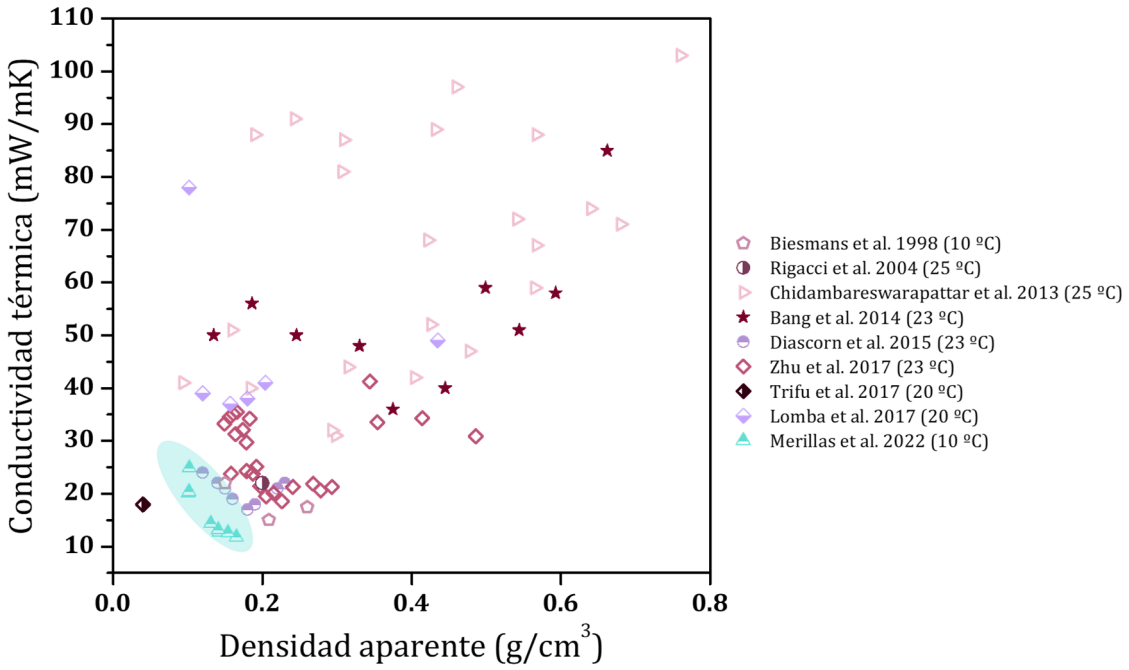

Figura R.18. Conductividad térmica en función de la densidad aparente de los aerogeles de poliuretano y poliisocianurato de la literatura y los producidos en esta tesis.

Adición de nanotubos de carbono

La incorporación y dispersión efectiva de distintos contenidos (0,5, 1,0 y 3,0 wt.%) de nanotubos de carbono modificados en las formulaciones de aerogeles de poliuretano llevó a descubrimientos interesantes (**Capítulo 5, sección 5.3**):

- El proceso de gelificación se ve afectado por la inclusión de estas partículas, modificando las cinéticas de reacción. Pequeñas cantidades de nanotubos de carbono aumentan la velocidad de gelificación, mientras que un mayor aumento en la cantidad de partículas conduce a la ralentización de las velocidades de reacción.
- Cuando se añaden nanotubos de carbono, se alcanzan densidades ligeramente menores. Esto es debido al menor encogimiento de los aerogeles cuando se dispersan estas partículas en su estructura, contribuyendo a un mayor aguante durante el proceso de secado supercrítico y, por lo tanto, a un incremento de la porosidad final.
- La modificación estructural de los aerogeles de poliuretano producida por los nanotubos empeoran su rigidez, reduciendo el módulo de elasticidad. A pesar de este efecto, estos nanocompuestos pueden ser comprimidos hasta más del 80 % sin romperse. Por el contrario, la elasticidad se mejora, y el coeficiente de pérdida de energía se reduce.
- La conductividad térmica de las muestras que contienen nanotubos de carbono se reduce notablemente, y esta reducción es mayor para contenidos más altos de partículas. La mayor reducción conseguida en este trabajo es desde 15.07 mW/mK obtenida para el aerogel de referencia producido con un 4 wt.% de catalizador hasta 12.02 mW/mK para el aerogel con un 3.0 wt.% de nanotubos de carbono. Esta reducción se analizó en detalle teniedo en cuenta los diferentes mecanismos de transferencia de calor:
  - Debido al menor encogimiento que tiene lugar se forman poros de mayor tamaño, conduciendo a un ligero aumento de la conducción de la fase gaseosa.
  - La adición de CNTs reduce la conectividad de las partículas (lo que reduce la rigidez del aerogel), restringiendo la transferencia de fonones y reduciendo la conducción de la fase sólida.
  - La dispersión y absorción producida por los CNTs bloquea la radiación infrarroja, incrementando el coeficiente de extinción de las muestras conteniendo estas partículas.

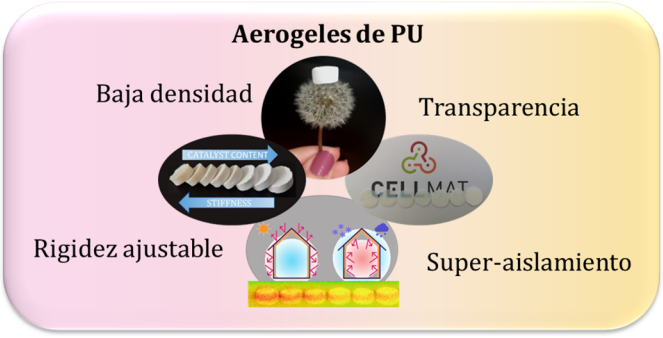

Figura R.19. Principal conclusión de la sección VIII b.

Aerogeles de poliisocianurato-poliuretano que presentan transparencia se han sintetizado por primera vez. Estos materiaes también presentan la mayor capacidad aislante encontrada en la literatura para esta matriz, así como una rigidez modificable a través de las cinéticas de reacción.

Adicionalmente, la incorporación de partículas bloqueadoras de infrarrojo, como nanotubos de carbono, contribuyen a mejorar aún más la capacidad aislante.

Por lo tanto, estos aerogeles son materiales prometedores para aplicaciones en las que se precisa una densidad baja, buenas propiedades mecánicas, transparencia, y buen aislamiento térmico.

Línea b: Producción de composites utilizando espumas de poliuretano flexible como estructura de soporte

VIII.c Síntesis de composites de espuma de poliuretano-areogel de poliuretano (PU_F-PU_A)

- Se ha desarrollado una nueva metodología para reducir la conductividad térmica de las espumas de poliuretano flexible reticulado [71] (**Capítulo 6**, **sección 6.2**). Se basa en reducir la contribución de la conducción de la fase gaseosa de los materiales iniciales rellenando toda su estructura abierta con un aerogel de poliuretano que presenta muy baja conductividad térmica.
- Se han obtenido composites con bajas densidades (desde 123 hasta 134 kg/m^3) y un alto contenido en aerogel (ca. 80 wt.%).

Los principales resultados obtenidos durante el studio de estos novedosos materiales están incluidos en los siguientes párrafos.

Efectos sinérgicos

- Se encuentra un efecto sinérgico entre las espumas de PU reticuladas flexibles empleadas y los aerogeles. No solo los aerogeles reducen la conductividad térmica total de las espumas reticuladas, sino que las espumas también protegen la estructura del aerogel contra el colapso.
- De hecho, el efecto de la estructura reticulada sobre los aerogeles de poliuretano es un efecto de soporte que reduce la contracción durante el secado, reduciendo por tanto su densidad aparente y aumentando la porosidad de los aerogeles (del 88 al 91 %).

Estructura de los composites

- Los composites producidos presentan una buena cohesión entre ambos materiales (espuma de PU y aerogeles) estando constituidos por una red continua de aerogel adherida a las aristas de las espumas reticuladas.

Propiedades mecánicas

- La inclusión de aerogel en el interior de las espumas flexibles conduce a un gran aumento del módulo elástico y a un esfuerzo de compresión necesario para alcanzar una deformación del 10 % 12 veces superior respecto a las espumas iniciales.
- Los composites de PU_F-PU_A pueden comprimirse hasta altas deformaciones (más de un 70 %) sin romperse, experimentando una fuerte densificación desde el 60 % de deformación.
- Los composites producidos adquieren flexibilidad y elasticidad recuperando prácticamente su altura inicial tras una deformación del 10 % en compresión.

Conductividad térmica

- Se ha alcanzado un rendimiento de aislamiento térmico significativamente mayor con los composites de PU_F-PU_A. Se han conseguido valores de conductividad térmica de 16 mW/mK (a 10 °C), pudiendo así estar enmarcados en el rango de los super aislantes, mientras que las conductividades térmicas de las espumas iniciales estaban comprendidas entre los 34 y 50 mW/mK.
- La baja conductividad térmica de los aerogeles incorporados a la estructura de la espuma reduce drásticamente la contribución del gas en las espumas iniciales y el posible mecanismo convectivo.
- Adicionalmente, las medidas de conductividad térmica a diferentes temperaturas permiten concluir que la contribución de la radiación se reduce notablemente por la inclusión de aerogeles, debido a un mayor coeficiente de extinción producido por el aumento de densidad.

Efecto del tamaño de celda de la espuma

El uso de tres espumas con diferentes tamaños de poros conduce a la determinación del tamaño de celda óptimo para la inclusión de aerogel:

- Aunque la masa del aerogel es casi la misma para cada composite, su densidad aparente se reduce al aumentar el tamaño de poro de la espuma (tamaño L) ya que se produce una menor contracción en el aerogel.
- La rigidez del compuesto es menor a mayor tamaño de poro (tamaño L), siendo estas muestras las que presentan mayor elasticidad, al igual que ocurre con la espuma inicial. Por lo tanto, algunas de las propiedades iniciales de las espumas reticuladas se transmiten a los compuestos finales.
- Los poros más pequeños llevan a un mayor rendimiento de aislamiento térmico, alcanzando valores de 15,79, 16,61 y 16,07 mW/mK para los tamaños S, M y L, respectivamente. Sin embargo, a pesar de los valores iniciales significativamente diferentes de conductividad térmica para las espumas iniciales (34, 40 y 50 mW/mK), todos los compuestos alcanzaron una capacidad aislante de en torno a 16 mW/mK.

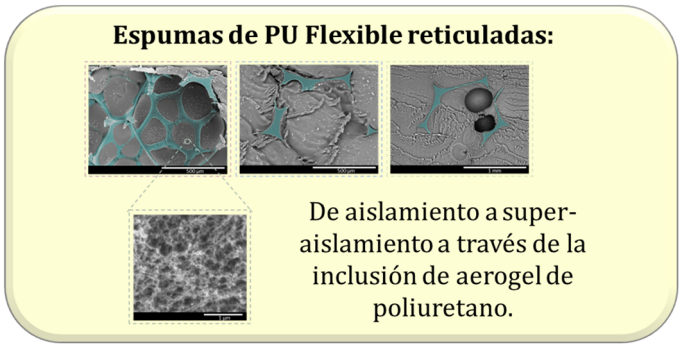

Figura R.20. Conclusiones principales de la sección VIII c.

La inclusión de aerogeles de poliuretano en los poros de espumas flexibles de poliuretano reticulado lleva a una cohesión efectiva entre ambas matrices. Promueve una fuerte reducción de la conducción del gas a través de los poros, disminuyendo así su conductividad térmica y permitiendo de este modo alcanzar valores en la región superaislante. Además, los composites muestran un excelente comportamiento mecánico.

VIII.d Síntesis de composites de aerogeles de sílice-espumas de poliuretano (Sil-PU)

- Se ha desarrollado una estrategia novedosa para reforzar eficazmente los aerogeles de sílice basada en el uso de espumas de poliuretano reticulado flexible como soporte [72] (**Capítulo 7, sección 7.2**).
- Se ha incluido un alto porcentaje de masa de aerogel en los composites finales, alcanzando valores aproximadamente del 87 %.
- Los principales resultados obtenidos durante el estudio de estos novedosos materiales se recogen en los siguientes párrafos.

Propiedades mecánicas

- Los módulos elásticos de los compuestos sintetizados aumentan significativamente con el empleo de esta estrategia, aumentando de 130 a 307 kPa.
- Mientras que los monolitos de aerogel de sílice se rompen en pequeños pedazos a deformaciones de compresión del 12 %, los aerogeles reforzados por este método pueden deformarse por encima del 80 % sin romperse, experimentando una fuerte densificación.
- A pesar de que la rigidez de los aerogeles de sílice se mejora considerablemente, se mantiene su flexibilidad y elasticidad a una deformación del 10 % y el 25 %.
- Se alcanzan altos índices de recuperación en torno al 95 % tras la realización de ensayos compresión-descompresión hasta una deformación del 25 %.

Conductividad térmica

- La conductividad térmica de los composites producidos muestra valores similares a los de los aerogeles de sílice pura, no disminuyendo por la adición del refuerzo reticulado.

Efecto del secado

- Se obtienen mayores densidades para los composites secados a presión atmosférica como consecuencia de una mayor contracción, reduciéndose así su porosidad. Por el contrario, los composites secados en condiciones supercríticas alcanzan menores densidades, contracciones y una mayor porosidad en comparación con los composites secados a presión atmosférica.

Efecto de la modificación superficial

- El agente de sililación (HMDZ) reduce la densidad final de los composites producidos, alcanzando densidades de 117 kg/m^3. Este hecho revela que se producen menores contracciones al modificar estos composites e incluso, para algunos casos específicos, se logran contracciones negativas, ya que estas espumas se hinchan durante la etapa de gelificación.
- Adicionalmente, los composites modificados presentan una mayor estabilidad y cohesión entre las aristas de poliuretano y del aerogel de sílice, obteniendo así menores desconexiones y aumentando el porcentaje másico de aerogel en el composite final (del 76 al 82 % para los composites secados supercríticamente y del 74 al 87 % para los compuestos secados a presión atmosférica).
- La combinación de la modificación superficial con el secado supercrítico conduce a una notable mejora de la rigidez del aerogel puro (de 130 a 450 kPa), así como a un valor superaislante para la conductividad térmica de 14 mW/mK.

Efecto del tamaño de poro de la espuma

- Las espumas con mayor tamaño de poro disminuyen la densidad final de los composites Sil-PU (**Capítulo 7, sección 7.3**) [73].
- El aumento progresivo del tamaño de los poros de la espuma contribuye a la aparición de grietas y pequeños huecos entre la espuma y el aerogel de sílice. Por lo tanto, los poros más pequeños conducen a una red de aerogel más continua que los poros más grandes.
- Los composites con poros de espuma más pequeños alcanzan mayor rigidez, en concordancia con su mayor densidad. No obstante, los composites fabricados con mayor tamaño de poro son los que presentan mayor elasticidad.
- El tamaño de poro óptimo para producir composites Sil-PU debe estar por encima de las 1000 micras, ya que los poros más pequeños dan lugar a altas densidades, contracciones y, por tanto, altas conductividades térmicas. Espumas con poros de 1 y 4 mm permiten obtener composites Sil-PU con una conductividad térmica de 13,0 y 12,3 mW/mK, respectivamente.

Figura R.21. Principales conclusions de la sección VIII d.

Las espumas de poliuretano reticulado flexible proporcionan un refuerzo eficaz para los aerogeles de sílice actuando como refuerzos que mejoran su fragilidad. Además de producir composites con mayor rigidez que soportan altas resistencias a la compresión sin roturas, se mantiene su excelente rendimiento aislante, no siendo alterado por la inclusión de la matriz de espuma.

VIII.e Anexo

Tres artículos [74]–[76] incluidos en el anexo de esta tesis dieron lugar a interesantes conclusiones en relación con las espumas de poliuretano que se recogen en los siguientes apartados (**sección Anexo**).

VIII.e.1 Influencia de las nanopartículas en la estructura celular de las espumas de poliuretano: estudio del mecanismo real detrás de la estrategia

- El diseño de tres procedimientos de fabricación diferentes para la producción de espumas rígidas de poliuretano con contenido de nanoarcillas (tipos: Clay Na+ y 30B, contenidos: 0,5 y 1,0 wt.%) permite controlar la cantidad de aire atrapado durante el proceso de mezclado. Así, se alcanzan diferentes niveles de aire atrapado durante la producción de estas espumas (**Anexo, sección 2**).
- La fabricación de espumas que contienen arcillas en condiciones de vacío conduce a estructuras celulares que tienen un tamaño de celda y una densidad de nucleación similares a la espuma de referencia. Por lo tanto, se descarta la posibilidad de un mecanismo en el que las nanoarcillas reduzcan el tamaño de la celda por una reducción de la tensión superficial.
- Sin embargo, las espumas producidas en condiciones atmosféricas indican que a mayor cantidad de aire se incluye durante el proceso de mezclado, mayor es el efecto de nucleación.
- Se ha encontrado una correlación entre el aumento de la viscosidad del poliol cuando se añaden nanoarcillas a la mezcla y la posibilidad de atrapar aire, lo que permite proponer un mecanismo que actúa bajo la adición de nanoarcillas a la mezcla reactiva:
  - El efecto de nucleación y la subsiguiente reducción del tamaño celular, debido a la incorporación de nanopartículas a una formulación rígida de poliuretano, es promovido por la presencia de un mayor número de burbujas de aire, que actúan como centros de nucleación.

- La presencia de un mayor número de burbujas de aire es consecuencia directa del aumento de la viscosidad del poliol cuando se añaden nanopartículas, lo que permite un atrapamiento de aire más efectivo.

El mecanismo detrás de la reducción del tamaño de la celda cuando se agregan nanoarcillas a las espumas rígidas de poliuretano consiste en una mayor cantidad de aire atrapado en la mezcla reactiva que aumenta la densidad de nucleación, reduciendo así el tamaño final de la celda. Este efecto de atrapar burbujas de aire en la mezcla se debe al aumento de la viscosidad del poliol cuando se añaden nanopartículas.

VIII.e.2 Descripción de nuevos parámetros estructurales para evaluar el aislamiento acústico de espumas de poliuretano semi-rígidas

- Se han definido nuevos parámetros estructurales para describir la estructura celular de las espumas semirrígidas de PU para correlacionarlos con la absorción acústica (**Anexo, sección 3**). Son espumas que se caracterizan por la presencia de pequeños agujeros en las paredes de las celdas.
- Con el fin de desarrollar una metodología precisa basada exclusivamente en la estructura celular de las espumas de poliuretano, se han evitado los cambios de densidad, contenido de celda abierta y tamaño de celda.
- El área de los agujeros (S_h), el número de agujeros por unidad de área (N_h) y el porcentaje del área de la pared celular ocupada por estos agujeros (%HCW) son los parámetros clave que conectan los agujeros característicos en las paredes celulares de estas espumas y su rendimiento de aislamiento acústico.
- Estos novedosos parámetros se han relacionado con el coeficiente de absorción acústica a diferentes frecuencias, y los resultados obtenidos permiten concluir que una estructura que contiene un pequeño número de huecos con una gran superficie presenta una absorción acústica más efectiva que una con un mayor número de huecos más pequeños.
- El parámetro clave que describe el comportamiento de absorción acústica de estas espumas es el porcentaje de agujeros por pared celular (%HCW). Cuanto mayor sea este parámetro, mayor será el coeficiente de absorción. Así, la estructura celular óptima para una absorción eficaz del sonido consiste en paredes que contienen un pequeño número de agujeros con una gran superficie.

Las propiedades de absorción acústica de las espumas de poliuretano semirrígidas se pueden predecir mediante el análisis de su estructura celular. El principal parámetro relacionado con esta propiedad es el porcentaje de huecos en las paredes de las celdas (%HCW), que favorece una mayor absorción acústica cuanto mayor es. Por lo tanto, debe haber pocos orificios con un área grande en las paredes de la celda para obtener excelentes absorbentes de sonido.

VIII.e.3 Adsorción de nitratos por espumas flexibles de poliuretano que contienen sepiolitas

- La incorporación de sepiolitas funcionalizadas con sales de amonio cuaternarias en la mezcla reactiva de espumas de poliuretano flexibles hidrófilas conduce a una gran capacidad de adsorción de nitratos (unos 23 mg/g) de fuentes hídricas (**Anexo, sección 4**).
- Emplear el material propuesto (Se-PU) mejora las metodologías anteriores descritas en la literatura, ya que no es necesario controlar la temperatura y el pH durante el proceso de adsorción, así como tampoco se requiere un proceso de filtración final.
- La interacción entre las sepiolitas tratadas y los nitratos se describe mediante el modelo de Langmuir.
- El estudio de diferentes contenidos de sepiolitas permite concluir que el contenido más alto que conduce a una estructura celular no dañada es del 8% en peso.
- La combinación de una espuma hidrófila de celda abierta con sepiolitas activas permite una adecuada interacción entre el agua contaminada y estas partículas por absorción de la matriz de poliuretano y adsorción en los sitios activos de la sepiolita. Además, se ha demostrado que no se produce liberación de nitratos tras el proceso de adsorción.
- Se ha utilizado agua real contaminada con nitratos que contiene iones adicionales para comprobar la eficacia real de los compuestos producidos, logrando capacidades aceptables de adsorción de nitratos alrededor de 11 mg/g.

Las espumas de poliuretano hidrofílicas que contienen sepiolitas modificadas son adsorbentes de nitratos en aguas contaminadas altamente efectivos. Existe un efecto sinérgico entre la matriz de poliuretano, que permite la absorción de agua, y las sepiolitas, que actúan como centros de adsorción de nitratos. Esta estrategia es una alternativa a otros métodos, y permite mejorar su costo-efectividad, seguridad y manejo, ya que no es necesario el control de filtración, temperatura o pH.

IX Referencias

[1] J. M. Buist, S. J. Grayson, and W. D. Woolley, *Fire and Cellular Polymers*. London and New York: Elsevier applied science, 1986. doi: 10.1007/978-94-009-3443-6.

[2] S. S. Kistler, "Coherent Expanded Aerogels and Jellies," *Nature*, vol. 127, p. 741, **1931**.

[3] S. S. Kistler, "Coherent expanded aerogels," *J. Phys. Chem.*, vol. 36, no. 1, pp. 52–64, **1932**, doi: https://doi.org/10.1021/j150331a003.

[4] C. Nägeli and C. Cramer, *Pflanzenphysiologische Untersuchungen*, no. 1. Schulthess, 1855.

[5] S. S. Kistler, "Method of producing aerogels," 2,093,454, 1937. doi: 10.1038/209966a0.

[6] S. S. Kistler and W. Boylston, "Treatment of aerogels to render them waterproof," 2,589,705, 1952.

[7] S. J. Teichner and G. A. Nicolaon, "Method of preparing inorganic aerogels," 3,672,833, 1972.

[8] R. W. Pekala, "Low density, Resorcinol-Formaldehyde aerogels," 4,873,218, 1989.

[9] R. W. Pekala, "Synthetic control of molecular structure in organic aerogels," *MRS Online Proc. Libr.*, vol. 171, pp. 285–291, **1989**, doi: https://doi.org/10.1557/PROC-171-285.

[10] R. W. Pekala, "Organic aerogels from the polycondensation of resorcinol with formaldehyde," *J. Mater. Sci.*, vol. 24, no. 9, pp. 3221–3227, **1989**, doi: 10.1007/BF01139044.

[11] G. Biesmans, D. Randall, E. Francais, and M. Perrut, "Polyurethane-based organic aerogels' thermal performance," *J. Non. Cryst. Solids*, vol. 225, pp. 36–40, **1998**, doi: http://dx.doi.org/10.1016/S0022-3093(98)00103-3.

[12] G. Biesmans, "Polyurethane based organic aerogels and their transformation into carbon aerogels," pp. 64–68, **1998**.

[13] M. B. Bryning, D. E. Milkie, M. F. Islam, L. A. Hough, J. M. Kikkawa, and A. G. Yodh, "Carbon nanotube aerogels," *Adv. Mater.*, vol. 19, no. 5, pp. 661–664, **2007**, doi: 10.1002/adma.200601748.

[14] N. Leventis, N. Chandrasekaran, C. Sotiriou-Leventis, and A. Mumtaz, "Smelting in the age of nano: Iron aerogels," *J. Mater. Chem.*, vol. 19, no. 1, pp. 63–65, **2009**, doi: 10.1039/b815985h.

[15] M. A. Aegerter, N. Leventis, and M. M. Koebel, *Aerogels Handbook*. Berlin, Germany: Springer, 2011. doi: 10.1007/978-1-4419-7589-8_4.

[16] H. Guo, M. A. B. Meador, L. McCorkle, D. J. Quade, J. Guo, B. Hamilton, M. Cakmak, and G. Sprowl, "Polyimide aerogels cross-linked through amine functionalized polyoligomeric silsesquioxane," *ACS Appl. Mater. Interfaces*, vol. 3, no. 2, pp. 546–552, **2011**, doi: 10.1021/am101123h.

[17] H. Guo, M. A. B. Meador, L. McCorkle, D. J. Quade, J. Guo, B. Hamilton, and M. Cakmak, "Tailoring properties of cross-linked polyimide aerogels for better moisture resistance, flexibility, and strength," *ACS Appl. Mater. Interfaces*, vol. 4, no. 10, pp. 5422–5429, **2012**, doi: 10.1021/am301347a.

[18] M. A. B. Meador, E. J. Malow, R. Silva, S. Wright, D. Quade, S. L. Vivod, H. Guo, J. Guo, and M. Cakmak, "Mechanically strong, flexible polyimide aerogels cross-linked with aromatic triamine," *ACS Appl. Mater. Interfaces*, vol. 4, no. 2, pp. 536–544, **2012**, doi: 10.1021/am2014635.

[19] M. Betz, C. A. García-González, R. P. Subrahmanyam, I. Smirnova, and U. Kulozik, "Preparation of novel whey protein-based aerogels as drug carriers for life science applications," *J. Supercrit. Fluids*, vol. 72, pp. 111–119, **2012**, doi: 10.1016/j.supflu.2012.08.019.

[20] J. C. Arboleda, M. Hughes, L. A. Lucia, J. Laine, K. Ekman, and O. J. Rojas, "Soy protein-nanocellulose composite aerogels," *Cellulose*, vol. 20, no. 5, pp. 2417–2426, **2013**, doi: 10.1007/s10570-013-9993-4.

[21] N. Asim, M. Badiei, M. A. Alghoul, M. Mohammad, A. Fudholi, M. Akhtaruzzaman, N. Amin, and K. Sopian, "Biomass and Industrial Wastes as Resource Materials for Aerogel Preparation: Opportunities, Challenges, and Research Directions," *Ind. Eng. Chem. Res.*, vol. 58, no. 38, pp. 17621–17645, **2019**, doi: 10.1021/acs.iecr.9b02661.

[22] K. Lee, L. Shabnam, S. N. Faisal, V. C. Hoang, and V. G. Gomes, "Aerogel from fruit biowaste produces ultracapacitors with high energy density and stability," *J. Energy Storage*, vol. 27, p. 101152, **2020**, doi: 10.1016/j.est.2019.101152.

[23] B. Zeng, X. Wang, and N. Byrne, "Development of cellulose based aerogel utilizing waste denim—A Morphology study," *Carbohydr. Polym.*, vol. 205, no. October 2018, pp. 1–7, **2019**, doi: 10.1016/j.carbpol.2018.09.070.

[24] C. Zhu, T. Y. J. Han, E. B. Duoss, A. M. Golobic, J. D. Kuntz, C. M. Spadaccini, and M. A. Worsley, "Highly compressible 3D periodic graphene aerogel microlattices," *Nat. Commun.*, vol. 6, pp. 1–8, **2015**, doi: 10.1038/ncomms7962.

[25] L. Kocon, F. Despetis, and J. Phalippou, "Ultralow density silica aerogels by alcohol supercritical drying," *J. Non. Cryst. Solids*, vol. 225, pp. 96–100, **1998**, doi: 10.1016/S0022-3093(98)00322-6.

[26] I. Smirnova and P. Gurikov, "Aerogel production: Current status, research directions, and future opportunities," *J. Supercrit. Fluids*, vol. 134, no. December 2017, pp. 228–233, **2018**, doi: 10.1016/j.supflu.2017.12.037.

[27] D. Urge-Vorsatz, K. Petrichenko, M. Staniec, and J. Eom, "Energy use in buildings in a long-term perspective," *Curr. Opin. Environ. Sustain.*, vol. 5, no. 2, pp. 141–151, **2013**, doi: 10.1016/j.cosust.2013.05.004.

[28] N. Azimi Fereidani, E. Rodrigues, and A. R. Gaspar, "A review of the energy implications of passive building design and active measures under climate change in the Middle East," *J. Clean. Prod.*, vol. 305, p. 127152, **2021**, doi: 10.1016/j.jclepro.2021.127152.

[29] "Directive 2010/31/EU of the European Parliament and of the Council on the energy performance of buildings," European Council: Brussels , Belgium, **2010**.

[30] A. Almusaed and A. Almssad, *Insulation Materials in Context of Sustainability*. IntechOpen Science, 2016. doi: 10.5772/61361.

[31] L. D. Hung Anh and Z. Pásztory, "An overview of factors influencing thermal conductivity of building insulation materials," *J. Build. Eng.*, vol. 44, p. 102604, **2021**, doi: 10.1016/j.jobe.2021.102604.

[32] "Aerogel Market Size & Share Report, 2020-2028," 2021. https://www.grandviewresearch.com/industry-analysis/aerogel-market

[33] F. P. Soorbaghi, M. Isanejad, S. Salatin, M. Ghorbani, S. Jafari, and H. Derakhshankhah, "Bioaerogels: Synthesis approaches, cellular uptake, and the biomedical applications," *Biomed. Pharmacother.*, vol. 111, no. January, pp. 964–975, **2019**, doi: 10.1016/j.biopha.2019.01.014.

[34] F. M. Husain, A. Khan, R. A. Khan, J. A. Siddique, M. Oves, A. A. P. Khan, M. O. Ansari, and H. D. Cancar, "Bio-based aerogels and their environment applications: an overview," in *Advances in Aerogel Composites for Environmental Remediation*, Elsevier Inc., 2021, pp. 347–356. doi: 10.1016/b978-0-12-820732-1.00018-7.

[35] "http://cellmat.es/."

[36] M. Á. Rodríguez-Pérez, "Propiedades Térmicas y Mecánicas de Espumas Poliolefinas," University of Valladolid, 1998.

[37] L. O. Arcos y Rábago, "Propiedades térmicas y mecánicas de espumas de poliolefinas fabricadas en un proceso de moldeo por compresión," University of Valladolid, 2002.

[38] C. Saiz-Arroyo, "Fabricación de materiales celulares mejorados basados en poliolefinas.

Relación procesado-composición-estructura-propiedades.," University of Valladolid, 2012.

[39] J. A. Reglero Ruiz, "Fabricación y caracterización de espumas de aluminio: aplicaciones en el sector aeronáutico," University of Valladolid, 2007.

[40] E. Solórzano, "Espumas de Aluminio: Proceso de Espumado, Estructura Celular y Propiedades," Úniversity of Valladolid, 2008.

[41] J. A. Reglero, M. A. Rodríguez-Pérez, D. Lehmhus, M. Windmann, J. A. de Saja, and A. Fernández, "An Experimental Study on the Inhomogeneities of Aluminum Foams Measuring the Thermal Conductivity by Using the Transient Plane Source Method," *Mater. Sci. Forum*, vol. 480–481, pp. 133–138, **2005**, doi: 10.4028/www.scientific.net/msf.480-481.133.

[42] E. Solórzano, M. A. Rodríguez-Pérez, J. A. Reglero, and J. A. De Saja, "Density gradients in aluminium foams: Characterisation by computed tomography and measurements of the effective thermal conductivity," *J. Mater. Sci.*, vol. 42, no. 8, pp. 2557–2564, **2007**, doi: 10.1007/s10853-006-1233-y.

[43] E. Solórzano, J. A. Reglero, M. Á. Rodríguez-Pérez, J. A. De Saja, and M. L. Rodríguez-Méndez, "Improvement of the foaming process for 4045 and 6061 aluminium foams by using the Taguchi methodology," *J. Mater. Sci.*, vol. 42, no. 17, pp. 7227–7238, **2007**, doi: 10.1007/s10853-007-1529-6.

[44] J. A. Reglero Ruiz, C. Saiz-Arroyo, M. Dumon, M. A. Rodríguez-Perez, and L. Gonzalez, "Production, cellular structure and thermal conductivity of microcellular (methyl methacrylate)-(butyl acrylate)-(methyl methacrylate) triblock copolymers," *Polym. Int.*, vol. 60, no. 1, pp. 146–152, **2011**, doi: 10.1002/pi.2931.

[45] M. Dumon, J. A. R. Ruiz, J. P. Sanz, M. A. R. Perez, J. M. Tallon, M. Pedros, E. Cloutet, and P. Viot, "Block copolymer-assisted microcellular supercritical CO2 foaming of polymers and blends," *Cell. Polym.*, vol. 31, no. 4, pp. 207–222, **2012**, doi: 10.1177/026248931203100402.

[46] B. Notario, A. Ballesteros, J. Pinto, and M. A. Rodríguez-Pérez, "Nanoporous PMMA: A novel system with different acoustic properties," *Mater. Lett.*, vol. 168, pp. 76–79, **2016**, doi: 10.1016/j.matlet.2016.01.037.

[47] M. Á. Rodríguez-Pérez, R. D. Simoes, C. J. L. Constantino, and J. A. de Saja, "Structure and Physical Properties of EVA/Starch Precursor Materials for Foaming Applications," *J. Appl. Polym. Sci.*, vol. 121, pp. 2324–2330, **2011**, doi: 10.1002/app.

[48] M. Á. Rodriguez-Perez, R. D. Simoes, S. Roman-Lorza, M. Alvarez-Lainez, C. Montoya-Mesa, C. J. L. Constantino, and J. A. de Saja, "Foaming of EVA/Starch Blends: Characterization of the Structure, Physical Properties, and Biodegradability," *Polym. Eng. Sci.*, **2012**, doi: 10.1002/pen.22046.

[49] A. Lopez-Gil, F. Silva-Bellucci, D. Velasco, M. Ardanuy, and M. A. Rodriguez-Perez, "Cellular structure and mechanical properties of starch-based foamed blocks reinforced with natural fibers and produced by microwave heating," *Ind. Crops Prod.*, vol. 66, pp. 194–205, **2015**, doi: 10.1016/j.indcrop.2014.12.025.

[50] A. López Gil, "Development of Environmentally Friendly Cellular Polymers for Packaging and Structural Applications . Study of the Relationship Cellular Structure-Mechanical Properties," University of Valladolid, 2016.

[51] L. O. Salmazo, "Cinéticas de espumación y control de la estructura celular en materiales basados en caucho natural y poliolefinas," University of Valladolid, 2015.

[52] J. I. Velasco, M. Antunes, O. Ayyad, J. M. López-Cuesta, P. Gaudon, C. Saiz-Arroyo, M. A. Rodríguez-Pérez, and J. A. de Saja, "Foaming behaviour and cellular structure of LDPE/hectorite nanocomposites," *Polymer (Guildf).*, vol. 48, no. 7, pp. 2098–2108, **2007**, doi: 10.1016/j.polymer.2007.02.008.

[53] C. Saiz-Arroyo, J. Escudero, M. A. Rodríguez-Pérez, and J. A. De Saja, "Improving the structure and physical properties of LDPE foams using silica nanoparticles as an additive," *Cell. Polym.*,

vol. 30, no. 2, pp. 63–78, **2011**, doi: 10.1177/026248931103000202.

[54] V. Bernardo, J. Martín-de León, E. Laguna-Gutiérrez, and M. Á. Rodríguez-Pérez, "PMMA-sepiolite nanocomposites as new promising materials for the production of nanocellular polymers," *Eur. Polym. J.*, vol. 96, no. August, pp. 10–26, **2017**, doi: 10.1016/j.eurpolymj.2017.09.002.

[55] E. Laguna-Gutierrez, J. Escudero, V. Kumar, and M. A. Rodriguez-Perez, "Microcellular foaming by using subcritical CO2 of crosslinked and non-crosslinked LDPE/clay nanocomposites," *J. Cell. Plast.*, vol. 54, no. 2, pp. 257–282, **2018**, doi: 10.1177/0021955X16681451.

[56] S. Pardo-Alonso, E. Solórzano, S. Estravís, M. A. Rodríguez-Perez, and J. A. De Saja, "In situ evidence of the nanoparticle nucleating effect in polyurethane-nanoclay foamed systems," *Soft Matter*, vol. 8, no. 44, pp. 11262–11270, **2012**, doi: 10.1039/c2sm25983d.

[57] S. Pardo-Alonso, E. Solórzano, and M. A. Rodriguez-Perez, "Time-resolved X-ray imaging of nanofiller-polyurethane reactive foam systems," *Colloids Surfaces A Physicochem. Eng. Asp.*, vol. 438, pp. 119–125, **2013**, doi: 10.1016/j.colsurfa.2013.01.045.

[58] S. Pardo-Alonso, E. Solórzano, L. Brabant, P. Vanderniepen, M. Dierick, L. Van Hoorebeke, and M. A. Rodríguez-Pérez, "3D Analysis of the progressive modification of the cellular architecture in polyurethane nanocomposite foams via X-ray microtomography," *Eur. Polym. J.*, vol. 49, no. 5, pp. 999–1006, **2013**, doi: 10.1016/j.eurpolymj.2013.01.005.

[59] P. Acuña, M. Santiago-Calvo, F. Villafañe, M. A. Rodríguez-Perez, J. Rosas, and D. Y. Wang, "Impact of expandable graphite on flame retardancy and mechanical properties of rigid polyurethane foam," *Polym. Compos.*, **2018**, doi: 10.1002/pc.25127.

[60] J. Pinto, "Fabrication et Caractérisation de Polymères Micro et Nano Cellulaires à partir de Polymères Nanostructurés à base PMMA," University of Bordeaux and University of Valladolid, 2014.

[61] B. Notario, "Fabricación y Caracterización de las Propiedades Físicas de Polímeros Nanocelulares : Transición de la Escala Micro a la Nano," University of Valladolid, 2016.

[62] J. Martín-de León, V. Bernardo, and M. Á. Rodríguez-Pérez, "Key Production Parameters to Obtain Transparent Nanocellular PMMA," *Macromol. Mater. Eng.*, vol. 302, no. 12, p. 1700343, **2017**, doi: 10.1002/mame.201700343.

[63] V. Bernardo, J. Martin-de Leon, J. Pinto, U. Schade, and M. A. Rodriguez-Perez, "On the interaction of infrared radiation and nanocellular polymers: First experimental determination of the extinction coefficient," *Colloids Surfaces A Physicochem. Eng. Asp.*, vol. 600, **2020**, doi: 10.1016/j.colsurfa.2020.124937.

[64] J. Martín-De León, V. Bernardo, and M. Á. Rodriguez-Perez, "Cyclic gas dissolution foaming as an approach for simultaneously reducing cell size and relative density in nanocellular pmma," *Polymers (Basel).*, vol. 13, p. 2383, **2021**, doi: 10.3390/polym13142383.

[65] J. Martín-de León, M. Jiménez, J. L. Pura, V. Bernardo, and M. A. Rodriguez-Pérez, "Easy-way production of highly transparent nanocellular polymers films," *Polymer (Guildf).*, vol. 236, **2021**, doi: 10.1016/j.polymer.2021.124298.

[66] B. Merillas, J. P. Vareda, J. Martín-de León, M. Á. Rodríguez-Pérez, and L. Durães, "Thermal Conductivity of Nanoporous Materials : Where Is the Limit ?," *Polymers (Basel).*, vol. 14, **2022**.

[67] B. Merillas, J. Martín-de León, F. Villafañe, and M. A. Rodríguez-Pérez, "Transparent Polyisocyanurate-Polyurethane-Based Aerogels: Key Aspects on the Synthesis and Their Porous Structures," *ACS Appl. Polym. Mater.*, vol. 3, no. 9, pp. 4607–4615, **2021**, doi: 10.1021/acsapm.1c00712.

[68] B. Merillas, J. Martín-de León, F. Villafañe, and M. Á. Rodríguez-Pérez, "Optical Properties of Polyisocyanurate – Polyurethane Aerogels : Study of the Scattering Mechanisms," *Nanomaterials*, vol. 12, p. 1522, **2022**, doi: https://doi.org/10.3390/nano 12091522.

[69] B. Merillas, F. Villafañe, and M. Á. Rodríguez-Pérez, "Super-insulating transparent polyisocyanurate-polyurethane aerogels: Analysis of the thermal conductivity and mechanical properties," *Nanomaterials*, vol. 12, no. 14, p. 2409, **2022**, doi: 10.3390/ nano12142409.

[70] R. Trifu, G. Gould, and S. White, "Flexible Polyisocyanate Based Aerogels," *MRS Adv.*, vol. 357, **2017**, doi: 10.1557/adv.201.

[71] B. Merillas, F. Villafañe, and M. Á. Rodríguez-Pérez, "Improving the Insulating Capacity of Polyurethane Foams through Polyurethane Aerogel Inclusion: From Insulation to Superinsulation," *Nanomaterials*, vol. 12, p. 2232, **2022**, doi: 10.3390/nano12132232.

[72] B. Merillas, A. Lamy-Mendes, F. Villafañe, L. Durães, and M. Á. Rodríguez-Pérez, "Silica-Based Aerogel Composites Reinforced with Reticulated Polyurethane Foams: Thermal and Mechanical Properties," *Gels*, vol. 8, no. 7, p. 392, **2022**, doi: 10.3390/gels8070392.

[73] B. Merillas, A. Lamy-Mendes, F. Villafañe, L. Durães, and M. Á. Rodríguez-Pérez, "Polyurethane foam scaffold for silica aerogels : effect of cell size on the mechanical properties and thermal insulation," *Mater. Today Chem.*, vol. 26, p. 101257, **2022**, doi: 10.1016/j.mtchem.2022.101257.

[74] B. Merillas, F. Villafañe, and M. Á. Rodríguez-Pérez, "Nanoparticles addition in pu foams: The dramatic effect of trapped-air on nucleation," *Polymers (Basel).*, vol. 13, no. 17, pp. 1–11, **2021**, doi: 10.3390/polym13172952.

[75] B. Merillas, F. Villafañe, and M. Á. Rodríguez-Pérez, "A New Methodology Based on Cell-Wall Hole Analysis for the Structure-Acoustic Absorption Correlation on Polyurethane Foams," *Polymers (Basel).*, vol. 14, p. 1807., **2022**, doi: 10.3390/polym14091807.

[76] S. Barroso-Solares, B. Merillas, P. Cimavilla-Roman, M. A. Rodriguez-Perez, and J. Pinto, "Enhanced nitrates-polluted water remediation by polyurethane / sepiolite cellular nanocomposites," *J. Clean. Prod.*, vol. 254, p. 120038, **2020**, doi: 10.1016/j.jclepro.2020.120038.

CHAPTER 1

INTRODUCTION

Chapter 1. Introduction

1.1 Introduction

In the early 20th century, namely in 1920, synthetic cellular polymers were discovered with the aim of replacing natural products owing to their attractive properties [1]. These materials are formed by two phases; a polymeric solid matrix and a gaseous phase dispersed along the material. The inclusion of the gaseous phase contributes to significantly reduce the density of the solid polymer, as well as providing interesting properties to the cellular polymers, such as energy absorption, vibration absorption, acoustic and thermal insulation, as well as lightening the structures, among others. These properties can be even more exceptional when the size of the pores forming the gaseous phase are reduced to reach the nanometric scale. The reduction of the size of these features to nanometers leads to remarkable changes in the optical and mechanical properties, and also in the thermal conductivity, spreading their use to unsuspected sectors and fields.

1.1.1 Aerogels

It was in the early thirties, in 1931, when a novel nanoporous material was reported by Kistler in the College of the Pacific in Stockton, California [2], [3]. The birth of this research arose from the controversy about the structure of gels. Although most of the forecast colloidal chemists accepted gels to be formed by a two-phase solid-liquid structure (Nägeli 1855 [4]), there was not enough experimental evidence to support this proposal. Kistler was the pioneer in demonstrating the independence between the solid phase of the gel and the fluid filling its voids. Trying to avoid the subsequent collapse of the solid gel component when the fluid evaporation took place, a new methodology was developed in order to extract the fluid. Since the gel collapse is produced by a capillary effect that the structure is not able to withstand, the replacement of the fluid should be carried out while preventing the liquid to recede from within the gel. In order to achieve this, the gel was placed into an autoclave and the temperature and pressure were set above the critical temperature and vapor pressure of the liquid, respectively, reaching the complete drying of the gel without collapsing the structure. The result of this drying is what is known as **aerogel** and nicknamed as the “blue smoke” or “frozen smoke” because of their usually cloudy appearance.

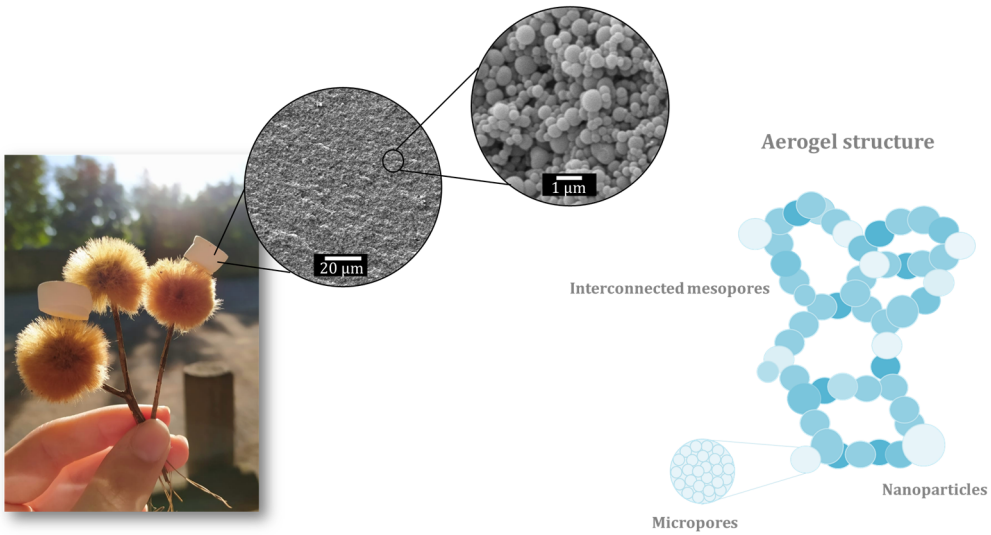

Figure 1. Scanning electron micrographs and scheme of an aerogel structure.

During that research, the first synthesized aerogel was a silica aerogel, using sodium silicate as silica precursor. Kistler's research was further extended to alumina, stannic oxide, tungstic oxide, nickel tartrate, agar, nitrocellulose, cellulose, rubber, and egg albumin aerogels. These obtained aerogels were materials with new physical properties never observed before.

As shown in **Figure 1**, aerogels are materials characterized by a highly porous structure formed by more than a 90 % of interconnected pores in the nanoscale. The solid skeleton, typically formed by particles or fibers, leads to the presence of a bimodal porous structure; the micropores comprised between the nanoparticles (primary particles) and pores typically in the mesoscale between the particle aggregates (secondary particles). As explained before with the pioneer work of Kistler, the solid matrix can be based on a great variety of materials. The small size of the structural features contributes to the appearance of exceptional properties.

1.1.2 Evolution of aerogels

Although the first patents for large-scale production of silica aerogels were filled in the 1950's [5], [6], it was not until 1972 when aerogels were commercialized by Teichner and Nicoloan [7]. These researchers substituted the sodium silicate precursor employed by Kistler by tetramethyl orthosilicate (TMOS), which would become one the most used silica precursors. Since then, researchers around the world started to synthesize aerogels with a wide spectrum of materials, both organic and inorganic. The main milestones reached in this field have been gathered in **Figure 2**.

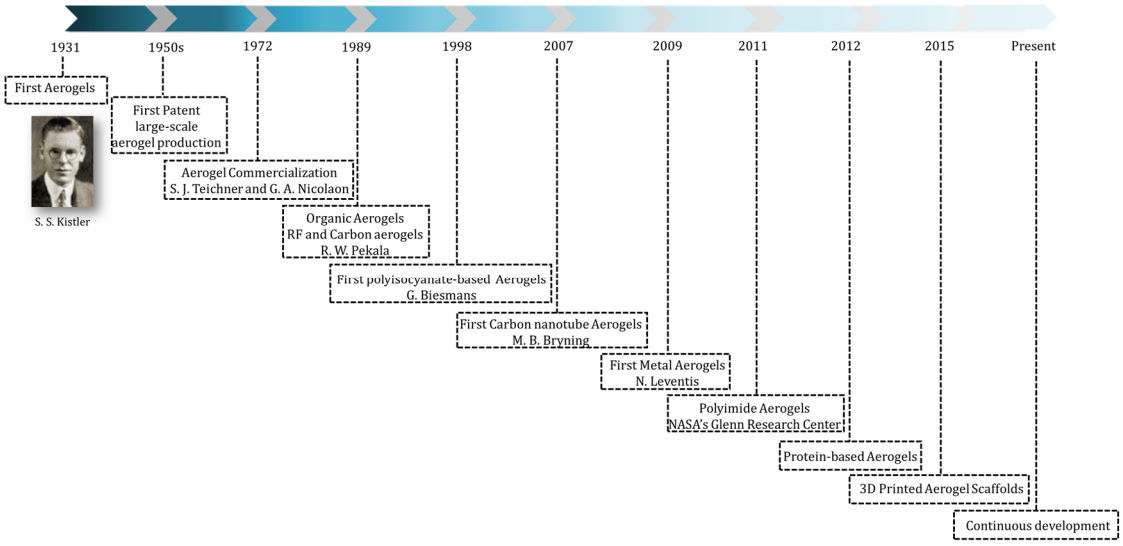

Figure 2. Main milestones in the aerogel research.

Organic aerogels were deeply studied by Pekala, who for the first time at the end of the 1980's, synthesized resorcinol-formaldehyde aerogels and carbon aerogels through the pyrolysis thereof [8]–[10]. In 1989 the first polyisocyanate-based aerogels were produced by Biesmans et al. and also transformed into carbon aerogels [11], [12]. Later, in 2001, the Aspen

Aerogels and Cabot Corporation companies started to commercialize silica-based aerogels which would become referents in the aerogel trade. Aerogels based on carbon nanotubes were first described in 2007 by drying aqueous-gels, reaching an excellent heat and electricity conduction [13]. Later, in 2009, metal aerogels were first made by Leventis et al., finding new magnetic and electric properties [14]. Most of these advances in the aerogel sphere, until 2009, have been gathered in an interesting handbook which describes the synthesis, properties, and applications of these materials [15]. More recently, other polymerized aerogels were synthesized for the first time, such as polyimide aerogels at NASA's Glenn Research Center in Ohio in 2011 [16]–[18]. In the last decade, protein-based aerogels have been explored by different authors looking for biodegradable and biocompatible nanoporous materials for drug delivery and other pharmaceutical and medical applications [19], [20]. Following the same line, recent research is focused on the obtention of bio-based aerogels and aerogels produced from biomass wastes [21]–[23]. In 2015, the three-dimensional printing of graphene aerogels was first reported by Zhu et al. [24], enabling a new generation of technological advances for aerogel production. This technology leads to personalized and complex shapes not available by the traditional production methods.

From these milestones on, widespread research has been carried out concerning aerogels focused on their development, with novel matrixes and the improvement of their main properties. There is no doubt that, in the coming years, the aerogel field will continue its rapid development searching for both the reduction of the production prices, the improvement of the physical properties as well as for the readiness for new practical applications.

1.1.3 Aerogel properties and applications

The interest that aerogels have aroused during their progress is due to their exceptional properties. Their low densities are comprised between 0.003 and 0.15 g/m^3 [25], as a result of their high porosity (typically up to 90 %). Additionally, the small size of the features forming the 3D network (particles or fibers) leads to huge surface areas (500 – 1000 m^2/g) [26]. Other specific properties have been defined for aerogels, all of them gathered in **Figure 3**. Among them, their low thermal conductivity and low speed of sound stand out, as well as the low dielectric constant and high loading capacity displayed by some of them. The chemistry of these materials allows to functionalize and perform chemical modifications through changes in the formulations or additional procedures.

The combination of unusual properties turns them into unique candidates for a great variety of applications which cannot be covered by other cellular polymers such as foams, non-woven fibers, 3D printed materials, etc. The main applications of aerogels are focused on the construction sector, textile sector, energy storage, waste removal, pharmaceutical and cosmetic sectors, and the food industry (see **Figure 3**).

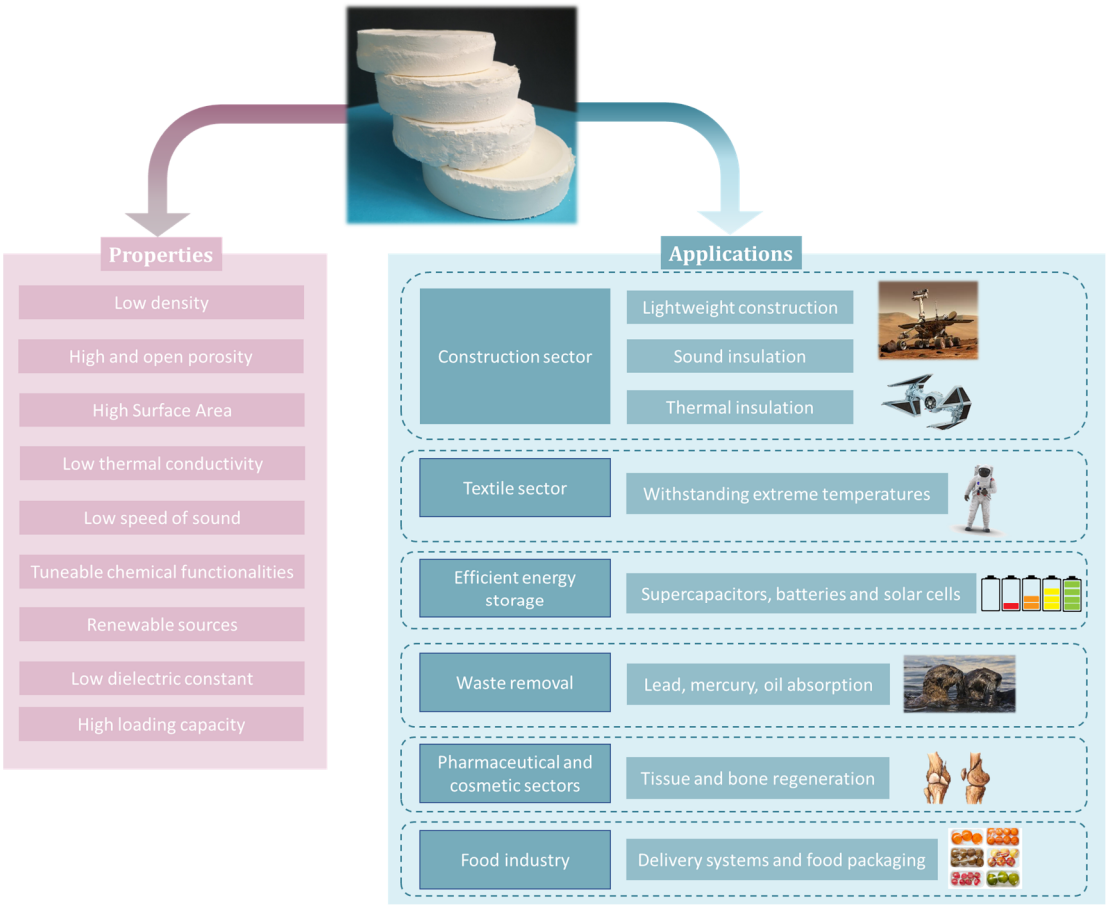

Figure 3. Specific properties and applications of aerogels.

Aerogels are mainly employed in the building sector because of their lightweight, and also thermal and sound insulation. This expands their applicability to related sectors such as automotive or aeronautics in which similar properties are required. Recently, the textile sector has started to incorporate aerogels into their clothing, aiming to face extreme temperatures, both hot and cold. Each time more industries are using aerogels for environmental applications as an efficient energy storage in supercapacitors, batteries or solar cells, or for pollution treatment processes such as heavy metal absorption, oil removal or water treatments. Additionally, promising advances in the pharmaceutical industry towards tissue and bones regeneration or drug delivery have been carried out, as well as in the food industry, especially for food packaging.

1.1.4 Future perspectives

More than a century ago, as early as 1820, scientists started to study the influence of greenhouse gases on Earth's climate. Many years later, in 1975, the first "global warming" appeared in a scientific magazine. This worldwide concern led to human adaptations and to the implementation of different strategies and measurements aiming to reduce the greenhouse gases emissions. Among the sectors contributing to detrimental effects, the building sector stands out accounting for a third of the total energy demand and the associated CO_2 emissions [27], [28]. Therefore, a sharp decrease of building energy consumption is a crucial requirement to fulfill the increasingly hardened regulations [29].

Thermal insulating materials are critical in this context. Regarding the Global Insulation Market (**Figure 4 a**), the construction sector is the main field in which insulating materials are applied, constituting a 34 % of the total insulation market. For this reason, and due to the fact that the commonly used insulating materials – such as polyurethane foams – provide thermal conductivities between 20 – 35 mW/(m·K), which are not enough to fulfill the future insulation normative, aerogels stand out as very promising substitutes [30],[31].

The growing interest in aerogels has become noticeable for many years, reaching a value of 818.9 million USD in the global market in 2020, and it is expected to grow at an annual rate of 15.1% reaching 2.2 billion USD by 2028 [32], as shown in **Figure 4 b**.

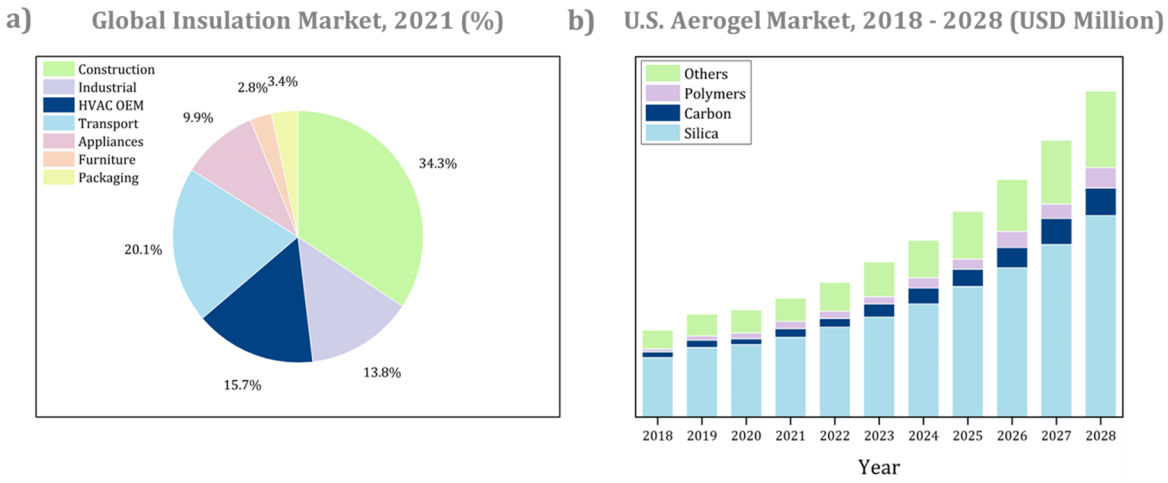

Figure 4. a) Global insulation Market during the year 2021 by sectors, b) U.S. Aerogel Market from 2018 to 2028 (from reference [32]).

As described in the previous figure, the most commonly employed aerogel matrix is silica. However, during the last years, a growing trend has been observed for carbon, polymeric and other aerogels, as well as on bio-based aerogels with various origins (cellulose, chitosan, alginate, starch, agar, among others [33], [34]). One of the reasons for this tendency could be based on the improvement of the mechanical properties offered by other matrixes in comparison to the silica matrix, often characterized by its brittleness.

The control of the final properties of these materials is closely linked to the initial matrix, the chemical formulation and the porous structure. Both, the processes and the structures of these materials are really complex and not well known, so there is a clear need for further research on these materials. Therefore, designing of specific properties is only possible by performing a thorough control of the production process and gel drying, as well as to delve on the parameters affecting the final porous structure of the aerogel. Additionally, the understanding of the relationship between process - porous structure - properties and, thus, applications, has to be extended.

The previous statements have encouraged the development of this thesis, carried out in CellMat Laboratory, as will be explained in the following sections, and has set the main goals and objectives (**section 1.3**). In addition to this research topic on aerogels, this thesis, also presents some contributions in the field of polyurethane foams, as explained below.

1.2 Framework of this thesis

This thesis, supervised by Prof. Dr. Miguel Ángel Rodríguez-Pérez and Prof. Dr. Fernando Villafañe González, has been developed at **CellMat Laboratory** [35], that belongs to the Condensed Matter Physics Department of the University of Valladolid, Spain.

CellMat is a research group which was founded in 1999 by both Prof. Dr. José Antonio de Saja and Prof. Dr. Miguel Angel Rodríguez- Pérez, who is the current leader of this group.

Since its beginning, this laboratory started to characterize commercially available polyolefin foams [36]–[38] and, two years later, to produce and characterize metal foams [39]–[43]. Afterward, the bases of CellMat Laboratory were set, reaching a wide expertise on the tetrahedron for cellular materials (Figure 5) for a wide collection of cellular polymers (PS, PU, PMMA, rubbers, etc.). This tetrahedron is based on understanding the production-structure-properties relationships and on the analysis of the applications of cellular polymers.

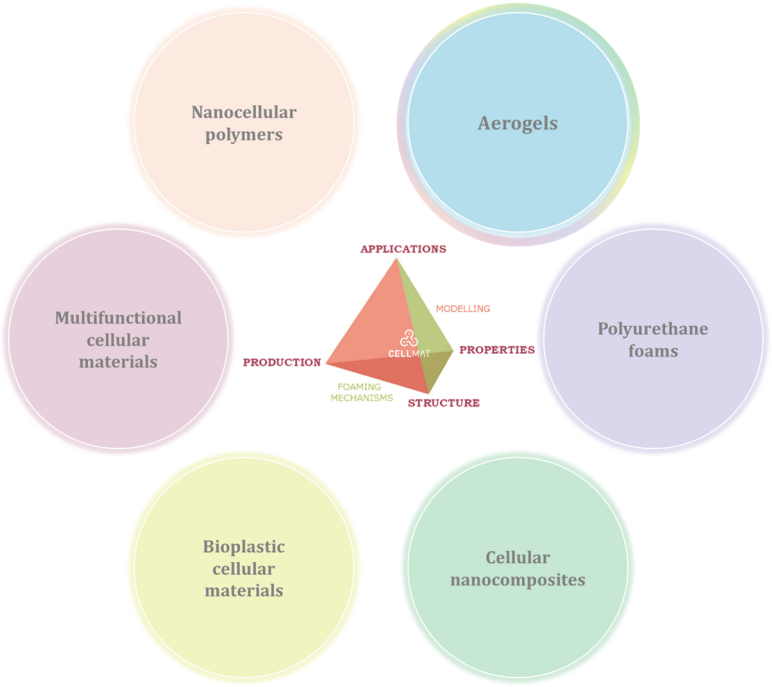

Figure 5. Cellular Materials tetrahedron and CellMat research areas.

One of the main objectives of CellMat is to develop new knowledge on these materials of interest for several sectors, such as automotive, renewable energies, building and construction, aeronautic, etc. and to carry out scientific research of interest in the field of cellular materials.

CellMat Laboratory covers different research topics: multifunctional cellular materials [44]–[46], bioplastic cellular materials [47]–[51], cellular nanocomposites [52]–[55], polyurethane foams [56]–[59], and nanocellular polymers [60]–[65]. In this thesis, a combination of the last two research lines has been carried out, joining the versatility of the polyurethane matrix with the interesting properties of cellular materials with cells is the nanoscale. This combination gives rise to a new research line based on polyurethane aerogels,

the main topic of this thesis, which benefits from the previous expertise of the group. Moreover, along this work, novel cellular composites have been synthesized expanding our knowledge in the field.

The main objective of this thesis is to develop new knowledge about aerogels, their synthesis, characterization, and possible final applications. Several theses have been previously finished in this group, dedicated to study the synthesis, kinetics, and physical properties of cellular nanocomposites based on rigid polyurethane. In those by Dr. Sergio Estravís Sastre in 2014 and by Dr. Mercedes Santiago Calvo in 2019, polyurethane was the main material.

The production process and porous structure have been studied in detail taking into account the possible factors affecting the final properties of the aerogels, as well as the optimization of the drying method. Then, the structure-properties relationship has been assessed and different physical properties have been studied, such as the textural, thermal, mechanical, and optical properties.

Afterward, the production of composites silica aerogel- flexible PU foam (Sil-PU) and PU aerogel- flexible PU foam (PU_A-PU_F) was carried out during an international three-month stay in the Computation and Materials (CeM) research group, belonging to The Chemical Process Engineering and Forest Products Research Centre (CIEPQPF) in the Chemical Engineering Department (DEQ) of the University of Coimbra (Portugal), under the supervision of Prof. Dr. Luisa Maria Rocha Durães. This institution was funded in 1994 with the objective of creating a structured framework for research activities. The vast expertise of the CeM group on silica aerogels and on their organically modified/reinforced counterparts has provided us with a very valuable knowledge and a solid framework to start working on these materials.

Additionally, the COST (European Cooperation in Science and Technology) CA18125 - Advanced Engineering and Research of aeroGels for Environment and Life Sciences has been also important for the development of this thesis. A Short-Term Scientific Mission (STSM) exchange of a three-month period was carried out in the same Portuguese university allowing the PhD candidate to learn new techniques and methods related to aerogels. This Cost Action through its funding, courses, and international conferences, gathers academia, industry and regulatory experts; thus, boosting the industry-academia interactions and training European young researchers via technical schools and STSM grants.

1.3 Objectives

The decision to research on aerogels in our laboratory was taken after considering the huge interest of aerogels, the need of further research on these materials, and the previous expertise of CellMat on cellular polymers. One of the major priorities was to expand our knowledge related to nanoporous materials. Additionally, the insulating performance of manufactured polyurethane foams and nanocellular polymers presented an interesting room for improvement, only possible by reducing both density and pore size. Thus, a research line of novel nanoporous materials was the main motivation to start with the development of this thesis.

The different objectives of this thesis are focused on the production of aerogels materials and on understanding the relation between porous structure and properties for the new developed materials.

Two main research lines have been considered when defining the objectives of this thesis, as gathered in **Figure 6**:

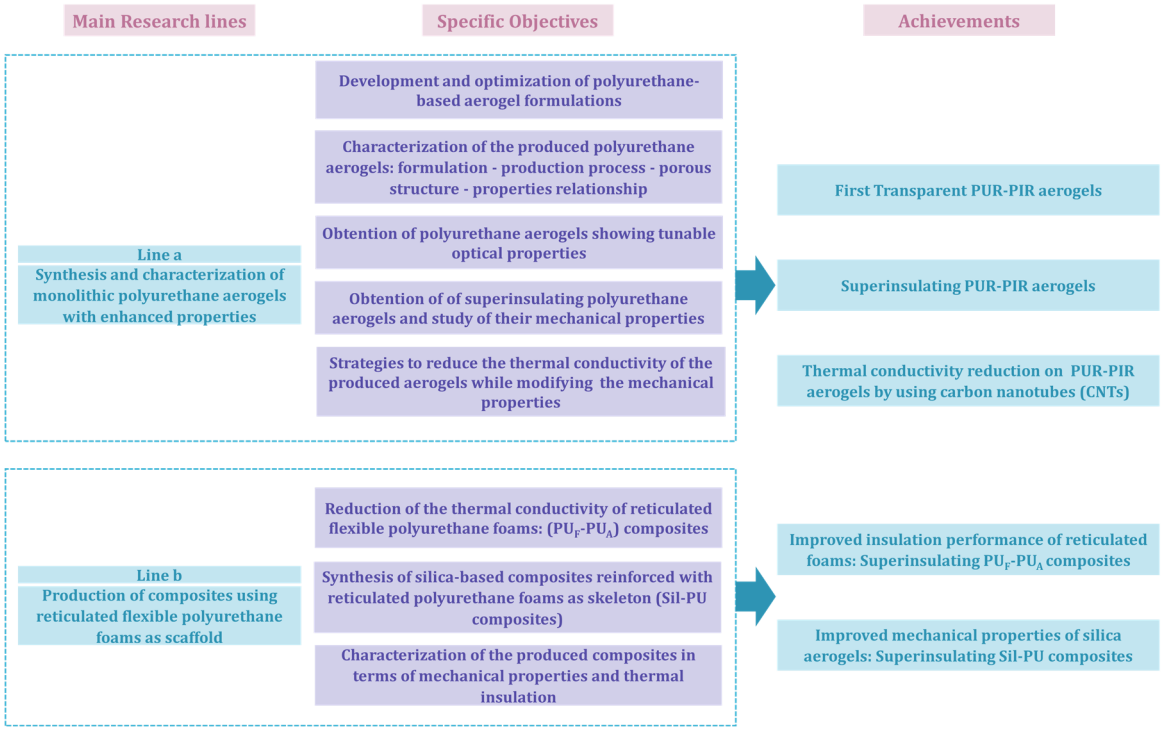

Figure 6. Main research lines, specific objectives, and summary of the achievements of this thesis.

a) Synthesis and characterization of monolithic polyurethane aerogels with enhanced properties

Two main topics are defined by this first line. On the one hand, synthesizing polyurethane aerogels with low densities, with a controlled nanoporous structure and with excellent physical properties. On the other hand, a detailed analysis of the structure-property relationships. The main goals of this line were to obtain aerogels with a great insulating performance and, if possible, reaching a high degree of transparency. This general objective can be divided into five specific objectives:

1. Development and optimization of polyurethane-based formulations for the obtention of nanoporous aerogels.

Different formulations were tested in order to select that leading to a homogeneous gel forming a nanoporous structure which does not collapse during the drying step. Different strategies were performed in order to carry out this study:

- Study of different catalysts
- Study of the influence of the catalyst content on the porous structure
- Effect of the drying method on the porous structure

2. Characterization of the produced polyurethane aerogels, in order to understand the formulation – production process – porous structure – properties relationship.

First of all, the specific techniques to characterize these materials were established. Aiming to fulfill this objective, different parameters and properties were evaluated:

- Bulk (ρ_B) and relative (ρ_r) densities were determined for the produced aerogels.
- Study of the porous structure: the gaseous and solid phase constituting these materials were described through different parameters. The solid phase was described by the average particle size (ϕ_{part}), particle size distribution and the specific surface area (S_{BET}), whereas the gaseous phase was defined by the average pore size (ϕ_{pore}) and porosity (Π).
- Study of the thermal insulating properties: thermal conductivity (λ) was evaluated.
- Study of the mechanical properties: the elastic modulus (E), and stress (σ) - strain (ε) curves were determined, as well as the energy loss coefficient (**ELC**).
- Study of the optical properties: light transmittance measurements (T) were carried out to assess the optical transparency of these aerogels. Two measurement methods were employed to obtain this parameter:
  - Laser measurements: different lasers with a characteristic light wavelength were used (450, 532 and 650 nm).
  - UV-vis measurements: a continuous spectrum scanning from 400 to 900 nm was measured.

3. Obtention of polyurethane aerogels showing tunable optical properties.

Transparency is, in combination with other characteristics, one of the most desired properties in aerogels. Thus, tailoring the porous structure of the produced aerogels would lead to tunable light transmittances. Additionally, their optical properties will be analyzed in detail in order to understand the scattering mechanisms taking place.

4. Obtention of superinsulating polyurethane aerogels and study of their mechanical properties.

The thermal conductivity of the produced aerogels was measured and the different contributions to the effective thermal conductivity were analyzed. In addition, the mechanical properties including compressive strength, elasticity and flexibility were studied.

5. Development of strategies to reduce the thermal conductivity of the produced aerogels while modifying the mechanical properties.

With the aim of reducing the radiative contribution, a well-known strategy in the field of cellular polymers consists on the addition of infrared opacifiers. This approach was tested in PU aerogels by the incorporation in the formulation of carbon nanotubes (**CNTs**).

For all the materials produced, a detailed analysis of the process-structure-properties relationships has been carried out.

b) Production of composites using reticulated flexible polyurethane foams as scaffold

The second research topic aims to produce PU foam-aerogel composites trying to improve both the initial properties of the foams (in the case of PU aerogels) and the properties of aerogels (in the case of silica aerogels). This includes the synthesis and evaluation of their mechanical and thermal insulating properties. The specific objectives for this line of research are as follows.

1. Reduction of the thermal conductivity of reticulated flexible polyurethane foams through the production of polyurethane foam-polyurethane aerogel (**PU_F–PU_A**) composites.

The inclusion of polyurethane aerogel into the foam pores of flexible PU foams contributes to significantly change the gaseous contribution of the heat transfer without altering the reaction kinetics of the PU foam, since it is already formed when the aerogel is included. Foams having different pore sizes were used in order to analyze the influence of this parameter on the final properties of the composites.

2. Synthesis of silica aerogel-based composites reinforced with reticulated polyurethane foams as skeleton (Sil-PU composites).

The same strategy has been used for silica aerogels with the purpose of improving the mechanical properties of the monolithic silica aerogels, while keeping their excellent insulating performance. Foams having different pore sizes were used to analyze the influence of this parameter on the final properties of the composites.

3. Characterization of the produced composites in terms of mechanical properties and thermal insulation.

Once the composites were produced, their mechanical properties and thermal conductivity were assessed, and the effect of the foam pore size on the final properties of the composites was analyzed.

Finally, a detailed analysis of the process-structure-property relationships was performed.

The specific objectives described for each main research line, together with the studied parameters, are gathered in **Figure 7**.

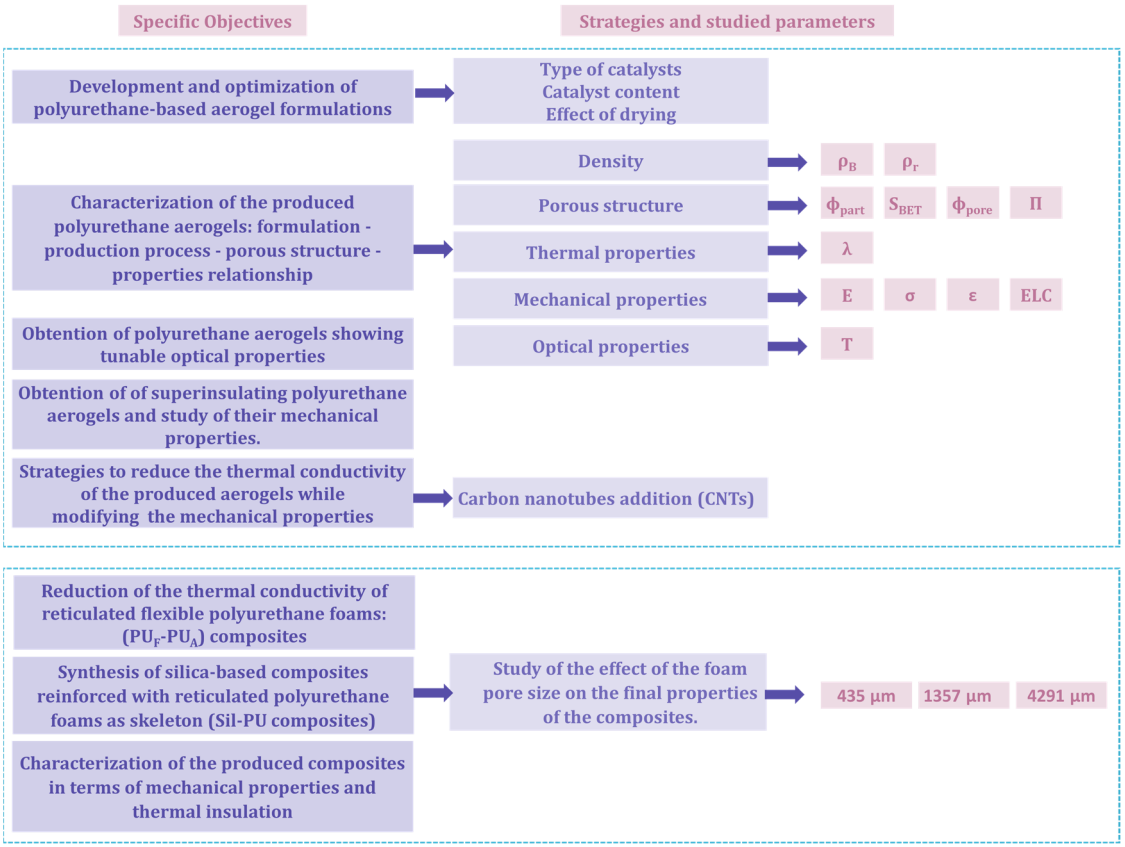

Figure 7. Specific objectives of this thesis and studied parameters.

By fulfilling these objectives, our knowledge in aerogels has been expanded reaching the possibility of producing aerogels on-demand at our facilities, through the control of their porous structures. Moreover, the assessment of the optical, thermal, and mechanical properties of the produced materials has been covered during this research.

Nonetheless, we are aware that several interesting properties such as acoustic properties, capillarity, or reaction kinetics, could be additionally studied, thus providing a more complete background. Therefore, an extensive future work is expected to be stemmed from this thesis.

Annex

During the period of training as Ph.D. student, some research on the field of polyurethane foams was also carried out. Although this is not the main topic of the thesis, an annex is included at the end of the document, collecting the main works produced on these materials. The objectives of the research carried out in PU foams are the following:

1. Studying the influence of adding nanoparticles to the reactive mixture of rigid polyurethane foams.

The effect of the addition of nanoparticles to PU formulations was assessed. Through avoiding the air inclusion into the reactive blend when mixing the components, the influence of air-trapping in the cell nucleation was analyzed.

2. Analyzing the influence of the porous structure on the acoustic absorption coefficient of a collection of semirigid polyurethane-based foams with different cellular structures.

To carry out this goal, a new methodology to characterize the holes and main features of the cells forming the polyurethane foams was developed.

3. Nitrates adsorption by using flexible hydrophilic PU foams.

Nanocomposites based on hydrophilic flexible PU foams and organomodified sepiolite as fillers were fabricated. Different sepiolite amounts were employed and the affinity of the produced nanocomposites by nitrates dissolved in water was evaluated.

1.4 Novelties

This research addresses different aspects of polyurethane and silica aerogels, as well as polyurethane foams, contributing to the scientific literature with some novelties, indicated below.

In the first place, **polyurethane-based aerogels** presenting **optical transparency** to visible light have been **synthesized for the very first time**. The size of the synthesized aerogels was incremented by optimizing the production procedures, allowing to measure their thermal conductivity with a higher reliability.

Moreover, owing to the interesting porous structure that these aerogels showed, the thermal conductivity of these monoliths revealed the **most insulating capacity for this matrix reaching the lowest values of thermal conductivity** known until now **for PU aerogels**.

The inclusion of carbon nanotubes (CNTs) in the polyurethane-based aerogel formulations led to a further reduction of the thermal conductivity for these materials as well as to modifications of the mechanical properties and porous structures.

Additionally, a **novel strategy** based on the inclusion of the **polyurethane-based aerogels into the pores of reticulated flexible polyurethane foams**, led to a significant reduction of their thermal conductivity never before explored, showing a simple and straightforward **method for improving the insulation performance of flexible reticulated PU foams** that could be applied to other cellular materials in future research. Furthermore, the **influence of the foam pore size** on the final properties of the produced composites has been analyzed, finding that, for all of them, **the cohesion between the aerogel and the PU struts is effective**, and that **final properties are similar to** those of the **monolithic aerogel**.

The same strategy was applied as **reinforcement for silica aerogels** reaching improved mechanical properties while **maintaining their super-insulating performance**. Therefore, an **innovative way for enhancing silica aerogels strength** and, thus, reducing their common brittleness is herein presented.

The latter **strategy has been optimized by the study of the effect of different foam pore sizes**, leading to a **more efficient aerogel-filling when the foam pores are smaller**.

In this way, the silica aerogel maintains its structure in the 3D network form without breaks and disconnections with the polymeric struts.

Moreover, as gathered in the Annex, different studies regarding polyurethane foams have been carried out:

The **effect of air-trapping in rigid PU foams filled with nanoclays** has been studied in detail, reaching to the conclusion that **the viscosity increase** that the reactive bend experiments when the nanoparticles are added, is the main factor **contributing to a nucleating effect, instead of being the effect of the particles themselves**. The reason would be the higher amount of gas trapped when increasing the viscosity of the polyol including the nanoparticles.

Novel parameters describing the porous structure of **semirigid PU foams** have been herein described. These parameters are helpful to describe the **relationship between acoustic absorption and structural parameters** for these materials.

Finally, the **inclusion of organomodified nanoclays on flexible hydrophilic PU** foam formulations has led to the improvement of the current methods for **nitrates adsorption in water solutions,** acting as **support of these particles** and, therefore, avoiding filtration steps, as well as **reaching high nitrates adsorption capacities**.

1.5 Structure of this thesis

This thesis has been formed by a compendium of publications. Eleven scientific articles have been published in international journals. Additionally, there are some unpublished results that have been included to provide additional information. Moreover, this thesis accomplishes the requirements to request the degree of Doctor in Philosophy (Ph.D.) with an International Mention.

This manuscript includes eight chapters and an annex at the end of the work. The different sections include the following information:

- **Chapter 1: Introduction.** A short introduction about aerogels, their birth, evolution, and main characteristics has been incorporated in this section. Then, the framework of this thesis, the general and specific objectives, and the novelties that this work provides are included. Finally, a section which gathers the scientific publications, international and national conferences, projects, and other additional information is presented. The structure of this thesis is also included.

- **Chapter 2: State of the art.** This chapter gathers the essential information to understand the concepts, processes, mechanisms involved during the synthesis of the produced materials, structure and properties. The main sections of this chapter describe the definitions of aerogel, types of aerogels depending on the matrix, synthesis, dryings, and structural parameters. Then, their optical, mechanical, and thermal properties are described including a revision of the existing bibliography and data found in the state of the art. At the end on the chapter, a summary of the main applications of these aerogels is found.

- **Chapter 3: Experimental section: Materials and Techniques.** The initial materials and formulations developed for synthesizing the materials produced in this thesis are described in detail in this chapter. Afterward, the production

methods followed during the materials manufacturing, the characterization techniques employed to analyze the structure, mechanical and optical properties, as well as the thermal conductivity are explained.

- **Chapter 4: Synthesis and Characterization of Transparent Polyurethane aerogel monoliths.** In this chapter, the synthesis and initial characterization of polyisocyanurate-polyurethane aerogels is described. The first results of polyurethane-based aerogels showing transparency are described and gathered in a scientific publication. A deeper analysis of the optical properties of these aerogels are merged in the second publication of this chapter, leading to the understanding of different parameters affecting the final transparency of the produced materials.

- **Chapter 5: Thermal Conductivity and Mechanical Properties of Transparent Polyurethane aerogel monoliths.** This chapter presents the results obtained regarding the mechanical properties and thermal conductivity of the polyisocyanurate-polyurethane aerogel formulations previously described in chapter 4. One scientific publication is herein included dealing with the relationship between formulation-structure-mechanical properties and thermal conductivity of these aerogels. Besides, an additional publication is attached gathering the results obtained for achieving a further reduction of the thermal conductivity of polyurethane aerogels through the incorporation of infrared blockers. This study analyzes in detail the contributions to the total thermal conductivity for this aerogel matrix.

- **Chapter 6: Improving the thermal insulation of Polyurethane foams by aerogel inclusion in the porous structure.** A novel strategy to drastically decrease the thermal conductivity of reticulated polyurethane foams is described in this chapter. This strategy consists of filling the foam pores with polyurethane aerogel which presents an excellent insulating performance. A scientific publication has been included containing the results of the synthesis and complete characterization of the novel polyurethane foam-polyurethane aerogel composites.

- **Chapter 7: Mechanical reinforcement of Silica Aerogels with Polyurethane foams as scaffold.** Chapter 7 merges the results of scaffolding silica aerogels with reticulated flexible polyurethane foams for improving their mechanical properties while maintaining their insulating behavior. The first publication found in this chapter describes the synthesis and characterization of these composites searching for the best synthesis route and formulation. The second publication studies the effect of different foam pore sizes on the final properties of the silica aerogel-polyurethane foam composites in order to find the optimum reinforcement.

- **Chapter 8: Conclusions and Future Work.** This chapter presents the main conclusions of this research. Additionally, the obtained results are compared with those found in the literature. Finally, some guidelines for future work are included at the end of the chapter.

- **Annex:** An annex is included at the end of this thesis gathering three publications related to polyurethane foams and the understanding of different properties thereof.

An overview of the structure and the distribution of the scientific publications along this thesis are represented in **Figure 8** and **Figure 9**, respectively:

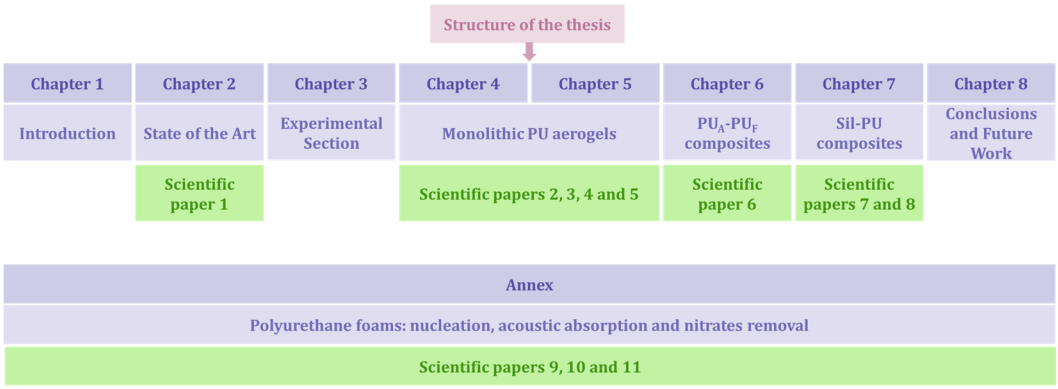

Figure 8. Structure of the thesis containing chapters and main research topic.

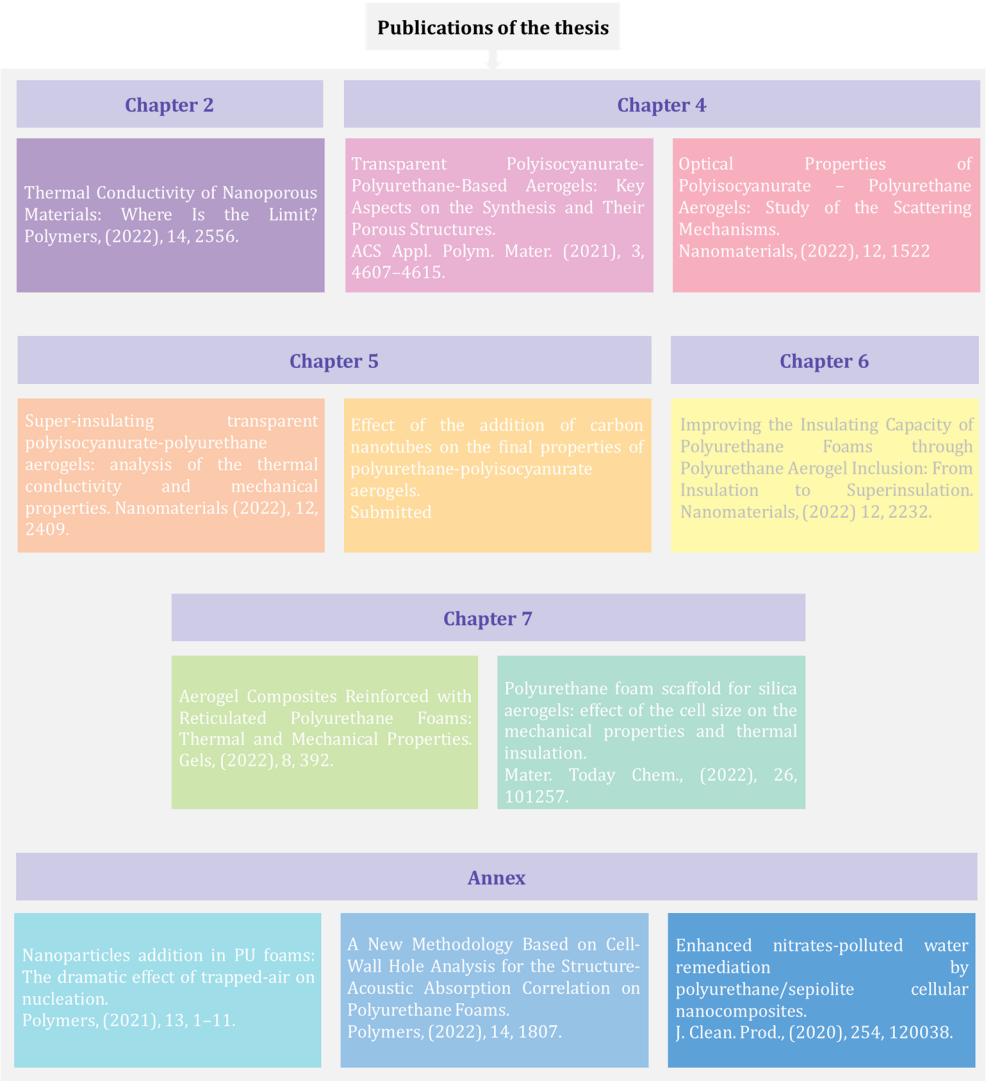

Figure 9. Publications included in this thesis.

1.6 Publications, conferences, projects, and courses

In this section, the scientific publications included in this thesis (**Table 1**), oral and poster contributions to national and international conferences related to the research from this thesis (**Table 2** and **Table 3**), industrial and research projects (**Table 4**), internships (**Table 5**), awards (**Table 6**), grants and contracts (**Table 7**), and additional activities such as supplementary papers and conferences, divulgation activities, and training courses (**Table 8**) are gathered.

A total of 11 scientific articles have been published in international journals during the development of the present thesis.

Table 1. Scientific publications included in this thesis.

Indexed Scientific publications			
Number	**Reference**	**Q/IF**	**Chapter**
1	Merillas B.; Vareda J.; Martín-de León J.; Rodríguez-Pérez MÁ.; Durães L. **Thermal Conductivity of Nanoporous Materials: Where Is the Limit?** Polymers, (2022), 14, 2556.	Q1/4.967	2
2	Merillas B.; Martín-de León J.; Villafañe F.; Rodríguez-Pérez MA. **Transparent Polyisocyanurate-Polyurethane-Based Aerogels: Key Aspects on the Synthesis and Their Porous Structures.** ACS Appl. Polym. Mater. (2021), 3, 4607–4615.	Q1/4.855	4
3	Merillas B.; Martín-de León J.; Villafañe F.; Rodríguez-Pérez MÁ. **Optical Properties of Polyisocyanurate – Polyurethane Aerogels: Study of the Scattering Mechanisms**. Nanomaterials, (2022), 12, 1522.	Q1/5.719	4
4	Merillas B.; Villafañe F.; Rodríguez-Pérez MÁ. **Super-insulating transparent polyisocyanurate-polyurethane aerogels: analysis of the thermal conductivity and mechanical properties**. Nanomaterials (2022), 12, 2409.	Q1/5.719	5
5	Merillas B.; Villafañe F.; Rodríguez-Pérez MÁ. **Effect of the addition of carbon nanotubes on the final properties of polyurethane-polyisocyanurate aerogels**. Submitted	-	5
6	Merillas B.; Villafañe F.; Rodríguez-Pérez MÁ. **Improving the Insulating Capacity of Polyurethane Foams through Polyurethane Aerogel Inclusion: From Insulation to Superinsulation**. Nanomaterials, (2022) 12, 2232.	Q1/5.719	6
7	Merillas B.; Lamy-Mendes A.; Villafañe F.; Durães L.; Rodríguez-Pérez MÁ. **Silica-Based Aerogel Composites Reinforced with Reticulated Polyurethane Foams: Thermal and Mechanical Properties**. Gels, (2022), 8, 392.	Q1/4.432	7
8	Merillas B.; Lamy-Mendes A.; Villafañe F.; Durães L.; Rodríguez-Pérez MÁ. **Polyurethane foam scaffold for silica aerogels: effect of the cell size on the mechanical properties and thermal insulation**. Mater. Today Chem., (2022), 26, 101257.	Q1/7.613	7
9	Merillas B.; Villafañe F.; Rodríguez-Pérez MÁ. **Nanoparticles addition in PU foams: The dramatic**	Q1/4.329	Annex

	effect of trapped-air on nucleation. Polymers, (2021), 13, 1–11.		
10	Merillas B.; Villafañe F.; Rodríguez-Pérez MÁ. **A New Methodology Based on Cell-Wall Hole Analysis for the Structure-Acoustic Absorption Correlation on Polyurethane Foams**. Polymers, (2022), 14, 1807.	Q1/4.329	Annex
11	Barroso-Solares S.; Merillas B.; Cimavilla-Roman P.; Rodríguez-Pérez MA.; Pinto J. **Enhanced nitrates-polluted water remediation by polyurethane/sepiolite cellular nanocomposites**. J. Clean. Prod., (2020), 254, 120038.	Q1/9.297	Annex

Non-Indexed Scientific publications	
Number	**Reference**
1	Barroso-Solares S.; Merillas B.; López-González E.; Rodríguez-Pérez MA.; Pinto J. Proceedings paper. EDULEARN18 – 10th International Conference on Education and new Learning Technologies. Page 6196-6206. **Development of a postgraduate training program on surface functionalization of polymers/polymer foams**.
2	Merillas B.; Martín-de León J.; Villafañe F.; Rodríguez-Pérez MÁ. Conference Proceedings. 18th International Conference on Advances in Foam Materials & Technology (FOAMS® 2021). **Highly Transparent Polyurethane-based Aerogels: effect of catalyst on the porous structure and final properties**.
3	Barroso-Solares S.; Vázquez-Corrales L.; Moral-Domingo, R.; Merillas B.; Cuadra-Rodríguez, D.; Rodríguez-Pérez MA.; Pinto J. Conference Proceedings. 18th International Conference on Advances in Foam Materials & Technology (FOAMS® 2021). **Water Pollutants Removal by Nanocomposite foamed Polymers**.

The results obtained in this thesis have been presented in several international and national conferences, gathered in the following tables.

Table 2. International conferences.

International conferences		
Number	**Conference**	**Contribution**
1	Barroso-Solares S.; Merillas B.; Cimavilla P.; Rodríguez-Pérez M.A.; Pinto J. **Nitrates and other pollutants removal from water resources using multifunctional polyurethane foams**. 4th International Congress on Water, Waste and Energy Management (WWEM-18), 2018, Madrid, Spain.	Oral contribution
2	Merillas B.; Barroso-Solares S.; Cimavilla P.; Pinto J.; Rodríguez-Pérez M.A. **Nitrate removal from aqueous solution by adsorption onto polyurethane/sepiolite cellular nanocomposites.** 17th International Conference on Advances in Foam Materials & Technology (FOAMS® 2019), 2019, Valladolid, Spain.	Poster contribution
3	Merillas B.; Villafañe F.; Rodríguez-Pérez MÁ. **Ex-situ analysis of the synthesis of PU aerogels: time evolution of particle size.** International Conference on Aerogels for Biomedical and Environmental Applications, 2020, Santiago de Compostela, Spain.	Poster contribution

4	Merillas B.; Villafañe F.; Rodríguez-Pérez MÁ. **Synthesis of polyurethane aerogels and the effect of the structure on thermal conductivity.** 6th Cellular Materials CellMAT 2020, 2020, Web-Conference (CEST), Germany.	Oral contribution
5	Merillas B.; Martín-de León J.; Villafañe F.; Rodríguez-Pérez MÁ. **Highly transparent polyurethane-based aerogels: effect of catalyst on the porous structure and final properties**. 18th International Conference on Advances in Foam Materials & Technology (FOAMS® 2021), 2021, Online conference.	Oral contribution
6	Barroso-Solares S.; Vázquez-Corrales L.; Moral-Domingo R.; Merillas B.; Cuadra-Rodríguez D.; Rodríguez-Pérez MA.; Pinto J. **Water Pollutants Removal by Nanocomposite foamed Polymers.** 18th International Conference on Advances in Foam Materials & Technology (FOAMS® 2021), 2021, Online conference.	Oral contribution
7	Merillas B.; Martín-de León J.; Villafañe F.; Rodríguez-Pérez MÁ. **Transparent Polyurethane-based aerogels with tunable optical properties**. Advanced Technologies for the processing and characterization of nanostructured materials. AERoGELS COST ACTION CA18125. AGH University of Science and Technology, 2021, Online conference, Cracow, Poland	Oral contribution
8	Merillas B.; Lamy-Mendes A.; Duraes L.; Villafañe F.; Rodríguez-Pérez MÁ. **Reinforced silica aerogels by using open cell polyurethane foams as skeleton: thermal and mechanical properties**. Spanish-Portuguese Industry-Academia Aerogel Meeting, 2022, Coimbra, Portugal.	Oral contribution
9	Merillas B.; Lamy-Mendes A.; Duraes L.; Villafañe F.; Rodríguez-Pérez MÁ. **Polyurethane foam scaffold for silica and polyurethane aerogels: effect of pore size on mechanical properties and thermal insulation**. 2nd International Conference on Aerogels for Biomedical and Environmental Applications, 2022, Athens, Greece.	Oral contribution
10	Merillas B.; Martín-de León J.; Villafañe F.; Rodríguez-Pérez MA. **Polyurethane aerogels: lightweight, transparency and super-insulation in one material**. 7th International Conference on Cellular Materials, CellMAT 2022, Online conference, Dresden, Germany.	Oral contribution
11	Barroso-Solares S.; Merillas B.; Cimavilla P **Nitrates and other pollutants removal from water resources using multifunctional porous polymers**. Workshop "Polymers for Environmental Preservation and Remediation". BioEcoUVA Research Institute on Bioeconomy (University of Valladolid) within the project "Functional polymeric FOams for WAter RemeDiation (FORWARD)" (RTI2018-097367-A-I00, founded by MCIN/ AEI /10.13039/501100011033/ and "FEDER Una manera de hacer Europa"). 2022, On-line.	Oral contribution

Table 3. National conferences.

National conferences		
Number	**Conference**	**Contribution**
1	Merillas B.; Arroyo M.; Cuéllar E.; Martín-Álvarez J. M..; Miguel D.; Villafañe F. **Green synthesis of 3-(2-Pyridyl)Pyrazole and its group 6 and 7 metal carbonyl complexes**. XXXVI Reunión Bienal de la Sociedad Española de Química, 2017, Sitges, Spain.	Poster contribution
2	Merillas B.; Villafañe F.; Rodríguez-Pérez M.A. **Synthesis and structural characterization of polyurethane aerogels**. X Congress of Young Researchers in Polymers, 2019, Burgos, Spain.	Oral contribution

The Ph.D. candidate was involved in the research activities of the following projects with public and private funding.

Table 4. Industrial and research projects.

Research projects		
Public funding		
1	**Project**	**Espumas poliméricas funcionales para el tratamiento de aguas.** RTI2018-097367-A- I00
	Funding body	Agencia Estatal de Investigación; Fondos FEDER
	Duration	January 2019 – June 2022
	Principal investigator	Javier Pinto Sanz
	Budget	72.600,00 €
2	**Project**	**Polímeros nanocelulares transparentes y aislantes térmicos, fabricación, caracterización y relación proceso-estructura-propiedades**. RTI2018-098749-B-I00
	Funding body	Proyecto Reto-Plan Nacional
	Duration	January 2019 – December 2021
	Principal investigator	Miguel Ángel Rodríguez Pérez
	Budget	157.300 €
3	**Project**	**Polímeros nanocelulares micronizados: una nueva generación de materiales para el core de aislantes térmicos avanzados basados en paneles de vacío (VIP)**. VA202P20
	Funding body	Junta de Castilla y León. Subvenciones del programa de apoyo a proyectos de investigación cofinanciadas por el Fondo Europeo de Desarrollo Regional.
	Duration	November 2020 – October 2023
	Principal investigator	Miguel Ángel Rodríguez Pérez
	Budget	240.000 €
4	**Project**	**Desarrollo de super aislantes térmicos basados en polímeros nanocelulares y bloqueadores de la radiación infrarroja.** PID2021- 127108OB-I00.
	Funding body	Agencia Estatal de Investigación; Fondos FEDER, Ministerio de Ciencia e Innovación. Unión Europea.
	Duration	September 2022 – August 2025
	Principal investigator	Miguel Ángel Rodríguez Pérez

	Budget	205.700,00 €
5	**Project**	**Hacia la producción industrial de polímeros nanocelulares transparentes.** PDC2022-133391- I00.
	Funding body	Agencia Estatal de Investigación; Ministerio de Ciencia e Innovación; Plan de recuperación, transformación y resiliencia. Unión Europea – Next Generation UE.
	Duration	December2022 – November 2024
	Principal investigator	Miguel Ángel Rodríguez Pérez
	Budget	149.500,00 €
6	**Project**	**Producción sostenible de super aislantes térmicos basados en polímeros nanocelulares con conductividad térmica reducida a través del incremento de la dispersión de fonones.** TED2021-130965B- I00.
	Funding body	Agencia Estatal de Investigación; Ministerio de Ciencia e Innovación; Plan de recuperación, transformación y resiliencia. Unión Europea – Next Generation UE.
	Duration	December2022 – November 2024
	Principal investigator	Miguel Ángel Rodríguez Pérez
	Budget	168.820,00 €
Private funding		
7	**Project**	**Investigación sobre aplicaciones de nanomateriales avanzados de carbono a la mejora de las prestaciones de matrices de poliuretano (PU) con interés en el sector de la automoción**.
	Funding body	Grupo Antolín Ingeniería
	Duration	April 2017 – December 2018
	Principal investigator	Miguel Ángel Rodríguez Pérez
	Budget	60000 €
8	**Project**	**Análisis comparativo de la estructura y cinética de reacción de sistemas en base poliuretano**.
	Funding body	Grupo Antolín Ingeniería
	Duration	September 2017 – May 2018
	Principal investigator	Miguel Ángel Rodríguez Pérez
	Budget	9000 €
9	**Project**	**Desarrollo y optimización de materiales celulares de celda abierta para aplicaciones de confort y de absorción de líquidos**.
	Funding body	CellMat Technologies SL
	Duration	December 2016 – December 2020
	Principal investigator	Miguel Ángel Rodríguez Pérez
	Budget	60000 €
10	**Project**	**Desarrollo y optimización de materiales celulares de elevada resistencia al impacto**.
	Funding body	CellMat Technologies SL
	Duration	December 2016 – December 2020
	Principal investigator	Miguel Ángel Rodríguez Pérez
	Budget	40000 €

The following table summarizes the research stays in other institutions during the development of this thesis. Two research stays in the Chemical Engineering Department at the University of Coimbra, under the supervision of Prof. Dr. Luisa Durães, lasted six months. During this time, some of the experiments included in **Chapter 7** were conducted, resulting in two publications and a collaboration (review included in **Chapter 2**).

Table 5. International internships.

Internships	
1	International internship (1) (3 months). **Computation and Materials (CeM)** Laboratory, Chemical Process Engineering and Forest Products Research Centre (CIEPQPF), Dept. Chemical Engineering, University of Coimbra (11/01/2021 – 12/04/2021)
2	International internship (2) (3 months). **Computation and Materials (CeM)** Laboratory, Chemical Process Engineering and Forest Products Research Centre (CIEPQPF), Dept. Chemical Engineering, University of Coimbra (01/07/2021 – 30/09/2021)

Some of the works presented in conferences and contests have been awarded, as gathered in the following table.

Table 6. Awards.

Awards	
1	**Second prize: IV Edition "Three-Minute Thesis"**. Doctoral School in the University of Valladolid (2019)
2	**Second prize: Best Poster Presentation from Early Career Researchers in International Conference on Aerogels for Biomedical and Environmental Application**. Organized by the AERoGELS COST Action. (2020)
3	**First prize: Young researchers'– Best Oral Presentation Award in the Spanish-Portuguese Industry-Academia Aerogel Meeting**. Organized by the AERoGELS COST Action and University of Coimbra. (2022)
4	**Finalist in the I Edition of the Divulgation Contest #HiloTesis"** organized by the group Divulgación y Cultura Científica (Red Divulga) de la sectorial de I+d+i de Crue. 1-23th April (2021).
5	Certificate of excellence, entrepreneurship and innovation as a member of "3IN-sole". **Finalist team of the IMFAHE´s Idea Competition-Nodal Award/Shark Tank Edition** celebrated during the VIII IMFAHE´s International Conference on May 30th, IMFAHE FOUNDATION, (2022).

The following table gathers the main grants and contracts received during the development of this thesis.

Table 7. Grants and contracts.

Grants and contracts	
1	**General Foundation of the University of Valladolid** (2017 – 2019)
2	**Predoctoral Contract of the University of Valladolid**, 2018. (2019)
3	**Predoctoral Contract from the Spanish Ministry of Science, Innovation and Universities FPU, 2017**. (2019 – 2023)
4	**Short Term Scientific Missions (STSM). AERoGELS COST Action (CA18125 - Advanced Engineering and Research of aeroGels for Environment and Life Sciences)**. Computation and Materials (CeM), Chemical Process Engineering and Forest Products Research Centre (CIEPQPF), Dept. Chemical Engineering, University of Coimbra. (2021).
5	**Mobility grants for short internships or temporary internships for FPU beneficiaries. Spanish Ministry of Universities FPU 2020**, (2021).
6	**Grants for the attendance at courses, congresses and conferences relevant to the development of doctoral theses of the University of Valladolid**, (2021).
7	**Grants for the attendance at courses, congresses and conferences relevant to the development of doctoral theses of the University of Valladolid**, (2022).

Other contributions to international and national conferences, publications, divulgation and training activities are summarized in the following table.

Table 8. Additional activities.

Additional scientific publications	
Number	**Reference**
1	Merillas B.; Cuéllar E.; Diez-Varga A.; Asensio-Bartolomé M.; García-Herbosa G.; Torroba T.; Martín-Álvarez J.M..; Miguel Daniel.; Villafañe Fernando. **Whole microwave syntheses of pyridylpyrazole and of Re and Ru luminescent pyridylpyrazole complexes**. Inorganica Chim Acta. (2019), 484, 1–7.
2	Merillas B.; Cuéllar E.; Diez-Varga A.; Torroba T.; García-Herbosa G.; Fernández S.; Lloret-Fillol Julio.; Martín-Álvarez J.M..; Miguel Daniel.; Villafañe Fernando. **Luminescent Rhenium(I)tricarbonyl Complexes Containing Different Pyrazoles and Their Successive Deprotonation Products: CO_2 Reduction Electrocatalysts**. Inorg Chem. (2020), 59, 15, 11152–65.
3	Linhares T.; Carneiro VH.; Merillas B.; Pessoa De Amorim M.T.; Durães L. **Textile waste-reinforced cotton-silica aerogel composites for moisture regulation and thermal / acoustic barrier**. J Sol-Gel Sci Technol. (2022), 102, 574–588.
4	Sánchez-Calderón I.; Merillas B.; Bernardo V.; Rodríguez-Pérez MÁ. **Methodology for measuring the thermal conductivity of insulating samples with small dimensions by heat flow meter technique**. J. Therm. Anal. Calorim. (2022), 147, 12523–12533.
Additional conferences	
1	Barroso-Solares S.; Merillas B.; López-González E.; Rodríguez-Pérez M.A.; Pinto J. **Development of a postgraduate training program on surface functionalization of polymers/polymer foams.** EDULEARN18: 10th International Conference on Education and New Learning Technologies, 2018, Mallorca, Spain
2	Merillas B.; Cuéllar E.; Diez-Varga A.; Asensio-Bartolomé M.; Torroba T.; Martín-Álvarez J.M..; Miguel Daniel.; Villafañe Fernando. **Tricarbonylrhenium(I) luminescent complexes with mono- and bidentate pyrazoles.** 7th EuCheMS Conference on Nitrogen Ligands, 2018, Lisbon, Portugal.
3	Merillas B.; Cuéllar E.; Diez-Varga A.; Asensio-Bartolomé M.; García-Herbosa G.; Torroba T.; Martín-Álvarez J.M..; Miguel Daniel.; Villafañe Fernando. **Deprotonation studies, luminescent properties and catalytic CO_2 reduction activity of $Re(CO)_3$ complexes with pyrazole and (3-(2pyridyl)pyrazole).** UK-Spain Organometallic Chemistry Symposium (USOCS2019), 2019, Alcalá de Henares, Spain.
Divulgation activities	
1	Cycle of conferences "Women Researchers in the University of Valladolid". Oral contribution: **"Rhenium(I) luminescent complexes with the ligand 3-(2-pyridyl)pyrazole"**. (2017)
2	Theoretical classes for the preparation, supervision and development of laboratory experiments for the students participating in the workshop "Foams in Operation" of the 2018 **Summer Scientific Campus** promoted by the Spanish Foundation for Science and Technology (FECYT) held at the University of Valladolid.
3	**Three-Minute Thesis Contest 2019** organized by the School of Doctoral in the University of Valladolid. Finalist of the contest with the intervention "Air bricks to build the future".
4	**Oral presentation in the National "Pint of Science". 2021** online Edition. Entitled "¿Tienes ya una casa en Marte?" in the "Tech me out" section. Spain

5	Finalist in the I Edition of the **Divulgation Contest #HiloTesis"** organized by the group Divulgación y Cultura Científica (Red Divulga) de la sectorial de I+d+i de Crue. 1-23th April (2021)
6	2021 - **Divulgation Activity #Cuéntame11FUVa**, promoted by the Unidad de Cultura Científica y de la Innovación from the University of Valladolid on social media YouTube, Twitter e Instagram. 7-13th February, (2022)
7	**Scientist Photography Contest (DIL)** organized by the Unidad de Cultura Científica y de la Innovación of the University of Valladolid, (2022)
8	**IX Jornadas de Investigadoras de Castilla y León,** comunicación oral "Aerogeles de poliuretano: superaislantes contra el cambio climático." Promovido por las universidades de Burgos, León, Salamanca y Valladolid, 9-10th February, (2023)
	Training activities
1	Taller de autores. "**Guía práctica para la publicación de trabajos**", University of Valladolid, 2017.
2	**Infrared Thermography with image processing**. Organized by the School of Doctoral in the University of Valladolid, 2018.
3	**Conference "Plastic, Containers, Fundamentals, Regulations and Trends"** organized by LEICAL, 2018
4	**5th International Summer School on Aerogels**. 19th -21st September 2018, Cologne, Germany. Department of Aerogels and Aerogel Composites of the Institute of Materials Research at the **German Aerospace Center (DLR)**.
5	**Introduction to Project Management**. Polytechnic University of Valencia, 2020.
6	**6th International Online Summer School on Aerogels** (IOSSA). 16th September 2021, Online, Department of Aerogels and Aerogel Composites of the Institute of Materials Research at the **German Aerospace Center (DLR)**.
7	**AERoGELS COST Action WG1&5-Virtual Hands-On Trainning School**. Held in Virtual Lab Simulation – LABSTER, 2021.
8	**Workshop: Advices and Regulatory Aspects on Health Risk, LCA and Production Management of Aerogels**. AERoGELS COST ACTION CA18125, 2021, On-line.
9	**Webinar: Sustainable silica-based nanomaterials for thermal protection systems.** 2022. On-Line event, University of Coimbra, Nanofire, Tyre4build Ins, AeroXtreme.
10	IMFAHE´s Online **Quarter Course on "Professional Development"**. IMFAHE FOUNDATION, 2022.
11	IMFAHE´s Online **Quarter Course on "Innovation, Entrepreneurship and Leadership"**. IMFAHE FOUNDATION, 2022.
12	IMFAHE´s Online **Quarter Course on "Careers in Science"**. IMFAHE FOUNDATION, 2022.
13	**Mentee of the International Mentor Program (IMP).** IMFAHE FOUNDATION, 2022.
14	Certificate of excellence, entrepreneurship and innovation as a member of "3IN-sole". Finalist team of the **IMFAHE´s Idea Competition-Nodal Award/Shark Tank Edition** celebrated during the VIII IMFAHE´s International Conference on May 30th, IMFAHE FOUNDATION, 2022.
15	**IMFAHE´s VIII International Conference Innovation Camp "Connecting Talent Worldwide, Promoting Innovation and Excellence in Higher Education"** IMFAHE FOUNDATION, 2022, Online on May 30th.

1.7 References

[1] J. M. Buist, S. J. Grayson, and W. D. Woolley, *Fire and Cellular Polymers*. London and New York: Elsevier applied science, 1986. doi: 10.1007/978-94-009-3443-6.

[2] S. S. Kistler, "Coherent Expanded Aerogels and Jellies," *Nature*, vol. 127, p. 741, **1931**.

[3] S. S. Kistler, "Coherent expanded aerogels," *J. Phys. Chem.*, vol. 36, no. 1, pp. 52–64, **1932**, doi: https://doi.org/10.1021/j150331a003.

[4] C. Nägeli and C. Cramer, *Pflanzenphysiologische Untersuchungen*, no. 1. Schulthess, 1855.

[5] S. S. Kistler, "Method of producing aerogels," 2,093,454, 1937. doi: 10.1038/209966a0.

[6] S. S. Kistler and W. Boylston, "Treatment of aerogels to render them waterproof," 2,589,705, 1952.

[7] S. J. Teichner and G. A. Nicolaon, "Method of preparing inorganic aerogels," 3,672,833, 1972.

[8] R. W. Pekala, "Low density, Resorcinol-Formaldehyde aerogels," 4,873,218, 1989.

[9] R. W. Pekala, "Synthetic control of molecular structure in organic aerogels," *MRS Online Proc. Libr.*, vol. 171, pp. 285–291, **1989**, doi: https://doi.org/10.1557/PROC-171-285.

[10] R. W. Pekala, "Organic aerogels from the polycondensation of resorcinol with formaldehyde," *J. Mater. Sci.*, vol. 24, no. 9, pp. 3221–3227, **1989**, doi: 10.1007/BF01139044.

[11] G. Biesmans, D. Randall, E. Francais, and M. Perrut, "Polyurethane-based organic aerogels' thermal performance," *J. Non. Cryst. Solids*, vol. 225, pp. 36–40, **1998**, doi: http://dx.doi.org/10.1016/S0022-3093(98)00103-3.

[12] G. Biesmans, "Polyurethane based organic aerogels and their transformation into carbon aerogels," pp. 64–68, **1998**.

[13] M. B. Bryning, D. E. Milkie, M. F. Islam, L. A. Hough, J. M. Kikkawa, and A. G. Yodh, "Carbon nanotube aerogels," *Adv. Mater.*, vol. 19, no. 5, pp. 661–664, **2007**, doi: 10.1002/adma.200601748.

[14] N. Leventis, N. Chandrasekaran, C. Sotiriou-Leventis, and A. Mumtaz, "Smelting in the age of nano: Iron aerogels," *J. Mater. Chem.*, vol. 19, no. 1, pp. 63–65, **2009**, doi: 10.1039/b815985h.

[15] M. A. Aegerter, N. Leventis, and M. M. Koebel, *Aerogels Handbook*. Berlin, Germany: Springer, 2011. doi: 10.1007/978-1-4419-7589-8_4.

[16] H. Guo, M. A. B. Meador, L. McCorkle, D. J. Quade, J. Guo, B. Hamilton, M. Cakmak, and G. Sprowl, "Polyimide aerogels cross-linked through amine functionalized polyoligomeric silsesquioxane," *ACS Appl. Mater. Interfaces*, vol. 3, no. 2, pp. 546–552, **2011**, doi: 10.1021/am101123h.

[17] H. Guo, M. A. B. Meador, L. McCorkle, D. J. Quade, J. Guo, B. Hamilton, and M. Cakmak, "Tailoring properties of cross-linked polyimide aerogels for better moisture resistance, flexibility, and strength," *ACS Appl. Mater. Interfaces*, vol. 4, no. 10, pp. 5422–5429, **2012**, doi: 10.1021/am301347a.

[18] M. A. B. Meador, E. J. Malow, R. Silva, S. Wright, D. Quade, S. L. Vivod, H. Guo, J. Guo, and M. Cakmak, "Mechanically strong, flexible polyimide aerogels cross-linked with aromatic triamine," *ACS Appl. Mater. Interfaces*, vol. 4, no. 2, pp. 536–544, **2012**, doi: 10.1021/am2014635.

[19] M. Betz, C. A. García-González, R. P. Subrahmanyam, I. Smirnova, and U. Kulozik, "Preparation of novel whey protein-based aerogels as drug carriers for life science applications," *J. Supercrit. Fluids*, vol. 72, pp. 111–119, **2012**, doi: 10.1016/j.supflu.2012.08.019.

[20] J. C. Arboleda, M. Hughes, L. A. Lucia, J. Laine, K. Ekman, and O. J. Rojas, "Soy protein-nanocellulose composite aerogels," *Cellulose*, vol. 20, no. 5, pp. 2417–2426, **2013**, doi: 10.1007/s10570-013-9993-4.

[21] N. Asim, M. Badiei, M. A. Alghoul, M. Mohammad, A. Fudholi, M. Akhtaruzzaman, N. Amin, and K. Sopian, "Biomass and Industrial Wastes as Resource Materials for Aerogel Preparation: Opportunities, Challenges, and Research Directions," *Ind. Eng. Chem. Res.*, vol. 58, no. 38, pp. 17621–17645, **2019**, doi: 10.1021/acs.iecr.9b02661.

[22] K. Lee, L. Shabnam, S. N. Faisal, V. C. Hoang, and V. G. Gomes, "Aerogel from fruit biowaste produces ultracapacitors with high energy density and stability," *J. Energy Storage*, vol. 27, p. 101152, **2020**, doi: 10.1016/j.est.2019.101152.

[23] B. Zeng, X. Wang, and N. Byrne, "Development of cellulose based aerogel utilizing waste denim—A Morphology study," *Carbohydr. Polym.*, vol. 205, no. October 2018, pp. 1–7, **2019**, doi: 10.1016/j.carbpol.2018.09.070.

[24] C. Zhu, T. Y. J. Han, E. B. Duoss, A. M. Golobic, J. D. Kuntz, C. M. Spadaccini, and M. A. Worsley, "Highly compressible 3D periodic graphene aerogel microlattices," *Nat. Commun.*, vol. 6, pp. 1–8, **2015**, doi: 10.1038/ncomms7962.

[25] L. Kocon, F. Despetis, and J. Phalippou, "Ultralow density silica aerogels by alcohol supercritical drying," *J. Non. Cryst. Solids*, vol. 225, pp. 96–100, **1998**, doi: 10.1016/S0022-3093(98)00322-6.

[26] I. Smirnova and P. Gurikov, "Aerogel production: Current status, research directions, and future opportunities," *J. Supercrit. Fluids*, vol. 134, no. December 2017, pp. 228–233, **2018**, doi: 10.1016/j.supflu.2017.12.037.

[27] D. Urge-Vorsatz, K. Petrichenko, M. Staniec, and J. Eom, "Energy use in buildings in a long-term perspective," *Curr. Opin. Environ. Sustain.*, vol. 5, no. 2, pp. 141–151, **2013**, doi: 10.1016/j.cosust.2013.05.004.

[28] N. Azimi Fereidani, E. Rodrigues, and A. R. Gaspar, "A review of the energy implications of passive building design and active measures under climate change in the Middle East," *J. Clean. Prod.*, vol. 305, p. 127152, **2021**, doi: 10.1016/j.jclepro.2021.127152.

[29] "Directive 2010/31/EU of the European Parliament and of the Council on the energy performance of buildings," European Council: Brussels , Belgium, **2010**.

[30] A. Almusaed and A. Almssad, *Insulation Materials in Context of Sustainability*. IntechOpen Science, 2016. doi: 10.5772/61361.

[31] L. D. Hung Anh and Z. Pásztory, "An overview of factors influencing thermal conductivity of building insulation materials," *J. Build. Eng.*, vol. 44, p. 102604, **2021**, doi: 10.1016/j.jobe.2021.102604.

[32] "Aerogel Market Size & Share Report, 2020-2028," 2021. https://www.grandviewresearch.com/industry-analysis/aerogel-market

[33] F. P. Soorbaghi, M. Isanejad, S. Salatin, M. Ghorbani, S. Jafari, and H. Derakhshankhah, "Bioaerogels: Synthesis approaches, cellular uptake, and the biomedical applications," *Biomed. Pharmacother.*, vol. 111, no. January, pp. 964–975, **2019**, doi: 10.1016/j.biopha.2019.01.014.

[34] F. M. Husain, A. Khan, R. A. Khan, J. A. Siddique, M. Oves, A. A. P. Khan, M. O. Ansari, and H. D. Cancar, "Bio-based aerogels and their environment applications: an overview," in *Advances in Aerogel Composites for Environmental Remediation*, Elsevier Inc., 2021, pp. 347–356. doi: 10.1016/b978-0-12-820732-1.00018-7.

[35] "http://cellmat.es/."

[36] M. Á. Rodríguez-Pérez, "Propiedades Térmicas y Mecánicas de Espumas Poliolefinas," University of Valladolid, 1998.

[37] L. O. Arcos y Rábago, "Propiedades térmicas y mecánicas de espumas de poliolefinas fabricadas en un proceso de moldeo por compresión," University of Valladolid, 2002.

[38] C. Saiz-Arroyo, "Fabricación de materiales celulares mejorados basados en poliolefinas.

Relación procesado-composición-estructura-propiedades.," University of Valladolid, 2012.

[39] J. A. Reglero Ruiz, "Fabricación y caracterización de espumas de aluminio: aplicaciones en el sector aeronáutico," University of Valladolid, 2007.

[40] E. Solórzano, "Espumas de Aluminio: Proceso de Espumado, Estructura Celular y Propiedades," Úniversity of Valladolid, 2008.

[41] J. A. Reglero, M. A. Rodríguez-Pérez, D. Lehmhus, M. Windmann, J. A. de Saja, and A. Fernández, "An Experimental Study on the Inhomogeneities of Aluminum Foams Measuring the Thermal Conductivity by Using the Transient Plane Source Method," *Mater. Sci. Forum*, vol. 480–481, pp. 133–138, **2005**, doi: 10.4028/www.scientific.net/msf.480-481.133.

[42] E. Solórzano, M. A. Rodríguez-Pérez, J. A. Reglero, and J. A. De Saja, "Density gradients in aluminium foams: Characterisation by computed tomography and measurements of the effective thermal conductivity," *J. Mater. Sci.*, vol. 42, no. 8, pp. 2557–2564, **2007**, doi: 10.1007/s10853-006-1233-y.

[43] E. Solórzano, J. A. Reglero, M. Á. Rodríguez-Pérez, J. A. De Saja, and M. L. Rodríguez-Méndez, "Improvement of the foaming process for 4045 and 6061 aluminium foams by using the Taguchi methodology," *J. Mater. Sci.*, vol. 42, no. 17, pp. 7227–7238, **2007**, doi: 10.1007/s10853-007-1529-6.

[44] J. A. Reglero Ruiz, C. Saiz-Arroyo, M. Dumon, M. A. Rodríguez-Perez, and L. Gonzalez, "Production, cellular structure and thermal conductivity of microcellular (methyl methacrylate)-(butyl acrylate)-(methyl methacrylate) triblock copolymers," *Polym. Int.*, vol. 60, no. 1, pp. 146–152, **2011**, doi: 10.1002/pi.2931.

[45] M. Dumon, J. A. R. Ruiz, J. P. Sanz, M. A. R. Perez, J. M. Tallon, M. Pedros, E. Cloutet, and P. Viot, "Block copolymer-assisted microcellular supercritical CO2 foaming of polymers and blends," *Cell. Polym.*, vol. 31, no. 4, pp. 207–222, **2012**, doi: 10.1177/026248931203100402.

[46] B. Notario, A. Ballesteros, J. Pinto, and M. A. Rodríguez-Pérez, "Nanoporous PMMA: A novel system with different acoustic properties," *Mater. Lett.*, vol. 168, pp. 76–79, **2016**, doi: 10.1016/j.matlet.2016.01.037.

[47] M. Á. Rodríguez-Pérez, R. D. Simoes, C. J. L. Constantino, and J. A. de Saja, "Structure and Physical Properties of EVA/Starch Precursor Materials for Foaming Applications," *J. Appl. Polym. Sci.*, vol. 121, pp. 2324–2330, **2011**, doi: 10.1002/app.

[48] M. Á. Rodriguez-Perez, R. D. Simoes, S. Roman-Lorza, M. Alvarez-Lainez, C. Montoya-Mesa, C. J. L. Constantino, and J. A. de Saja, "Foaming of EVA/Starch Blends: Characterization of the Structure, Physical Properties, and Biodegradability," *Polym. Eng. Sci.*, **2012**, doi: 10.1002/pen.22046.

[49] A. Lopez-Gil, F. Silva-Bellucci, D. Velasco, M. Ardanuy, and M. A. Rodriguez-Perez, "Cellular structure and mechanical properties of starch-based foamed blocks reinforced with natural fibers and produced by microwave heating," *Ind. Crops Prod.*, vol. 66, pp. 194–205, **2015**, doi: 10.1016/j.indcrop.2014.12.025.

[50] A. López Gil, "Development of Environmentally Friendly Cellular Polymers for Packaging and Structural Applications . Study of the Relationship Cellular Structure-Mechanical Properties," University of Valladolid, 2016.

[51] L. O. Salmazo, "Cinéticas de espumación y control de la estructura celular en materiales basados en caucho natural y poliolefinas," University of Valladolid, 2015.

[52] J. I. Velasco, M. Antunes, O. Ayyad, J. M. López-Cuesta, P. Gaudon, C. Saiz-Arroyo, M. A. Rodríguez-Pérez, and J. A. de Saja, "Foaming behaviour and cellular structure of LDPE/hectorite nanocomposites," *Polymer (Guildf).*, vol. 48, no. 7, pp. 2098–2108, **2007**, doi: 10.1016/j.polymer.2007.02.008.

[53] C. Saiz-Arroyo, J. Escudero, M. A. Rodríguez-Pérez, and J. A. De Saja, "Improving the structure and physical properties of LDPE foams using silica nanoparticles as an additive," *Cell. Polym.*,

vol. 30, no. 2, pp. 63–78, **2011**, doi: 10.1177/026248931103000202.

[54] V. Bernardo, J. Martín-de León, E. Laguna-Gutiérrez, and M. Á. Rodríguez-Pérez, "PMMA-sepiolite nanocomposites as new promising materials for the production of nanocellular polymers," *Eur. Polym. J.*, vol. 96, no. August, pp. 10–26, **2017**, doi: 10.1016/j.eurpolymj.2017.09.002.

[55] E. Laguna-Gutierrez, J. Escudero, V. Kumar, and M. A. Rodriguez-Perez, "Microcellular foaming by using subcritical CO2 of crosslinked and non-crosslinked LDPE/clay nanocomposites," *J. Cell. Plast.*, vol. 54, no. 2, pp. 257–282, **2018**, doi: 10.1177/0021955X16681451.

[56] S. Pardo-Alonso, E. Solórzano, S. Estravís, M. A. Rodríguez-Perez, and J. A. De Saja, "In situ evidence of the nanoparticle nucleating effect in polyurethane-nanoclay foamed systems," *Soft Matter*, vol. 8, no. 44, pp. 11262–11270, **2012**, doi: 10.1039/c2sm25983d.

[57] S. Pardo-Alonso, E. Solórzano, and M. A. Rodriguez-Perez, "Time-resolved X-ray imaging of nanofiller-polyurethane reactive foam systems," *Colloids Surfaces A Physicochem. Eng. Asp.*, vol. 438, pp. 119–125, **2013**, doi: 10.1016/j.colsurfa.2013.01.045.

[58] S. Pardo-Alonso, E. Solórzano, L. Brabant, P. Vanderniepen, M. Dierick, L. Van Hoorebeke, and M. A. Rodríguez-Pérez, "3D Analysis of the progressive modification of the cellular architecture in polyurethane nanocomposite foams via X-ray microtomography," *Eur. Polym. J.*, vol. 49, no. 5, pp. 999–1006, **2013**, doi: 10.1016/j.eurpolymj.2013.01.005.

[59] P. Acuña, M. Santiago-Calvo, F. Villafañe, M. A. Rodríguez-Perez, J. Rosas, and D. Y. Wang, "Impact of expandable graphite on flame retardancy and mechanical properties of rigid polyurethane foam," *Polym. Compos.*, **2018**, doi: 10.1002/pc.25127.

[60] J. Pinto, "Fabrication et Caractérisation de Polymères Micro et Nano Cellulaires à partir de Polymères Nanostructurés à base PMMA," University of Bordeaux and University of Valladolid, 2014.

[61] B. Notario, "Fabricación y Caracterización de las Propiedades Físicas de Polímeros Nanocelulares : Transición de la Escala Micro a la Nano," University of Valladolid, 2016.

[62] J. Martín-de León, V. Bernardo, and M. Á. Rodríguez-Pérez, "Key Production Parameters to Obtain Transparent Nanocellular PMMA," *Macromol. Mater. Eng.*, vol. 302, no. 12, p. 1700343, **2017**, doi: 10.1002/mame.201700343.

[63] V. Bernardo, J. Martin-de Leon, J. Pinto, U. Schade, and M. A. Rodriguez-Perez, "On the interaction of infrared radiation and nanocellular polymers: First experimental determination of the extinction coefficient," *Colloids Surfaces A Physicochem. Eng. Asp.*, vol. 600, **2020**, doi: 10.1016/j.colsurfa.2020.124937.

[64] J. Martín-De León, V. Bernardo, and M. Á. Rodriguez-Perez, "Cyclic gas dissolution foaming as an approach for simultaneously reducing cell size and relative density in nanocellular pmma," *Polymers (Basel).*, vol. 13, p. 2383, **2021**, doi: 10.3390/polym13142383.

[65] J. Martín-de León, M. Jiménez, J. L. Pura, V. Bernardo, and M. A. Rodriguez-Pérez, "Easy-way production of highly transparent nanocellular polymers films," *Polymer (Guildf).*, vol. 236, **2021**, doi: 10.1016/j.polymer.2021.124298.

CHAPTER 2

STATE OF THE ART

Chapter 2. State of the Art

2.1 Introduction

This chapter provides a fundamental background for the understanding of this thesis by defining the main concepts, parameters and mechanisms employed along the manuscript, as well as a study of the state of the art by analyzing and gathering data from prior works regarding aerogels.

Therefore, it starts from the definition of aerogel, existing types thereof, the synthetic methods to produce them, the drying processes and the main parameters intended to describe their porous structures. Additionally, a revision of some properties of aerogels, studying the optical, mechanical and thermal properties is also herein supplied. Finally, the fields in which the main applications of these materials are framed are mentioned while explaining the fundamentals thereof.

2.2 Aerogels

2.2.1 Concept

Prior to the definition of aerogels, gels should be described. Gels are a structure of the matter consisting of a three-dimensional sponge-like network surrounded by a fluid. From this general meaning, several daily products fit the definition, from gelatin to gel glue. Depending on the solvent filling the gel pores, these are known as hydrogels (water), alcogels (alcohol), oleogels (non-polar organic solvent) or aquagels if the solid phase is a colloidal network and the solvent is water [1].

The definition of aerogels has ever caused a great controversy and it is still being a challenge. The classic definition of aerogels was firstly given by Kistler (1931) [2] who defined as those gels in which the liquid phase is substituted by air, with slight shrinkage of the solid structure. In 1987 the International Union of Pure and Applied Chemistry (IUPAC) [3] specified that the pores forming the structure must be micropores, ie. smaller than 2 nm. Owing to the extremely low pore size reported by that statement, this definition has been considered incorrect by the scientific aerogel community and it has been modified along the time by several authors (see **Table 2.1**, which collects different definitions of aerogels).

Since the slight shrinkage mentioned in the definitions was not quantified, it was commonly accepted that aerogels should be obtained by supercritical drying (process described in **section 2.2.4**) as explained by Brinker and Scherer in 1990 in the book *Sol-Gel Science: The Physics and Chemistry of Sol-Gel Processing* [4]. Nevertheless, advances on drying technology led to different drying techniques that produced moderate shrinkage of the gel structure and, thus, aerogels definition was once again not accurate.

It was in 2006 when Hüsing and Schubert [5] returned to a definition more similar to that of Kistler making reference to the non-strongly damaged structure when the liquid is extracted from the gel. In this way, the multiple sizes of pores present in these materials, which are typically meso- (2 – 50 nm) and macro- (> 50 nm) pores are included in the definition. More recently, in 2010, Leventis et al. [6] proposed a more extensive definition of aerogel. The explanation was based on their open porous structure, formed by the dispersion of a gaseous phase along the solid network. This definition was then completed according to Smirnova and Gurikov [7]. The latter gave a deeper insight about their solid network, stating

that it is formed by loosely packaged particles or fibers which lead to a material with really low density and high surface area. The same year, Eychmüller [8] specified a maximum pore size of few hundred nanometers and a minimum porosity of 95 %.

Table 2.1. Definitions of aerogel along the time.

Year	Author	Definition
1931	Kistler	"gels in which the liquid has been replaced by air, with very moderate shrinkage of the solid network"
1987	IUPAC	"gel comprised of a microporous solid in which the dispersed phase is a gas"
1990	Brinker and Scherer	"if the wet gel is placed in an autoclave and dried under supercritical conditions (…) the product is called an aerogel"
2006	Hüsing and Schubert	"materials in which the typical pore structure and network are largely maintained when the pore liquid of a gel is replaced by air"
2010	Leventis	"an open nonfluid colloidal network or polymer network that is expanded throughout its whole volume by a gas, and is formed by the removal of all swelling agents from a gel without substantial volume reduction or network compaction"
2017	Smirnova and Gurikov	"an open colloidal or polymeric network consisting of loosely packed, bonded particles or fibers that is expanded throughout its volume by a gas and therefore exhibits very low density and high specific surface area"
2017	Eychmüller	"a solid with meso- and macropores with diameters up to a few hundred nanometers and a porosity of more than 95% in which the dispersed phase is a gas"
2021	Ratke and Gurikov	"aerogels are open porous nanostructured solids obtained from a sol–gel process, irrespective of the way a wet gel is dried (…) if the majority of pores are in the mesoporous range, meaning the pores are mostly below 50 nm"

Nowadays, the scientific community continues trying to find an accurate definition for these exceptional materials and the IUPAC definition might be changed [9]. Very recently, in 2021, Ratke and Gurikov defined in their book *The Chemistry and Physics of Aerogels: Synthesis, Processing, and Properties* [10] aerogels as "open porous nanostructured solids obtained from a sol–gel process, irrespective of the way a wet gel is dried (…) if the majority of pores are in the mesoporous range, meaning the pores are mostly below 50 nm". In this way, it excludes porous materials made by foaming, micelles or templating that contain pores mainly in the macroscale. This is currently the preferred definition by the aerogel community, and it will be used along this thesis.

2.2.2 Types of aerogels depending on the matrix

Aerogels can be obtained in the form of monoliths, granulates, or powders. The main classification is based on the chemical nature of the solid network:

- **Inorganic aerogels:** the inorganic aerogels, par excellence, are silica aerogels (SiO_2 aerogels) which have been the most explored from the very beginning. However, several inorganic skeletons are also able to produce aerogels from a variety of transition and main group metal oxides, such as metal oxides obtained from alumina [11], titania [12], zirconia [13], vanadium [14], chromium [15], iron [16], molybdenum [17], manganese [18], nickel [19] and cadmium or even multicomponent oxides [20]–[22].
- **Organic aerogels:** these aerogels are synthesized by polymerization of multifunctional monomers in dilute solution. Some of the typical organic aerogels are synthetic aerogels like resorcinol/formaldehyde (RF) [23], melamine/formaldehyde (MF) [24], phenol – furfural (PF) [25], polyacrylamides [26], polyacrylates [27], polyisocyanates [28], polyimides [29], polystyrenes [30], polyvinyl alcohol (PVA) [31], epoxies and polyurethanes [32]. Some of these organic aerogels can be converted into carbon aerogels by pyrolysis [33], [34]. Other carbon-based aerogels (although can be considered as inorganic) are graphite [35], graphene [36], and carbon nanotube aerogels [37]. Additionally, there exist bio-based aerogels which present higher biosafety, and biodegradability than the previously mentioned aerogels. They are based on proteins or polysaccharides such as agar [38], alginate [39], cellulose [40], chitosan [41], starch [42], lignin [43], pectin [44] or collagen [45].
- **Inorganic/Organic Hybrid Aerogels:** some synergistic effects have been found when combining inorganic and organic materials [46]. This strategy can be carried out by chemical bonding during the synthesis process or by interpenetration or doping of the aerogels. The most common hybrid aerogels are silica aerogels containing organic compounds such as alkoxides or silica precursors with alkyl, aryl, and alkenyl [47], [48] to improve some properties such as their hydrophobicity or mechanical strength.

2.2.3 Synthesis procedure

The main method for aerogel synthesis is the well-known sol-gel process. In general terms, gelation process consists on the following steps:

1. Precursors are dissolved into the corresponding solvent or mixture of solvents.
2. After a certain time in which precursors start to react from monomers to oligomers, then to polymers and, finally, forming particles until a colloidal sol is formed, consisting on a system in which particles between 1 nm and 1 μm are dispersed [1]. These particles exhibit Brownian motion, i.e. particles are randomly moving and collide between them [49], and can also move by sedimentation or solvent-driven encountering with other particles and forming particle clusters.
3. Gelation occurs. This process is defined by IUPAC as the "process of passing through the gel point to form a gel or network" and the gelation point as the "point of incipient network formation in a process forming a chemical or physical polymer network." In this step, polymerization and crosslinking of polymer chains take place forming a tridimensional solid network, typically formed by particles or fibers, which is soaked in the initial solvent. It is worth noting that the gelation point, taken as the time when the gel is occupying the whole volume and it does not flow, is not an accurate time and

may change depending on the measuring technique (rheology, viscometry or visually).

4. In order to achieve an aerogel, the obtained gel should be dried (by eliminating the solvent between particles and the solvent inside each particle) while avoiding damaging the porous structure. The different drying methods are described in the following section (**Section 2.2.4**).

These steps are represented in **Figure 2.1**:

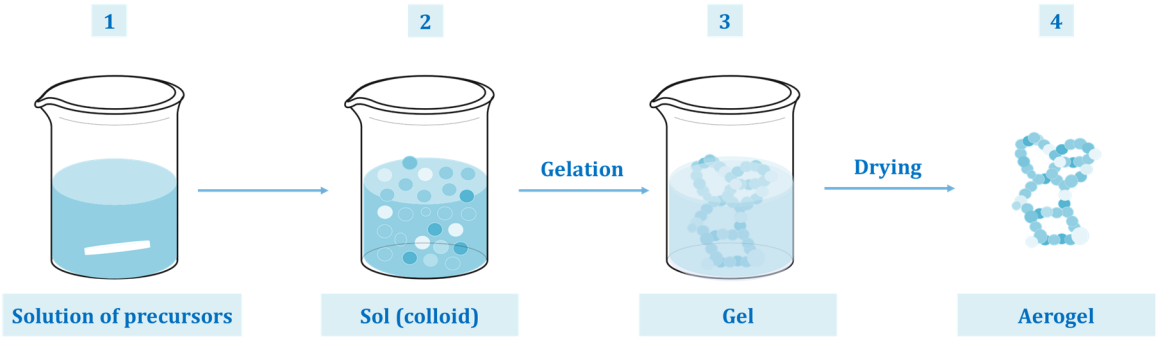

Figure 2.1. Sol-gel procedure.

In summary, the sol-gel process is based on a progressive chemical linking (by polymerization or condensation) of the initial precursors. These precursors initially form small particles, and, after the subsequent creation of chemical bonds and particles aggregation, a solid network is formed, whose pores are completely filled with a solvent.

Gels can also be obtained from a preformed colloidal suspension which undergoes an aggregation process leading to phase separation and to the consequent sedimentation, what is known as flocculation. The main difference lays on the chemical bonds. In the traditional sol-gel process, covalent bonds are formed and the obtained gel is usually monolithic, whereas by the flocculation procedure, in which particles are joined by weak physical interactions, flake-like gels are usually obtained [8].

In the 1980s and 1990s two diffusion models were reported in order to describe the transition from colloidal sol to gel: the diffusion-limited aggregation of particles model (DLA), and the diffusion-limited aggregation of clusters model (DLCA) [50]–[52]. These models allowed to study the aerogels fractality and fractal patterns numerically in order to understand the network formation. They are based on the statements that the Brownian diffusion of particles leads to build aggregates and clusters, giving rise to fractal structures. Starting from a seed particle that is fixed in the space, additional particles randomly moving in all possible directions are added. Once a particle collides, the seed particle will be attached to it and fixed at that position (see **Figure 2.2**). This process continues until the formation of branched spanning clusters, which can be considered as the onset of gelation.

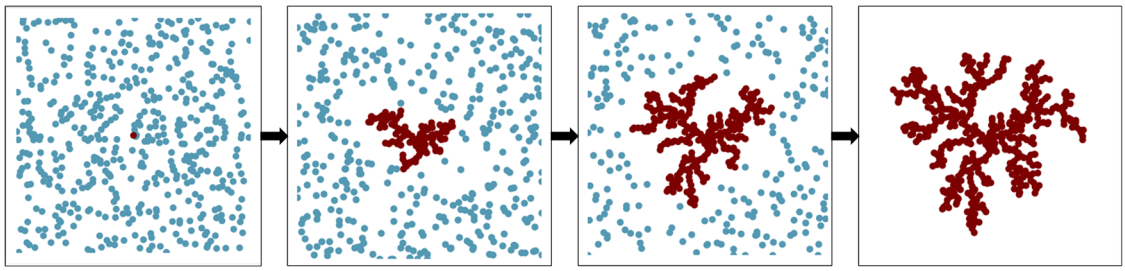

Figure 2.2. DLA theory for 500 particles starting from a seed particle in the center (red particle). Images created by the online tool developed by Sayama H. [53].

One of the crucial aspects in the aerogel synthesis is the reaction kinetics, that strongly affect the composition and structure of the final aerogels. It is evident that a higher amount of catalyst leads to faster chemical reactions, existing several mechanisms depending on the reaction kinetics:

Smoluchoswki [54] described a competition between the particles **aggregation** by the Brownian motion and **sedimentation** mechanisms caused by the action of gravity. The conclusions are that, at short times, the Brownian diffusion dominates, while for larger reaction times gravity will have a significant effect and particles will follow a Boltzmann distribution with height. Mason and Weaver [55] carefully studied these coupled mechanisms using the previously described DLCA approach. They concluded that large particles will sediment at the bottom of the container, not having thus time to aggregate, whereas the smaller ones will not settle but aggregate. Therefore, small particles should be obtained to avoid sedimentation.

The diameter of the gel particles depends on the reaction conditions. Factors such as the catalyst content, pH of the reaction medium, precursor ratio, or gelation temperature will influence the gelation mechanisms and, therefore, the aerogel network formation [56]. Dixit et al. [57] achieved fine tunability of the synthesis of silica nanoparticles through the control of the reaction kinetics. The authors were able to halt the reaction at a certain time by modulating the reaction medium. The addition of a huge excess of water against ethanol allowed to remove the unreacted silica precursor (TEOS). Particles ranging from 50 nm to 400 nm were obtained with high monodispersity, reaching higher particles when the polymerization time was larger.

Additionally, for silica aerogels, which are formed through hydrolysis and condensation reactions at acidic and basic conditions, respectively, the pH of the reaction medium will control the growth of the tridimensional network. Under acidic conditions, more hydroxyl groups will be available for siloxane bond formation by the so-called monomer-cluster addition [10]. In this case, the aerogel network tend to be open forming branched polymeric-like structures [58], [59]. In contrast to this situation, under basic conditions, the nucleophilic attack occurs preferably at the central silicon atoms, leading to compact structures. The structure disposition is not only the main parameter changing with the pH, but the hydrophobicity is affected by the -OH or alkoxy groups present on the final composition, which also depends on the pH and reaction rate.

Keysar et al. [60] studied the particle aggregation in alumina aerogels, observing that the size of the aerogel clusters was strongly influenced by the amount of acid added during the gelation step. The addition of nitric acid reduced the interparticle repulsion, allowing the sol particles to connect at an early stage and, therefore, obtaining smaller particles.

These are some examples which show the complexity of the gelation process, which is affected by numerous variables triggering different growing mechanisms. This fact makes difficult to control the reaction kinetics of each system.

Commonly further steps are added after the gelation process. Once gels are produced, they usually undergo an **ageing** process in which, due to the presence of unreacted monomers, chemical reactions still running strengthening the solid network. One of the most common mechanisms occurring when new particles are formed is the Ostwald ripening or coarsening [61]. This mechanism (summarized in **Figure 2.3**) consists on neck-joining between the small particles created during ageing and the bigger ones constituting the gel network (**Figure 2.3 a**). Additionally, particles on the surface can be dissolved and precipitate on the interparticle necks enlarging their size.

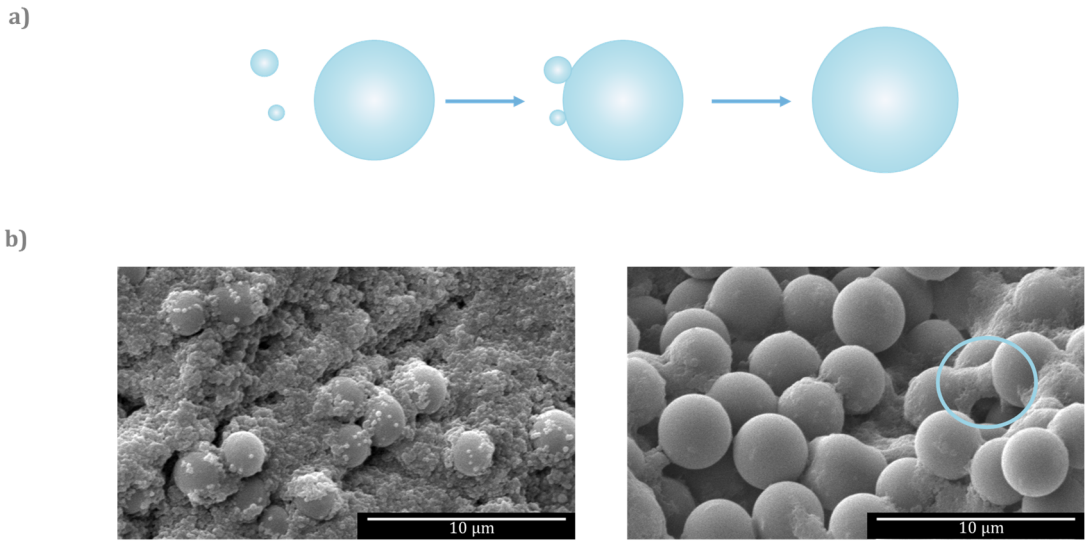

Figure 2.3. a) Scheme of the Ostwald ripening mechanism, b) Example of scanning electron micrographs of an aerogel produced during this thesis (catalyst Dabco® T) where Ostwald ripening mechanism is taking place.

Figure 2.3 b shows experimental examples in which the newest small particles are deposited into the surface of the bigger ones (left image) or strengthening the interparticle necks (right image).

Another additional step that is usually performed is a **washing and solvent-exchange**. The former consists on washing out the non-reacted chemicals, whereas the latter allows changing, by diffusion, the solvent placed into the gel pores by other solvent in which the monomers are less soluble, or with better physical and toxicological properties for the subsequent drying step. Sometimes both processes can be performed in a single step.

2.2.4 Drying methods

As previously mentioned in the definition of aerogel, only slight shrinkage of the gel structure should occur during drying, in order to maintain as much as possible the porous structure. This critical step has promoted the development of different drying techniques to achieve the elimination of the liquid solvent while avoiding shrinkage. Most of the controversy with the aerogel definition lays on the drying method, since several authors stated that only those gels which are dried under supercritical conditions are named aerogels. Following this idea, dried gels have been traditionally labeled according to the employed method for drying, as explained in **Figure 2.4.**:

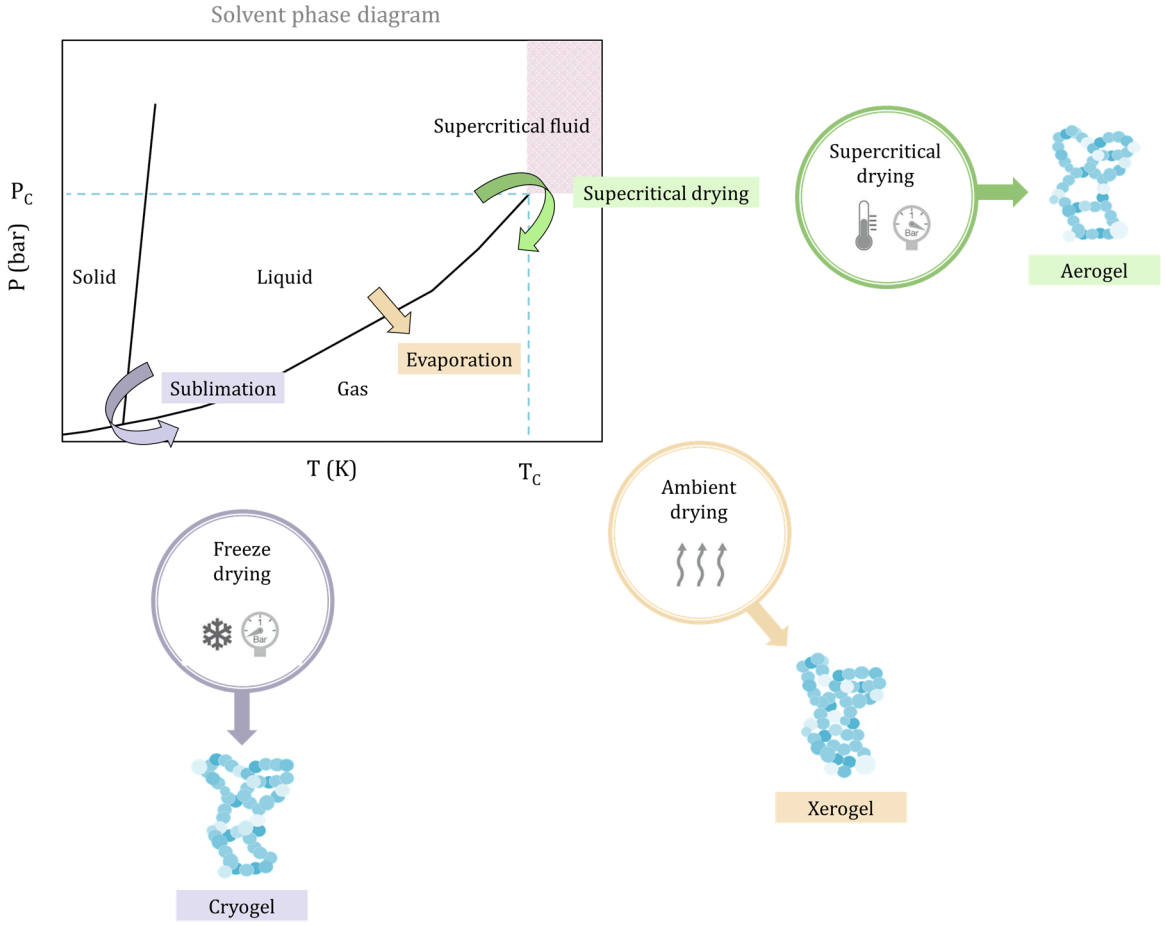

Figure 2.4. Different drying methods and final product names.

This scheme shows the possible ways to obtain a gaseous phase surrounding the pores starting from the initial liquid state. Each of the different drying techniques are described in detail in the following subsections:

Ambient drying

The fundamentals of the process are to increase the temperature at ambient pressure conditions to promote solvent evaporation, so a phase change of the solvent molecules from liquid to gas phase occurs. The basic issue are the capillary forces performed by the pore liquid meniscus, as displayed in **Figure 2.5.**, and the consequent pressure gradient induced by these forces, which contributes to the shrinkage of the structure. This process follows the Young-Laplace equation [62]:

$$p_c = \frac{2\,\sigma_{LG}\cos\theta}{R} \qquad (2.1)$$

Where the capillary pressure (p_c) is described by the interfacial tension liquid-gas (σ_{LG}), the radius of the cylindrical pore (R = d/2) and the wetting angle between the liquid and the pore wall (θ).

These forces (which may reach 100–200 MPa [63]) could lead to a pore collapse. This capillary pressure increases with the reduction of the pore size, being significantly higher (1000 times) for pores in the nanoscale (nm) than those in the microscale (μm).

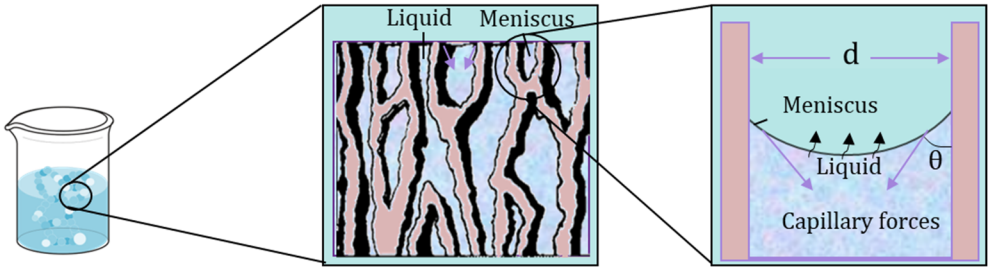

Figure 2.5. Scheme of the capillary forces acting during solvent evaporation.

The material obtained by this method is called xerogel, as derived from the Greek word '*xeros*', meaning dry. These materials usually have a higher density, thus, lower porosity and higher thermal conductivity, than the so-called aerogels.

This technique is very interesting because allows a significant reduction of the final cost of the production process, but it could lead to moderate shrinkages when optimizing the drying conditions and finding the most favorable solvent. Some possible strategies to reduce the final shrinkage are exchanging the solvent, ageing the gel to increase its strength (**section 2.2.3**), adding surfactants to reduce the surface tension of the liquid [64], or performing chemical modifications on the gel surface. The latter is commonly used for silica aerogels [65]–[67].

Freeze drying

Freeze drying technique was developed aiming to avoid the previously explained capillary forces. It consists on freezing the gel fluid and evaporating it along the sublimation line (**Figure 2.4**). In this way, by not existing a liquid-solid interface, capillary pressure will not affect the gel structure and, therefore, volume shrinkage could be lower.

The overall process starts by lowering the temperature below the melting point. Generally, the freezing temperatures are between -50 and -85 °C. Several nuclei can be created and, when reaching a critical size, the solid phase starts to grow, since the volume free energy of the solid is lower than that of the liquid. This nucleation might occur as a consequence of a lower interfacial energy caused by impurities in the liquid or simply due to the pore walls. It is common that the growing solid forms perpendicular lines in agreement with the isotherms of the thermal field. The size of the crystals depends on the freezing rate, being in general larger for lower freezing rates [68].

Once the solvent is completely solidified, several drying steps are carried out. First, a primary drying in which a high percentage of the overall solvent is sublimated by increasing the temperature and decreasing the pressure. Additional drying steps can be performed with the purpose of removing the remaining solvent that has not been previously frozen during the primary phase. The temperature now is usually raised to higher temperatures than in the previous drying procedure [69]. Both parameters, temperature and vacuum pressure should be optimized in order to control the drying rates that influence the aerogel textural properties. A simple scheme of the process is represented in **Figure 2.6**.

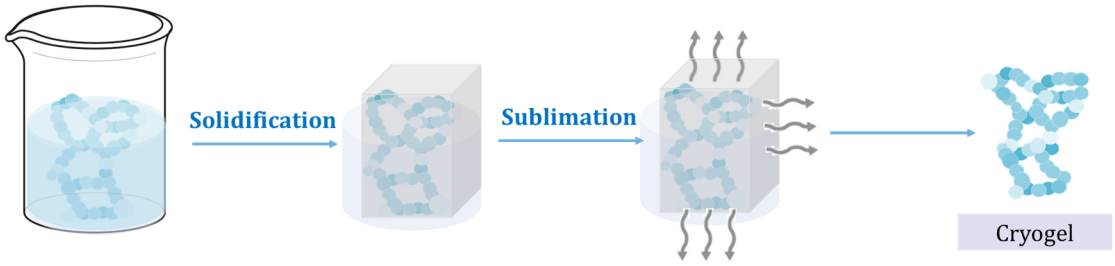

Figure 2.6. Freeze drying process.

Depending on the pore size, supercooling below the freezing point is sometimes needed to start the solidification process [70]. This supercooling step (ΔT) is dependent on the pore size, as expressed by the following equation:

$$\Delta T = \frac{-2\,\sigma_{SL}\cos\theta}{r_p\,\Delta S_m} \qquad (2.2)$$

With ΔS_m as the melting entropy, the wetting angle between the liquid and the pore wall (θ), the interfacial tension solid-liquid (σ_{SL}) and r_p the pore radius.

It should be outlined that the whole process is more complex than what has been summarized, since not only consists on several drying steps to ensure the complete removal of the solidified solvent, but also the search for the optimum solvent. The major disadvantages of this method are the formation of crystals which may damage the gel network and the heterogeneity of the solidification process, which begins in the largest pores being those likely to deform the pore network. The materials obtained from this process are called cryogels, and usually tend to show high densities (> 250 kg/m^3) [71] because of the induced pore collapse. Nevertheless, the price of the aerogels obtained by this method is generally affordable, estimating to be around 30 €/m^2 for 5 mm thickness on an industrial scale [72].

Supercritical Drying

Undoubtedly supercritical drying is the most explored and the drying technique that has attracted more attention to obtain aerogels. The procedure is based on transforming the liquid contained in the gel pores into a supercritical fluid (high temperature supercritical drying HT – SCD) or replacing the solvent by supercritical carbon dioxide (sc-CO_2) (low temperature supercritical drying LT – SCD).

In a phase diagram (**Figure 2.4**), the liquid-vapor equilibrium line ends at the critical point. Such point marks the beginning of a region named supercritical fluid. This state of the matter is characterized by a high diffusivity, low viscosity and low surface tension in comparison with a typical liquid, as well as a high density in comparison with an ideal gas [73]. Therefore, it presents an intermediate behavior between liquid and gas. The key of using supercritical fluids is avoiding capillary forces from the liquid-vapor interface (ambient drying), which is not present in this state, since it presents zero surface tension and, thus, there is not a strong shrinkage due to capillary forces.

Different fluids can be employed at their supercritical state, but by far the most commonly used is sc-CO_2 because of its non-toxicity, non-flammability, cost-effectiveness and, mainly, their mild critical conditions of pressure and temperature and its GRAS status (Generally Recognizes As Safe) according to the CFR – Code of Federal Regulations. Other alternative fluids have been gathered in **Table 2.2**. Nevertheless, their critical point occurs at higher temperatures and pressures (water, ethanol, acetone), or are hazardous (NH_3, N_2O) and flammable (methanol).

Table 2.2. Critical properties of different fluids.

Fluid	Critical pressure/MPa	Critical temperature/ K
CO_2	7.4	304
NH_3	11.3	405
Water	22.1	647
N_2	3.4	126
EtOH	6.4	517
Acetone	4.7	508
MeOH	8.1	512
N_2O	7.3	306

Nowadays, the low temperature supercritical drying (LT – SCD) is widely adopted. The procedure depends on the drying setup which is constituted by robust stainless-steel vessels but always follow similar principles. In general terms, the wet gel is placed into the autoclave and covered with the corresponding solvent to prevent preliminary evaporation and, as a consequence, shrinkage. Then, CO_2 is fed into the vessel in a continuous way or in batches (depending on whether the process is continuous or static). Temperature and pressure are increased until reaching the critical point. It has to be taken into account that, owing to the presence of an additional solvent into the autoclave, the supercritical conditions of the mixture slightly differ from those of the sc-CO_2 (for instance for ethanol or acetone mixed with CO_2 the supercritical mixture can be obtained around 313 K and 8 MPa [10]). Then, the mixture of the solvent and the CO_2 is progressively extracted from the reactor while clean carbon dioxide is fed to keep the pressure constant. It is crucial that during drying significant pressure changes should not occur in order to avoid deformations of the gel. This

mixture can be sent to an expander where, due to the pressure drop, the liquid (solvent) and gas (CO_2) can be separated. This process continues until extracting all the solvent and, thus, drying completely the wet gel. The last step of the process is removing the pressure of the vessel. This process has to be done carefully and extremely slowly in order to avoid significant pressure gradients that could deteriorate the aerogel porous structure.

There exist several critical parameters in the SCD process. The **operating conditions of temperature and pressure** should be chosen carefully, as well as the **solvent** used for drying, that must be miscible with CO_2. Each systems requires the use of an "optimum solvent" that leads to the lowest shrinkage and, thus, to lower densities and higher surface areas. Some aspects to consider when selecting a drying solvent are:

- Availability and price
- Solvent consumption and recyclability
- Minimum risks (health, safety and flammability)
- Critical point of solvent-CO_2 mixture

Additionally, the **aerogel geometry and size** will significantly affect the **drying time**. The cycle time will depend mainly on the sample thickness since, at a constant pressure and temperature, the diffusion coefficient remains constant, and the time for the solvent replacement is related to the sample diameter by [74]:

$$\frac{t_2}{t_1} = \left(\frac{d_2}{d_1}\right)^2 \qquad (2.3)$$

Where t is the required time, and d the sample diameter.

Several models have been developed to optimize the drying conditions, as such reported by Selmer et al. [75], which evaluates the mass transport for the SCD of gels in different shapes and dimensions for the system CO_2/ethanol. The authors defined the minimal drying time (t_{min}) of each system as depending on the ratio between porosity Π and tortuosity τ_g of the gel, as indicated in Equation 2.4:

$$t_{min} = \frac{1}{K_{eff}} \cdot \frac{\tau_g}{\Pi} R^2 \qquad (2.4)$$

Being K_{eff} and R the effective diffusion coefficient and gel size, respectively.

The sample geometry also plays a fundamental role, since monoliths will usually require a batch drying process, while beads and small particles allow a possible continuous process. Therefore, increasing production of aerogels to a larger scale requires an optimization of the drying time.

Supercritical drying has been considered the best method in order to preserve the gel structure. Thus, it has been widely known as the main process to obtain aerogels, since it allows obtaining low density aerogels with very small pore sizes and great specific surface areas. The main disadvantage of this process is the long times usually required to obtain a totally dry gel, what increases the cost of the product (15–50 €/m² for 5 mm thickness are estimated on an industrial scale [76]–[78]).

2.2.5 Porous structure

The porous structure of aerogels is responsible for most of their exceptional properties. According to this feature, aerogels can be classified into particulate aerogels or fibrillar aerogels, as schematized in **Figure 2.7 a** and **b**, respectively.

Most of the aerogels present a particulate structure formed by interconnected chemically bonded particles. During the polymerization, primary particles of few nanometers are formed. Then, these particles coarsen or joint together by different mechanisms such as Ostwald ripening (**section 2.2.3**), giving rise to larger secondary particles, that are the ones typically detected by SEM (**Figure 2.7 c**).

Therefore, the porous structure in these materials has two different contributions: the micropores between the primary particles, that can be very small in size (a few nm), and the open mesopores between the particulate skeleton, forming channels and connecting the whole structure (**Figure 2.7 c**). These open pores are typically larger in size, (tens or hundreds of nanometers).

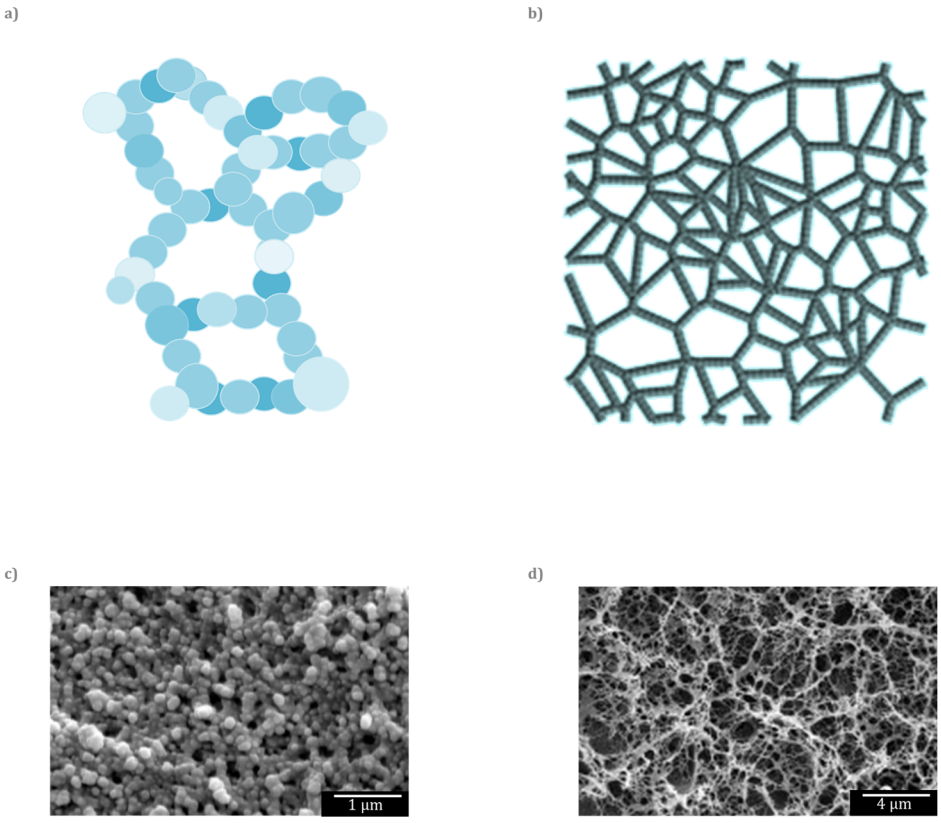

Figure 2.7. a) Scheme of an aerogel formed by particles, b) Scheme of a fibrillar aerogel, c) SEM micrograph of a silica aerogel [79], d) SEM micrograph of a cellulose aerogel [80].

Another type of porous structure found mainly in biopolymeric aerogels (for instance cellulose aerogels) is a fibrillar structure (**Figure 2.7 b** and **d**). These fibrils form a random three-dimensional (3D) network with cross points formed by covalent bonds which differentiate them from dispersed fibers with non-chemically-bonded nodes.

2.2.6 Parameters defining an aerogel

In this section, the most common macroscopic and microscopic parameters describing aerogels are defined. **Figure 2.8** summarizes the main structural features of a particulate aerogel and the parameters needed to characterize them.

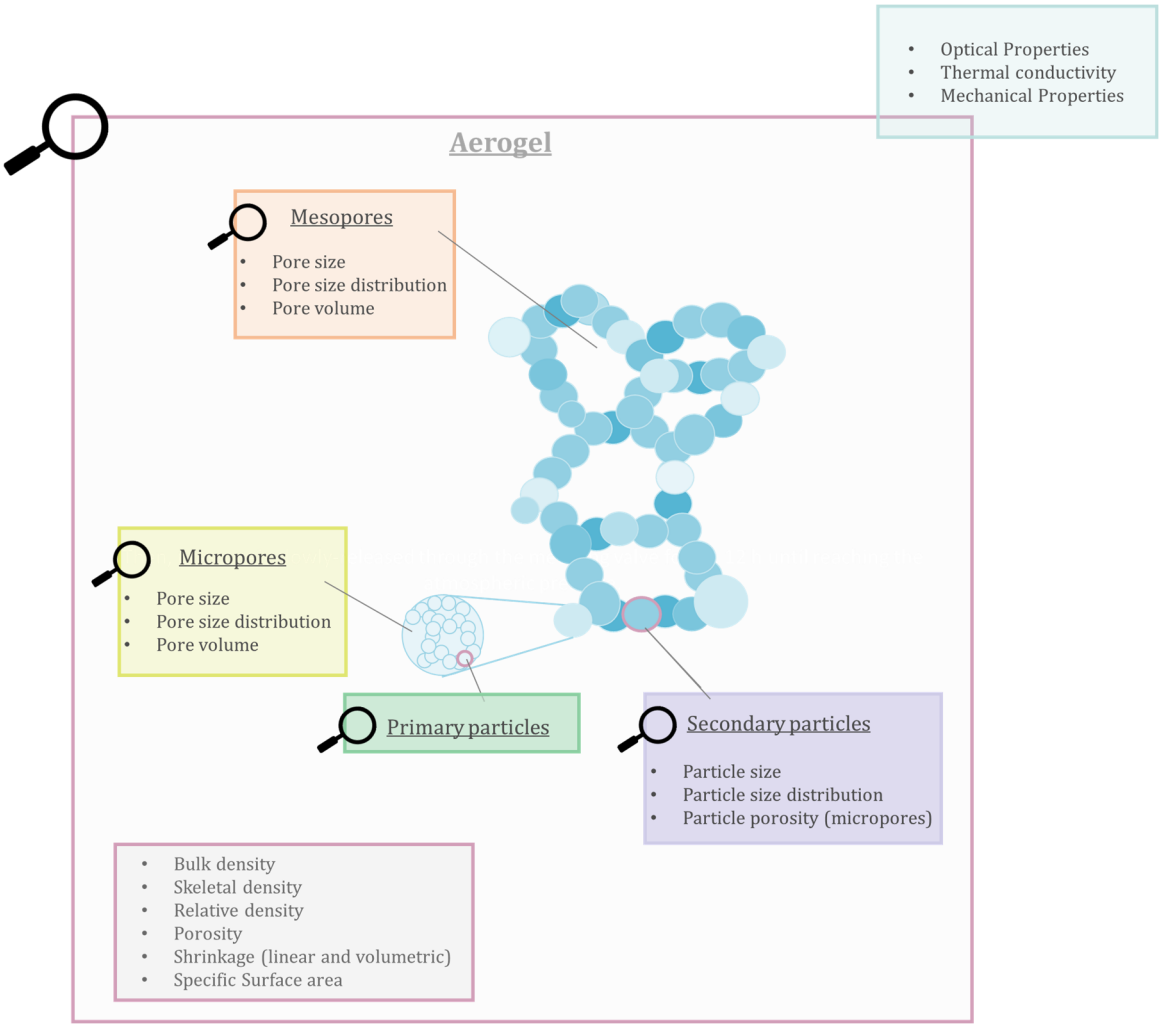

Figure 2.8. Parameters to characterize each of the structural features of aerogels.

Macroscopic parameters

Gelation time (t_g)

Gelation time or gel time is a parameter which accounts for the time when the gel has been formed. The viscosity of the initial sol increases progressively during the sol-gel transition until reaching the maximum at the gelation time. One of the possible simple measuring procedures used nowadays is by tilting the container where the sol is being produced and, once the gel does not flow anymore and it is not deformed, taking that time as gel time. Additionally, some sol-gel transitions induce a change on the solution appearance when the polymerization reaction takes place, which usually turn rather cloudy. So, this is another way to estimate the gel time.

Owing to the difficulty of measuring gelation time, it is typically taken as a qualitative (not quantitative) measurement, useful to make only coarse comparisons between samples.

Bulk density (ρ_b)

Bulk or geometrical density (ρ_b) is obtained as the ratio between the aerogel mass and the aerogel volume. It is a macroscopic descriptor of aerogels, and it is one of the most relevant parameters when defining these materials.

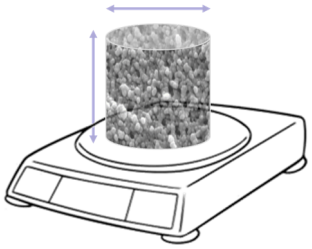

Figure 2.9. Geometrical density (ρ_b).

Skeletal density (ρ_s)

Solid density or skeletal density (ρ_s) gives the density of the solid backbone of the aerogel. By measuring the gas volume present in the sample (by means of a pycnometer), the solid volume can be subtracted and, therefore, its density can be calculated. Each matrix has a typical range of solid densities, since this a parameter inherent of each raw material.

Relative density (ρ_r)

Relative density (ρ_r) describes the volumetric solid fraction which is present in the aerogel. It can be calculated as the ratio between the geometrical density and the skeletal density, as shown in **Equation 2.3**:

$$\rho_r = \frac{\rho}{\rho_s} \qquad (2.5)$$

Porosity (Π)

Porosity (Π) describes the volume fraction of the gas phase dispersed along the sample. It is a characteristic parameter describing aerogels, since these materials usually present high porosity values, typically above 95 %. It can be calculated by subtracting the volumetric solid fraction from 1:

$$\Pi = 1 - \rho_r \qquad (2.6)$$

Shrinkage (S)

The volumetric (S_v) and linear (S_l) shrinkages are typically calculated to determine the volume contraction that occurs during the drying process as a consequence of the pore collapse and damage of the porous structure. These parameters are key when developing a synthesis route and the selection of the corresponding solvents for the synthesis and drying steps, as well as the effectiveness of the solvent exchange step. It is typically larger for ambient dried aerogels than for the supercritical counterparts, although shrinkage is always present and can reach values as high as 80% [81], [82]. These parameters are calculated by taking into account the initial and final diameters (S_l) (for cylindrical samples) or volumes (S_v) of the gel and aerogel, respectively.

$$S_l(\%) = \left(1 - \frac{d}{d_0}\right) \cdot 100 \qquad (2.7)$$

$$S_v(\%) = \left(1 - \frac{V}{V_0}\right) \cdot 100 \qquad (2.8)$$

Where d is the final diameter of the sample after drying, d_o is the diameter of the gel before drying, V is the final volume of the sample after the drying and V_o is the diameter of the gel before drying.

These are important parameters related to the sample density, since the higher the shrinkage the higher the bulk density of the aerogel. Sometimes a reverse shrinkage called 'springback effect' is observed when the forces compressing the sample have been released and the structure can be extended at to certain extent.

The previously described parameters are macroscopic descriptors of the aerogel samples. However, a detailed analysis of the microscopic features of the solid and gaseous phases are also necessary to understand their influence on the final properties.

Specific surface area (S_{BET})

One important characteristic of aerogels is their surface area per unit volume. This parameter has an inverse dependence with the particle size forming the 3D network, since smaller particles will lead to a larger surface area. Therefore, owing to the small particles forming these materials that are generally in the nanoscale, the specific surface areas of aerogels are normally large. Feng et al. [83] reached high specific surface areas of 945.8 m^2/g for silica aerogels synthesized from rice husk ash and dried under ambient conditions. Similar specific surface areas were obtained by Ren et al. [84] for hybrid silica aerogel containing polyhedral oligomeric silsesquioxane (POSS), with values comprised between 945 and 1283 m^2/g. Organic aerogels also show high specific surface areas. A summary of the typical specific surface areas for aerogel produced from different matrixes is gathered in **Table 2.3**:

Table 2.3. Typical specific surface areas for different aerogels. Data obtained from references [5], [85]–[87] where R-F is resorcinol formaldehyde and M-F melamine formaldehyde.

Aerogel matrix	Specific Surface Area (m^2/g)
Silica	100 - 1600
Cellulose	10 – 975
R-F	350 – 900
M-F	875 – 1025
Metal oxides	81 – 785
Carbon	600 – 800
Polyurethane	10 – 800

This parameter is typically measured by the nitrogen adsorption technique (see **Chapter 3**) or Small Angle Neutron Scattering (SANS).

Additional parameters can be extracted from the nitrogen sorption measurements such as the pore volume, the total area in pores, or the nitrogen quantity absorbed per unit mass that complement the structural characterization. These parameters are explained in the following sections.

Microscopic parameters

As displayed in **Figure 2.8.** Parameters to characterize each of the structural features of aerogels.secondary particles conforming the skeletal network are composed by smaller primary particles. The diameter of these secondary particles is a crucial parameter when characterizing aerogels, since it will affect the specific surface area of the sample and, therefore, the final properties. The distribution of these particles along the sample volume leads to the formation of branched pores that usually are in the nanoscale. In addition to these interparticle pores, smaller micropores can be found inside the secondary particles (filling the space between the primary particles). Owing to the extremely small size of the aerogel pores, the difficulty of measuring their volume and size becomes notable. In the following sections, these parameters are defined and the common techniques for their characterization are explained.

Particle size ($\phi_{particle}$)

The size of the particles (or fibers) forming the backbone skeleton has a strong influence on the aerogel characteristics such as the size of the pores between them, the specific surface area, their optical properties, or the heat transfer through the solid phase. This parameter can be measured through the scanning electron micrographs and by an adequate software that allows measuring the particle contour and determine the average diameter (**Figure 2.10 a**). As expected, the accuracy of this measurement lies on the visualization technique, which requires a high resolution. The mean particle size depends strongly on the solvent system used for gelation, the pH of the reaction medium, the attractive or repulsive interactions between particles, and the aggregation mechanisms that take place during that process (Ostwald ripening).

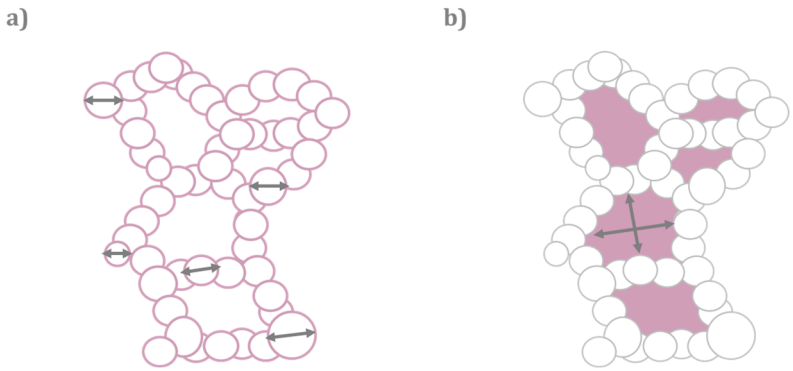

Figure 2.10. Scheme of the particle size and pore size measurements.

It is also worth mentioning that the homogeneity or heterogeneity of the particles affects the aerogel performance. Therefore, the particle size distribution is usually calculated through the particle size measurements.

Pore size (ϕ_{pore})

The structure of an aerogel differs significantly from a conventional micro- or nano-cellular foam, what creates great difficulties for analyzing their porous structures. The main method to characterize the gas phase of the aerogels is by means of the pore size, pore size distribution, and pore volume, i.e. the total gas volume present in the aerogel. Nitrogen sorption technique is commonly used for their measurement, and the employment of the well-known Barret-Joyner-Halenda (BJH) method allows to estimate a pore size value (**Figure 2.10 b**) from the desorption curve. This method makes some assumptions that are not entirely accurate, like considering the aerogel pores as cylinders and the application of the Kelvin equation. The homogeneity of the pore size distribution will determine whether there are homogeneous or heterogeneous pores along the aerogel.

As it can be seen in **Figure 2.8**, a double pore size can be found even for the most homogeneous aerogels. The presence of micropores in combination with meso- or even macropores is a challenge when a pore size value has to be given. Additionally, it has to be noted that the BJH evaluation can only be applied for pores smaller than ca. 100 nm, since capillary condensation occurs from this size on. The main problem lies on measuring the pore volume, since the nitrogen sorption technique does not always provide the correct value and there exists a significant volume fraction (of pores above 100 nm) that is generally underestimated. Authors such as Diascorn et al. [88] employed the mercury porosimetry technique as alternative for measuring the pore size of polyurethane aerogels. By varying the catalyst content, the average pore size of these samples sifted from 15 – 45 nm obtained for the lowest catalyst content to 30 – 210 nm for the highest content. Nevertheless, this technique is not always valid for aerogels, since their commonly brittle structure could be damaged by the mercury intrusion at high pressures. Pirard et al. [89] experimentally demonstrated that aerogels were compacted and pressurized under mercury, causing the destruction of the inner pores. The proposed solution to evaluate an average pore size in our research is explained in detail in **Chapter 3**.

2.3 Properties

A thorough control of the structural parameters is crucial to tailor the final properties of the produced aerogels. Thus, through the tuning of the aerogel composition and structure, different properties can be achieved which leads to on-demand applications. The promising combination of excellent properties makes aerogels outstanding materials in comparison with other porous materials such as microcellular or nanocellular foams, allowing them to be suitable for novel and unexplored applications, as well as for providing a better performance on those already known.

These materials present a high potential for prospective research. Among their interesting properties, the optical, mechanical, and thermal properties are those in which huge advances are taking place nowadays and the ones in which this research is focused. Thus, the following sections describe the theoretical background and gather data from the literature in relation to these properties.

2.3.1 Optical properties

Regarding the optical properties of aerogels, transparency is undoubtedly one of the most-wanted features. An aerogel can be transparent only when the light wave is able to pass through it without a strong interaction with its structure. This interaction that attenuates the radiation can be described by two mechanisms: light absorption of the aerogel matrix, and light scattering produced by the aerogel porous structure. Transmittance is defined as the amount of light able to pass through a material in comparison with the incident intensity. Different factors can affect light transmittance, such as sample thickness, light wavelength, or structural parameters (particle size, pore size, particle size distribution, etc.).

According to the Beer-Lambert law [90], the transmitted light depends on the sample thickness (L) and on an attenuation coefficient (μ):

$$T = \frac{I}{I_0} = e^{-\mu \cdot L} \qquad (2.9)$$

Where I is the intensity through the sample, and I_0 is the incident intensity. Deriving from this law, the transmitted intensity for any thickness can be calculated from the experimental data, as described by Equation 2.8:

$$T = T_0^{\frac{L}{L_0}} \qquad (2.10)$$

Being T_0 and L_0 the reference transmittance and thickness values, respectively, and L the selected thickness at which transmittance needs to be calculated.

The **attenuation coefficient (μ)** comprises the mechanisms contributing to reduce the transmission of light by absorption or scattering (**Figure 2.11**):

- **Absorption** of radiation by the aerogel matrix would lead to a transformation of light radiation into thermal energy. This is not an independent process but it is linked to the scattering mechanisms [91]. Nevertheless, due to the usual low density of aerogels, this mechanism will not be predominant. In particular, for polymeric aerogels this mechanism is typically very low because most polymers have little or no absorption of visible light.

- **Scattering mechanism** deviates light with a certain angle when interacting with the internal structure of aerogels and with what is known as 'scatterer centers'. Because

of the open porosity of aerogels, their structure can be seen as a continuous air phase in which interconnected particles are distributed. Thus, it could be considered as an air medium where light can pass through nanometric particles which scatter the incident light. Taking into account the previous description of the aerogel structure, transparency will depend mainly on the particle size, the particle size distribution, and the packaging of these particles, which give rise to the aerogel density.

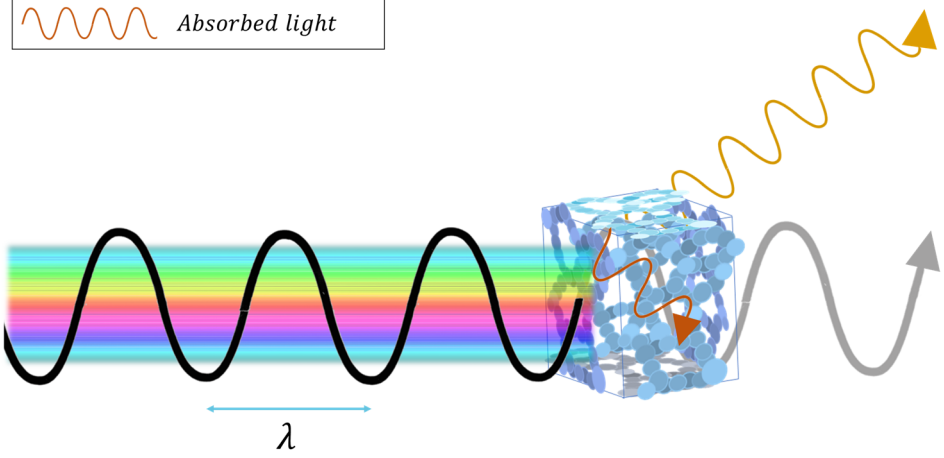

Figure 2.11. Mechanisms taking place when light passes through an aerogel.

The size of the scatterer centers affects the amount of dispersed light as well as its direction. In this way, when the incident wavelength (visible light ranges from 450 to 750 nm) is above one tenth of the scatter size, Mie scattering takes place [92], [93], scattering most of the incident light in the forward direction with a high angle since the scatterers are hindering the light passage. Nevertheless, if the size of the scatterer features is smaller than a tenth of the wavelength of the incident light, an elastic scattering mechanism takes place which is the well-known **Rayleigh scattering** [94] (**Figure 2.12**). The latter mechanism presents a stronger dependence with the light wavelength and a reduced amount of light is dispersed. For samples in which this mechanism is taking place, a higher transparency is expected, since these particles would be considered almost invisible to the visible light. The scattered intensity from Rayleigh scattering produced by a particle of diameter $\phi_{particle}$ is described by the following equation [95]:

$$I_{scattered} = \frac{8\,\pi^4 \phi_{particle}^6}{r^2\,\lambda^4}\left[\frac{n^2-1}{n^2+2}\right](1+\cos^2\theta) \qquad (2.11)$$

Where r is the radial distance from the scatterer, θ the scattering angle, and n the refractive index.

This formula clearly shows the strong dependence of the scattered light with the particle size, which is to the sixth power. It has to be highlighted that, according to the

Rayleigh mechanism, the scattering intensity varies with the fourth power of the inverse of the wavelength of the incident light. That means that smaller wavelengths (bluish colors) will be higher dispersed than the larger ones (reddish colors). Transmittance for materials in which Rayleigh scattering can be expressed by the following equation [96]:

$$T = A\, e^{-\frac{BL}{\lambda^4}} \qquad (2.12)$$

With A and B constants and L the sample thickness.

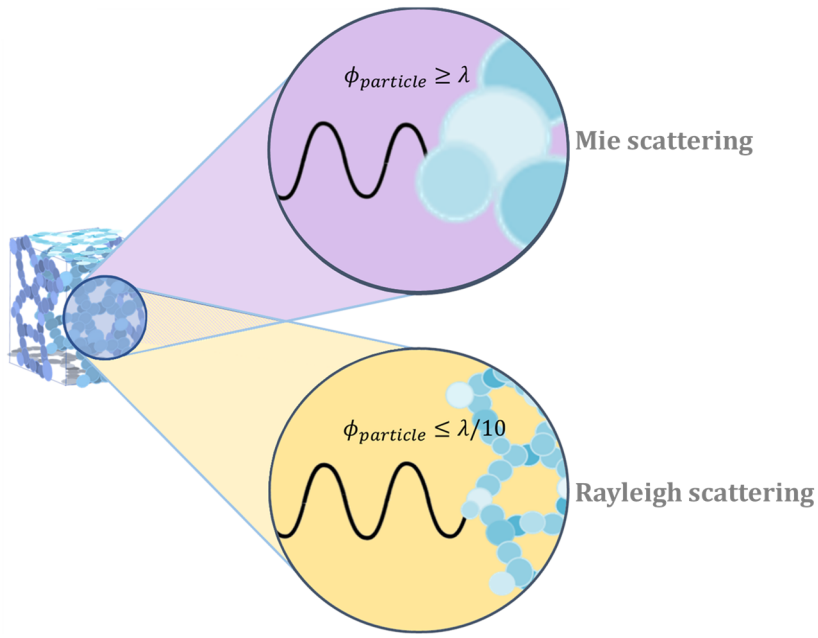

Figure 2.12. Scattering mechanisms depending on the aerogel particle size.

However, if the diameter of the scatterers is larger than one-tenth of the wavelength, the scattering mechanisms that takes place is known as **Mie scattering** [92]. After solving the Maxwell's equations [97], [98], the scattering intensity presents the following dependence:

$$I_{scattered} = I_i \int_{\alpha_0}^{\alpha_1} |S(\theta, \alpha)|^2 f(\alpha) d\alpha \qquad (2.13)$$

Where I_i is the total transmission, $S(\theta, \alpha)$ the scattering function, and $f(\alpha)$ the distribution for the particle size parameter (α). This particle size parameter is influenced by the wavelength (λ) and the particle radius ($r_{particle}$):

$$\alpha = \frac{2\,\pi n_m}{\lambda} r_{particle} \qquad (2.14)$$

In this case, the dependence with the light wavelength is to the first power, causing a larger amount of scattered light. Therefore, less light can be transmitted, and the samples will show a significant loss in visible-light transparency.

- Additionally, the different **refractive index** between the polymeric matrix and air contributes to scatter the incident light. Thus, when light reaches the aerogel an inhomogeneous interaction in the air-aerogel interface takes place [99]. Since aerogels contain air in a high percentage of their total volume, the refractive index is similar to that of air (1), and can be calculated by the Clausius-Mosotti formula [100]:

$$n - 1 = \frac{3\,\rho}{2\,\rho_s}\left(\frac{n_s^2-1}{n_s^2+2}\right) \qquad (2.15)$$

  Where ρ_s and n_s are the solid density and the refractive index of the polymer matrix.

According to the previous mechanisms that contribute to decrease the amount of transmitted light, the following conclusions can be extracted:

- A thorough control of the gelation and drying steps should be taken to obtain transparent aerogels, since light transmittance will be remarkably decreased by factors such as shrinkage or structural damage that can generate particle aggregates and clusters, or a strong Ostwald ripening which generates large particles [101].
- The diameter of the particles forming the skeleton of the aerogel plays an essential role in their final optical properties, since different scattering mechanisms with a different dependence on the light wavelength will take place depending on the size of these scatterers.

When thinking about a transparent aerogel, **silica aerogels** are those that usually come to our minds [102]–[104]. Several authors have analyzed the reasons behind their high transparency. In relation to the factors previously explained that reduce the light transmittance, some statements can be done:

- There exists a negligible light absorption of the silica matrix in comparison to other matrixes [105], [106].
- The nanoparticles forming the silica aerogel solid network are smaller than a tenth of the visible wavelength and, thus, a high transmittance is observed.
- Some silica aerogels present a bluish color [107], caused by the dispersion of the light with the smallest wavelength (blue).

By joining these factors, it can be concluded that it is Rayleigh scattering the mechanism that better describes the optical behavior of silica aerogels [91], [108]–[110]. Additionally, analysis of experimental data confirmed the scattering dependence with wavelength of λ^{-4}, as reported by Zhao et al. [111].

Despite the interesting properties of silica aerogels, their poor mechanical strength is still one of their main drawbacks. For this reason, several researchers have focused their attention on obtaining **organic aerogels** that could present high transparency levels to visible light. Organic aerogels usually improve the mechanical strength in comparison with silica ones, as explained in the following section. Additionally, their synthesis procedure allows to control and obtain a more predictable structure, as well as modifying their functional groups to increase their hydrophobicity [112].

There are some examples in the literature of organic aerogels showing high levels of light transmittance:

- **Resorcinol-Formaldehyde aerogels (RF aerogels)** as those synthesized by Pekala [113], [114] and Liang et al. [115] (no quantitative light transmittance data are reported).
- **Melamine-Formaldehyde aerogels (MF aerogels)** such as the aerogels reported by Ruben et al. [116], and those recently produced by Nakanishi et al. [24] (**Figure 2.13 a,** Adapted with permission from Ref. [24]. Copyright © 2020, American Chemical Society) reaching 84 % of transmittance at 550 nm for 10-mm thick samples.
- **Chitosan aerogels** as, for instance, the chitosan aerogels produced by Takeshita et al. [117], [118], [119] (**Figure 2.13 b,** Adapted with permission from Ref. [119]. Copyright © 2015, American Chemical Society.) with values of light transmittance ca. 30 % at 550 nm for samples of thicknesses comprised between 4.0 and 4.4 mm of thickness. The same group recently synthesized a type of aldehyde-free chitosan aerogels by thermal decomposition of urea that induces the gelation of a chitosan solution [41]. In this work, higher light transmittances were reached, being of ca. 70 % of transmittance at 550 nm for the aerogels with the lowest urea concentration at 2.7 mm of thickness.
- **Cellulose aerogels (aerocellulose)** as those aerogels produced by Mi et al. [40] (**Figure 2.13 c,** Adapted with permission from Ref. [40]. Copyright © 2016, American Chemical Society) which reached a maximum transmittance of ca. 60 % for 2 mm-thick samples at a wavelength of 550 nm. These results were improved by Ayadi et al. [120] until reaching a 70 % of transmittance for film samples of 1 mm at the same wavelength. The nanocellulose-based aerogels of Kobayashi et al. [121] showed higher transmittance of ca. 80 % at that wavelength for 1 mm-thick aerogels.
- **Polyimide aerogels** as those reported by Hou et al. [122]. They fabricated polyimide aerogel membranes (PIAMs) with an 80% of transmittance at 550 nm for samples of 1 mm in thickness. There exists other recent works that reported polyimide aerogels with high transparency to visible light as the work of Tafreshi et al. [123] and that of Vivod et al. [124] (**Figure 2.13 d,** Adapted with permission from Ref. [124]. Copyright © 2020, American Chemical Society).
- **Other polymeric aerogels**. Meckler et al. [125] reported polymeric aerogels based on divinylbenzene as monomer (DVB; 80% pure with a balance of ethylvinylbenzene) and AIBN as a radical initiator by nitroxide mediated stable free radical polymerization (SFRP) (**Figure 2.13 e,** Adapted with permission from Ref. [125]. Copyright © 2022, American Chemical Society). These samples showed visible transmittance >60% (for 2.8 mm thickness) at 550 nm. Additionally, some patents have been filed in the last years based on the fabrication of other polymers presenting transparency to visible light by using monomers with low refractive index [126] or using chain transfer agents [127].
- **Hybrid inorganic-organic aerogels** have been synthesized by the combination of different matrixes to obtain synergistic effects, reaching higher transmittances. Wang et al. [128] reached values of 92.3 % of transmittance (550 nm wavelength with 2 mm-thick) for hydrophobic polyvinylpolysilsesquioxane aerogels. Liu et al. [129] combined cellulose nanofibers with polysiloxane to synthesize optically transparent aerogels which reached an 85 % of transmittance (at 550 nm for 2 mm-thick aerogels). Similar values were obtained for ethylene-bridged polymethylsiloxane aerogels at 10 mm [130] and slightly lower values (between 20 and 40 %) for cellulose–silica composite aerogels [131] (at 550 nm for 3 mm-

thick aerogels) (**Figure 2.13 f,** Adapted with permission from Ref. [131]. Copyright © 2017, American Chemical Society).

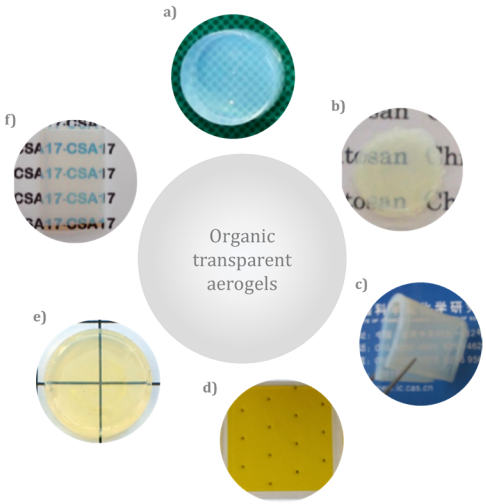

Figure 2.13. Examples of organic aerogels presenting transparency to visible light.

The previous examples, together with additional values found in the literature for organic aerogels, have been gathered in **Figure 2.14**, representing their light transparency at 550 nm of wavelength. For the lowest thickness of ca. 1 mm, the highest transmittance is 80 % for cellulose aerogels. However, the obtention of higher values of ca. 90 % (for a thickness of 2 mm) is only possible for hybrid aerogels in which an inorganic matrix is present (green colour).

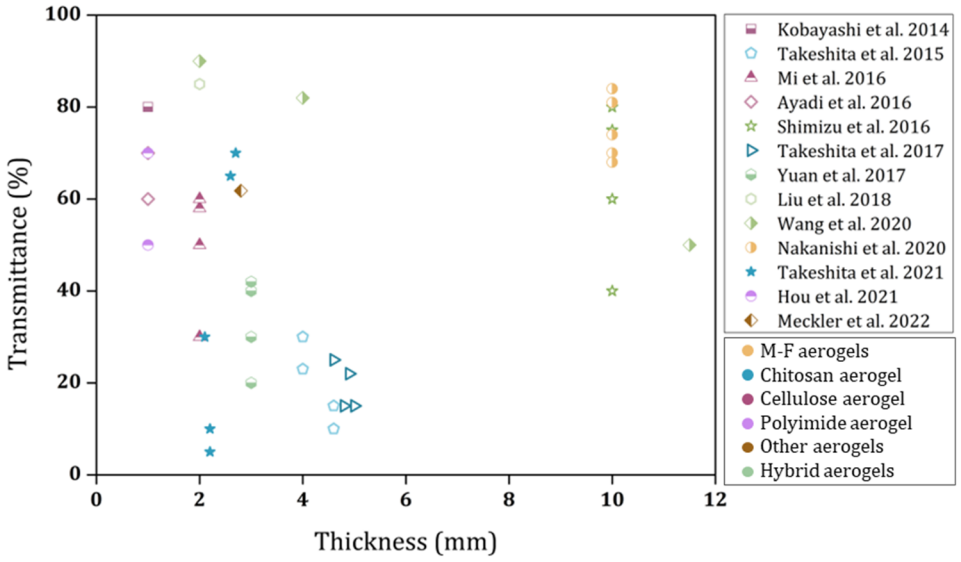

Figure 2.14. Light transmittance at 550 nm as a function of the sample thickness for different organic aerogels. Data obtained from the literature.

A thorough search for organic matrixes that lead to transparent or traslucent aerogels while enhancing the mechanical endurance of silica aerogels is being carried out during the last years. This search revealed that there are several interesting polymers which have not been explored yet. For instance, cost-effective materials usually presenting a combination of

excellent properties (high mechanical strength and low thermal conductivity) are polyurethane and polyisocianurate, well-known polymers widely used in the construction sector as foamed materials. For these especific materials, transparent aerogels had not been reported when this research started. Thus, there exists a promising and wide room for exploring novel transparent organic aerogels.

2.3.2 Mechanical properties

It is commonly stated that the main drawback of aerogels is their low mechanical endurance, which restricts their use in some practical applications exceeding the breaking stress [132]. The mechanical properties of aerogels are related to the stress propagation through the solid backbone. Apart from the aerogel density, both the size of the particles forming the skeleton and the interparticle pores influence the stress concentration and the deformation mechanisms taking place along the structure. The necks formed between particles act as 'springs', determining the strength of the aerogel against an applied force [133]. Additionally, the huge pore volume conforming these materials contributes to a plastic behavior when a large force is applied, since the solid structure is irreversibly deformed, and a strong densification can take place.

Different strategies can be used to improve the mechanical strength of aerogels. The most straightforward way is to increase their bulk density (**Figure 2.15 b)**. In 1988, Fricke [134] stablished a dependence between the aerogel density (ρ) and the elastic modulus (E) that was later confirmed by Pekala et al. [135]:

$$E \propto \rho^{\gamma}$$

This is a scaling law where $\gamma \simeq 3 - 3.7$, instead of the value of ca. 2 usually obtained for most of the polymeric foams.

The relationship between density and mechanical strength was further studied, widening the range for the value of the exponent γ from 2 to 4, since this parameter mainly depends on the connectivity of the solid backbone that can hugely vary between materials [136]. Chidambareswarapattar et al. [137] calculated the exponent γ for polyurethane aerogels, obtaining values from 3.49 to 7.75, what reflects the change in the morphology of these specimens, the interparticle connectivity, and how matter fills the air voids.

Another approach to increase the mechanical strength of aerogels is through an ageing step (**Figure 2.15 c**) to modify the structure and, in particular, the interparticle necks and particle diameter. As explained in **section 2.2.3**, the Ostwald ripening mechanism contributes to enlarge the interparticle necks and secondary particles, leading to an increase on the gel strength that is maintained in the final aerogel. Sometimes the ageing step requires a heat treatment or even a post-curing process can be applied for this purpose [138].

Other strategies to reinforce aerogels can be employed. For instance, chemical bonding between reactive functional groups on the surface of the solid backbone and the corresponding reinforcing compounds (**Figure 2.15 d**). Polymers are promising materials from this point of view, because cross-linking can be used to strengthen the aerogel matrix [138].

Finally, one of the most common approaches is enhancing the aerogel mechanical properties through the addition of different fillers, such as clays [139], fibers [140] or carbon nanotubes [141] among others (**Figure 2.15 e**) [142].

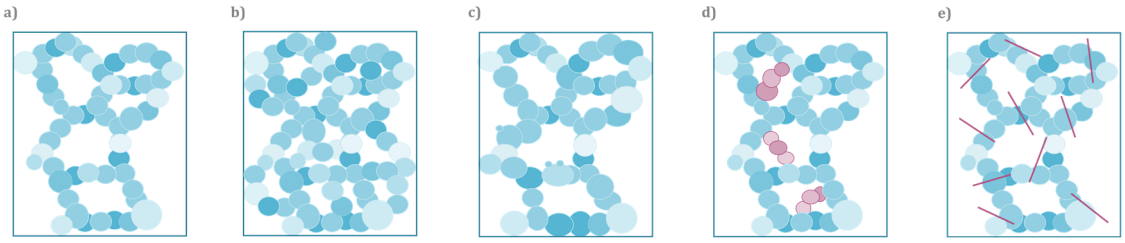

Figure 2.15. Different strengthening techniques for aerogels: a) reference aerogel, b) density increase, c) ageing, d) polymer crosslinking, e) fiber reinforcement.

It is well-known that silica aerogels are prone to present a brittle behavior because of the fragility of the O-Si-O bonds under an impact force [142], [143], joined to the presence of flaws acting as stress concentrators [144]. Apart from the small flaws that could appear during the drying process, pores are considered as an integral part of flaws causing the brittleness of these materials [132]. Some statistical models have been developed to stablish a correlation between the relative density of silica aerogels and some mechanical parameters such as elastic modulus or yield stress. These models allow the tailoring of the mechanical properties by controlling the pore size distribution along the inner structure, the particle size and particle strings [145].

More recently, research has focused its efforts on developing aerogels with better mechanical strength that are suitable for applications in which bearing load is essential. Organic aerogels usually present an improved mechanical performance than inorganic aerogels because of the higher toughness of the polymeric matrix [146].

Focusing on polyurethane-based aerogels, plots gathering data from quasi-static compression tests as a function of the bulk density have been created. **Figure 2.16** shows the correlation between elastic modulus and bulk density, whereas in **Figure 2.17** (see below) density is related with the compressive strength at a strain of 50 %.

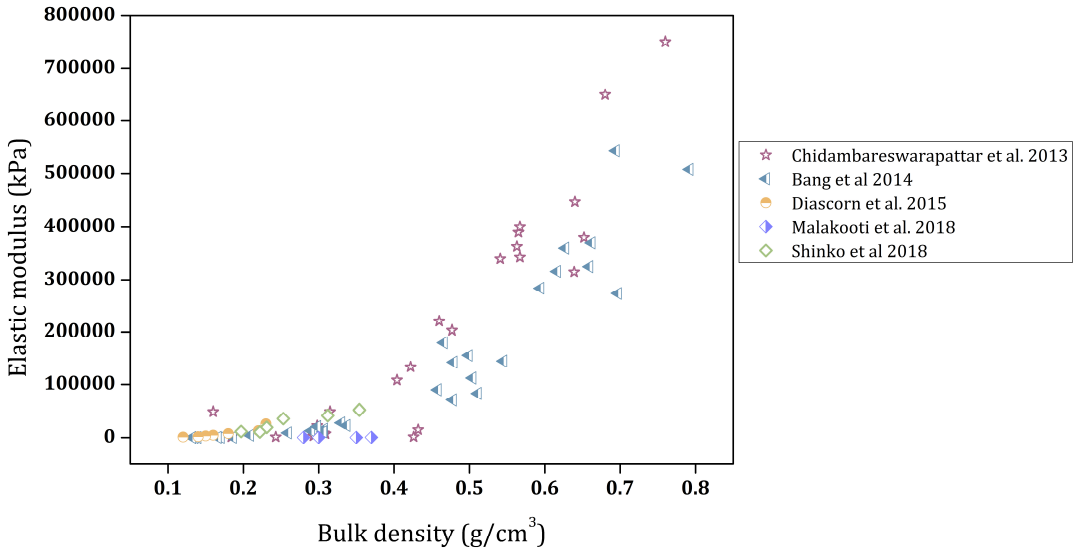

Figure 2.16. Elastic modulus as a function of bulk density for polyurethane-based aerogels from the literature.

Malakooti et al. [147] reached a wide range of elastic modulus for a family of polyisocyanurate-urethane aerogels from 37 to 265 kPa, for a range of densities between 0.28 and 0.37 g/cm^3. These aerogels showed great stability and resilience under compression cyclic loadings at 50 % strain. Significantly higher elastic moduli were obtained by Diascorn et al. [88] for polyurethane aerogels obtaining a range from 1 to 26 MPa and a relationship between bulk density (0.120 to 0.230 g/cm^3) and the elastic moduli with a scaling law with an exponent γ= 3.7. These wide differences on the mechanical strength are also promoted by the noticeable changes observed in the nanostructure of the polyurethane aerogel samples with pore sizes between 15 nm and 210 nm. Even higher elastic moduli were obtained by Chidambareswarapattar et al. [137]. These authors synthesized from flexible to significantly hard polyurethane aerogels with elastic moduli values comprised between 1 and 750 MPa when promoting the reaction of a triisocyanate with different di- and triols. In this way, the different monomer structures led to a wide range of bulk densities (0.160 – 0.760 g/cm^3) that allowed to tailor the final response to mechanical stress. Bang et al. [148] produced flexible aerogels by using hyperbranched polyurethanes as precursors and studied the effect of using flexible (aliphatic) or rigid (aromatic) precursors. One of the main conclusions of their work is that flexible aerogels can be achieved for aerogels with low densities (about 0.140 g/cm^3) and an exponent γ higher than 5. At higher densities (0.300 – 0.700 g/cm^3), aerogels were stiff and tough. It has been demonstrated that the crucial parameter influencing the flexibility of aerogels is the contact area between particles. Thus, low interparticle contact, that is, fewer covalent bonds between particles are required to obtain flexible aerogels. In this way, by a thorough selection of the functional group density present on the initial precursors, the final mechanical properties can be tuned. These works were focused on the influence of the bulk density and changes in the nanoporous structure to tailor the mechanical properties (**Figure 2.15 b**). More recently, one of the polymer crosslinking strategy previously described (**Figure 2.15 d**) was used by Shinko et al. [149] between polyurea and polyurethane, leading to organic aerogels. The polyol weight fraction influenced the aerogel shrinkage and, therefore, the aerogel density ranged from 0.197 to 0.354 g/cm^3. This effect was analyzed on the final properties of the produced materials, obtaining elastic moduli between 10 and 52 MPa.

Other parameter that is commonly employed for characterizing the stiffness of the synthesized materials is the stress at a certain strain. **Figure 2.17** collects these data (at a strain of 50 %) which have been selected from the previous works in order to identify the influence of density on the mechanical strength. There exists a strong effect of the bulk density on the compressive stress since the particle distribution, particle size, and interparticle neck thickness are modified with density and, therefore, they modify the way that an external force deforms the material and how the compressive load is distributed along the nanoporous structure.

Polyurethane-based aerogels with densities between 0.1 and 0.4 g/cm^3 show a stress at 50 % of strain in a range from 1 to 20 MPa. Nevertheless, when density increases above 0.5 g/cm^3 the stress needed to deform the aerogel at 50 % can reach values of 120 MPa.

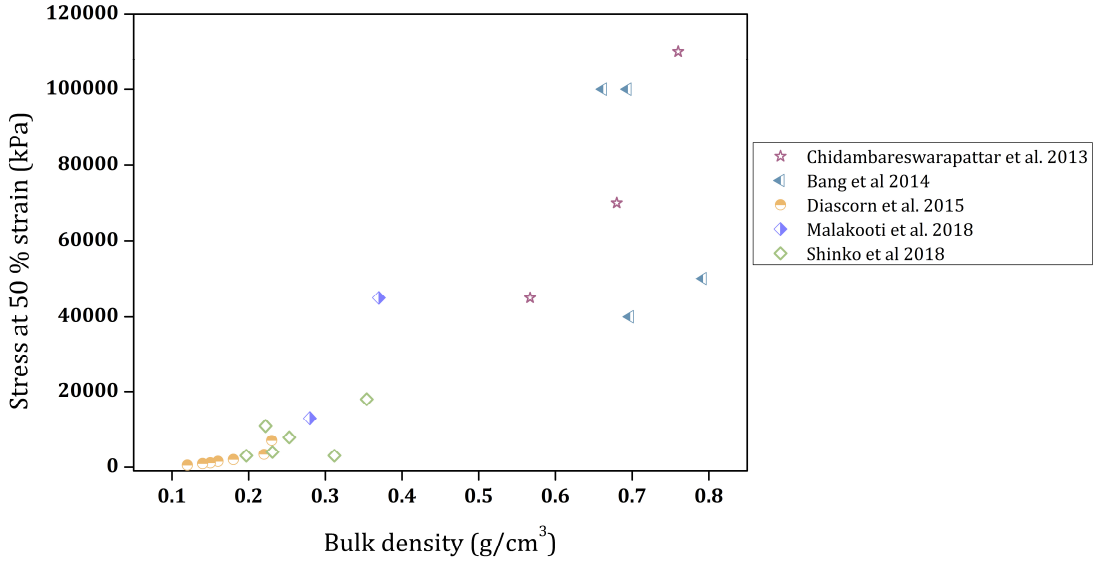

Figure 2.17. Stress at a 50 % strain as a function of bulk density for polyurethane-based aerogels from the literature.

Other additional mechanical tests that are performed to evaluate the mechanical properties of aerogels are quasi-static load–unload compressive tests that allow to study the recovery capacity after a mechanical stress and the energy dissipated through the hysteresis area, or three-point bending tests providing the flexural modulus.

The recovery capacity of each sample lies on the rearranging ability of their 3D network along the empty space. It is common that part of the energy is dissipated, and the unloading cycle presents a lower compressive stress than the loading one, thus showing a hysteresis area. There exist different mechanisms for the energy dissipation, such as adhesion and friction between polymeric chains, microstructural buckling and crack formation [147].

The aerogel flexibility is usually evaluated by bending experiments. If a plastic deformation is performed, a reverse force would be necessary to recover the original shape. It has been demonstrated that the key parameter to be controlled in order to achieve flexible aerogels is the interparticle contact area per unit volume. The manipulation of the interparticle bonding can be adjusted by a careful selection of the initial monomers and the crosslinking chemistry. Considering the molecular properties of the monomers, such as their chemical structure or functional group density, a low number of functional groups gives rise to a lower number of covalent bonds, therefore, to a lower particle – particle contact areas. The crosslinking chemistry during the gelation process also presents a great influence on the interparticle connections. Covalent or Van der Waals interactions lead to increase the interparticle bonding, as well as the polymeric accumulation on the already formed primary nanoparticle-chains. Thus, narrow interparticle contacts are required to obtain flexibility as final property on aerogels [150]. Some examples from the literature for aerogels based on polyurethane and polyisocyanate are gathered in **Figure 2.18**.

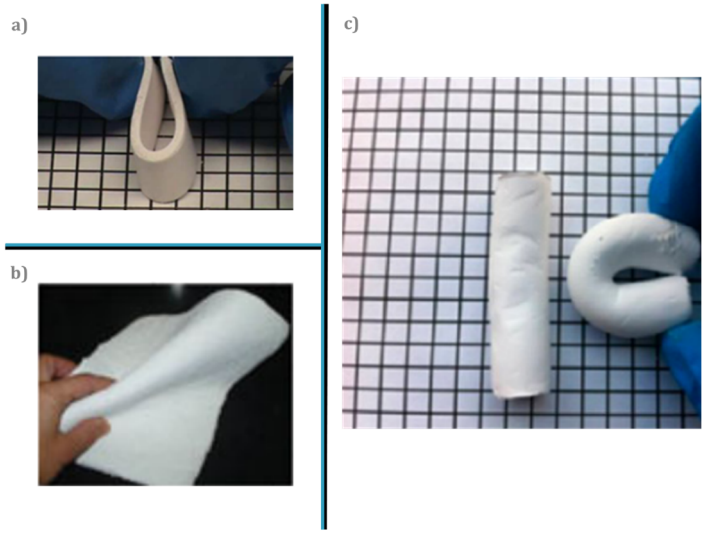

Figure 2.18. Examples of polyurethane and polyisocyanate-based aerogels from the literature: References a) Bang et al. [148], Adapted with permission from Ref. [148]. Copyright © 2014, American Chemical Society. b) Trifu et al. [151], Adapted by permission from Springer Nature, MRS Advances [151], Copyright © 2017. c) Chidambareswarapattar et al. [152], Adapted with permission from Ref. [152]. Copyright © 2013, American Chemical Society.

The elasticity and flexibility of aerogels are promising properties that allow the implementation of these materials in different fields such as the medical sector, as it will be explained in the final section of this chapter.

2.3.3 Thermal Conductivity

2.3.3.1. Mechanisms of heat transfer for nanoporous materials and techniques to measure the thermal conductivity of these materials.

One of the most promising properties of aerogels is their low thermal conductivity that points them out as potential advanced thermal insulators. Prior to the analysis of the literature data regarding this property, the heat transfer mechanisms should be described. In order to address this issue, one literature review has been published and it is herein included. The publication "Merillas, B.; Vareda, J.P.; Martín-de León, J.; Rodríguez-Pérez, M.Á.; Durães, L. **Thermal Conductivity of Nanoporous Materials: Where Is the Limit?** Polymers 2022, 14, 2556" includes the following contents:

- A revision of the current aerogel insulators and their insulating capacities.
- The effectiveness, pros, and cons of the typical measuring techniques used nowadays for materials with low thermal conductivities have been analyzed: In particular the transient and steady-state methods have been discussed in detail.
- Experimental data of silica aerogel composites and PMMA nanocellular foams produced for this publication have been analyzed by employing different measuring techniques.
- Thermal conductivity data from the literature focused on PMMA polymer foams and silica-based and polyurethane-based aerogels have been gathered.
- The heat transfer mechanisms have been described in detail for these materials.
- The essential structural features for achieving superinsulating materials (i.e. materials with thermal conductivities lower than that of air) have been described.

Graphical abstract

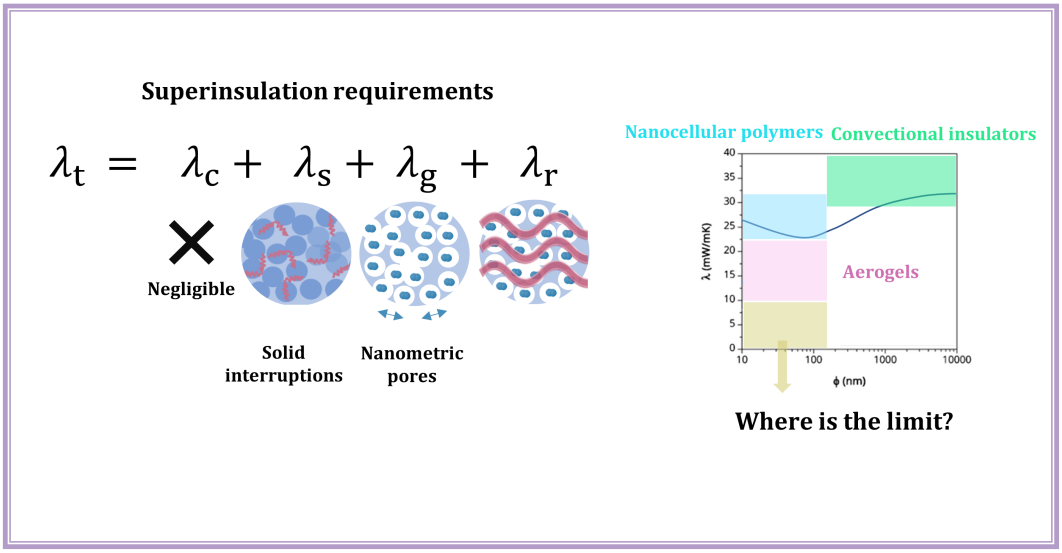

Figure 2.19. Graphical abstract of "Thermal Conductivity of Nanoporous Materials: Where Is the Limit?"

Polymers, 14, 13, 2556, 2022.

Thermal Conductivity of Nanoporous Materials: Where Is the Limit?

Beatriz Merillas[1], João Pedro Vareda[2], Judith Martín-de León[1], Miguel Ángel Rodríguez-Pérez[1,3], and Luisa Durães[2,*]

[1] Cellular Materials Laboratory (CellMat), Department of Condensed Material Physics, Facultad de Ciencias, University of Valladolid, 47011 Valladolid, Spain; b.merillas@fmc.uva.es (B.M.); j.martin@cellmattechnologies.com (J.M.-d.L.); marrod@fmc.uva.es (M.Á.R.-P.)

[2] University of Coimbra, CIEPQPF, Department of Chemical Engineering, Rua Sílvio Lima, 3030-790 Coimbra, Portugal; jvareda@eq.uc.pt

[3] BioEcoUVA Research Institute on Bioeconomy, University of Valladolid, 47011 Valladolid, Spain

** Correspondence: luisa@eq.uc.pt*

Abstract: Nowadays, our society is facing problems related to energy availability. Owing to the energy savings that insulators provide, the search for effective insulating materials is a focus of interest. Since the current insulators do not meet the increasingly strict requirements, developing materials with a greater insulating capacity is needed. Until now, several nanoporous materials have been considered as superinsulators achieving thermal conductivities below that of the air (26 mW/(m K), like nanocellular PMMA/TPU, silica aerogels, and polyurethane aerogels reaching 24.8, 10, and 12 mW/(m K), respectively. In the search for the minimum thermal conductivity, still undiscovered, the first step is understanding heat transfer in nanoporous materials. The main features leading to superinsulation are low density, nanopores, and solid interruptions hindering the phonon transfer. The second crucial condition is obtaining reliable thermal conductivity measurement techniques. This review summarizes these techniques, and data in the literature regarding the structure and thermal conductivity of two nanoporous materials, nanocellular polymers and aerogels. The key conclusion of this analysis specifies that only steady-state methods provide a reliable value for thermal conductivity of superinsulators. Finally, a theoretical discussion is performed providing a detailed background to further explore the lower limit of superinsulation to develop more efficient materials.

Keywords: nanoporous materials; thermal conductivity; thermal superinsulators; aerogels; nanocellular polymers.

DOI: 10.3390/polym14132556

2.3.3.2. Thermal Conductivity of PU based aerogels. State of the art.

This Section includes a thorough study of the thermal conductivities reported in the literature of polyurethane and isocyanate-based aerogels as a function of their bulk densities. Starting from 1998, Biesmans et al. [32] provided data for polyurethane and polyisocyanurate aerogels that presented significantly low thermal conductivities at 10 °C and ambient pressure conditions. These values ranged from 15 to 22 mW/mK for densities between 0.100 and 0.260 g/cm^3, becoming the greatest polyurethane-based insulators for several decades. It was in 2004 when Rigacci et al. [153] prepared polyurethane-based aerogel-like materials by using different drying routes obtaining a thermal conductivity of 22 mW/mK when supercritical drying was applied. Since then, several studies have tried to further decrease the thermal conductivity of polyurethane or polyisocyanurate aerogels. Since it was crucial to understand the correlation between the initial monomers and the final properties of aerogels, Chidambareswarapattar et al. [137] studied the influence of the monomer structure on the macroscopic properties of polyurethane aerogels. An initial decrease in the thermal conductivity was found when increasing density until reaching a minimum value (31 mW/mK for a density of 0.298 g/cm^3). Then, thermal conductivity increased significantly. Similarly, Bang et al. [154] tuned the rigidity of the initial triisocyanate, alcohols, and difunctional acrylates in order to analyze their influence on the mechanical properties and thermal conductivity of the produced aerogels, achieving a lowest thermal conductivity value of 36 mW/mK. This value was noticeably reduced by Diascorn et al. in 2015 [155] by modifying the catalyst concentration and, therefore, the gelation reaction rate. The polyurethane aerogel with the lowest thermal conductivity reached a value of 17 mW/mK. A different strategy was followed by Zhu et al. [28] who searched for the optimum solvent systems when preparing polyisocyanate-based aerogels. Through the exploration of the Hansen solubility parameters of different solvent mixtures, ultralow thermal conductivities were reached. Trifu et al. [151] synthesized polyisocyanate-based aerogels and their thermal conductivity could be correlated with the isocyanate functionality (lowest thermal conductivity of 18 mW/mK). Additionally, a patent has been published by Lomba et al. [156] which reports aerogels with an isocyanate and cyclic ether compounds. The obtained polymeric aerogels showed a moderate insulating capacity with a minimum of 37 mW/mK.

Figure 2.20 gathers the data of the thermal conductivity as a function of the bulk density for the polyurethane or polyisocyanate-based aerogels which are mentioned in these scientific publications. It is observed that there exist low thermal conductivity values for a range of densities comprised between 0.1 and 0.3 g/cm^3, with a minimum value of 15 mW/mK. However, in spite of all the research on this topic, an unexplored region remains for polyurethane-based aerogels with densities below 0.2 g/cm^3, which are expected to show excellent insulating capacities. In addition, we have not found any detailed study of the relation between the porous structure and the thermal conductivity of these materials.

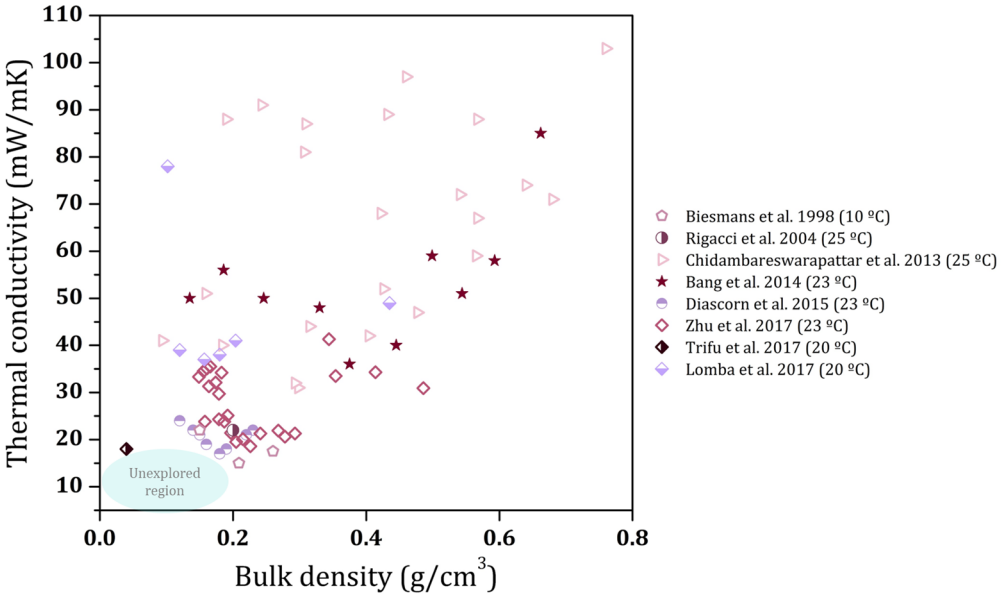

Figure 2.20. Thermal conductivity as a function of the bulk density of polyurethane and polyisocyanurate aerogels from literature data.

2.4 Aerogel applications

There exists an infinity of fields in which aerogels are applied or their potential implementation is being studied. In this section, the main fields and those relevant to this thesis are described in more detail, whereas those that are not involved in the development of this thesis are only briefly mentioned.

Building sector

The unique thermal and acoustic insulating properties of aerogels in conjunction with a high light transmittance open a new world of possibilities and applications. One of the main fields in which transparent aerogels could be applied is the building sector as window-panes, solar collector covers, or aerogel blankets. Nowadays, several silica aerogels have been employed in novel applications. Reim et al. [157] **(Figure 2.21 a,** Reprinted from Ref. [157], Copyright © 2002, with permission from Elsevier) set granular silica aerogel between two PMMA sheets to produce a window glazing (35 % of solar transmittance with a total thickness of 5 cm). Some aerogel-window glazings are being commercialized reaching higher transmittances of 90 % and being anti-reflective [109] (**Figure 2.21 b,** from Ref. [109] by permission of Oxford University Press). Owing to the energy savings that these materials allow, some current buildings have implemented this novel technology, such as a the roof of a pharmacy in Switzerland using Nanogel® Aerogel from Cabot Corporation [158] (**Figure 2.21 c**), or even granular products have been developed in the last years such as a product based on aerogel in polycarbonate sheets at a multifunctional building in Seattle, Washington's Freemont District (**Figure 2.21 d**, Reprinted by permission from Springer Nature, Nano and Biotech Based Materials for Energy Building Efficiency by Buratti et al. Ref [159], Copyright © 2016) and a Gymnasium at BBS Mainz (Germany) (**Figure 2.21 e,** Reprinted by permission from Springer Nature, Nano and Biotech Based Materials for Energy Building Efficiency by Buratti et al. Ref [159], Copyright © 2016) [159], at a primary school in Norway [160] (**Figure 2.21 f,** from Ref. [160], Permission is not required for this non-

commercial use), the Halls at SUNY Stony Brook, NY, USA (**Figure 2.21 g,** Reprinted from Ref. [161], Copyright © 2015, with permission from Elsevier) or the Detroit School of Arts, MI, USA (**Figure 2.21 h,** Reprinted from Ref. [161], Copyright © 2015, with permission from Elsevier) [161], or even at the Buchwiesen School Sports Hall in Zurich (**Figure 2.21 i**, Reprinted from Ref. [162], Copyright © 2018, with permission from Elsevier) [162].

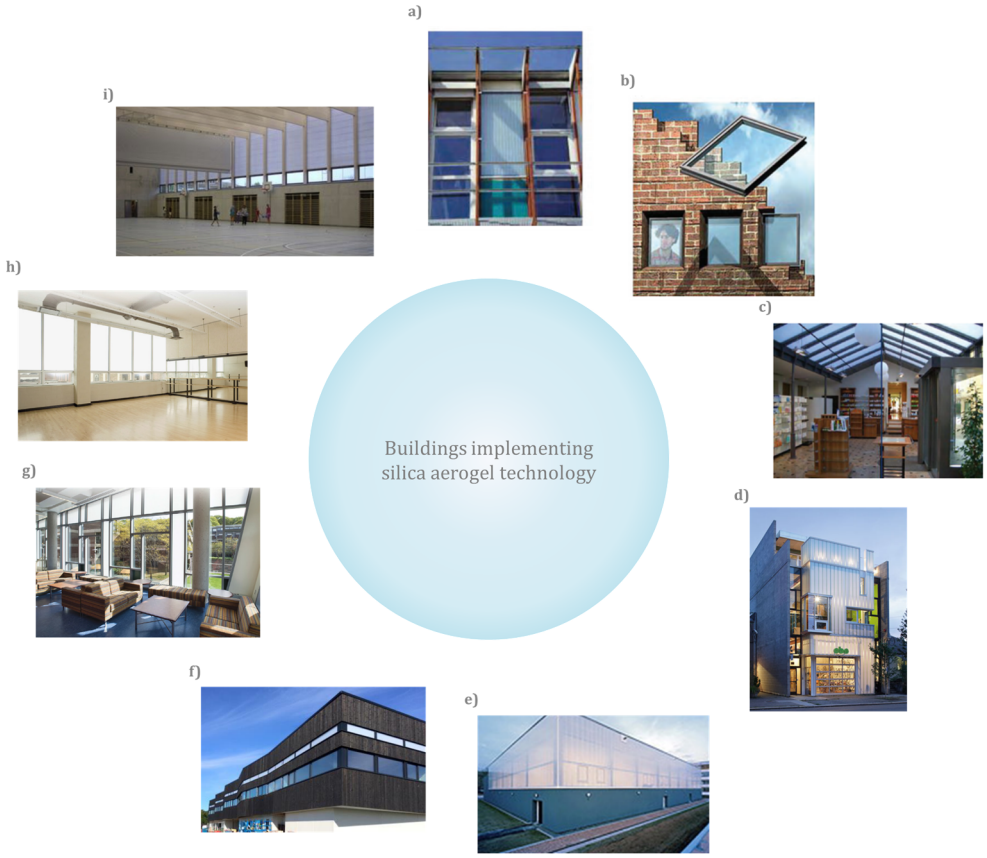

Figure 2.21. Examples of buildings including silica aerogel on their structures.

Automotive sector and aeronautics

The extremely insulating capacity of aerogels combined with their low densities and, therefore, lightweight, offers the opportunity of being applied in the automotive and aeronautics sectors, where these features are essential [163], [164]. Additionally, aerogels have been pointed out as particle detectors and counters using the Cherenkov effect since the early 1980s [165]–[167].

The European Retrieval Carrier EURECA satellite and other NASA's projects such as Mars Pathfinder, Mars Exploration Rovers, and Mars Science Lander use aerogels for purposes related with capturing cosmic dust and thermal insulation [168], [169].

Energy and electronics field

Specially carbon aerogels, due to their electrically conductive behavior, have been employed for supercapacitors in which the aerogels act as electrodes. Their high surface area and electrical properties allow them to store and release energy in a controlled way.

The electrical properties of aerogels can be modulated in order to achieve different applications. Dielectric [170], [171], superconductive, thermoelectric [172], or piezoelectric properties [173], [174] can be reached by the addition of different compounds or the employment of metallic matrixes.

Environmental applications: Waste removal

It is well-known the worldwide concerns of polluted water resources. Different pollutants are usually present as a result of poorly regulated recycling of industrial or household wastes [175]. Specially organic aerogels are being used for pollutants removal as for instance water purification [176], dye removal [177], [178], heavy metals removal [179], or oil spill removal [180] among other pollutants.

Pharmaceutical and biomedical sector

The pharmaceutical and biomedical sectors are thoroughly studying the implementation of advanced drug delivery systems based on aerogel, what has been studied during the last decade, reaching to novel and improved performances [181]. Challenges such as poor solubility or low diffusion can be faced by aerogels, which combine unique features. It has been proved the significant safety and biocompatibility [182], [183] of some aerogels in toxicological studies and, as future perspectives, aerogels will be produced in capsule, ointment, tablet, powders or injectable forms.

2.5 References

[1] J. Alemán, A. V. Chadwick, J. He, M. Hess, K. Horie, R. G. Jones, P. Kratochvíl, I. Meisel, I. Mita, G. Moad, S. Penczek, and R. F. T. Stepto, "Definitions of terms relating to the structure and processing of sols, gels, networks, and inorganic-organic hybrid materials (IUPAC recommendations 2007)," *Pure Appl. Chem.*, vol. 79, no. 10, pp. 1801–1829, **2007**, doi: 10.1351/pac200779101801.

[2] S. S. Kistler, "Coherent Expanded Aerogels and Jellies," *Nature*, vol. 127, p. 741, **1931**.

[3] A. D. McNaught and A. Wilkinson, *Compendium of chemical Terminology: IUPAC Recommendations*. Blackwell Scientific Publications, 1987. doi: 10.1016/0022-328x(88)83113-9.

[4] C. J. Brinker and G. W. Scherer, *Sol-Gel Science: The Physics and Chemistry of Sol-Gel Processing*. Oxford, UK: Academic Press, 1990. doi: 10.1016/C2009-0-22386-5.

[5] N. Hüsing and U. Schubert, "Aerogels," in *Ullmann's Encyclopedia of Industrial Chemistry*, Wiley-VCH Verlag GmbH & Co. KGaA, Weinheim, 2006. doi: 10.1002/14356007.c01.

[6] N. Leventis, A. Sadekar, N. Chandrasekaran, and C. Sotiriou-Leventis, "Click synthesis of monolithic silicon carbide aerogels from polyacrylonitrile-coated 3D silica networks," *Chem. Mater.*, vol. 22, pp. 2790–2803, **2010**, doi: 10.1021/cm903662a.

[7] I. Smirnova and P. Gurikov, "Aerogels in chemical engineering: Strategies toward tailor-made aerogels," *Annu. Rev. Chem. Biomol. Eng.*, vol. 8, pp. 307–334, **2017**, doi: 10.1146/annurev-chembioeng-060816-101458.

[8] C. Ziegler, A. Wolf, W. Liu, A. K. Herrmann, N. Gaponik, and A. Eychmüller, "Modern Inorganic Aerogels," *Angew. Chemie - Int. Ed.*, vol. 56, no. 43, pp. 13200–13221, **2017**, doi: 10.1002/anie.201611552.

[9] J. P. Vareda, A. Lamy-Mendes, and L. Durães, "A reconsideration on the definition of the term aerogel based on current drying trends," *Microporous Mesoporous Mater.*, vol. 258, pp. 211–216, **2018**, doi: 10.1016/j.micromeso.2017.09.016.

[10] L. Ratke and P. Gurikov, *The Chemistry and Physics of Aerogels: Synthesis, Processing, and Properties*. Cambridge University Press, 2021. doi: 10.1007/BF02705298.

[11] G. Zu, J. Shen, X. Wei, X. Ni, Z. Zhang, J. Wang, and G. Liu, "Preparation and characterization of monolithic alumina aerogels," *J. Non. Cryst. Solids*, vol. 357, no. 15, pp. 2903–2906, **2011**, doi: 10.1016/j.jnoncrysol.2011.03.031.

[12] V. Štengl, S. Bakardjieva, J. Šubrt, and L. Szatmary, "Titania aerogel prepared by low temperature supercritical drying," *Microporous Mesoporous Mater.*, vol. 91, no. 1–3, pp. 1–6, **2006**, doi: 10.1016/j.micromeso.2005.10.046.

[13] R. C. Walker, A. E. Potochniak, A. P. Hyer, and J. K. Ferri, "Zirconia aerogels for thermal management: Review of synthesis, processing, and properties information architecture," *Adv. Colloid Interface Sci.*, vol. 295, no. June, p. 102464, **2021**, doi: 10.1016/j.cis.2021.102464.

[14] V. Augustyn and B. Dunn, "Vanadium oxide aerogels: Nanostructured materials for enhanced energy storage," *Comptes Rendus Chim.*, vol. 13, no. 1–2, pp. 130–141, **2010**, doi: 10.1016/j.crci.2009.05.002.

[15] E. J. Carlson, J. N. Armor, W. J. Cunningham, and A. M. Smith, "Chromium aerogel method of producing same and fluorinating process utilizing same," 1989. [Online]. Available: https://patents.google.com/patent/US4828818A/en

[16] J. K. Yoo, H. J. Kong, R. Wagle, B. H. Shon, I. K. Kim, and T. H. Kim, "A study on the methods for making iron oxide aerogel," *J. Ind. Eng. Chem.*, vol. 72, pp. 332–337, **2019**, doi: 10.1016/j.jiec.2018.12.033.

[17] W. Dong and B. Dunn, "Sol-gel synthesis of monolithic molybdenum oxide aerogels and

xerogels," *J. Mater. Chem.*, vol. 8, no. 3, pp. 665–670, **1998**, doi: 10.1039/a706537j.

[18] I. V. Elmanovich and V. V. Zefirov, "Manganese Oxide Aerogels Obtained in a One-Step Process Directly in Supercritical CO2 at Different Temperatures," *Ineos Open*, vol. 4, no. 3, pp. 112–116, **2021**, doi: 10.32931/io2115a.

[19] Z. Zhang, Q. Gao, H. Gao, Z. Shi, J. Wu, M. Zhi, and Z. Hong, "Nickel oxide aerogel for high performance supercapacitor electrodes," *RSC Adv.*, vol. 6, no. 113, pp. 112620–112624, **2016**, doi: 10.1039/C6RA24436J.

[20] M. Chaaban and H. El-Rassy, "Nickel–aluminum oxide aerogels: Super-adsorbents for azo dyes for water remediation," *ACS Omega*, vol. 5, no. 42, pp. 27401–27412, **2020**, doi: 10.1021/acsomega.0c03828.

[21] A. Feinle and N. Hüsing, "Mixed metal oxide aerogels from tailor-made precursors," *J. Supercrit. Fluids*, vol. 106, pp. 2–8, **2015**, doi: 10.1016/j.supflu.2015.07.015.

[22] I. Sádaba, M. Ojeda, R. Mariscal, R. Richards, and M. López Granados, "Preparation and characterization of Mg-Zr mixed oxide aerogels and their application as aldol condensation catalysts," *ChemPhysChem*, vol. 13, no. 14, pp. 3282–3292, **2012**, doi: 10.1002/cphc.201200440.

[23] M. Schwan, R. Tannert, and L. Ratke, "New soft and spongy resorcinol-formaldehyde aerogels," *J. Supercrit. Fluids*, vol. 107, pp. 201–208, **2016**, doi: 10.1016/j.supflu.2015.09.010.

[24] Y. Nakanishi, Y. Hara, W. Sakuma, T. Saito, K. Nakanishi, and K. Kanamori, "Colorless Transparent Melamine-Formaldehyde Aerogels for Thermal Insulation," *ACS Appl. Nano Mater.*, vol. 3, no. 1, pp. 49–54, **2020**, doi: 10.1021/acsanm.9b02275.

[25] R. W. Pekala, "Organic aerogels from the sol-gel polymerization of phenolic-furfural mixtures," 1995.

[26] L. Mo, S. Zhang, F. Qi, and A. Huang, "Highly stable cellulose nanofiber/polyacrylamide aerogel via in-situ physical/chemical double crosslinking for highly efficient Cu(II) ions removal," *Int. J. Biol. Macromol.*, vol. 209, no. PB, pp. 1922–1932, **2022**, doi: 10.1016/j.ijbiomac.2022.04.167.

[27] M. Papastergiou, A. Kanellou, D. Chriti, G. Raptopoulos, and P. Paraskevopoulou, "Poly(urethane-acrylate) aerogels via radical polymerization of dendritic urethane-acrylate monomers," *Materials (Basel).*, vol. 11, no. 11, **2018**, doi: 10.3390/ma11112249.

[28] Z. Zhu, G. M. B. F. Snellings, M. M. Koebel, and W. J. Malfait, "Superinsulating Polyisocyanate Based Aerogels: A Targeted Search for the Optimum Solvent System," *ACS Appl. Mater. Interfaces*, vol. 9, no. 21, pp. 18222–18230, **2017**, doi: 10.1021/acsami.7b03344.

[29] B. Shi, B. Ma, C. Wang, H. He, L. Qu, B. Xu, and Y. Chen, "Fabrication and applications of polyimide nano-aerogels," *Compos. Part A Appl. Sci. Manuf.*, vol. 143, no. January, p. 106283, **2021**, doi: 10.1016/j.compositesa.2021.106283.

[30] A. M. Joseph, B. Nagendra, P. Shaiju, K. P. Surendran, and E. B. Gowd, "Aerogels of hierarchically porous syndiotactic polystyrene with a dielectric constant near to air," *J. Mater. Chem. C*, vol. 6, no. 2, pp. 360–368, **2018**, doi: 10.1039/c7tc05102f.

[31] R. Zhang, W. Wan, L. Qiu, Y. Wang, and Y. Zhou, "Preparation of hydrophobic polyvinyl alcohol aerogel via the surface modification of boron nitride for environmental remediation," *Appl. Surf. Sci.*, vol. 419, pp. 342–347, **2017**, doi: 10.1016/j.apsusc.2017.05.044.

[32] G. Biesmans, D. Randall, E. Francais, and M. Perrut, "Polyurethane-based organic aerogels' thermal performance," *J. Non. Cryst. Solids*, vol. 225, pp. 36–40, **1998**, doi: http://dx.doi.org/10.1016/S0022-3093(98)00103-3.

[33] G. Biesmans, "Polyurethane based organic aerogels and their transformation into carbon aerogels," pp. 64–68, **1998**.

[34] M. Aghabararpour, M. Naderi, S. Motahari, and M. Najafi, "A study on resorcinol formaldehyde

carbon aerogel/epoxy nanocomposites: the effect of carbon aerogel pyrolysis time," *J. Polym. Res.*, vol. 26, no. 3, pp. 1–8, **2019**, doi: 10.1007/s10965-019-1721-9.

[35] M. Li, J. Liu, J. Liu, S. Pan, J. Zhang, Y. Liu, Y. Liu, J. Liu, J. Liu, and H. Lu, "Highly Oriented Graphite Aerogel Fabricated by Confined Liquid-Phase Expansion for Anisotropically Thermally Conductive Epoxy Composites," *ACS Appl. Mater. Interfaces*, vol. 12, no. 24, pp. 27476–27484, **2020**, doi: 10.1021/acsami.0c02151.

[36] G. Nassar, E. Daou, R. Najjar, M. Bassil, and R. Habchi, "A review on the current research on graphene-based aerogels and their applications," *Carbon Trends*, vol. 4, p. 100065, **2021**, doi: 10.1016/j.cartre.2021.100065.

[37] S. Y. Moon, B. R. Kim, C. W. Park, S. H. Lee, and S. M. Kim, "High-crystallinity single-walled carbon nanotube aerogel growth: Understanding the real-time catalytic decomposition reaction through floating catalyst chemical vapor deposition," *Chem. Eng. J. Adv.*, vol. 10, no. November 2021, p. 100261, **2022**, doi: 10.1016/j.ceja.2022.100261.

[38] W. Zhang, S. Shi, W. Zhu, L. Huang, C. Yang, S. Li, X. Liu, R. Wang, N. Hu, Y. Suo, Z. Li, and J. Wang, "Agar Aerogel Containing Small-Sized Zeolitic Imidazolate Framework Loaded Carbon Nitride: A Solar-Triggered Regenerable Decontaminant for Convenient and Enhanced Water Purification," *ACS Sustain. Chem. Eng.*, vol. 5, no. 10, pp. 9347–9354, **2017**, doi: 10.1021/acssuschemeng.7b02376.

[39] R. R. Mallepally, I. Bernard, M. A. Marin, K. R. Ward, and M. A. McHugh, "Superabsorbent alginate aerogels," *J. Supercrit. Fluids*, vol. 79, pp. 202–208, **2013**, doi: 10.1016/j.supflu.2012.11.024.

[40] Q. Y. Mi, S. R. Ma, J. Yu, J. S. He, and J. Zhang, "Flexible and Transparent Cellulose Aerogels with Uniform Nanoporous Structure by a Controlled Regeneration Process," *ACS Sustain. Chem. Eng.*, vol. 4, pp. 656–660, **2016**, doi: 10.1021/acssuschemeng.5b01079.

[41] S. Takeshita, S. Zhao, and W. J. Malfait, "Transparent, Aldehyde-Free Chitosan Aerogel," *Carbohydr. Polym.*, vol. 251, no. September 2020, p. 117089, **2021**, doi: 10.1016/j.carbpol.2020.117089.

[42] V. Baudron, M. Taboada, P. Gurikov, I. Smirnova, and S. Whitehouse, "Production of starch aerogel in form of monoliths and microparticles," *Colloid Polym. Sci.*, vol. 298, no. 4–5, pp. 477–494, **2020**, doi: 10.1007/s00396-020-04616-5.

[43] Z. Zeng, X. Y. D. Ma, Y. Zhang, Z. Wang, B. F. Ng, M. P. Wan, and X. Lu, "Robust Lignin-Based Aerogel Filters: High-Efficiency Capture of Ultrafine Airborne Particulates and the Mechanism," *ACS Sustain. Chem. Eng.*, vol. 7, pp. 6959–6968, **2019**, doi: 10.1021/acssuschemeng.8b06567.

[44] S. Groult and T. Budtova, "Tuning structure and properties of pectin aerogels," *Eur. Polym. J.*, vol. 108, no. August, pp. 250–261, **2018**, doi: 10.1016/j.eurpolymj.2018.08.048.

[45] D. Govindarajan, N. Duraipandy, K. V. Srivatsan, R. Lakra, P. S. Korapatti, R. Jayavel, and M. S. Kiran, "Fabrication of Hybrid Collagen Aerogels Reinforced with Wheat Grass Bioactives as Instructive Scaffolds for Collagen Turnover and Angiogenesis for Wound Healing Applications," *ACS Appl. Mater. Interfaces*, vol. 9, no. 20, pp. 16939–16950, **2017**, doi: 10.1021/acsami.7b05842.

[46] K. Y. Lee, D. B. Mahadik, V. G. Parale, and H. H. Park, "Composites of silica aerogels with organics: a review of synthesis and mechanical properties," *J. Korean Ceram. Soc.*, vol. 57, pp. 1–23, **2020**, doi: 10.1007/s43207-019-00002-2.

[47] Q. Li, M. Afeworki, N. M. Callen, R. J. Colby, M. Gopinadhan, M. L. N. Kochersperger, B. K. Peterson, M. Sansone, S. C. Weston, and D. C. Calabro, "Template-Free Self-Assembly of Mesoporous Organosilicas," *Chem. Mater.*, vol. 30, pp. 2218–2228, **2018**, doi: 10.1021/acs.chemmater.7b04480.

[48] K. J. Shea and D. A. Loy, "Bridged Polysilsesquioxanes . Molecular-Engineered Hybrid Organic - Inorganic Materials," *Chem. Mater.*, vol. 13, pp. 3306–3319, **2001**.

[49] G. M. Hidy, "On the theory of the coagulation of noninteracting particles in Brownian motion,"

J. Colloid Sci., vol. 20, no. 2, pp. 123–144, **1965**, doi: 10.1016/0095-8522(65)90003-6.

[50] P. Meakin, "Formation of fractal clusters and networks by irreversible diffusion-limited aggregation," *Phys. Rev. Lett.*, vol. 51, no. 13, pp. 1119–1122, **1983**, doi: 10.1103/PhysRevLett.51.1119.

[51] T. A. Witten and L. M. Sander, "Diffusion-limited aggregation, a kinetic critical phenomenon," *Phys. Rev. Lett.*, vol. 47, no. 19, pp. 1400–1403, **1981**, doi: 10.1103/PhysRevLett.47.1400.

[52] M. Kolb, R. Botet, and R. Julien, "Scaling of Kinetically Growing Clusters," *Phys. Rev. …*, vol. 51, no. 13, pp. 1123–1126, **1983**, [Online]. Available: http://journals.aps.org/prl/abstract/10.1103/PhysRevLett.69.3354

[53] H. Sayama, "'Diffusion-Limited Aggregation: A Real-Time Agent-Based Simulation' http://demonstrations.wolfram.com/DiffusionLimitedAggregationARealTimeAgentBasedSimulation/," *Wolfram Demonstrations Project*, 2011.

[54] M. Smoluchowski, "Drei Vorträge über Diffusion, Brownsche Molekularbewegung und Koagulation von Kolloidteilchen," *Phys. Z.*, vol. 17, pp. 557–571, 585–599, **1916**.

[55] M. Mason and W. Weaver, "The settling of small particles in a fluid," *Phys. Rev.*, vol. 23, pp. 412–426, **1924**, doi: 10.1103/PhysRev.23.412.

[56] N. T. K. Thanh, N. Maclean, and S. Mahiddine, "Mechanisms of nucleation and growth of nanoparticles in solution," *Chem. Rev.*, vol. 114, no. 15, pp. 7610–7630, **2014**, doi: 10.1021/cr400544s.

[57] C. K. Dixit, S. Bhakta, A. Kumar, S. L. Suib, and J. F. Rusling, "Fast nucleation for silica nanoparticle synthesis using a sol-gel method," *Nanoscale*, vol. 8, no. 47, pp. 19662–19667, **2016**, doi: 10.1039/c6nr07568a.

[58] T. Vicsek, *Fractal Growth Phenomena*, 2nd ed. 1992. doi: 10.1142/1407.

[59] D. Schaefer, "What Factors Control the Structure of Silica Aerogels ?," *J. Phys. Colloq.*, vol. 50, no. C4, pp. C4-121-C4-126, **1989**, doi: 10.1051/jphyscol:1989418.

[60] S. Keysar, Y. De Hazan, Y. Cohen, T. Aboud, and G. S. Grader, "Particle aggregation in alumina aerogels," *J. Mater. Res.*, vol. 12, no. 2, pp. 430–433, **1997**, doi: 10.1557/JMR.1997.0063.

[61] M. Shahadat, A. A. Wani, Y. K. Manea, R. Adnan, S. Z. Ahammad, and S. W. Ali, "Heavy metals scavenging using multidentate/multifunctional aerogels and their composites," in *Advances in Aerogel Composites for Environmental Remediation*, Elsevier Inc., 2021, pp. 275–296. doi: 10.1016/B978-0-12-820732-1.00015-1.

[62] P. Montero De Hijes, K. Shi, E. G. Noya, E. E. Santiso, K. E. Gubbins, E. Sanz, and C. Vega, "The Young-Laplace equation for a solid-liquid interface," *J. Chem. Phys.*, vol. 153, p. 191102, **2020**, doi: 10.1063/5.0032602.

[63] G. W. Scherer and D. M. Smith, "Cavitation during drying of a gel," *J. Non. Cryst. Solids*, vol. 189, pp. 197–211, **1995**, doi: 10.1016/0022-3093(95)00222-7.

[64] H. Y. Nah, V. G. Parale, H. N. R. Jung, K. Y. Lee, C. H. Lim, Y. S. Ku, and H. H. Park, "Role of oxalic acid in structural formation of sodium silicate-based silica aerogel by ambient pressure drying," *J. Sol-Gel Sci. Technol.*, vol. 85, no. 2, pp. 302–310, **2018**, doi: 10.1007/s10971-017-4553-2.

[65] R. B. Torres, J. P. Vareda, A. Lamy-Mendes, and L. Durães, "Effect of different silylation agents on the properties of ambient pressure dried and supercritically dried vinyl-modified silica aerogels," *J. Supercrit. Fluids*, vol. 147, no. February, pp. 81–89, **2019**, doi: 10.1016/j.supflu.2019.02.010.

[66] H. Gao, L. Bo, P. Liu, D. Chen, A. Li, Y. Ou, C. Dong, J. Wang, X. Chen, C. Hou, W. Dong, and G. Wang, "Ambient pressure dried flexible silica aerogel for construction of monolithic shape-stabilized phase change materials," *Sol. Energy Mater. Sol. Cells*, vol. 201, no. March, p. 110122, **2019**, doi: 10.1016/j.solmat.2019.110122.

[67] F. Shi, L. Wang, and J. Liu, "Synthesis and characterization of silica aerogels by a novel fast ambient pressure drying process," *Mater. Lett.*, vol. 60, pp. 3718–3722, **2006**, doi: 10.1016/j.matlet.2006.03.095.

[68] C. Simón-Herrero, S. Caminero-Huertas, A. Romero, J. L. Valverde, and L. Sánchez-Silva, "Effects of freeze-drying conditions on aerogel properties," *J. Mater. Sci.*, vol. 51, pp. 8977–8985, **2016**, doi: 10.1007/s10853-016-0148-5.

[69] T. Kramer, D. M. Kremer, M. J. Pikal, W. J. Petre, E. Y. Shalaev, and L. A. Gatlin, "A Procedure to Optimize Scale-Up for the Primary Drying Phase of Lyophilization," *J. Pharm. Sci.*, vol. 98, pp. 307–318, **2009**, doi: 10.1002/jps.

[70] K. Grosse, L. Ratke, and B. Feuerbacher, "Solidification and melting of succinonitrile within the porous network of an aerogel," *Phys. Rev. B - Condens. Matter Mater. Phys.*, vol. 55, no. 5, pp. 2894–2902, **1997**, doi: 10.1103/PhysRevB.55.2894.

[71] C. Alié, N. Tcherkassova, F. Ferauche, S. Lambert, B. Heinrichs, R. Pirard, and J. P. Pirard, "Multigram scale synthesis and characterization of low-density silica xerogels," *J. Non. Cryst. Solids*, vol. 352, pp. 2763–2771, **2006**, doi: 10.1016/j.jnoncrysol.2006.03.054.

[72] S. Członka, M. F. Bertino, J. Kośny, and N. Shukla, "Freeze-drying method as a new approach to the synthesis of polyurea aerogels from isocyanate and water," *J. Sol-Gel Sci. Technol.*, vol. 87, no. 3, pp. 685–695, **2018**, doi: 10.1007/s10971-018-4769-9.

[73] S. Zheng, X. Hu, A. R. Ibrahim, D. Tang, Y. Tan, and J. Li, "Supercritical fluid drying: Classification and applications," *Recent Patents Chem. Eng.*, vol. 3, pp. 230–244, **2010**, doi: 10.2174/1874478811003030230.

[74] M. J. van Bommel and A. B. de Haan, "Drying of silica gels with supercritical carbon dioxide," *J. Mater. Sci.*, vol. 29, pp. 943–948, **1994**, doi: 10.1007/BF00351414.

[75] I. Selmer, A. S. Behnecke, J. Quiño, A. S. Braeuer, P. Gurikov, and I. Smirnova, "Model development for sc-drying kinetics of aerogels: Part 1. Monoliths and single particles," *J. Supercrit. Fluids*, vol. 140, no. April, pp. 415–430, **2018**, doi: 10.1016/j.supflu.2018.07.002.

[76] "Aspen Aerogels. http://www.aerogel.com."

[77] "CABOT Aerogel. http://www.cabot-corp.com/Aerogel."

[78] "BASF. http://www.basf.es/ecp1/Spain/es/."

[79] M. Kéri, A. Forgács, V. Papp, I. Bányai, P. Veres, A. Len, Z. Dudás, I. Fábián, and J. Kalmár, "Gelatin content governs hydration induced structural changes in silica-gelatin hybrid aerogels – Implications in drug delivery," *Acta Biomater.*, vol. 105, pp. 131–145, **2020**, doi: 10.1016/j.actbio.2020.01.016.

[80] J. Cai, S. Kimura, M. Wada, S. Kuga, and L. Zhang, "Cellulose aerogels from aqueous alkali hydroxide-urea solution," *ChemSusChem*, vol. 1, pp. 149–154, **2008**, doi: 10.1002/cssc.200700039.

[81] K. Ganesan and L. Ratke, "Facile preparation of monolithic κ-carrageenan aerogels," *Soft Matter*, vol. 10, pp. 3218–3224, **2014**, doi: 10.1039/c3sm52862f.

[82] R. Subrahmanyam, P. Gurikov, P. Dieringer, M. Sun, and I. Smirnova, "On the road to biopolymer aerogels—dealing with the solvent," *Gels*, vol. 1, pp. 291–313, **2015**, doi: 10.3390/gels1020291.

[83] Q. Feng, K. Chen, D. Ma, H. Lin, Z. Liu, S. Qin, and Y. Luo, "Synthesis of high specific surface area silica aerogel from rice husk ash via ambient pressure drying," *Colloids Surfaces A Physicochem. Eng. Asp.*, vol. 539, pp. 399–406, **2018**, doi: 10.1016/j.colsurfa.2017.12.025.

[84] J. Ren, J. Feng, L. Wang, G. Chen, Z. Zhou, and Q. Li, "High specific surface area hybrid silica aerogel containing POSS," *Microporous Mesoporous Mater.*, vol. 310, p. 110456, **2021**, doi: 10.1016/j.micromeso.2020.110456.

[85] U. Schubert, N. Hiising, and A. Lorenz, "Hybrid Inorganic-Organic Materials by Sol-Gel," *Chem.*

Mater., vol. 7, pp. 2010–2027, **1995**.

[86] M. A. Aegerter, N. Leventis, and M. M. Koebel, *Aerogels Handbook*. Berlin, Germany: Springer, 2011. doi: 10.1007/978-1-4419-7589-8_4.

[87] D. Biesmans, G and Randall, "Polyurethane-Based Aerogels for Use as Environmentally Acceptable Super Insulants in the Future Appliance Market," *J. Cell. Plast.*, vol. 34, **1998**.

[88] N. Diascorn, S. Calas, H. Sallée, P. Achard, and A. Rigacci, "Polyurethane aerogels synthesis for thermal insulation - textural, thermal and mechanical properties," *J. Supercrit. Fluids*, vol. 106, pp. 76–84, **2015**, doi: 10.1016/j.supflu.2015.05.012.

[89] R. Pirard, S. Blacher, F. Brouers, and J. P. Pirard, "Interpretation of mercury porosimetry applied to aerogels," *J. Mater. Res.*, vol. 10, no. 8, pp. 2114–2119, **1995**, doi: 10.1557/JMR.1995.2114.

[90] D. A. Bostain, J. S. Brenizer, and P. M. Norris, "Neutron radioscopic measurement of water adsorption coefficients in aerogels," *Res. Nondestruct. Eval.*, vol. 14, no. 1, pp. 47–57, **2002**, doi: 10.1080/09349840209409703.

[91] C. F. Bohren and D. R. Huffman, *Absorption and scattering of light by small particles*. Wiley-VCH, Germany, 1983. doi: 10.1088/0031-9112/35/3/025.

[92] A. Wolf, B. Terheiden, and R. Brendel, "Light scattering and diffuse light propagation in sintered porous silicon," *J. Appl. Phys.*, vol. 104, no. 3, p. 033106, **2008**, doi: 10.1063/1.2956690.

[93] D. Jackel and B. Walter, "Modeling and Rendering of the Atmosphere Using Mie-Scattering," *Comput. Graph. forum*, vol. 16, no. 4, pp. 201–210, **1997**.

[94] D. J. Lockwood, "Rayleigh and Mie Scattering," *Encycl. Color Sci. Technol.*, pp. 1098–1107, **2016**, doi: 10.1007/978-1-4419-8071-7.

[95] W. Cao and A. J. Hunt, "Improving the visible transparency of silica aerogels," *J. Non. Cryst. Solids*, vol. 176, pp. 18–25, **1994**.

[96] J. Martín-de León, J. L. Pura, V. Bernardo, and M. Á. Rodríguez-Pérez, "Transparent nanocellular PMMA: Characterization and modeling of the optical properties," *Polymer (Guildf).*, vol. 170, no. December 2018, pp. 16–23, **2019**, doi: 10.1016/j.polymer.2019.03.010.

[97] R. Acharya, "Interaction of waves with medium," in *Satellite Signal Propagation, Impairments and Mitigation*, Academic Press, 2017, pp. 57–86. doi: 10.1016/b978-0-12-809732-8.00003-x.

[98] W. K. Pendleton and T. Wriedt, *The Mie Theory-Basics and Applications*, vol. 169. Florida, USA: Springer Series in Optical Sciences, 2012. doi: 10.1088/0031-9112/32/10/032.

[99] J. Wang, D. Petit, and S. Ren, "Transparent thermal insulation silica aerogels," *Nanoscale Adv.*, vol. 2, no. 12, pp. 5504–5515, **2020**, doi: 10.1039/d0na00655f.

[100] G. Poelz and R. Riethmüller, "Preparation of silica aerogel for Cherenkov counters," *Nucl. Instruments Methods*, vol. 195, pp. 491–503, **1982**.

[101] C. Mandal, S. Donthula, R. Soni, M. Bertino, and N. Leventis, "Light scattering and haze in TMOS-co-APTES silica aerogels," *J. Sol-Gel Sci. Technol.*, vol. 90, pp. 127–139, **2019**, doi: 10.1007/s10971-018-4801-0.

[102] M. Tabata, I. Adachi, Y. Ishii, H. Kawai, T. Sumiyoshi, and H. Yokogawa, "Development of transparent silica aerogel over a wide range of densities," vol. 623, no. 1, pp. 339–341, **2010**, doi: 10.1016/j.nima.2010.02.241.

[103] A. Venkateswara Rao, D. Haranath, G. M. Pajonk, and P. B. Wagh, "Optimisation of supercritical drying parameters for transparent silica aerogel window applications," vol. 14, pp. 1194–1199, **1998**.

[104] J. C. Bernardes, D. Müller, K. Pinheiro, and C. R. Rambo, "Enhancing the optical transparency of TiO 2 aerogels with high surface area through water-based synthesis," vol. 109, p. 110359, **2020**, doi: 10.1016/j.optmat.2020.110359.

[105] H. Wang, A. Du, X. Ji, C. Zhang, B. Zhou, Z. Zhang, and J. Shen, "Enhanced Photothermal Conversion by Hot-Electron Effect in Ultrablack Carbon Aerogel for Solar Steam Generation," *ACS Appl. Mater. Interfaces*, vol. 11, no. 45, pp. 42057–42065, **2019**, doi: 10.1021/acsami.9b12918.

[106] R. Du, Y. Hu, R. Hübner, J. O. Joswig, X. Fan, K. Schneider, and A. Eychmüller, "Specific ion effects directed noble metal aerogels: Versatile manipulation for electrocatalysis and beyond," *Sci. Adv.*, vol. 5, no. 5, pp. 1–10, **2019**, doi: 10.1126/sciadv.aaw4590.

[107] A. Venkateswara Rao, G. M. Pajonk, and N. N. Parvathy, "Effect of solvents and catalysts on monolithicity and physical properties of silica aerogels," *J. Mater. Sci.*, vol. 29, no. 7, pp. 1807–1817, **1994**, doi: 10.1007/BF00351300.

[108] A. A. Pisal and A. Venkateswara Rao, "Development of hydrophobic and optically transparent monolithic silica aerogels for window panel applications," *J. Porous Mater.*, vol. 24, no. 3, pp. 685–695, **2017**, doi: 10.1007/s10934-016-0305-x.

[109] S. B. Riffat and G. Qiu, "A review of state-of-the-art aerogel applications in buildings," *Int. J. Low-Carbon Technol.*, vol. 8, no. 1, pp. 1–6, **2013**, doi: 10.1093/ijlct/cts001.

[110] A. Soleimani Dorcheh and M. H. Abbasi, "Silica aerogel; synthesis, properties and characterization," *J. Mater. Process. Technol.*, vol. 199, no. 1, pp. 10–26, **2008**, doi: 10.1016/j.jmatprotec.2007.10.060.

[111] L. Zhao, S. Yang, B. Bhatia, E. Strobach, and E. N. Wang, "Modeling silica aerogel optical performance by determining its radiative properties," *AIP Adv.*, vol. 6, no. 2, p. 025123, **2016**, doi: 10.1063/1.4943215.

[112] R. W. Pekala, "Synthetic control of molecular structure in organic aerogels," *MRS Online Proc. Libr.*, vol. 171, pp. 285–291, **1989**, doi: https://doi.org/10.1557/PROC-171-285.

[113] R. W. Pekala, "Low density, Resorcinol-Formaldehyde aerogels," 4,873,218, 1989.

[114] R. W. Pekala, "Organic aerogels from the polycondensation of resorcinol with formaldehyde," *J. Mater. Sci.*, vol. 24, no. 9, pp. 3221–3227, **1989**, doi: 10.1007/BF01139044.

[115] C. Liang, G. Sha, and S. Guo, "Resorcinol-formaldehyde aerogels prepared by supercritical acetone drying," *J. Non. Cryst. Solids*, vol. 271, pp. 167–170, **2000**, doi: 10.1016/S0022-3093(00)00108-3.

[116] G. C. Ruben and R. W. Pekala, "High-resolution transmission electron microscopy of the nanostructure of melamine-formaldehyde aerogels," *J. Non. Cryst. Solids*, vol. 186, pp. 219–231, **1995**, doi: 10.1016/0022-3093(95)00082-8.

[117] S. Takeshita, S. Akasaka, and S. Yoda, "Structural and acoustic properties of transparent chitosan aerogel," *Mater. Lett.*, vol. 254, pp. 258–261, **2019**, doi: 10.1016/j.matlet.2019.07.064.

[118] S. Takeshita and S. Yoda, "Translucent, hydrophobic, and mechanically tough aerogels constructed from trimethylsilylated chitosan nanofibers," *Nanoscale*, vol. 9, pp. 12311–12315, **2017**, doi: 10.1039/c7nr04051b.

[119] S. Takeshita and S. Yoda, "Chitosan Aerogels: Transparent, Flexible Thermal Insulators," *Chem. Mater.*, vol. 27, pp. 7569–7572, **2015**, doi: 10.1021/acs.chemmater.5b03610.

[120] F. Ayadi, B. Martín-García, M. Colombo, A. Polovitsyn, A. Scarpellini, L. Ceseracciu, I. Moreels, and A. Athanassiou, "Mechanically flexible and optically transparent three-dimensional nanofibrous amorphous aerocellulose," *Carbohydr. Polym.*, vol. 149, pp. 217–223, **2016**, doi: 10.1016/j.carbpol.2016.04.103.

[121] Y. Kobayashi, T. Saito, and A. Isogai, "Aerogels with 3D Ordered Nanofiber Skeletons of Liquid-Crystalline Nanocellulose Derivatives as Tough and Transparent Insulators," *Angew. Chemie*, vol. 126, pp. 10562–10565, **2014**, doi: 10.1002/ange.201405123.

[122] X. Hou, R. Zhang, and D. Fang, "Polyimide Aerogel Membranes with Adjustable Transparency

and High Flexibility for Highly Efficient Solar Thermal Collection," *ACS Sustain. Chem. Eng.*, vol. 9, pp. 7638–7648, **2021**, doi: 10.1021/acssuschemeng.1c02042.

[123] O. A. Tafreshi, S. Ghaffari-Mosanenzadeh, S. Karamikamkar, Z. Saadatnia, S. Kiddell, C. B. Park, and H. E. Naguib, "Novel, flexible, and transparent thin film polyimide aerogels with enhanced thermal insulation and high service temperature," *J. Mater. Chem. C*, vol. 10, pp. 5088–5108, **2022**, doi: 10.1039/d1tc06122d.

[124] S. L. Vivod, M. A. B. Meador, C. Pugh, M. Wilkosz, K. Calomino, and L. McCorkle, "Toward Improved Optical Transparency of Polyimide Aerogels," *ACS Appl. Mater. Interfaces*, vol. 12, no. 7, pp. 8622–8633, **2020**, doi: 10.1021/acsami.9b17796.

[125] S. M. Meckler, G. Iftime, A. Nallapaneni, Q. Van Overmeere, B. Keoshkerian, E. Bulger, A. S. Ho, C. Zhu, J. B. Rivest, and M. Chintapalli, "Optically Transparent Polymer Aerogels Via Controlled Radical Polymerization," *ACS Appl. Polym. Mater.*, vol. 4, pp. 1565–1569, **2022**, doi: 10.1021/acsapm.1c01854.

[126] E. Bulger, M. Chintapalli, G. Iftime, Q. Van Overmeere, J. B. Rivest, R. Neelakantan, and S. M. Meckler, "High optical transparency polymer aerogels using low refractive index monomers," 2020.

[127] M. Chintapalli, B. Keoshkerian, G. Iftime, and Q. Van Overmeere, "Method to produce transparent polymer aerogels using chain transfer agents," 2020.

[128] L. Wang, J. Feng, Y. Jiang, S. Zhang, L. Li, and J. Feng, "Facile fabrication of hydrophobic polyvinylpolysilsesquioxane aerogels with improved optical properties," *J. Sol-Gel Sci. Technol.*, vol. 94, pp. 88–97, **2020**, doi: 10.1007/s10971-019-05148-3.

[129] Q. Liu, A. W. Frazier, X. Zhao, J. A. De La Cruz, A. J. Hess, R. Yang, and I. I. Smalyukh, "Flexible transparent aerogels as window retrofitting films and optical elements with tunable birefringence," *Nano Energy*, vol. 48, no. February, pp. 266–274, **2018**, doi: 10.1016/j.nanoen.2018.03.029.

[130] T. Shimizu, K. Kanamori, A. Maeno, H. Kaji, and K. Nakanishi, "Transparent Ethylene-Bridged Polymethylsiloxane Aerogels and Xerogels with Improved Bending Flexibility," *Langmuir*, vol. 32, pp. 13427–13434, **2016**, doi: 10.1021/acs.langmuir.6b03249.

[131] B. Yuan, J. Zhang, Q. Mi, J. Yu, R. Song, and J. Zhang, "Transparent Cellulose-Silica Composite Aerogels with Excellent Flame Retardancy via an in Situ Sol-Gel Process," *ACS Sustain. Chem. Eng.*, vol. 5, pp. 11117–11123, **2017**, doi: 10.1021/acssuschemeng.7b03211.

[132] T. Woignier, J. Primera, A. Alaoui, P. Etienne, F. Despestis, and S. Calas-Etienne, "Mechanical properties and brittle behavior of silica aerogels," *Gels*, vol. 1, pp. 256–275, **2015**, doi: 10.3390/gels1020256.

[133] M. Gronauer, A. Kadur, and J. Fricke, "Mechanical and Acoustic Properties of Silica Aerogel," in *First International Symposium, Würzburg, Fed. Rep. of Germany September 23–25, 1985*, 1986, no. 167, pp. 167–173. doi: 10.1007/978-3-642-93313-4_22.

[134] J. Fricke, "Aerogels - highly tenuous solids with fascinating properties," *J. Non. Cryst. Solids*, vol. 100, pp. 169–173, **1988**, doi: 10.1016/0022-3093(88)90014-2.

[135] R. W. Pekala, L. W. Hrubesh, T. Tillotson, C. T. Alviso, J. F. Poco, and J. . Lemay, "A comparison of mechanical properties and scaling law relationships for silica aerogels and their organic counterparts," 1990.

[136] J. Groß and J. Fricke, "Scaling of elastic properties in highly porous nanostructured aerogels," *Nanostructured Mater.*, vol. 6, pp. 905–908, **1995**, doi: 10.1016/0965-9773(95)00206-5.

[137] C. Chidambareswarapattar, P. M. Mccarver, H. Luo, H. Lu, C. Sotiriou-leventis, and N. Leventis, "Fractal Multiscale Nanoporous Polyurethanes : Flexible to Extremely Rigid Aerogels from Multifunctional Small Molecules," *Chem. Mater.*, vol. 25, no. 15, pp. 3205–3224, **2013**, doi: 10.1021/cm401623h.

[138] J. P. Randall, M. A. B. Meador, and S. C. Jana, "Tailoring mechanical properties of aerogels for aerospace applications," *ACS Appl. Mater. Interfaces*, vol. 3, pp. 613–626, **2011**, doi: 10.1021/am200007n.

[139] O. A. Madyan, M. Fan, L. Feo, and D. Hui, "Enhancing mechanical properties of clay aerogel composites: An overview," *Compos. Part B Eng.*, vol. 98, pp. 314–329, **2016**, doi: 10.1016/j.compositesb.2016.04.059.

[140] X. Yang, Y. Sun, D. Shi, and J. Liu, "Experimental investigation on mechanical properties of a fiber-reinforced silica aerogel composite," *Mater. Sci. Eng. A*, vol. 528, pp. 4830–4836, **2011**, doi: 10.1016/j.msea.2011.03.013.

[141] M. Piñero, M. M. Mesa-Díaz, D. de los Santos, M. V. Reyes-Peces, J. A. Díaz-Fraile, N. de la Rosa-Fox, L. Esquivias, and V. Morales-Florez, "Reinforced silica-carbon nanotube monolithic aerogels synthesised by rapid controlled gelation," *J. Sol-Gel Sci. Technol.*, vol. 86, no. 2, pp. 391–399, **2018**, doi: 10.1007/s10971-018-4645-7.

[142] H. Maleki, L. Durães, and A. Portugal, "An overview on silica aerogels synthesis and different mechanical reinforcing strategies," *J. Non. Cryst. Solids*, vol. 385, pp. 55–74, **2014**, doi: 10.1016/j.jnoncrysol.2013.10.017.

[143] J. Lin, G. Li, W. Liu, R. Qiu, H. Wei, K. Zong, and X. Cai, "A review of recent progress on the silica aerogel monoliths: synthesis, reinforcement, and applications," *J. Mater. Sci.*, vol. 56, no. 18, pp. 10812–10833, **2021**, doi: 10.1007/s10853-021-05997-w.

[144] A. G. Evans, "Slow crack growth in brittle materials under dynamic loading conditions," *Int. J. Fract.*, vol. 10, no. 2, pp. 251–259, **1974**, doi: 10.1007/BF00113930.

[145] H. Ma, X. Zheng, X. Luo, Y. Yi, and F. Yang, "Simulation and analysis of mechanical properties of silica aerogels: From rationalization to prediction," *Materials (Basel).*, vol. 11, no. 2, pp. 1–12, **2018**, doi: 10.3390/ma11020214.

[146] C. Tan, B. M. Fung, J. K. Newman, and C. Vu, "Organic aerogels with very high impact strength," *Adv. Mater.*, vol. 13, no. 9, pp. 644–646, **2001**, doi: 10.1002/1521-4095(200105)13:9<644::AID-ADMA644>3.0.CO;2-#.

[147] S. Malakooti, S. Rostami, H. G. Churu, H. Luo, J. Clark, F. Casarez, O. Rettenmaier, S. Daryadel, M. Minary-Jolandan, C. Sotiriou-Leventis, N. Leventis, and H. Lu, "Scalable, hydrophobic and highly-stretchable poly(isocyanurate-urethane) aerogels," *RSC Adv.*, vol. 8, no. 38, pp. 21214–21223, **2018**, doi: 10.1039/c8ra03085e.

[148] A. Bang, C. Buback, C. Sotiriou-Leventis, and N. Leventis, "Flexible aerogels from hyperbranched polyurethanes: Probing the role of molecular rigidity with poly(Urethane Acrylates) versus poly(Urethane Norbornenes)," *Chem. Mater.*, vol. 26, no. 24, pp. 6979–6993, **2014**, doi: 10.1021/cm5031443.

[149] A. Shinko, S. C. Jana, and M. A. Meador, "Crosslinked polyurea-co-polyurethane aerogels with hierarchical structures and low stiffness," *J. Non. Cryst. Solids*, vol. 487, no. February, pp. 19–27, **2018**, doi: 10.1016/j.jnoncrysol.2018.02.020.

[150] R. Rajamanickam, S. Kumari, D. Kumar, S. Ghosh, J. C. Kim, G. Tae, S. Sen Gupta, and G. Kumaraswamy, "Soft colloidal scaffolds capable of elastic recovery after large compressive strains," *Chem. Mater.*, vol. 26, no. 17, pp. 5161–5168, **2014**, doi: 10.1021/cm502643a.

[151] R. Trifu, G. Gould, and S. White, "Flexible Polyisocyanate Based Aerogels," *MRS Adv.*, vol. 357, **2017**, doi: 10.1557/adv.201.

[152] C. Chidambareswarapattar, P. M. McCarver, H. Luo, H. Lu, C. Sotiriou-Leventis, and N. Leventis, "Fractal multiscale nanoporous polyurethanes: Flexible to extremely rigid aerogels from multifunctional small molecules," *Chem. Mater.*, vol. 25, no. 15, pp. 3205–3224, **2013**, doi: 10.1021/cm401623h.

[153] A. Rigacci, J. C. Marechal, M. Repoux, M. Moreno, and P. Achard, "Preparation of polyurethane-based aerogels and xerogels for thermal superinsulation," *J. Non. Cryst. Solids*, vol. 350, pp. 372–

378, **2004**, doi: 10.1016/j.jnoncrysol.2004.06.049.

[154] A. Bang, C. Buback, C. Sotiriou-Leventis, and N. Leventis, "Flexible aerogels from hyperbranched polyurethanes: Probing the role of molecular rigidity with poly(Urethane Acrylates) versus poly(Urethane Norbornenes)," *Chem. Mater.*, vol. 26, no. 24, pp. 6979–6993, **2014**, doi: 10.1021/cm5031443.

[155] N. Diascorn, S. Calas, H. Sallée, P. Achard, and A. Rigacci, "Polyurethane aerogels synthesis for thermal insulation - textural, thermal and mechanical properties," *J. Supercrit. Fluids*, vol. 106, pp. 76–84, **2015**, doi: 10.1016/j.supflu.2015.05.012.

[156] M. Lomba, J. Garduno, E. Torres, F. Salhi, S. Bassaganas, and A. Sakalyte, "Organic aerogels based on isocyanate and cyclic ether polymer networks," EP 3 124 516 A1, 2017.

[157] M. Reim, A. Beck, W. Körner, R. Petricevic, M. Glora, M. Weth, T. Schliermann, J. Fricke, C. Schmidt, and F. J. Pötter, "Highly insulating aerogel glazing for solar energy usage," *Sol. Energy*, vol. 72, no. 1, pp. 21–29, **2002**, doi: 10.1016/S0038-092X(01)00086-X.

[158] "https://www.cabotcorp.com/."

[159] C. Buratti, Moretti, Elisa, and E. Belloni, "Nanogel Windows for Energy Building Efficiency," in *Nano and Biotech Based Materials for Energy Building Efficiency*, Switzerland: Springer International Publishing, 2016, pp. 41–69. doi: 10.1007/978-3-319-27505-5.

[160] T. Gao, B. P. Jelle, and A. Gustavsen, "Building Integration of Aerogel Glazings," *Procedia Eng.*, vol. 145, pp. 723–728, **2016**, doi: 10.1016/j.proeng.2016.04.090.

[161] U. Berardi, "The development of a monolithic aerogel glazed window for an energy retrofitting project," *Appl. Energy*, vol. 154, pp. 603–615, **2015**, doi: 10.1016/j.apenergy.2015.05.059.

[162] M. A. Mujeebu, "Nano aerogel windows and glazing units for buildings' energy efficiency," in *Nanotechnology in Eco-efficient Construction.*, Woodhead Publishing, 2018, pp. 417–439. doi: 10.1016/B978-0-08-102641-0.00018-9.

[163] E. J. Hogan, M. T. Krajewski, and P. Muthukumaran, "Aerogel-based vehicle thermal management systems and methods," 0238008, 2007.

[164] Y. S. Kishore, "Aerogel : Future Material of Automobile Industry," *Int. Res. J. Eng. Technol.*, vol. 7, no. 6, pp. 5244–5246, **2020**.

[165] L. W. Hrubesh, "Aerogel applications," *J. Non. Cryst. Solids*, vol. 225, no. 1–3, pp. 335–342, **1998**, doi: 10.1016/S0022-3093(98)00135-5.

[166] S. Henning, G. Jarlskog, U. Mjörnmark, A. Nilsson, and L. Svensson, "An aerogel cerenkov counter for the AFS experiment," *Phys. Scr.*, vol. 23, no. 4, pp. 703–707, **1981**, doi: 10.1088/0031-8949/23/4B/019.

[167] D. E. Fields, H. van Hecke, J. Boissevain, B. V. Jacak, W. E. Sondheim, J. P. Sullivan, W. J. Willis, K. Wolf, E. Noteboom, P. M. Peters, and R. Burke, "Use of aerogel for imaging Cherenkov counters," *Nucl. Inst. Methods Phys. Res. A*, vol. 349, no. 2–3, pp. 431–437, **1994**, doi: 10.1016/0168-9002(94)91207-6.

[168] N. Bheekhun, A. Rahim, A. Talib, and M. R. Hassan, "Aerogels in Aerospace: A Review," *Adv. Mater. Sci. Eng.*, vol. 2013, **2013**.

[169] S. M. Jones, "Aerogel: Space exploration applications," *J. Sol-Gel Sci. Technol.*, vol. 40, no. 2–3, pp. 351–357, **2006**, doi: 10.1007/s10971-006-7762-7.

[170] K. Maex, M. R. Baklanov, D. Shamiryan, F. Iacopi, S. H. Brongersma, and Z. S. Yanovitskaya, "Low dielectric constant materials for microelectronics," *J. Appl. Phys.*, vol. 93, no. 11, pp. 8793–8841, **2003**, doi: 10.1063/1.1567460.

[171] Y. J. Kim, S. H. Yoo, H. G. Lee, Y. Won, J. Choi, and K. Kang, "Structural Analysis of silica aerogels for the interlayer dielectric in semiconductor devices," *Ceram. Int.*, vol. 47, pp. 29722–29729, **2021**, doi: 10.1016/j.ceramint.2021.07.144.

[172] X. Wang, L. Liang, H. Lv, Y. Zhang, and G. Chen, "Elastic aerogel thermoelectric generator with vertical temperature-difference architecture and compression-induced power enhancement," *Nano Energy*, vol. 90, no. PA, p. 106577, **2021**, doi: 10.1016/j.nanoen.2021.106577.

[173] Q. Zheng, H. Zhang, H. Mi, Z. Cai, Z. Ma, and S. Gong, "High-performance flexible piezoelectric nanogenerators consisting of porous cellulose nanofibril (CNF)/poly(dimethylsiloxane) (PDMS) aerogel films," *Nano Energy*, vol. 26, pp. 504–512, **2016**, doi: 10.1016/j.nanoen.2016.06.009.

[174] F. Ram, K. Suresh, A. Torris, G. Kumaraswamy, and K. Shanmuganathan, "Highly compressible ceramic/polymer aerogel-based piezoelectric nanogenerators with enhanced mechanical energy harvesting property," *Ceram. Int.*, vol. 47, pp. 15750–15758, **2021**, doi: 10.1016/j.ceramint.2021.02.147.

[175] S. R. Kurundawade, R. S. Malladi, R. M. Kulkarni, and A. A. Parwaz Khan, *Natural aerogels for pollutant removal*. Elsevier Inc., 2021. doi: 10.1016/B978-0-12-820732-1.00002-3.

[176] R. Ganesamoorthy, V. K. Vadivel, R. Kumar, O. S. Kushwaha, and H. Mamane, "Aerogels for water treatment: A review," *J. Clean. Prod.*, vol. 329, p. 129713, **2021**, doi: 10.1016/j.jclepro.2021.129713.

[177] V. T. Nguyen, L. Q. Ha, T. D. L. Nguyen, P. H. Ly, D. M. Nguyen, and D. Hoang, "Nanocellulose and Graphene Oxide Aerogels for Adsorption and Removal Methylene Blue from an Aqueous Environment," *ACS Omega*, vol. 7, no. 1, pp. 1003–1013, **2022**, doi: 10.1021/acsomega.1c05586.

[178] A. Lamy-Mendes, R. B. Torres, J. P. Vareda, D. Lopes, M. Ferreira, V. Valente, A. V. Girão, A. J. M. Valente, and L. Durães, "Amine modification of silica aerogels/xerogels for removal of relevant environmental pollutants," *Molecules*, vol. 24, no. 20, pp. 2–4, **2019**, doi: 10.3390/molecules24203701.

[179] I. Ihsanullah, M. Sajid, S. Khan, and M. Bilal, "Aerogel-based adsorbents as emerging materials for the removal of heavy metals from water: Progress, challenges, and prospects," *Sep. Purif. Technol.*, vol. 291, p. 120923, **2022**, doi: 10.1016/j.seppur.2022.120923.

[180] T. Paulauskiene, J. Uebe, A. U. Karasu, and O. Anne, "Investigation of Cellulose-Based Aerogels for Oil Spill Removal," *Water. Air. Soil Pollut.*, vol. 231, p. 424, **2020**, doi: 10.1007/s11270-020-04799-1.

[181] C. A. García-González, A. Sosnik, J. Kalmár, I. De Marco, C. Erkey, A. Concheiro, and C. Alvarez-Lorenzo, "Aerogels in drug delivery: From design to application," *J. Control. Release*, vol. 332, pp. 40–63, **2021**, doi: 10.1016/j.jconrel.2021.02.012.

[182] N. S. Sani, N. A. N. N. Malek, K. Jemon, M. R. A. Kadir, and H. Hamdan, "Preparation and characterization of hydroxyapatite incorporated silica aerogel and its effect on normal human dermal fibroblast cells," *J. Sol-Gel Sci. Technol.*, vol. 90, no. 2, pp. 422–433, **2019**, doi: 10.1007/s10971-019-04946-z.

[183] P. Veres, G. Király, G. Nagy, I. Lázár, I. Fábián, and J. Kalmár, "Biocompatible silica-gelatin hybrid aerogels covalently labeled with fluorescein," *J. Non. Cryst. Solids*, vol. 473, pp. 17–25, **2017**, doi: 10.1016/j.jnoncrysol.2017.07.016.

CHAPTER 3

EXPERIMENTAL SECTION: MATERIALS AND TECHNIQUES

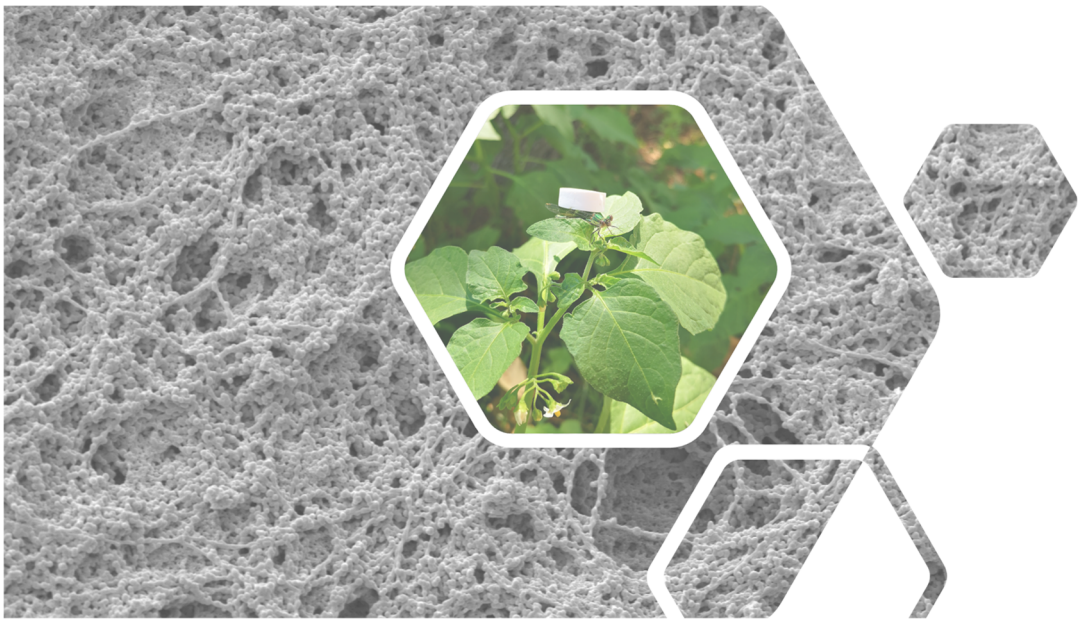

Chapter 3. Experimental section: Materials and Techniques

3.1 Introduction

The third chapter gathers the experimental methods concerning this thesis. First, the materials used along this research, the formulations developed for the aerogels (both, silica and polyurethane-based), the flexible PU foams used to produce the composites, and the production methods are carefully described.

Then, the characterization techniques employed for the analysis of the porous structure and the methodologies used to determine the optical, mechanical and thermal properties are herein described.

3.2 Materials and formulations

3.2.1 Polyurethane aerogel formulations

Polyurethane is an organic polymer based on the repetition of urethane linkages. Its chemistry was discovered and patented in 1937 by Otto Bayer, who developed the novel polyisocyanate-polyaddition process. The widespread use of this polymer is mainly owing to its cost-effectiveness, versatility, and interesting properties. The traditional synthesis of this polymer consists of the reaction between an organic isocyanate (diisocyanate or a polymeric isocyanate) and a compound containing hydroxyl groups in presence of the corresponding catalysts and additives, as described in **Figure 3.1**.

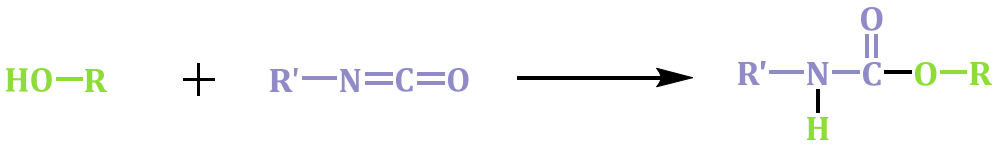

Figure 3.1. Polyurethane reaction.

The starting point for the manufacturing of PU aerogels in this thesis were several formulations previously developed in CellMat for PU foams. The use of different catalysts resulted in significant changes on the aerogels structure, as shown in **Figure 3.2**.

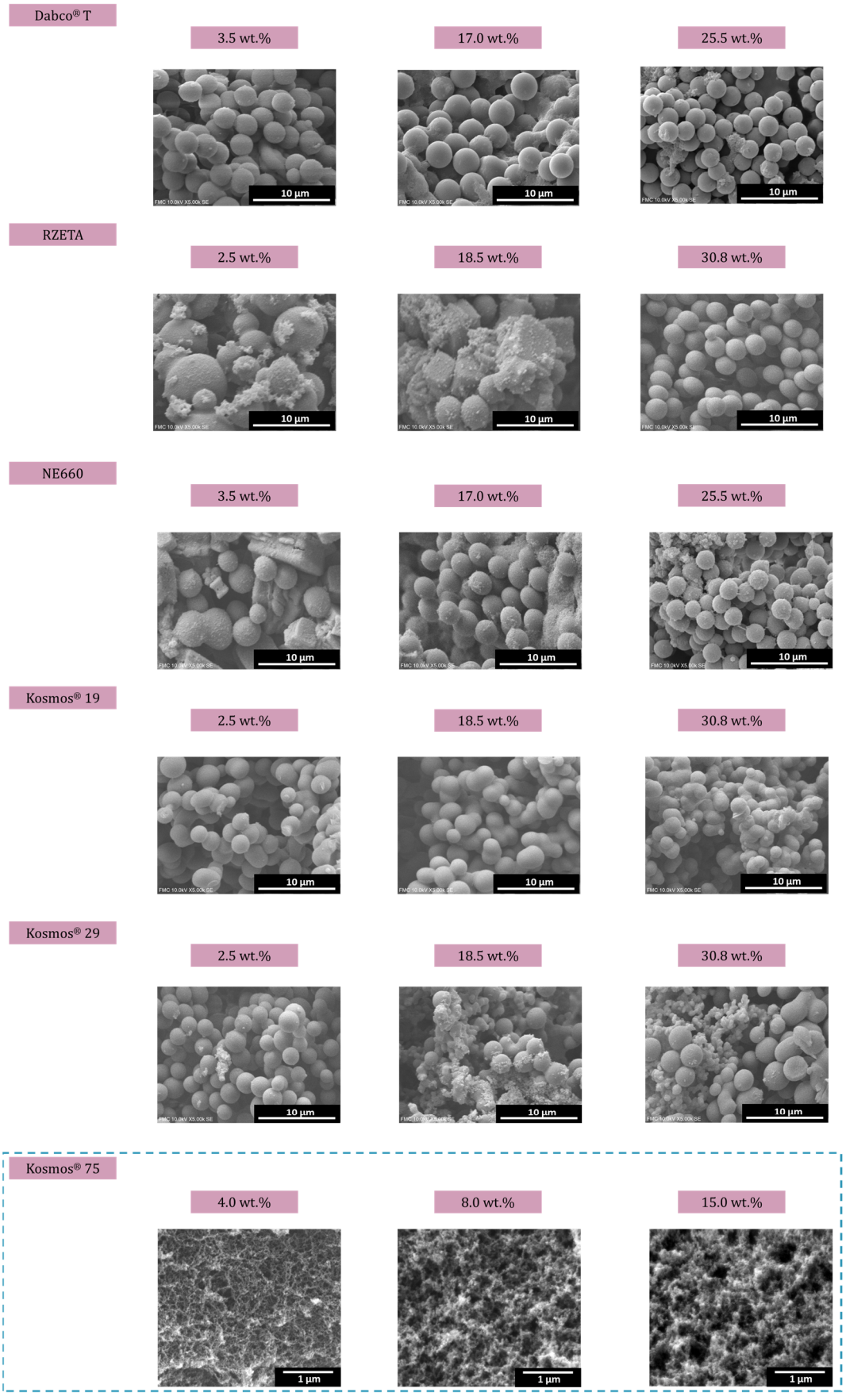

Figure 3.2. Scanning electron micrographs for different polyurethane-based aerogels produced with different catalysts and catalyst contents.

After a thorough study of the different structures produced with these catalysts, one of them was selected. The catalyst chosen, KOSMOS® 75 MEG, to carry out the herein presented research was the one which led to the porous structure with the smallest features. The employed reactants for the formulation used to produce the PUR-PIR aerogels and their main properties are described in **Table 3.1.**

Table 3.1. Components and characteristics for polyurethane aerogels.

Reactant	Density (g/cm^3)	Viscosity (mPa·s)	Concentration (g/L)	Solvent
IsoPMDI® 92140	1.230	170 – 250 (25°C)	44	65 % vol CH_3CN/35 % vol THF
Pentaerythritol	1.396	-	100	DMSO
KOSMOS® 75 MEG	-	< 3500 (23°C)	70	THF

The formulation was based on a polymeric isocyanate (methylene diphenyl diisocyanate) (p-MDI) corresponding to the formulation 4,4'-diphenylmethane diisocyanate, IsoPMDI® 92140 (ρ = 1.230 g/cm^3 at 25 °C), purchased from BASF Polyurethane. The employed polyol was pentaerythritol (purity > 98%) with a density of ρ = 1.396 g/cm^3 (at 20 °C) provided by Alfa Aesar. This polyol was received as a solid material (**Figure 3.3b**). The catalyst promoting the chemical reaction is a potassium octoate compound dissolved in ethylene glycol that is commercialized as KOSMOS® 75 MEG, by Evonik. The solvents employed for the dissolutions were tetrahydrofurane (THF) extra pure (purity > 99.5 %) stabilized with 250 ppm of butylated hydroxytoluene (BHT), acetonitrile (CH_3CN) HPLC grade (purity > 99.9 %), dimethyl sulfoxide synthesis grade (DMSO) (purity > 99.5 %) and acetone synthesis grade (purity > 99.5 %). All of them were supplied by Scharlab, S. L.

The FT-IR spectra of the two main reactants and a scanning electron micrograph of the solid polyol can be found in **Figure 3.3**. Both spectra display the main peaks corresponding to their functional groups. The granular polyol showed particles in the millimetric scale.

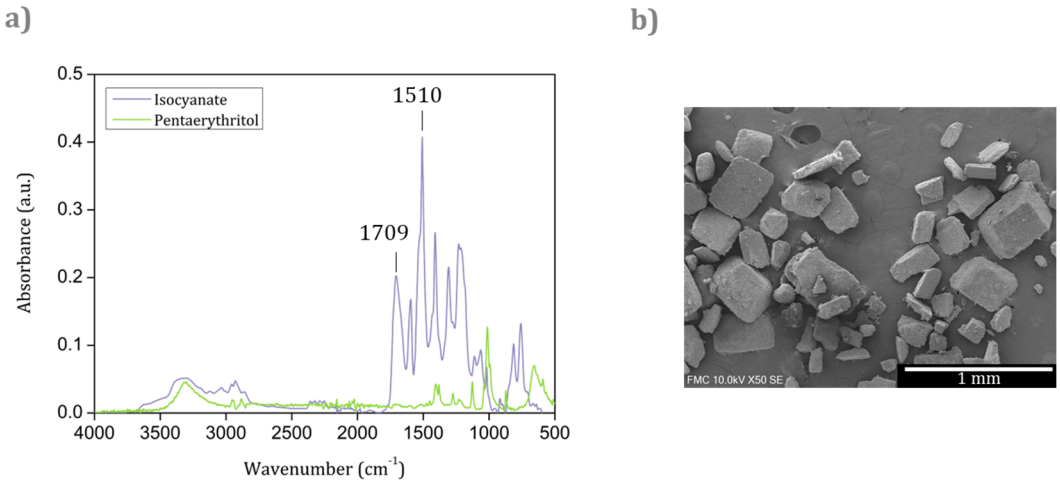

Figure 3.3. a) FT-IR spectra of the polyol and isocyanate, b) Scanning electron micrograph of the solid polyol.

The complete formulation for a final solution of ca. 100 mL is described in **Table 3.2**. The catalyst volume varies from 0.65 to 12.89 mL depending on the desired formulation. A range of catalyst content from 1 to 20 wt.% was used for these studies. The weight percentage of the catalyst is calculated from the total mass of both precursors, polyol, and isocyanate.

Table 3.2. Concentration and volume of the initial reactants for a final solution of ca. 100 mL.

Reactant	Concentration (mmol)	Volume (mL)
IsoPMDI® 92140	14.60	83.00
Pentaerythritol	6.30	8.58
KOSMOS® 75 MEG	-	[0.65 – 12.89]

This formulation was used for several studies of this thesis, gathered in **Chapter 4, 5 and 6**, in order to study the optical, mechanical and thermal properties of polyisocyanurate-polyurethane (PIR-PUR) based aerogels and for the synthesis of polyurethane aerogel-polyurethane foam composites. The reaction between the diisocyanate and the selected branched polyol leads to the formation of a hyperbranched solid network as described by **Figure 3.4**.

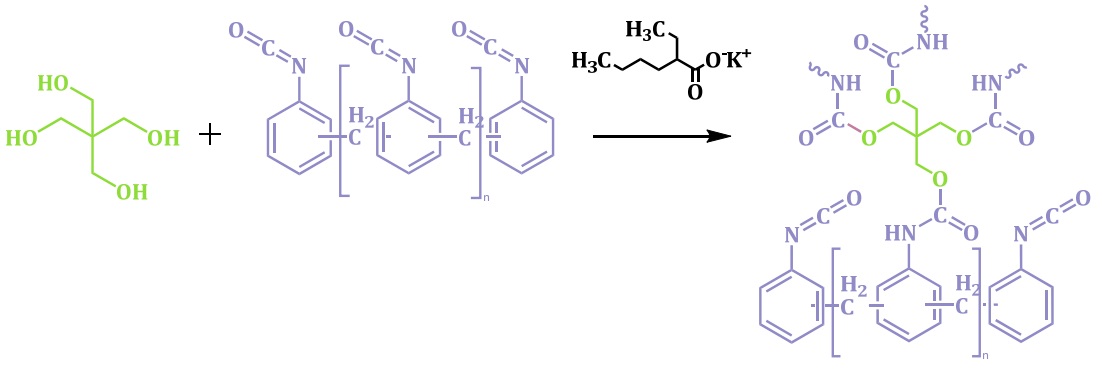

Figure 3.4. Polycondensation reaction between polyol and polymeric isocyanate to form the polyurethane aerogel network.

The molar relationship between polyol and isocyanate was 0.43, thus, an excess of -NCO groups is present. This excess of isocyanate promotes a secondary reaction by trimerization leading to the formation of isocyanurate (**Figure 3.5**).

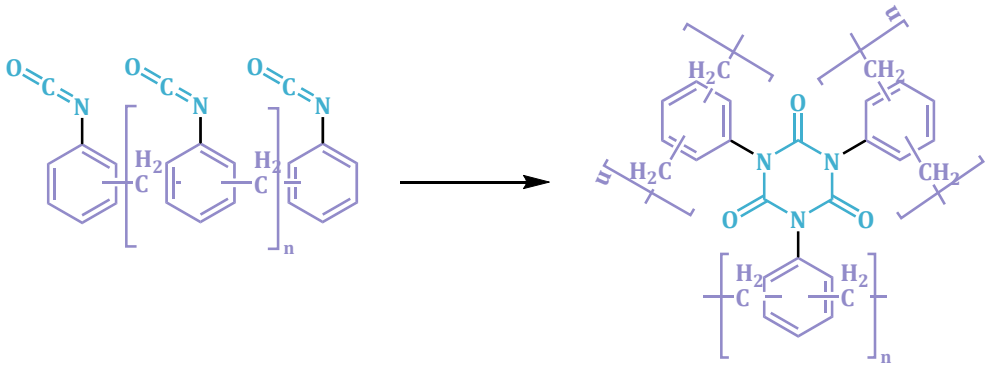

Figure 3.5. Isocyanate trimerization reaction to form isocyanurate.

3.2.2 Silica aerogel formulations

Silica aerogel formulations can be developed from a great variety of silica precursors. The silica formulations employed in this thesis are based on tetraethoxysilane (TEOS, $Si(OC_2H_5)_4$, 98%) supplied by Acros Organics. To promote the polymerization, a hydrolysis step followed by the condensation step are necessary. Therefore, acid and basic catalysts for inducing these chemical reactions were employed. The acid catalyst is based on oxalic acid ($C_2H_2O_4$, 99% in H_2O) and the basic ones on ammonium hydroxide (NH_4OH, 25% NH_3 in H_2O) purchased from Fluka Analytical. Ethanol (EtOH, absolute, C_2H_5OH), provided by Fluka Analytical was used as solvent for the silica precursor. The corresponding concentrations and properties are gathered in **Table 3.3**.

Table 3.3. Components and characteristics for silica aerogels.

Reactant	Density (g/cm^3)	Molar mass (g/mol)	Concentration (M, mol/L)	Solvent
TEOS	0.933	208.33	0.91	EtOH
NH_4OH	-	35.04	1	Distilled H_2O
$C_2H_2O_4$	-	90.03	0.01	Distilled H_2O

The specific molar proportion between the initial precursor, solvent and catalysts is defined in the following table:

Table 3.4. Molar proportion of the different chemical compounds.

Reactant	Reactant amount (mol)
TEOS	0.1
EtOH	1.5
NH_4OH (solution)	0.4
$C_2H_2O_4$ (solution)	0.4

The chemical reactions forming the silica-based aerogels are described in **Figure 3.6**:

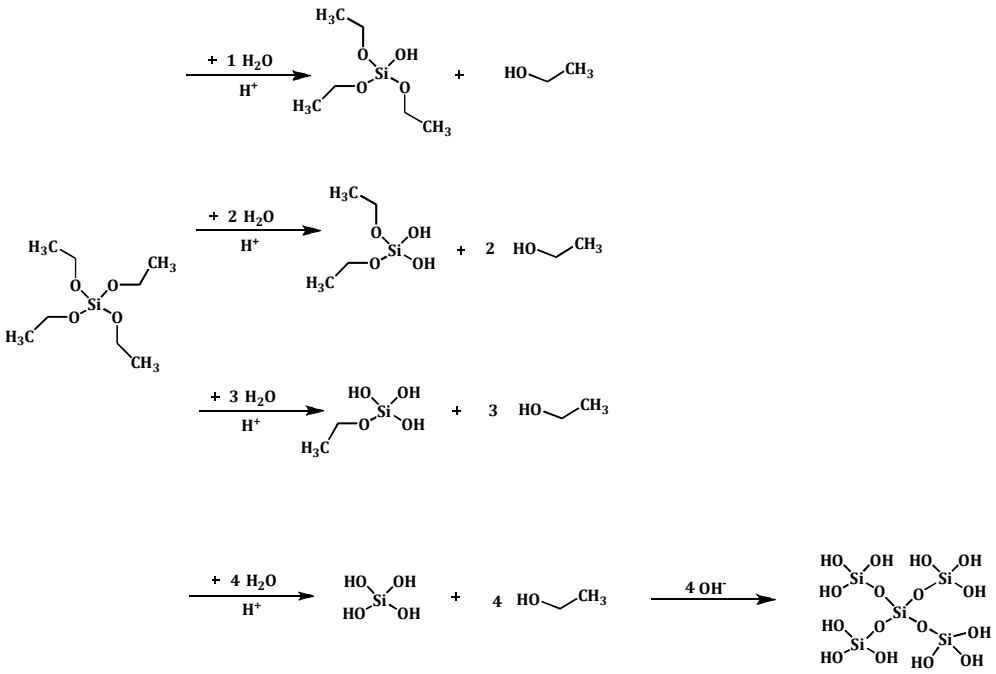

Figure 3.6. Hydrolysis and condensation reactions of the silica precursor.

For some of the aerogels produced, a silylating agent was used for carrying out a surface modification on the produced gels. The selected compound was hexamethyldisilazane (HMDZ, $(CH_3)_3SiNHSi(CH_3)_3$, > 98%) obtained from Alfa Aesar, which reacts with the silanol groups to avoid further condensation. Reaction of silanol groups with HMDZ are displayed in **Figure 3.7**.

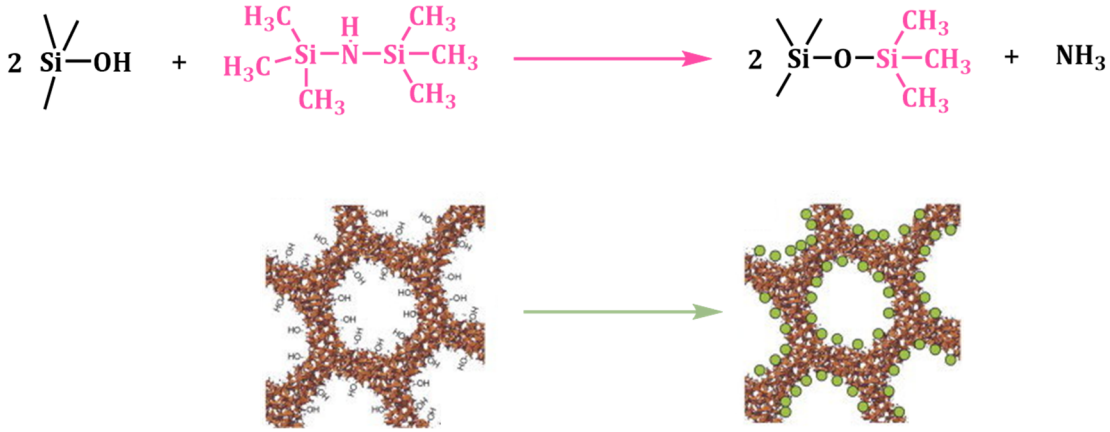

Figure 3.7. Reaction between silanol groups and hexamethyldisilazane [1].

3.2.3 Carbon nanotubes

Commercial multi-walled carbon nanotubes (CNTs) were purchased from Nanocyl (average length of 1.5 µm, average diameter of 9.5 nm, surface area of ca. 250 – 300 m^2/g). A silane modification was performed on these nanotubes as described by Kim et al. [2] to improve their dispersibility and interfacial bonding. The silinization treatment consists on two steps: first, refluxing for 20 h at 50 °C with nitric acid (Sigma Aldrich, 70 %). Afterwards, carbon nanotubes were filtered with a Büchner funnel and washed with water until reaching

an almost neutral pH. Then, carbon nanotubes were dried overnight in an oven at 60 °C. The second modification step consists on the silane modification. CNTs were submitted to a reflux for 4 h at 70 °C with a solution of tetramethyl orthosilicate (TMOS). This solution has a concentration of 10 % of TMOS and the solvent is a mixture of 70 % ethanol/30% water. Finally, CNTs were filtered and dried for 1 day at 60 °C. The hydrodynamic diameter after the modification is ca. 270.1 ± 5.03 nm [3].

Carbon nanotubes were visualized by means of transmission electron microscopy (**Figure 3.8**) and the average diameter after the silane modification was 14.31 ± 1.25 nm.

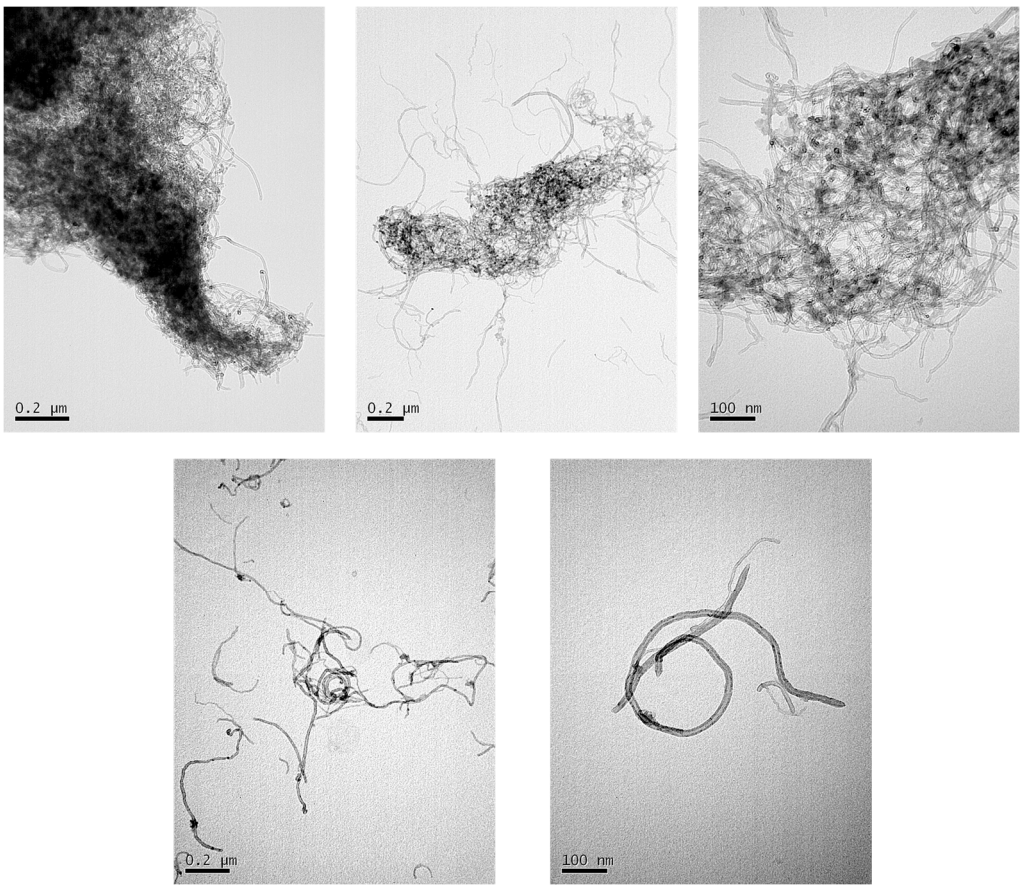

Figure 3.8. Transmission electron microscopy of the modified carbon nanotubes.

The characteristic chemical bonds of the modified nanotubes were confirmed by FT-IR (**Figure 3.9**). The following silica related peaks can be identified:

- Si-O-Si bending at 1020 cm^{-1}
- Si-O stretching vibration at 550 and 870 cm^{-1}
- O-H stretching (Si-O-H) at 3770 cm^{-1}

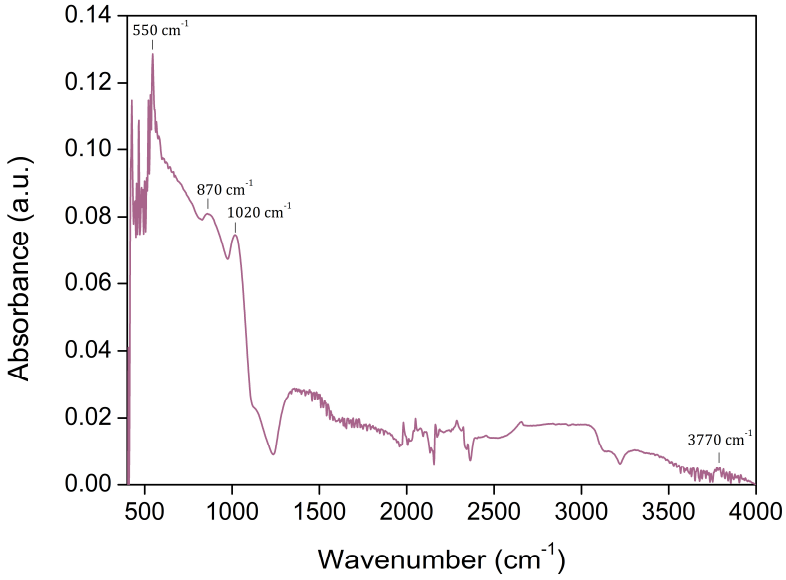

Figure 3.9. Infrared spectrum of the modified carbon nanotubes (CNTs-TMOS).

3.3 Production methods

The synthesized samples were produced by the sol-gel process and then dried by different methods, as described below.

3.3.1 Synthesis

The sol-gel method used for the aerogel syntheses consists of an initial solution containing the precursors and, after the addition of the corresponding catalysts which promotes the polymerization reactions, several colloidal particles form a sol. After further polymerization and growing of these particles, gelation step takes place forming a wet-gel.

3.3.1.1 Polyurethane aerogels

The polycondensation reaction occurs by mixing the isocyanate solution (44 g/L) with the secondly added polyol solution (100 g/L) (see **Table 3.1**) in a plastic cup. After the addition of both precursors, an amount of catalyst [1 – 20 wt.% over the total mass of polyol and isocyanate] is added to the mixture and stirred with an electric stirrer (EUROSTAR Power control-visc P1, IKA provided with a 50 mm diameter Lenart disc) at 500 rpm for 20 seconds at room temperature.

Once the gelation takes place, the wet-gel was covered with acetonitrile for 24 hours to prevent evaporation and to allow the non-reacted chemicals to react (ageing). Then, the gel was washed twice with acetonitrile every 24 hours to remove the remining compounds that are not attached to the polymeric structure. The whole process is summarized in **Figure 3.10**. The drying methods will be described in the following **section 3.3.2**.

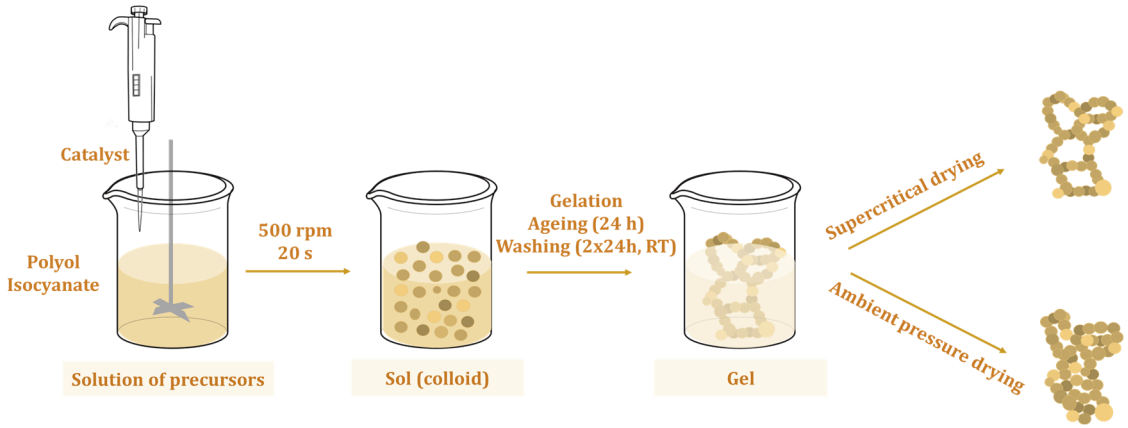

Figure 3.10. Synthesis procedure for PU aerogels.

Aerogels were produced with cylindrical shape of either ca. 10 mm height and 38 mm diameter for thermal conductivity characterization, or either ca. 8 mm in height, and 15 mm in diameter for mechanical characterization.

Polyurethane aerogels containing carbon nanotubes

The silane–modified CNTs (**section 3.2.3 Carbon nanotubes**) were used as fillers during the synthesis of the polyurethane aerogels. The corresponding amount of CNTs was added to the isocyanate solution. An initial dispersion of these fillers was performed by sonication for 30 minutes. Then, the solution was continuously stirred at 250 rpm with a magnetic stirrer and the polyol and catalyst solutions were added. This mixing was applied until reaching a viscosity that does not allow the stirrer to move which, at that moment, is removed from the gel (**Figure 3.11**).

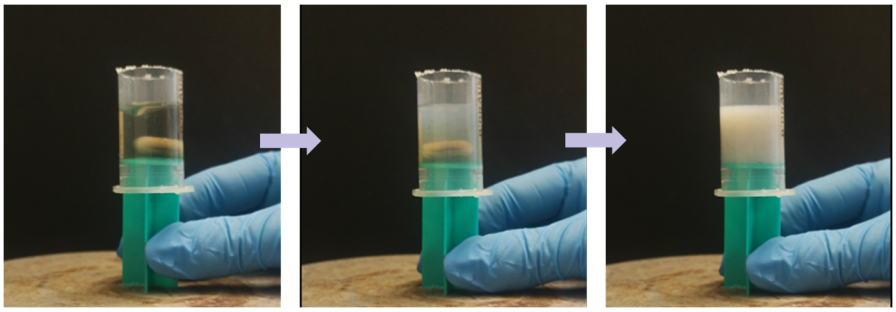

Figure 3.11. Pictures of the gelation process under magnetic stirring for the polyurethane aerogels containing CNTs.

Once gels were obtained, the same procedure previously described for the pristine polyurethane aerogels was followed.

The synthesized samples were cylinders of either ca. 40 mm diameter and 15 – 20 mm height or 16 mm diameter and 7 – 14 mm of height for the thermal conductivity and mechanical measurements, respectively.

3.3.1.2 Silica aerogels

Monolithic silica aerogels (modified and unmodified) were synthesized by using TEOS as precursor in a two-step acid-base catalyzed sol-gel method (**Figure 3.12**). First, a solution of the silica precursor in ethanol was prepared (concentrations can be found at **Table 3.3**). Then the acidic reaction was promoted by the addition of the corresponding amount of a solution of oxalic acid (0.01 M in distilled water). The resulting mixture was stirred by a magnetic stirrer at 300 rpm for 30 min at room temperature and then placed into an oven at 27 °C for 24 h, in order to ensure an effective hydrolysis. After the completion of the hydrolysis process, the basic catalyst (1 M in distilled water) was dropped, and the blend was mixed at 300 rpm for 45 s. A clear transition from sol to gel was observed after the gelation time obtaining a gelly-like monolith. The beaker containing the specimen was sealed and placed into an oven at 27 °C for 7 days following previously described procedures [4]. Finally, a washing step with ethanol (2 x 12 h at 50 °C) was performed after demolding the monoliths.

Once gels were washed, a surface modification was carried out for the modified samples by covering the produced gels with a mixture of 30 % vol. of HMDZ in ethanol at 50 °C for 24 h. Finally, gels were dried by the corresponding method as specified in the following section.

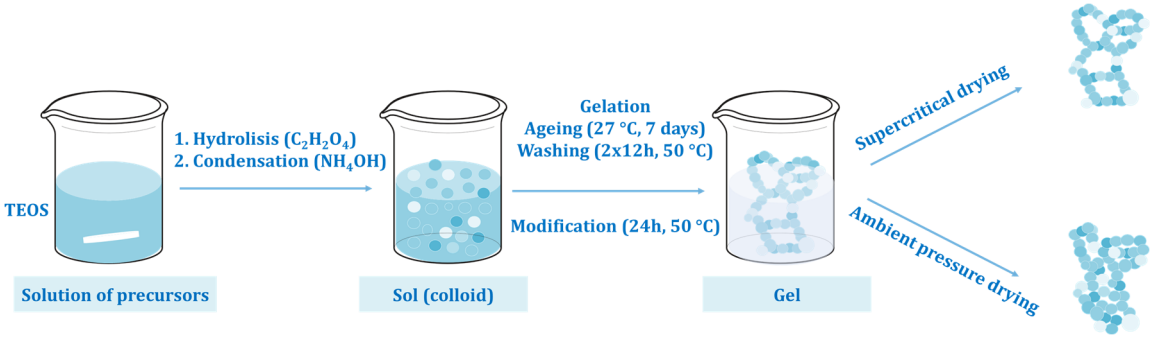

Figure 3.12. Synthesis procedure for silica aerogels.

The dimensions of the produced samples were diameters between 12 and 16 mm and heights of ca. 10 mm.

3.3.1.3 Polyurethane foam-Polyurethane aerogel composites

The inner structure of reticulated polyurethane foams was filled with polyurethane aerogel. The reticulated PU foams were purchased from Recticel Ibérica, S.L. (Spain). Three flexible reticulated foams having different pore sizes were chosen for the synthesis of the composites. The corresponding labels for these samples are S (small), M (medium) and L (large) according to their cell size. The main features of these foams are gathered in **Figure 3.13**.

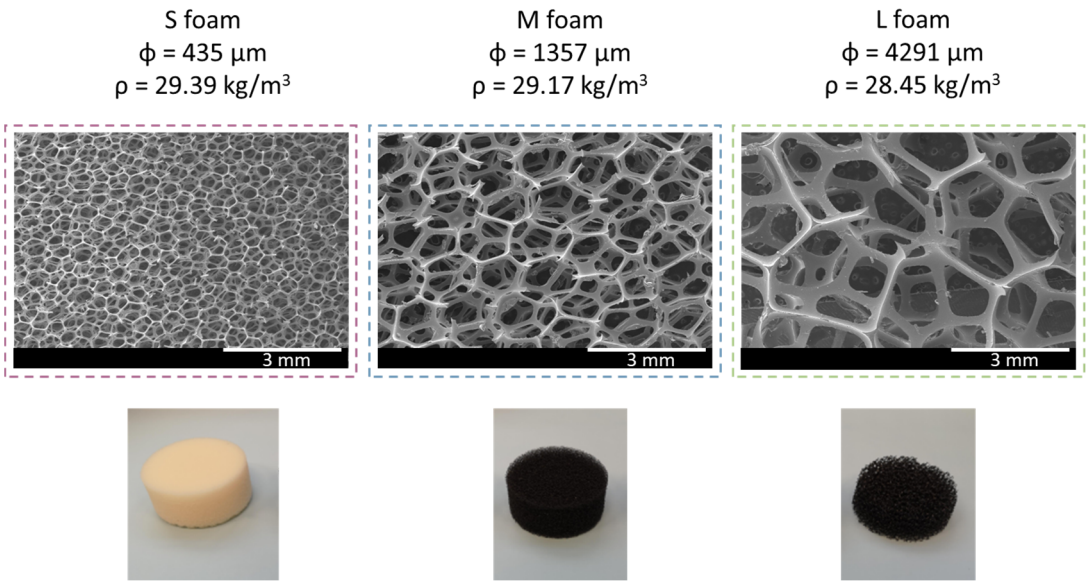

Figure 3.13. Flexible reticulated PU foams supplied by Recticel Ibérica, their pore size and SEM micrographs.

Polyurethane foam – Polyurethane aerogel (PU_F - PU_A) composites were produced following the same procedure as for the polyurethane aerogels, but using the flexible polyurethane foam as an scaffold for the aerogel. The catalyst amount selected for these materials was 4 wt.%. Once the corresponding amounts of polyol and catalyst were added to the isocyanate solution (n_{iso}/n_{pol} molar ratio of 2.32), the mixture was stirred with an electric mixer at 500 rpm for 20 s. The resultant sol was poured into a beaker containing the polyurethane foam until the latter was completely covered. The foams that floated in the solution were slightly pushed to the bottom until being hold by the viscous gel. Once the gelation was complete (gel time ca. 28 min), the gelly-like composites were covered with acetonitrile for 24 h and then washed twice with the same solvent at room temperature as previously described in **section 3.3.1.1** (**Figure 3.14**). Finally, the gels thus obtained were dried.

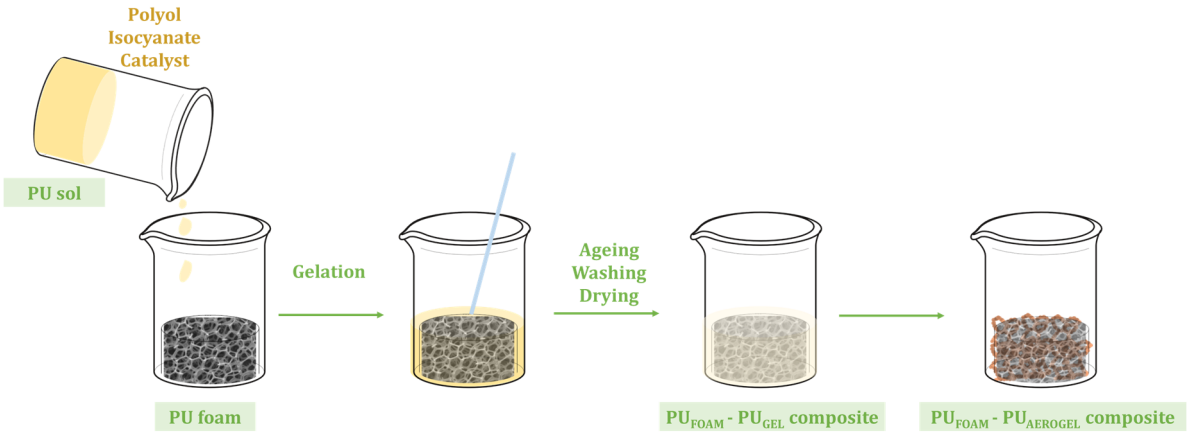

Figure 3.14. Synthesis procedure for PU_F-PU_A composites.

Cylinders of ca. 30 mm diameter and 12 mm height were used for the thermal conductivity measurements, and the mechanical tests were performed on cylindrical samples of 15 – 20 mm diameter and 10 – 12 mm height.

3.3.1.4 Silica aerogel-Polyurethane foam composites

Silica aerogels were reinforced by the incorporation of a polyurethane skeleton by using the flexible reticulated S, M, and L foams described in the previous section. The experimental steps are: preparing the silica precursor solution, running the hydrolysis reaction and, just after adding the basic catalyst to start the condensation process, and pouring the resultant sol into a beaker where the PU foam has been placed. After the gelation finishes, the same steps explained in section Silica aerogels3.3.1.2 were followed: 7 days in an oven at 27 °C and two 12 h washings with ethanol at 50 °C. The composites in which a surface modification with HMDZ is applied were submerged into a solution with the modifier (30 % vol. of HMDZ in ethanol) at 50 °C for 24 h. The obtained jelly composites were then dried.

Different sample sizes were produced: for the mechanical tests, cylinders with a diameter between 12 and 16 mm and height of ca. 10 mm; whereas cylinders with a diameter between 30 and 45 mm and a thickness between 20 and 22 mm were obtained for the thermal conductivity measurements.

3.3.2 Drying methods

Once the wet-gels were obtained, the removal of the solvent filling the gel pores must be carried out. Different drying techniques have been used in this thesis.

Ambient Pressure Drying (APD)

The monolithic polyurethane and silica aerogels were dried at ambient pressure to analyze the effect of this method on their density and shrinkage. The polyurethane aerogel samples were allowed to dry at room temperature for several days. However, the capillary forces caused by solvent evaporation led to a huge shrinkage, as shown in **Figure 3.15**, therefore, this method was not further applied along this thesis for the PU aerogels.

Figure 3.15. Polyurethane aerogels obtained once dried by supercritical drying (left) and by ambient pressure drying (right).

The silica aerogels followed a different APD process. First, by an initial drying step of 5 h at room temperature to keep a slow evaporation, followed by heating at 60 °C for 24 h. Finally, the samples were heated at 150 °C during 2 additional hours, in order to ensure a complete

drying of the samples. The APD aerogels were not able to withstand the capillary forces during the drying procedure and they were broken into small pieces (**Figure 3.16**).

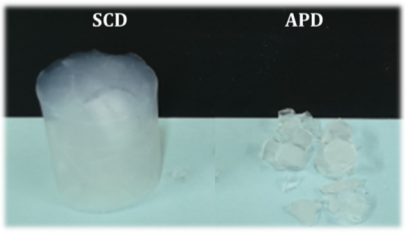

Figure 3.16. Silica aerogels dried by supercritical drying (left) and by ambient pressure drying (right).

Supercritical Drying (SCD)

The other drying process applied for the polyurethane and silica aerogels, as well as for the composites, was supercritical drying. The gas used for this procedure is carbon dioxide (CO_2). As observed in **Figure 3.17**, carbon dioxide is a gas at ambient conditions of temperature and pressure. However, reaching the critical point from which the supercritical state is achieved is possible at relatively mild conditions: 31 °C and 73 bar. The supercritical state consists on a hybrid behavior between gaseous and liquid state. In this case density is close to that of the liquid, whereas the viscosity and diffusion coefficients are higher and similar to those of the gas. These conditions facilitate the elimination of the biphasic system liquid-gas present if evaporation takes place, which would cause pressure gradients inside the gel pores.

The choice of CO_2 (medical grade liquid CO_2, purity > 99.9 %) is not only due to its "mild supercritical conditions" but this gas is considered as environmentally friendly in comparison with other possible alternatives, that could leave hazardous chemical compounds, be pollutant, or have a higher global warming potential [5].

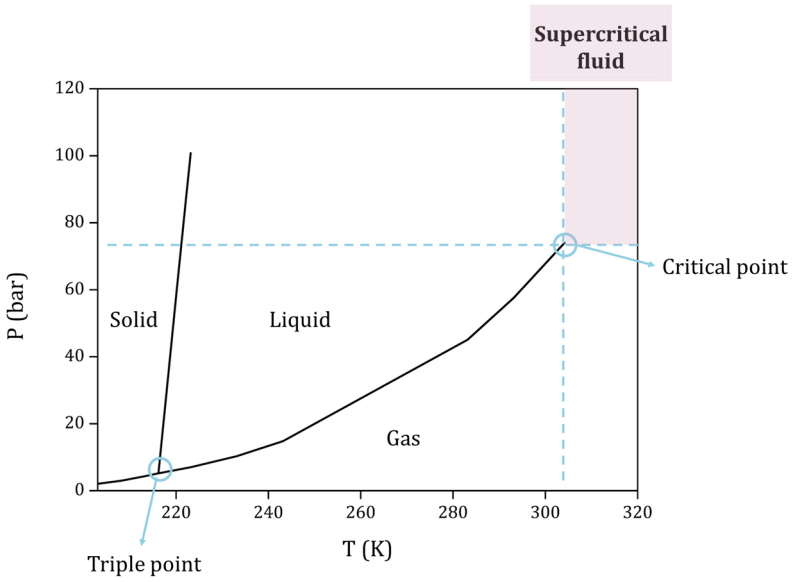

Figure 3.17. Phase diagram for CO_2.

The drying setup employed for this thesis is summarized in **Figure 3.18**. It consists of two non-stirred pressure vessels purchased from Parr Instrument Company (Moline, IL, USA), with a maximum working temperature of 350 °C. The capacity of the pressure vessels is 600 mL for vessel 1 (model PARR 4760) and 970 mL for vessel 2 (model PARR 4600), and the maximum allowable operating pressures (MAWP) are 20.68 MPa and 19.99 MPa, respectively. A thermowell with a type J thermocouple (5) is included in both reactors to accurately measure the inner temperature during the process.

Additionally, the pressure vessel number 2 (4600 reactor) includes a dip tube for solvent extraction (7) and a metering valve which allows a slow depressurization (8). Both reactors are placed into a thermal bath (Selecta, UNITRONIC 200) (9), and the whole system also includes a pressure pump (4), pressure regulator (6) and the CO_2 bottle (3).

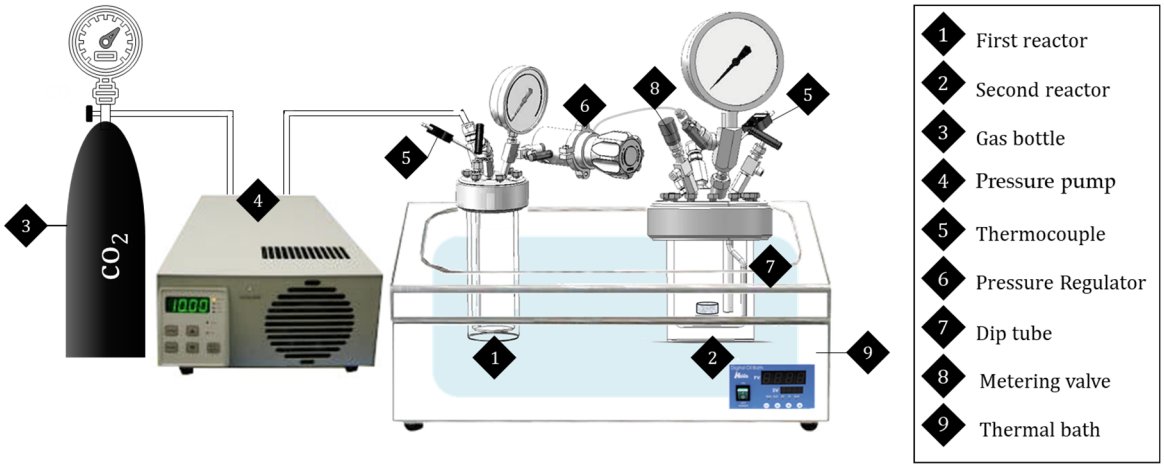

Figure 3.18. Supercritical drying setup.

The SCD process takes place as follows (**Figure 3.19**):

First, gels are placed into the pressure vessel 2 and covered with the corresponding solvent (acetone for the polyurethane aerogels and polyurethane-based composites, and ethanol for the silica aerogels and silica-based composites) which prevents the inner solvent from premature evaporation.

Then, carbon dioxide is pressurized over the critical pressure (up to 100 bar), and the thermal bath is heated at a constant temperature of 50 °C. Both thermocouples indicated that the temperature inside the reactors is constant and equal to that of the thermal bath (**Figure 3.19, step 1**).

Once supercritical conditions are reached (**Figure 3.19, step 2**), the covering solvent is extracted through the dip tube and collected into a beaker so its volume can be measured (**Figure 3.19, step 3**).

The drying process starts after the solvent extraction. Since it is a static process, the supercritical carbon dioxide ($scCO_2$) is in contact with the gel samples for a certain time which varies depending on the number and volume of the samples. Then, the CO_2 enriched in solvent (the solvent filling the gel pores) is slowly extracted (**Figure 3.19, step 4**). In order to maintain the supercritical pressure during the CO_2 evacuation, clean $scCO_2$ from the reactor

1 (which acts as $scCO_2$ storage) must replace the enriched ones. Thus, $scCO_2$ extracts the solvent contained inside the wet gel pores by diffusion during the contact time. This process is considered as one drying cycle. The number and length of the drying cycles depend on the volume and number of samples dried at the same time on each batch.

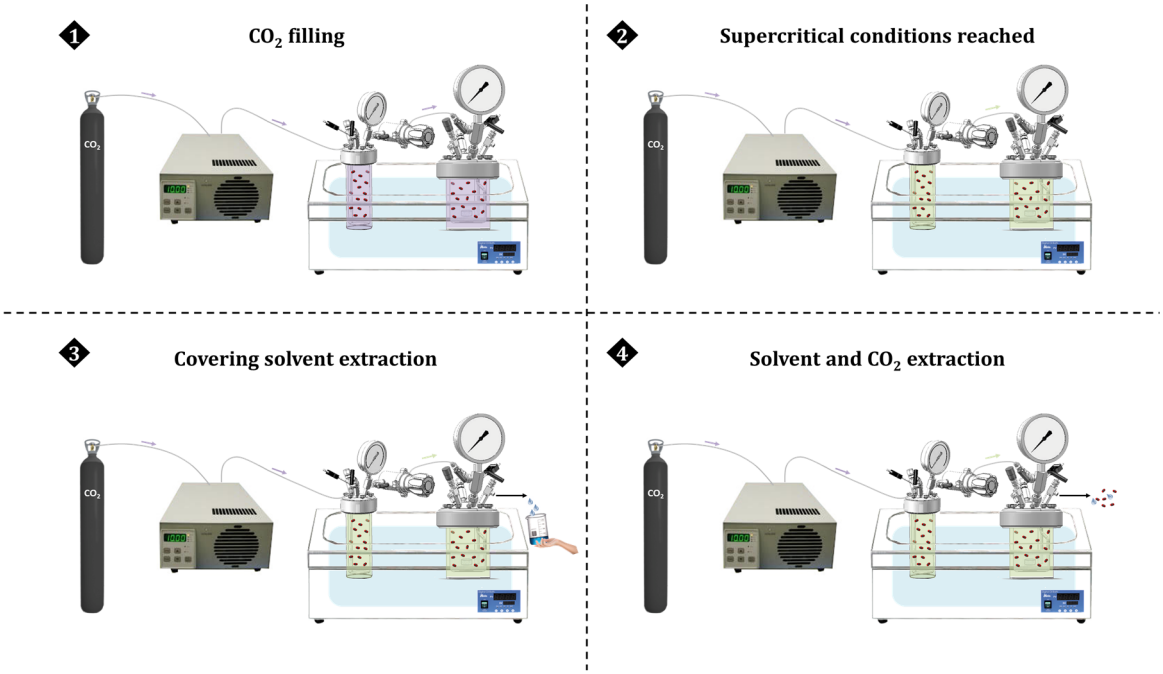

Figure 3.19. Supercritical drying steps.

Finally, once the gel pores are free of solvent, the clean CO_2 is extracted during the evacuation. A white color confirms the absence of solvent. Then, pressure is slowly-released through the metering valve for ca. 12 h until reaching the atmospheric pressure. **Table 3.5** shows the typical duration of each step using the drying setup herein described. Steps 2 and 3 must be repeated several times until almost dry CO_2 is obtained from the extraction.

Table 3.5. Typical time conditions for a SCD drying of the polyurethane aerogels produced in this thesis.

Step	Drying step	Duration (min)
1	Initial solvent extraction	30
2	Static solvent- $scCO_2$ exchange	50
3	Clean $scCO_2$ feeding – solvent enriched $scCO_2$ extraction	35
4	Slow final depressurization	600

3.4 Characterization methods

The aerogels and composites were characterized by their density and porosity, as well as by the shrinkage experimented during the drying step. Regarding their porous structure, scanning electron microscopy was used, thus allowing to measure parameters such as the particle size. In addition, nitrogen sorption was also used in order to measure the specific surface area and pore diameter. Additional properties have been also measured for some of the samples reported in this thesis, such as the mechanical behavior, thermal conductivity, optical properties, and the mass percentage of aerogel contained into the composites.

3.4.1 Bulk density, Solid density, Relative density and Porosity

Bulk density (ρ) was measured by dividing the mass of the sample (AT261 MettlerToledo balance) by its geometric volume (caliper of 0.01 mm resolution) following the corresponding standards ASTM D1622/ D1622M-14 [6].

Solid density or skeletal density (ρ_s) was measured by means of a pycnometer (AccuPyc II 1340, Micromeritics). Since the pores of the synthesized samples are mainly in the nanometric scale, the use of a gas with a large Van der Waals radius could lead to hinder some of the smallest pores, giving porosity values lower than the real one, and therefore lower solid densities. Nitrogen (N_2) is a diatomic molecule whose Van der Waals radius is around 155 pm, whereas the Van der Waals radius for helium (He) is ca. 140 pm (**Figure 3.20**). Thus, helium was the gas employed for the analysis. In order to guarantee the complete replacement of the gas inside the aerogel pores, 200 purges with helium were made. An initial pressure ramp was performed to determine the optimum measurement pressure, which would allow to measure the totality of pores without damaging the structure. After this analysis, a pressure of 0.13 MPa was employed for the measurements.

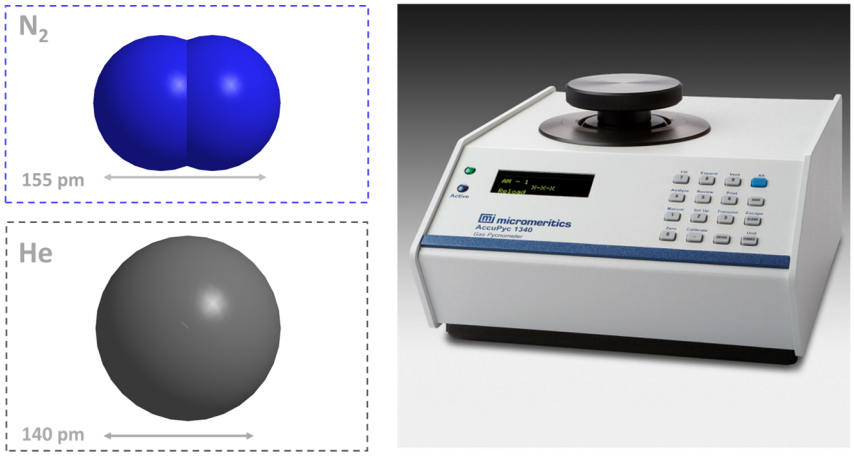

Figure 3.20. Van der Waals radius for diatomic nitrogen and helium and the pycnometer used to measure the solid density.

Once the volume of the solid phase in the sample is measured, the solid density, relative density and porosity can be calculated.

Solid density:

$$\rho_s = \frac{m}{V_s} \qquad (3.1)$$

Where m is the sample mass and V_s the volume occupied by solid.

Relative density:

$$\rho_r = \frac{\rho}{\rho_s} \qquad (3.2)$$

Porosity:

$$\Pi = 1 - \rho_r \qquad (3.3)$$

3.4.2 Linear and volumetric shrinkage

Unfortunately, aerogels suffer an unavoidable shrinkage during some of the production steps. In this thesis, the shrinkage that has been evaluated is that occurring during the drying step. Linear (S_l) and volumetric (S_v) shrinkages have been calculated to estimate the dimensional differences on the diameter or volume, respectively, between the initial wet gels and the obtained dried aerogels.

$$S_l(\%) = \left(1 - \frac{d}{d_0}\right) \cdot 100 \qquad (3.4)$$

$$S_v(\%) = \left(1 - \frac{V}{V_0}\right) \cdot 100 \qquad (3.5)$$

where d and d_0 are the final diameter of the sample after and before drying, respectively, and V and V_0 are the volume of the sample after and before the drying step.

3.4.3 Gelation time

When the transition from sol to gel takes place, several changes can be observed in the sample. Gelation time is taken when these changes are detected. For the polyurethane aerogels, the initial sol presents a transparent yellowish appearance and, when the polymerization reaction takes place, it turns out to either transparent bluish for lower amounts of catalyst or to opaque white for the highest concentrations (**Figure 3.21**). Additionally, since this color change is not always easy to identify, and viscosity notably changes from sol to gel, the container was carefully tilted each 30 seconds. The gel time was taken as that moment when the gel is not deformed by tilting, that is, when it does not flow anymore. In the case of the silica aerogels, changes in color were not detected since both, sol and gel, were transparent. Therefore, only the tilting technique could be used in this case.

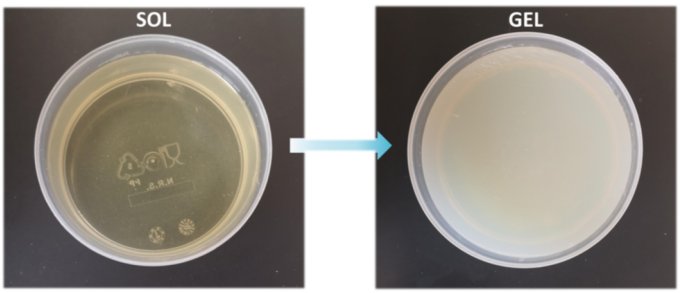

Figure 3.21. Sol-Gel transition for one of the PU aerogels.

3.4.4 Scanning electron microscopy

The sample's structure has been characterized by an ESEM Scanning Electron Microscope (QUANTA 200 FEG, Hillsboro, OR, USA, at the Instrumental Techniques Laboratory from the Scientific Park of the University of Valladolid) for the nanoporous structures and by a Scanning Electron Microscope (FlexSEM 1000, Hitachi) for the macroporous structures (reticulated PU foams and related composites). For the composites a BackScattered Electron Detector (BSE) was used.

Prior to the visualization, samples were cut with a metal blade and then coated with a layer (5 – 10 nm thickness) of iridium for the aerogels or gold for the PU foams through a sputter coater (EMITECH K575X Sputter Coater). The choice of the metal coating depends on the features to visualize. Since gold could form aggregates of several nanometers, it is not appropriate for samples with nanometric pores and particles (aerogels) [7].

Cell size for the polyurethane foams was measured by drawing the cell contour of enough number of cells on the scanning electron micrographs by using a software-based on Image J/FIJI [8].

Particle diameter ($\phi_{particle}$) was estimated from the scanning electron micrographs through the same software than for the PU foams. More than 50 individual particles were drawn in the SEM image (**Figure 3.22**) to estimate the average diameter in each sample. The normalized standard deviation (NSD) was calculated as the standard deviation of the particle distribution divided by the average particle diameter (SD/ $\phi_{particle}$). This parameter allows evaluating the homogeneity of the particle size distribution.

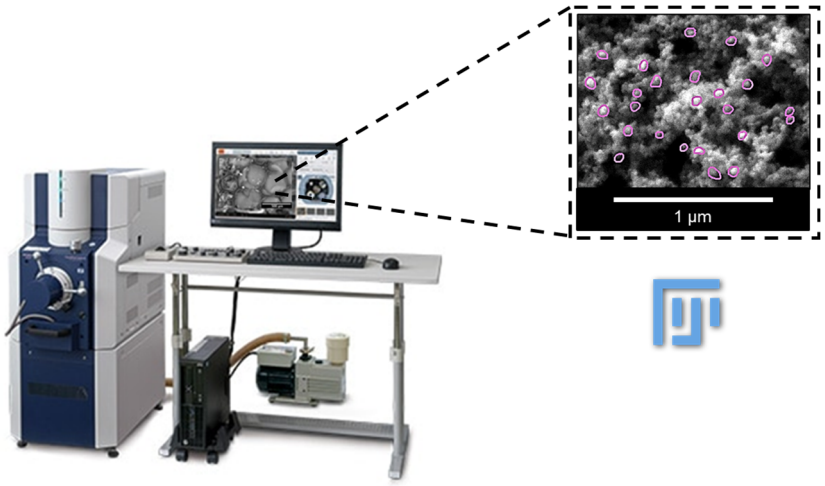

Figure 3.22. Example of particle drawing with Image J/FIJI for a polyurethane aerogel sample.

3.4.5 Transmission Electron Microscopy

The carbon nanotubes were visualized by Transmission Electron Microscopy (TEM) with a JEOL JEM1011 microscope at the Instrumental Techniques Laboratory from the Scientific Park of the University of Valladolid. Carbon nanotubes were directly placed into a carbon tape.

The nanotube diameter was measured by the Image J/FIJI software [8].

3.4.6 Nitrogen sorption

The Gas Adsorption Theory is based on the incompletely bounded atoms in a solid surface. These atoms, owing to Van der Waals interaction forces, are more reactive and the adsorption of gases, vapors or liquids could satisfy the imbalanced atomic forces on the surface.

The selected gas used as adsorbate is usually nitrogen, due to its strong interaction with most of the solids. In 1938, Brunauer, Emmett, and Teller developed a theory, well known as BET theory, which described the multilayer adsorption [9]. This theory is based on the Langmuir isotherm that describes the monolayer adsorption. However, BET theory assumes that each adsorbed molecule acts as a site for the adsorption in the next layer and, therefore, the physisorption of a gas on a solid adsorbent is not restricted to a monolayer formation. Thus, if the experiment pressure is high enough, a multilayer adsorption can take place.

BET analyses are most often carried out at the boiling temperature of nitrogen (77 K). This theory described the adsorbed gas molecules at a given relative pressure (P/P_0). First, nitrogen molecules will start to be adsorbed on the adsorbent surface (Stage 1 of **Figure 3.23 a**). Then, when the relative pressure continues increasing, a monolayer of one-molecule-thick is formed (Stage 2). At this stage BET equation can be applied:

$$\frac{1}{v\left[\left(\frac{p_0}{p}\right)-1\right]} = \frac{c-1}{v_m c}\left(\frac{p}{p_0}\right) + \frac{1}{v_m c} \quad (3.6)$$

Where υ is the total adsorbed gas quantity, υ_m is the monolayer adsorbed gas volume, p is the equilibrium pressure of the adsorbate, p_0 is the saturation pressure of the adsorbate and c is a BET constant.

In this way, the specific surface area (S_{BET}) can be calculated as:

$$S_{BET} = \frac{v_m N\, s}{V\, a}[=]\frac{m^2}{g} \quad (3.7)$$

Where N is Avogadro's number ($6.02 \cdot 10^{23}$ molecules/mol), s is the cross-sectional area of the adsorbed gas molecule, V is the molar volume of the adsorbed gas, and a is the mass of the sample (adsorbent). The validity of BET isotherm is restricted to a relative pressure (P/P_0) from 0.05 to 0.35.

The use of the nitrogen sorption technique for the analysis of the pore size dates from 1940s. It is the method developed by Barrett, Joyner and Halenda (BJH) the one which, in 1951, has become the most widely used [10]. When the nitrogen amount is further increased and, therefore, the relative pressure is higher, a complete coverage of the sample can be reached where the pores are filled with the adsorbate (Stages 3 and 4 in **Figure 3.23 a**). In this way, the BJH calculation can be applied to determine the pore volume, the pore diameter and the pore distribution. The upper limit of the pore size is in the mesopore range (**Figure 3.23 c**) since at a relative pressure of ca. 0.95 the saturation vapor pressure (p_0) is about to be reached and, therefore, capillary condensation will occur.

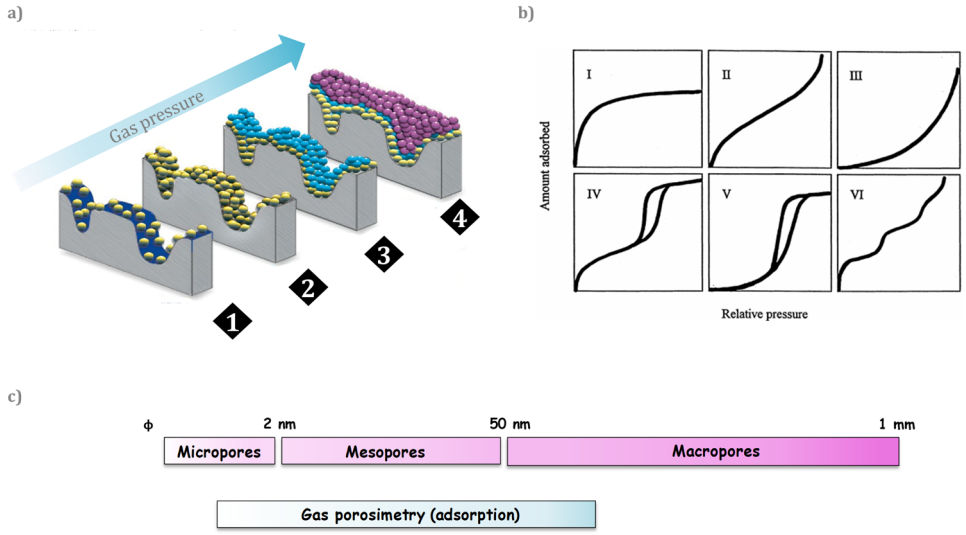

Figure 3.23. a) Stages of gas sorption on a porous surface, b) The IUPAC Classification of Adsorption Isotherms for Gas-Solid Equilibria [11], c) Pore size classification according to the IUPAC.

The adsorption isotherms can be classified into six categories according to IUPAC [12] as plotted in **Figure 3.23 b**.

- Type I: microporous solids having relatively small external surfaces.
- Type II: macroporous adsorbents with strong adsorbate-adsorbent interactions.
- Type III: macroporous adsorbents with weak adsorbate-adsorbent interactions.
- Type IV: monolayer absorption followed by capillary condensation*.
- Type V: multilayer absorption followed by capillary condensation*.
- Type VI: multilayer adsorption on a uniform non-porous surface.

* The hysteresis loop is associated with capillary condensation taking place in mesopores.

Finally, to sum up the different mechanisms occurring during these experiments have been displayed in **Figure 3.24**:

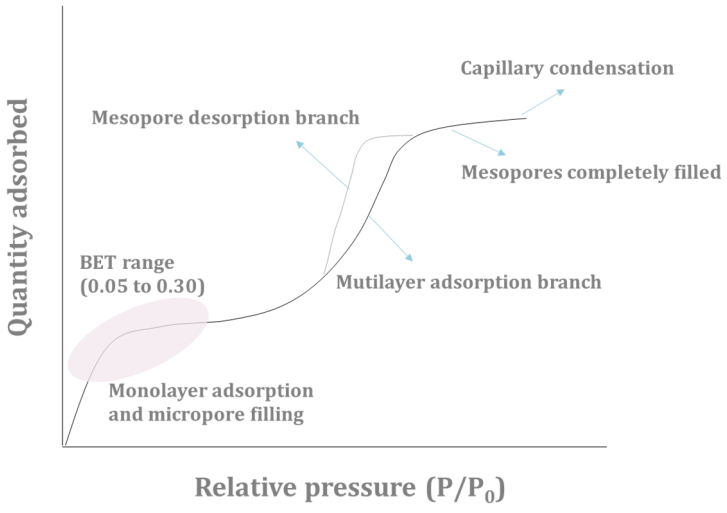

Figure 3.24. Nitrogen adsorption-desorption process in a mesoporous material.

In this thesis, nitrogen sorption measurements were carried out at 77 K with a Micromeritics ASAP 2020 instrument at the University of Málaga (Spain). Prior to the measurements, samples were degassed under high vacuum at 50 °C for 24 hours.

The specific surface areas (SBET) were obtained by the Brunauer-Emmett-Teller (BET) method [13] in the pressure range P/P_0 0.05 – 0.30.

Pore size distributions were determined by the Barrett–Joyner–Halenda (BJH) method through the desorption branch of the N_2-sorption isotherm, assuming that pores have a cylindrical shape. As previously explained, macroporosity could not be determined by this technique owing to capillary condensation, therefore, this technique is unable to detect the full, theoretically expected pore volume in high-porosity aerogels [14], [15]. For this reason, the average pore diameter was estimated by considering the pore volume as the free aerogel volume.

$$V_p = \frac{1}{\rho} - \frac{1}{\rho_s} \qquad (3.8)$$

Where the pore volume (V_p) is obtained as the difference between the whole volume of the sample and the solid volume.

Then, from the obtained surface areas (S_{BET}) and considering cylindrical pores, the following equation can be used to obtain the pore diameter (Φ_{pore}):

$$\Phi_{pore} = \frac{4V_p}{S_{BET}} \qquad (3.9)$$

3.4.7 Infrared Spectroscopy. FT-IR

Infrared spectroscopy allows to identify the characteristic functional groups that the produced aerogels present, as well as monitoring the isocyanate consumption (2000 – 2500 cm^{-1}). The amide I region (in the range of 1610 – 1760 cm^{-1}) contains the carbonyl stretching vibrations of several groups of interest: urethane generated during the polymerization (gelling) reaction, urea formed from water-traces present in the employed solvents, and isocyanurate formed by isocyanate trimerization. The corresponding peaks and areas are found as displayed in **Figure 3.25**:

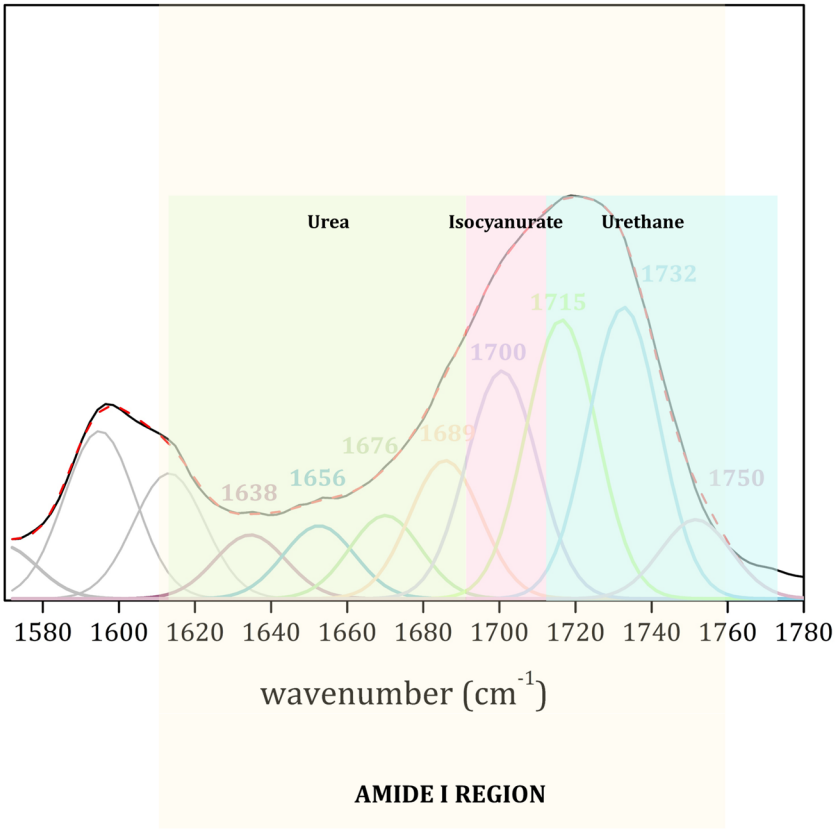

Figure 3.25. FT-IR spectrum of the Amide I region of a PUR-PIR aerogel.

The FT-IR spectra were collected as follows:

- A background spectrum was deduced initially.
- Baseline correction was applied to all the spectra.
- Spectra were normalized at an internal reference (asymmetric CH stretching band at 2972 cm^{-1}, whose concentration remains constant during the chemical reactions).
- The amide I region was deconvoluted to identify and quantify each peak.

The latter step has been carried out by means of a specific software – Peakfit. After the selection of the amide I region, gaussian bands were deconvoluted and fitted until reaching a correlation coefficient of at least 0.99. This method was described by Santiago et al. and more information can be found in references [16] and [17]. The identification of each peak can be found in **Figure 3.26**.

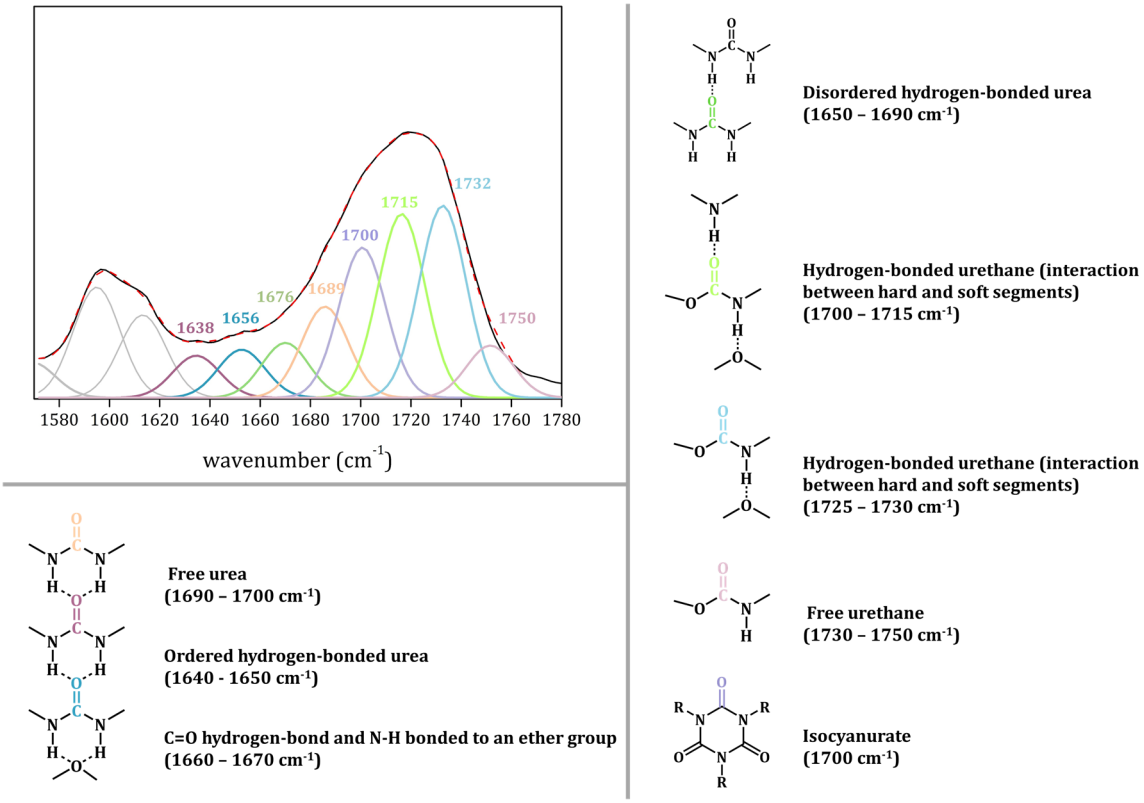

Figure 3.26. Peaks identification on the FT-IR spectra of a PUR-PIR aerogel.

The quantification of each peak corresponding to the reaction products is described in **Chapter 5, section 5.2**. The relative areas of urea, urethane, and isocyanurate can be calculated as the ratio between its area and the total area of amide I region.

3.4.8 Optical properties

The optical properties of the polyurethane aerogels were studied experimentally through transmittance measurements. These measurements have been carried out by means of both several lasers and a visible-ultraviolet spectrometer.

Laser measurements

Light transmittance was calculated as the ratio between the intensity passing through the aerogel sample (I), and the intensity without sample (I_0).

$$T = \frac{I}{I_0} \qquad (3.10)$$

Three lasers having different wavelengths were used: a red laser (650 nm) and a green laser (532 nm) provided by Laserlince S.L., as well as a blue laser (450 nm) model MLL-III-450L supplied by Lasing S.A. The experimental setup is displayed in **Figure 3.27 a**, consisting of the light source (laser), and a photodiode joined to an integrating sphere with 12.5 mm window (PRW0505, Gigahertz-Optik) connected to a photometer (X94, Gigahertz-Optik) as light detector. The detector – laser distance was fixed at 133 mm.

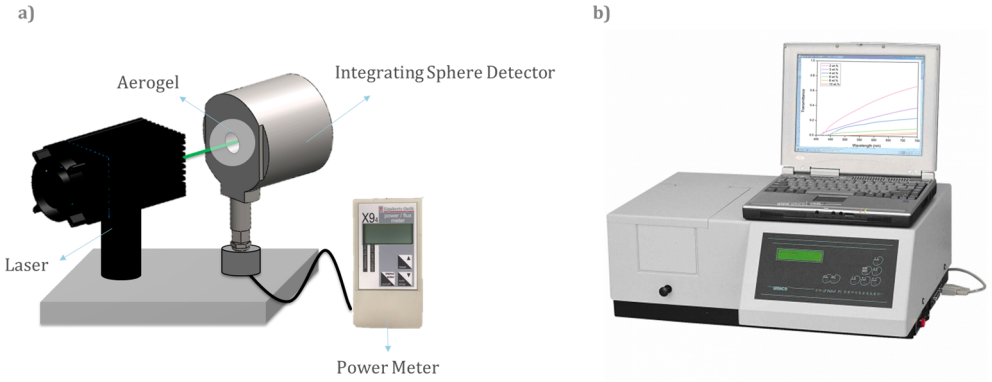

Figure 3.27. Scheme of the set-ups for the a) laser and b) UV-Vis measurements.

A thin slide of ca. 2 mm was removed from both cylinder base surfaces of the samples to maintain a homogeneous structure avoiding surface effects. Samples with different thicknesses were measured for each type of aerogel by cutting plane-parallel slices with a metal blade (thickness was modified from 0.4 mm to 12 mm).

Samples were directly placed in contact with the window of the integrating sphere to collect all the scattered light.

UV-Vis

An ultraviolet spectrometer (model UV-2102 PC, Shimadzu) was employed aiming to evaluate the wavelength dependence on the transmitted light in the range from 400 to 900 nm (**Figure 3.27 b**). The aperture of the slit was 1 nm. First, a background spectrum without any sample was obtained and the corresponding intensity was taken as 100 % of transmittance. The transmittances for the aerogels were taken as relative values to allow comparison between samples since, according to the UV-Vis setup, samples were placed at ca. 2 cm from the detector and some of the scattered light did not reach the detector. A gain factor of 2 was employed for the measurements. For the less transparent samples, the weak intensity of the spectrometer made difficult to obtain the transmittance values.

3.4.9 Mechanical properties

The mechanical tests were performed by using two different equipments. The measurements carried out in the University of Coimbra (**Chapter 7**) during a doctoral internship were performed in an Inspekt mini-series (Hegewald & Peschke, Nossen, Germany) (**Figure 3.28 a**), with a strain rate of 1 mm/min. Five compression–decompression cycles were performed with a maximum strain of 10 % and a loadcell of 50 N with a preload of ca. 0.1 N. In addition, a compression – decompression cycle at a strain of 25 % was performed with the same conditions. The destructive tests were carried out by using a loadcell of 3 kN until reaching a maximum load of 2.8 kN. The samples employed for the tests were cylindrical samples with a diameter between 12 and 16 mm and a height of ca. 10 mm.

On the other hand, the equipment for the uniaxial compression tests carried out in the University of Valladolid (**Chapter 5**) was an universal testing machine (Instron model 5500R6025) (**Figure 3.28 b**). The experiments were performed according to ASTM D1621-00 [18]. A load cell of ca. 1kN was selected and the displacement rate was [height/10] mm/min. Tests were performed on cylindrical samples with a diameter to height ratio of ca. 1.8 (cylinders of ca. 8 mm of height and 15 mm of diameter), at ambient conditions (23 ± 2 °C and 50 ± 10 % of relative humidity as indicated by ISO 291:2005 [19]). All samples were conditioned for 24 hours before evaluation.

Compression-decompression tests up to a 10 % of strain (**Figure 3.28 c**) were performed to evaluate the energy loss coefficient (ELC) [20]:

$$ELC\ (\%) = \frac{A_L - A_U}{A_L} \cdot 100 \qquad (3.11)$$

Where A_L and A_U are the corresponding areas under the loading and unloading curves, respectively.

The stress (σ) vs. strain (ε) curves were obtained from the following equations:

$$\sigma = \frac{F}{S} \qquad (3.12)$$

$$\varepsilon = \frac{\Delta h}{h_0} \qquad (3.13)$$

Being F the applied force, S the surface of the cross section of the specimen, h_0 the initial height of the samples, and Δh the displacement of the gauge.

From the stress vs. strain curves (**Figure 3.28 d**) the stress at different strains ($\sigma_{10\%}$, $\sigma_{25\%}$, $\sigma_{50\%}$, $\sigma_{75\%}$) can be extracted, as well as the elastic modulus, that was measured as the slope of the linear region at low strains.

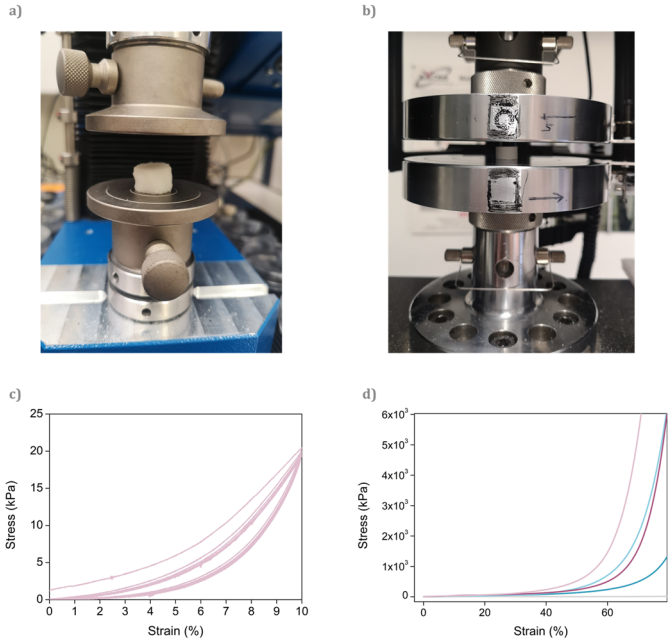

Figure 3.28. a) Inspekt mini-series, b) Instron model 5500R6025, c) An example of compression-decompression cycles at a strain of 10 %, d) An example of stress-strain curves up to high strains.

3.4.10 Thermal conductivity

The steady-state method was employed for measuring the thermal conductivity of the produced samples. This property was measured by means of a thermal heat flow meter model FOX 314 (TA Instruments/LaserComp, Inc.) according to the normative ASTM C518 [21] and ISO 8301 [22]. Since the sensor area of the instrument (100 x 100 mm^2) is larger than the surface area of the synthesized samples, an external heat flux sensor gSKIN® XM 27 9C (greenTEG AG) (sensing dimensions of 4.4 x 4.4 x 0.5 mm) connected to a data logger gSKIN® DLOG-4219 (greenTEG AG) [23]were used to measure the heat flow. The measurement range of this heat flux sensor is ± 550 W/m^2 and the resolution 0.41 W/m^2. As described in **Figure 3.29**, the sample is placed into an ethylene vinyl acetate (EVA) mask in order to avoid convection inside the FOX 314 cavity. This assembly was located in contact with two rubber sheets (300 mm x 300 mm x 1.5 mm) that minimize the heat flux fluctuations. The external sensor was placed in contact with the upper sample surface and the upper rubber sheet. Additionally, two thermocouples were located on both sides of the sample to collect the temperature gradient during the experiment. The average temperatures employed for the measurements were 10, 20, 30, and 40 °C with a temperature gradient of 20 °C. This methodology has been previously validated by our group, [23], [24], confirming that accurate values are provided for insulating samples.

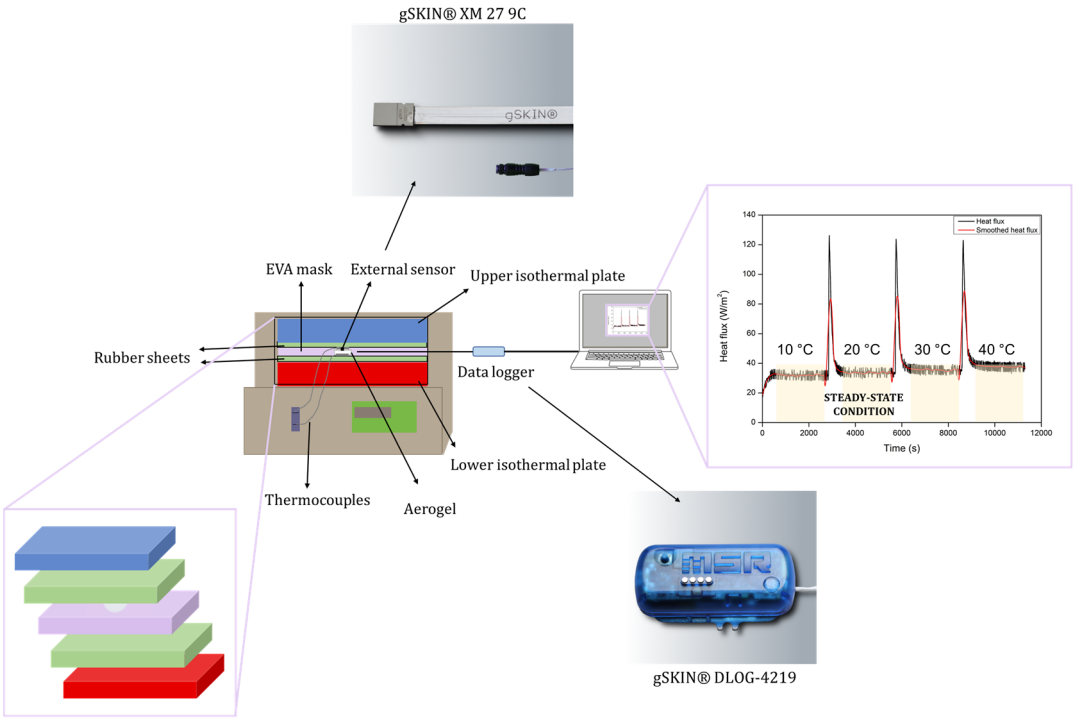

Figure 3.29. Thermal conductivity setup and an example of the heat flux measurement at different temperatures.

The sensitivity of the external sensor S(T) changes with the measurement temperature was calculated through the parameters obtained from the calibration performed by the company supplying the heat flux sensors, greenTEG AG, as described in the following equation:

$$S(T) = S_0 + (T_s - 22.5) \cdot S_c \quad (3.14)$$

In which S_c is the linear correction factor (0.0019 (μV/(W/m²))/°C), S_0 is the sensitivity at the calibration temperature of 22.5 °C (1.55 (μV/(W/m²)), and T_s is the mean sensor temperature.

The heat flux per unit area of each measurement (q) is calculated through a measured output voltage (U), which is obtained every second, and the sensor sensitivity (S) at that temperature:

$$q = \frac{U}{S} \quad (3.15)$$

The heat flux per unit area was smoothed with the adjacent-averaging method by taking a number of data points of 400. From this signal and once the steady state condition was reached, an average of 1200 seconds was taken. The thermal conductivity can be calculated through Equation 3.15:

$$\lambda = \frac{q \cdot d}{\Delta T} \quad (3.16)$$

Where d is the sample thickness and ΔT is the temperature difference between the hot and the cold plates.

3.5 References

[1] B. D. Hatton, K. Landskron, W. J. Hunks, M. R. Bennett, D. Shukaris, D. D. Perovic, and G. A. Ozin, "Materials chemistry for low-k materials," *Mater. Today*, vol. 9, no. 3, pp. 22–31, **2006**, doi: 10.1016/S1369-7021(06)71387-6.

[2] M. T. Kim, K. Y. Rhee, S. J. Park, and D. Hui, "Effects of silane-modified carbon nanotubes on flexural and fracture behaviors of carbon nanotube-modified epoxy/basalt composites," *Compos. Part B Eng.*, vol. 43, pp. 2298–2302, **2012**, doi: 10.1016/j.compositesb.2011.12.007.

[3] A. Lamy-Mendes, A. V. Girão, R. F. Silva, and L. Durães, "Polysilsesquioxane-based silica aerogel monoliths with embedded CNTs," *Microporous Mesoporous Mater.*, vol. 288, p. 109575, **2019**, doi: 10.1016/j.micromeso.2019.109575.

[4] R. B. Torres, J. P. Vareda, A. Lamy-Mendes, and L. Durães, "Effect of different silylation agents on the properties of ambient pressure dried and supercritically dried vinyl-modified silica aerogels," *J. Supercrit. Fluids*, vol. 147, no. February, pp. 81–89, **2019**, doi: 10.1016/j.supflu.2019.02.010.

[5] S. Zheng, X. Hu, A. R. Ibrahim, D. Tang, Y. Tan, and J. Li, "Supercritical fluid drying: Classification and applications," *Recent Patents Chem. Eng.*, vol. 3, pp. 230–244, **2010**, doi: 10.2174/1874478811003030230.

[6] *ASTM D1622-08: Standard Test Method for Apparent Density of Rigid Cellular Plastics*. West Conshohocken, PA, USA: ASTM International, 2008. doi: 10.1520/D1622-20.

[7] L. Juhász, K. Moldován, P. Gurikov, F. Liebner, I. Fábián, J. Kalmár, and C. Cserháti, "False morphology of aerogels caused by gold coating for sem imaging," *Polymers (Basel).*, vol. 13, no. 4, pp. 1–12, **2021**, doi: 10.3390/polym13040588.

[8] J. Pinto, E. Solórzano, M. A. Rodriguez-Perez, and J. A. De Saja, "Characterization of the cellular structure based on user-interactive image analysis procedures," *J. Cell. Plast.*, vol. 49, no. 6, pp. 555–575, **2013**, doi: 10.1177/0021955X13503847.

[9] M. Ghaedi, *Interface Science and Technology. Adsorption: Fundamental Processes and Applications*. London, UK: Elsevier, 2021.

[10] K. Sing, "The use of nitrogen adsorption for the characterisation of porous materials," *Colloids Surfaces A Physicochem. Eng. Asp.*, vol. 187–188, pp. 3–9, **2001**, doi: 10.1016/S0927-7757(01)00612-4.

[11] M. D. Donohue and G. L. Aranovich, "Classification of Gibbs adsorption isotherms," *Adv. Colloid Interface Sci.*, vol. 76–77, pp. 137–152, **1998**, doi: 10.1016/S0001-8686(98)00044-X.

[12] K. S. W. Sing, D. H. Everett, R. A. W. Haul, L. Moscou, R. A. Pierotti, J. Rouquerol, and T. Siemieniewska, "REPORTING PHYSISORPTION DATA FOR GAS/SOLID SYSTEMS with Special Reference to the Determination of Surface Area and Porosity," *Int. Union Pure Appl. Chem.*, vol. 57, no. 4, pp. 603–619, **1985**, doi: http://dx.doi.org/10.1351/pac198557040603.

[13] E. P. Barrett, L. G. Joyner, and P. P. Halenda, "The Determination of Pore Volume and Area Distributions in Porous Substances. I. Computations from Nitrogen Isotherms," *J. Am. Chem. Soc.*, vol. 73, no. 1, pp. 373–380, **1951**, doi: 10.1021/ja01145a126.

[14] G. Reichenauer and G. W. Scherer, "Nitrogen sorption in aerogels," *J. Non. Cryst. Solids*, vol. 285, no. 1–3, pp. 167–174, **2001**, doi: 10.1016/S0022-3093(01)00449-5.

[15] G. Reichenauer and G. W. Scherer, "Effects upon nitrogen sorption analysis in aerogels," *J. Colloid Interface Sci.*, vol. 236, no. 2, pp. 385–386, **2001**, doi: 10.1006/jcis.2000.7419.

[16] M. Santiago-Calvo, J. Tirado-Mediavilla, J. L. Ruiz-Herrero, M. Á. Rodríguez-Pérez, and F. Villafañe, "The effects of functional nanofillers on the reaction kinetics, microstructure, thermal and mechanical properties of water blown rigid polyurethane foams," *Polymer (Guildf).*, vol. 150, pp. 138–149, **2018**, doi: 10.1016/j.polymer.2018.07.029.

[17] M. Santiago-Calvo, "Synthesis, Foaming Kinetics and Physical Properties of Cellular Nanocomposites Based on Rigid Polyurethane," 2019.

[18] *ASTM D1621–00 Standard test method for compressive properties of rigid cellular plastics*. West Conshohocken, PA, USA, 1991.

[19] "ISO 291:2005 Plastics — Standard atmospheres for conditioning and testing," Geneva, Switzerland, **2005**.

[20] J. Bhinder and P. K. Agnihotri, "Effect of carbon nanotube doping on the energy dissipation and rate dependent deformation behavior of polyurethane foams," *J. Cell. Plast.*, **2020**, doi: 10.1177/0021955X20917280.

[21] "ASTM C518- Standard Test Method for Steady-State Thermal Transmission Properties by Means of the Heat Flow Meter Apparatus.," West Conshohocken, PA, USA, **2017**.

[22] "ISO 8301:1991- Thermal insulation — Determination of steady-state thermal resistance and related properties — Heat flow meter apparatus," Geneva, Switzerland, **1991**.

[23] I. Sánchez-Calderón, B. Merillas, V. Bernardo, and M. Á. Rodríguez-Pérez, "Methodology for measuring the thermal conductivity of insulating samples with small dimensions by heat flow meter technique," *J. Therm. Anal. Calorim.*, vol. 147, pp. 12523–12533, **2022**, doi: 10.1007/s10973-022-11457-7.

[24] I. Sánchez-Calderón, Á. Sillero, F. Lizalde-Arroyo, V. Bernardo, J. Martín-de-León, and M. Á. Rodríguez-Pérez, "Evaluation of methods to accurately characterize the thermal conductivity of micro-and nanocellular polymers based on poly(methyl-methacrylate) (PMMA) produced at lab-scale," *Polym. Test.*, vol. 117, p. 107842, **2023**, doi: 10.1016/j.polymertesting.2022.107842.

CHAPTER 4

SYNTHESIS AND CHARACTERIZATION OF TRANSPARENT POLYURETHANE AEROGEL MONOLITHS

Chapter 4. Synthesis and Characterization of Transparent Polyurethane aerogel monoliths

4.1 Introduction

According to the huge interest generated by the production of transparent organic aerogels, it was set as a key objective in this thesis.

The aim of this chapter is to synthesize transparent polyurethane aerogels by modifying the chemical formulation. This thesis presents the first reports on achieving transparency in aerogels with a polyurethane-based matrix. The details of the employed formulations can be found in **Tables 3.1** and **3.2** of Chapter 3. The characterization techniques employed for the study of the aerogel properties are herein described. Then, the optical properties of these aerogels are analyzed in detail determining the effect of different parameters in the final light transmittance of these materials, as well as the scattering mechanisms that take place. In order to fulfill these objectives, two scientific publications are herein gathered.

Section 4.2 reports the synthesis and characterization of the first transparent polyurethane-based aerogels. The optical properties of the produced materials have been tuned by changing the initial formulation, which leads to different porous structures.

Afterwards, section 4.3 describes a thorough study of the optical properties of these materials. Different aspects influencing their light transmittance have been analyzed in order to determine which features are mainly controlling their transparency. Additionally, the study of the scattering mechanisms responsible for dispersing part of the incident light have allowed to reach interesting conclusions.

4.2 Synthesis of transparent polyurethane aerogels

The results based on the synthesis, characterization, and preliminary light transmittance measurements are presented in the first publication: **B. Merillas, J. Martín-de León, F. Villafañe, M. A. Rodríguez-Pérez. Transparent Polyisocyanurate-Polyurethane-Based Aerogels: Key Aspects on the Synthesis and Their Porous Structures. ACS Appl. Polym. Mater., vol. 3, no. 9, pp. 4607–4615, 2021, doi: 10.1021/acsapm.1c00712**.

In this work, the textural properties of polyurethane aerogels obtained by supercritical drying have been modified by changes in the catalyst concentration. Different catalyst amounts ranging from 1 to 20 wt.% were used to produce these materials achieving tunable porous structures. The polyurethane aerogels showed really low densities (0.10−0.16 g/cm^3) and high porosities (above 85 %). Additional parameters such as gelation time, shrinkage during the drying step or size of the particles forming the polymeric skeleton, were determined in order to obtain a complete characterization. By means of the nitrogen sorption technique, the surface area, pore volume and pore size were determined.

A clear trend was observed between the catalyst amount employed during the synthesis procedure and the size of the particles and pores forming the nanostructure of the samples: reducing the catalyst amount led to a significant decrease in the particles and pore sizes. Therefore, a careful control of the reaction kinetics allowed to obtain particle sizes smaller than a tenth of the wavelength of visible light (40 nm), thus **reaching PU transparent aerogels for the very first time**.

Aiming to quantify their light transmittance, a laser with a wavelength of 532 nm was employed for the measurements. High transmittances (ca. 76 %, 1 mm thick) were reached for the samples with the lowest catalyst amounts that sharply decreased until almost 0 % for the highest catalyst concentrations (20 wt.%).

In conclusion, this publication describes new polyurethane aerogels with tunable optical properties which can be obtained by modifying the reaction kinetics. Thus, PU aerogels from highly transparent to almost opaque have been synthesized.

The presence of light transparency in these aerogels that also gather other interesting properties (low density, high porosities, high surface areas, etc.) makes them potential materials for applications such as sensors, glazing window-panes, or energy related applications.

Figure 4.1 shows the graphical abstract of the presented paper. The full publication is included in the next pages.

Graphical abstract

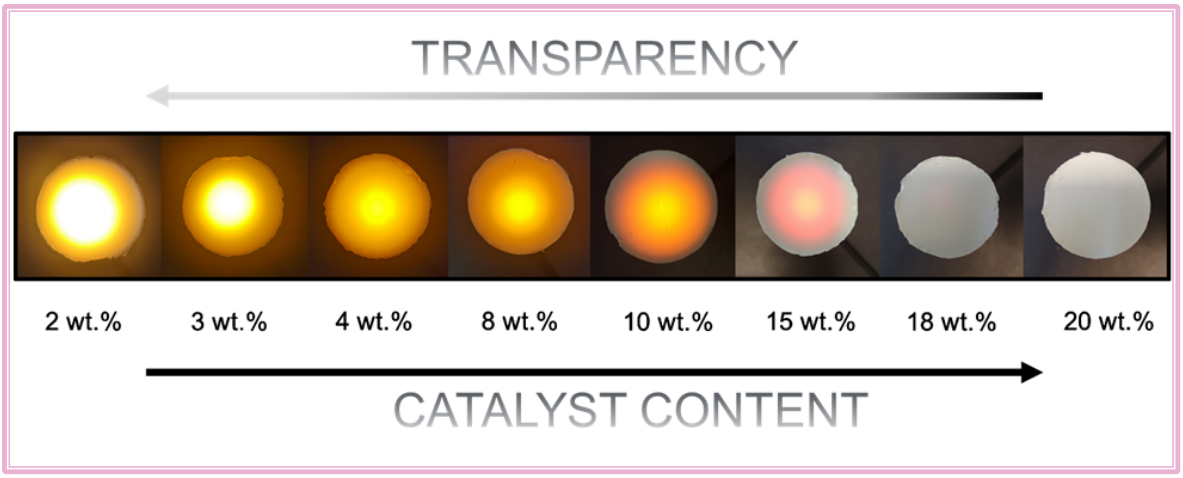

Figure 4.1. Graphical abstract of **"Transparent Polyisocyanurate-Polyurethane-based aerogels: key aspects on the synthesis and their porous structure."**

Transparent Polyisocyanurate-Polyurethane-based aerogels: key aspects on the synthesis and their porous structure

ACS Appl. Polym. Mater. 3, 9, 4607–4615, 2021.

Beatriz Merillas*, Judith Martín-de León, Fernando Villafañe†, and Miguel Ángel Rodríguez-Pérez†

Cellular Materials Laboratory (CellMat), Condensed Matter Physics Department, Faculty of Science, University of Valladolid, Campus Miguel Delibes, Paseo de Belén 7, 47011, Valladolid, Spain

** Corresponding author: b.merillas@fmc.uva.es*

Abstract: The effect of the catalyst concentration on the synthesis and textural properties of polyisocyanurate-polyurethane aerogels is analyzed. The use of different catalyst amounts allows obtaining low-density aerogels (0.10–0.16 g/cm^3) with high porosities (85–91%). Their porous structures were analyzed by scanning electron microscopy and nitrogen adsorption–desorption isotherm. A noticeable decrease in the size of the scattering centers, particles, and pores, was achieved when reducing the catalyst amount. In some samples, the small size of these features, much smaller than the wavelength of visible light, causes a bare light dispersion, leading to the first transparent polyisocyanurate-polyurethane aerogels. Light transmittance measurements at 532 nm have been made showing high values (ca. 76% for 1 mm thick samples) for the formulations with the smallest particle and pore sizes. These aerogels presenting optical transparency have many potential applications such as solar collectors, glazing systems for insulating windows, and sensors, among others.

Keywords: polyisocyanurate, polyurethane, aerogels, transparent, sol–gel, particle size.

DOI: 10.1021/acsapm.1c00712

4.3 Analysis of the optical properties of polyurethane aerogels

This section contains a paper which is the natural continuation of the previous one. The publication is entitled "Optical Properties of Polyisocyanurate – Polyurethane Aerogels: Study of the Scattering Mechanisms." This work has been published in Nanomaterials in 2022 (**B. Merillas, J. Martín-de León, F. Villafañe, and M. Á. Rodríguez-Pérez, "Optical Properties of Polyisocyanurate – Polyurethane Aerogels: Study of the Scattering Mechanisms," Nanomaterials, vol. 12, p. 1522, 2022, doi: https://doi.org/10.3390/nano 12091522.**).

Once novel transparent polyisocyanurate-polyurethane aerogels were synthesized, their optical properties must be analyzed in detail. For this purpose, light sources with different wavelengths were used: red laser (650 nm), green laser (532 nm), blue laser (450 nm). This made possible to analyze the effect of several parameters in the final light transmittance.

The first **parameter influencing the optical properties** of these aerogels was the sample **thickness**, what allowed to confirm the fulfillment of the Beer-Lambert law. In fact, the **attenuation coefficient** of each sample could be calculated and normalized by the sample density in order to stablish an accurate comparison.

Three groups could be differentiated in terms of the exhibited light transmittance and the **porous structure**. The first group was formed by the samples with the lowest catalyst amount (2, 3 and 4 wt.%), which therefore are the samples with the smallest particles (ca. 24 nm), and those reaching the highest transmittance value of 85 % (1 mm thick at 650 nm). Secondly, samples with an intermediate amount of catalyst (6, 8 and 10 wt.%) showed a slight decrease in the final transmittance, owing to their larger particle size (ca. 32 nm). Finally, a sharp reduction in the transmittance until reaching values near 0 was observed for the samples with the highest catalyst concentration (15 and 18 wt.%), as a consequence of having a structure formed by larger particle sizes (above 40 nm). This relationship confirms that the **particles** forming the solid network of the polyurethane aerogels **act as scatterer centers** for the incident light.

Finally, the dependence of transmittance with the **light wavelength** was evaluated through an ultraviolet-visible spectrophotometer (400 to 750 nm). These experiments allowed to determine the scattering mechanism that takes place for each sample. In this way, the dependence of transmittance with the light wavelength was analyzed by the fitting of this parameter to L/λ^4 (Rayleigh scattering) or L/λ (Mie scattering). A barrier between **Rayleigh and Mie scattering mechanisms** was found when going from particles of 23-32 nm to larger particles, thus demonstrating that the loss of transparency of some samples is due to a change in the scattering mechanism that leads to a strong light attenuation.

Figure 4.2 shows the graphical abstract of this article where the Rayleigh scattering mechanism can be observed. The light which is dispersed (that with the smallest wavelength, i.e. blue light) promotes a bluish colour on the polyurethane aerogels. However, the light which is transmitted will be that with the largest wavelength (red colour), giving an orangish appearance to the samples. The full publication is included in the next pages.

Graphical abstract

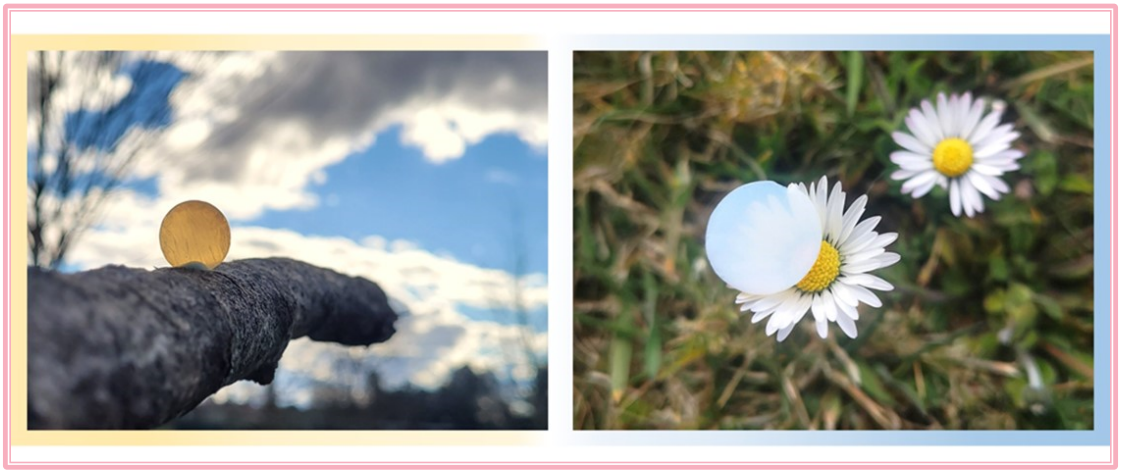

Figure 4.2. Graphical abstract of **"Optical Properties of Polyisocyanurate–Polyurethane Aerogels: Study of the Scattering Mechanisms."**

Optical Properties of Polyisocyanurate–Polyurethane Aerogels: Study of the Scattering Mechanisms

Beatriz Merillas[1,*], Judith Martín-de León[1], Fernando Villafañe[2], and Miguel Ángel Rodríguez-Pérez[1,3]

[1] Cellular Materials Laboratory (CellMat), Condensed Matter Physics Department, Faculty of Science, University of Valladolid, Campus Miguel Delibes, 47011 Valladolid, Spain; jmadeleon@fmc.uva.es (J.M.-d.L.); marrod@fmc.uva.es (M.Á.R.-P.)

[2] GIR MIOMeT-IU Cinquima-Química Inorgánica. Faculty of Science, University of Valladolid, Campus Miguel Delibes, 47011 Valladolid, Spain; fernando.villafane@uva.es

[3] BioEcoUVA Research Institute on Bioeconomy, University of Valladolid, 47011 Valladolid, Spain

** Correspondence: b.merillas@fmc.uva.es; Tel.: +34-983423194*

Nanomaterials, 12, 1522, 2022.

Abstract: Highly transparent polyisocyanurate–polyurethane (PUR–PIR) aerogels were synthesized, and their optical properties were studied in detail. After determining the density and structural parameters of the manufactured materials, we analyzed their optical transmittance. It was demonstrated that the catalyst content used to produce the aerogels can be employed to tune the internal structure and optical properties. The results show that the employment of lower catalyst amounts leads to smaller particles forming the aerogel and concomitantly to higher transmittances, which reach values of 85% (650 nm) due to aerogel particles acting as scattering centers. Thus, it was found that the lower this size, the higher the transmittance. The effect of the sample thickness on the transmittance was studied through the Beer–Lambert law. Finally, the scattering mechanisms involved in the light attenuation were systematically evaluated by measuring a wide range of light wavelengths and determining the transition between Rayleigh and Mie scattering when the particles were larger. Therefore, the optical properties of polyurethane aerogels were studied for the first time, opening a wide range of applications in building and energy sectors such as glazing windows.

Keywords: polyurethane–polyisocyanurate aerogels; optical properties; transparency; Rayleigh scattering; Mie scattering; scattering mechanisms.

DOI: 10.3390/nano12091522

4.4 Future perspectives

The exceptional optical properties that the synthesized PUR-PIR aerogels have shown, provide a promising search for other interesting properties in relation to their mechanical and thermal insulating behavior. Therefore, the potential properties of these samples will be analyzed in the following chapter (**Chapter 5**).

CHAPTER 5

THERMAL CONDUCTIVITY AND MECHANICAL PROPERTIES OF TRANSPARENT POLYURETHANE AEROGEL MONOLITHS

Chapter 5. Thermal Conductivity and Mechanical Properties of Transparent Polyurethane aerogel monoliths

5.1 Introduction

This chapter contains the results obtained on the thermal insulation capacity and mechanical behavior of polyisocyanurate-polyurethane aerogels.

The aim of this chapter is to analyze the effect of different factors, such as the reaction kinetics and the addition of carbon nanotubes, on the thermal conductivity and mechanical properties of polyurethane aerogels. The details of the employed formulations can be found in Tables 3.1 and 3.2 of Chapter 3. These results have been divided into two different sections.

Section 5.2 gathers the results obtained for polyurethane aerogel monoliths, which reach thermal conductivities never before achieved for this aerogel matrix. Minimum values of 12 mW/mK are obtained by controlling the reaction kinetics through changes in the catalyst concentration of the employed formulations. Additionally, the produced aerogels show tunable stiffness, great elasticity and recovery values after a compression force (10 % of deformation).

Section 5.3 includes the study of the inclusion of carbon nanotubes as infrared blockers in one of the previously described formulations of section 5.2. The influence of these fillers on the aerogel structure, mechanical properties and thermal insulation is analyzed in detail.

5.2 Insulating capacity and mechanical properties of transparent polyurethane aerogels

This section contains the publication entitled: **B. Merillas, F. Villafañe, M.Á. Rodríguez-Pérez. Super-insulating transparent polyisocyanurate-polyurethane aerogels: Analysis of the thermal conductivity and mechanical properties, Nanomaterials, 12, 2409, 2022, doi:10.3390/ nano12142409.**

The main goal of this research was to evaluate the relationship between formulation, nanostructure, and the thermal and mechanical properties of transparent polyisocyanurate-polyurethane (PUR-PIR) aerogels. Thus, aerogels are produced by employing different catalyst amounts and then fully characterized. The complete characterization consists on the analysis of the textural properties, thermal conductivity measured at different temperatures (10, 20, 30 and 40 °C), and uniaxial compression tests.

The catalyst concentration was found to modify the aerogel structure and, therefore, the thermal insulation performance. Owing to the small size of particles and pores with low catalyst concentrations, what is the cause of their transparency to visible light described in Chapter 4, the thermal conductivity reaches a minimum value of 12 mW/mK, the best thermal insulating performance found in the literature for polyurethane aerogels to the best of our knowledge. This value is increased to 24 mW/mK at 10 °C by enlarging the catalyst concentration.

A theoretical analysis of the thermal contributions acting in these samples is performed, concluding that the reduction of the gas conduction through the Knudsen effect is the key factor leading to such a low thermal conductivity. Additionally, the size effect affects the phonon transfer along the particulate skeleton, resulting in small solid conduction contributions. The radiation contribution is similar for all the samples, accounting for ca. 1 mW/mK of the total thermal conductivity.

The mechanical behavior also depends on the catalyst amount. Aerogels with smallest particles and pores and, therefore, a more compact and dense structure, show elastic modulus of ca. 6.32 MPa, a value that is progressively diminishing by increasing the size of the structural features until reaching 0.13 MPa. The significant differences on the aerogel's stiffness may be controlled through the reaction kinetics, obtaining tunable mechanical strength. One exceptional feature displayed the produced aerogels is their high deformations, since those above 70 % do not break the aerogels, instead promoting a densification of their structure. All the synthesized polyurethane aerogels show a good elastic behavior and recovery ratios after a deformation up to 10 %.

Figure 5.1 shows the graphical abstract of the presented paper. The full publication is included in the next pages.

Graphical abstract

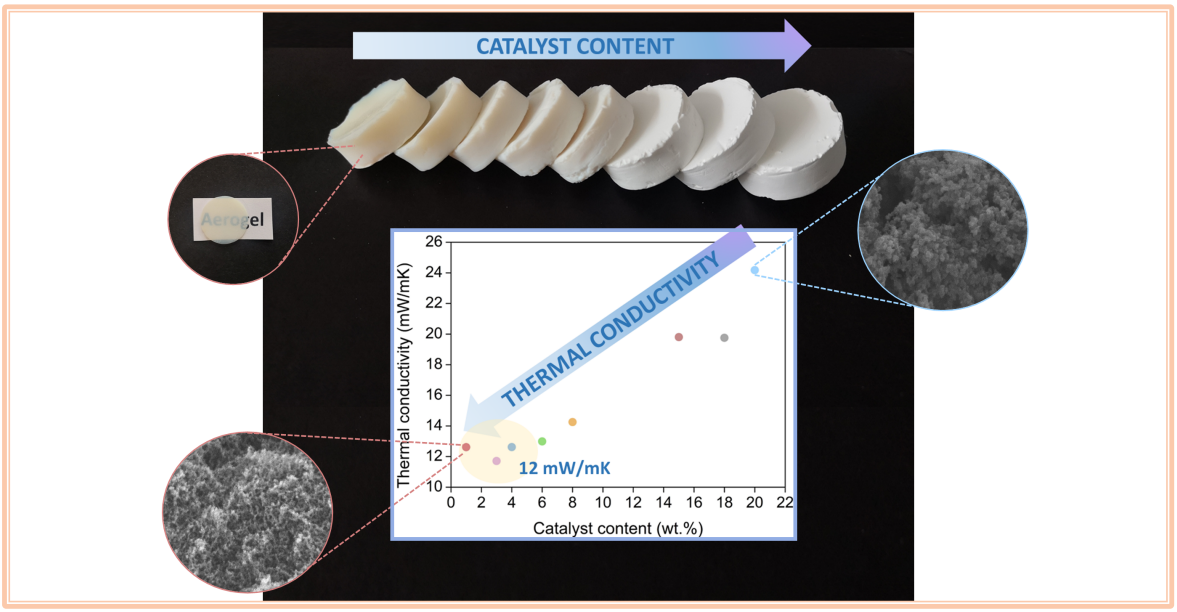

Figure 5.1. Graphical abstract of **"Super-Insulating Transparent Polyisocyanurate-Polyurethane Aerogels: Analysis of Thermal Conductivity and Mechanical Properties."**

The combination of the previously analyzed optical properties of these aerogels with their excellent thermal insulation make them exceptional materials for buildings, automotive or even aeronautics.

Super-insulating transparent polyisocyanurate-polyurethane aerogels: analysis of the thermal conductivity and mechanical properties

Beatriz Merillas[1*], Fernando Villafañe[2], and Miguel Ángel Rodríguez-Pérez[1,3*]

1 Cellular Materials Laboratory (CellMat), Condensed Matter Physics Department, Faculty of Science, University of Valladolid, Campus Miguel Delibes, Paseo de Belén 7, 47011 Valladolid, Spain

2 GIR MIOMeT-IU Cinquima-Química Inorgánica. Faculty of Science, University of Valladolid, Campus Miguel Delibes, Paseo de Belén 7, 47011 Valladolid, Spain

3 BioEcoUVA Research Institute on Bioeconomy, University of Valladolid, Spain

**Correspondence: Authors Email: b.merillas@fmc.uva.es, Tlf: +34 983 42 31 94, ORCID: 0000-0003-2995-6412,*

Email: marrod@fmc.uva.es, Tlf: +34 983 18 40 35, ORCID: 0000-0002-3607-690X

Nanomaterials, 12, 2409, 2022.

Abstract: A family of transparent polyisocyanurate-polyurethane (PUR-PIR) aerogels with an interesting combination of physical properties were synthesized. First, their textural properties were analyzed aiming to study catalyst influence on the final porous structures and densities. Their thermal conductivities were measured at different temperatures allowing to observe a clear trend relating the initial formulation with the porous structure and reaching values as low as 12 mW/mK, the lowest found in the literature for aerogels based on this polymer matrix. Contributions to the thermal conductivity were calculated improving the understanding of the porous structure-insulating performance relationship. Moreover, their mechanical properties were studied (elastic modulus, stress at different strains and elastic behavior). The aerogels showed tunable stiffness (elastic modulus from 6.32 to 0.13 MPa) by changing the catalyst concentration and significant elasticity. Thus, super-insulating transparent PUR-PIR aerogels with tailored mechanical properties were obtained opening a wide range of potential applications in the energy, building, automotive and aeronautical sectors, among others. The exceptional insulation of silica aerogels was reached at the same time that their general brittleness was improved while keeping good transparency to visible light (85 %, 650 nm). Therefore, these aerogels may constitute an alternative to silica aerogels.

Keywords: polyurethane; polyisocyanurate; aerogels; super-insulation; mechanical properties.

DOI: 10.3390/nano12142409

5.3 Further thermal conductivity reduction through the incorporation of carbon nanotubes as fillers and changes in the mechanical behavior

This section contains a paper which is a continuation of the previous one. The publication is entitled "Effect of the addition of carbon nanotubes on the final properties of polyurethane-polyisocyanurate aerogels".

The key purpose of this work is to study the influence on the mechanical and thermal properties of adding carbon-based fillers to one of the previously described formulations. To fulfill this purpose, different carbon nanotubes amounts of 0.5, 1.0 and 3.0 wt.% were added to a pure monolithic reference. After a thorough characterization of their density, porosity, shrinkage, nanostructure, mechanical properties and thermal conductivity, the following conclusions were extracted.

1. These fillers alter the reaction kinetics, thus promoting a faster gelation reaction for low CNTs amounts, and similar reaction rates when the fillers amount is increased to 3.0 wt.%.

2. Carbon nanotubes (CNTs) do not increase the initial density of the aerogel, since these fillers reduce the shrinkage experimented by the reference aerogel during the supercritical drying, thus leading to slightly higher porosities. Consequently, the size of the pores forming the structure are larger. The fact that pores are enlarged directly affects the mechanical properties of these aerogels, leading to lower mechanical strengths and elastic moduli. On the contrary, the elasticity of these nanocomposites improves, thus reducing the amount of energy dissipated during the compression experiments, as evaluated by the energy loss coefficient. It has to be also mentioned that, despite the loss of stiffness caused by CNTs , the nanocomposites withstand high deformations of above 80 % without breaking.

3. The effect of CNTs on the thermal insulation capacity is also studied in depth. The thermal conductivity of the pure aerogel is reduced in ca. 3 mW/mK for the highest amount of CNTs, starting from a value of 15 mW/mK, and reaching only 12 mW/mK. This reduction is due to the influence of these particles on the different heat transfer mechanisms. In order to analyze this effect, the contributions to the total thermal conductivity are estimated. Although the gas conduction is increased because of the larger pores of the samples containing CNTs, the solid conduction is minimized by decreasing the particle interconnectivity and, thus, restricting the phonon transfer. Finally, these fillers are proved to significantly decrease the radiative term by blocking the infrared radiation. This fact is demonstrated by the calculation of the extinction coefficients as a function of the wave number that are increased by the CNTs addition.

In summary, the incorporation of CNTs to polyurethane aerogel constitutes an effective strategy to further reduce their low thermal conductivity.

Figure 5.2 shows the graphical abstract of the presented paper. The full publication is included in the next pages.

Graphical abstract

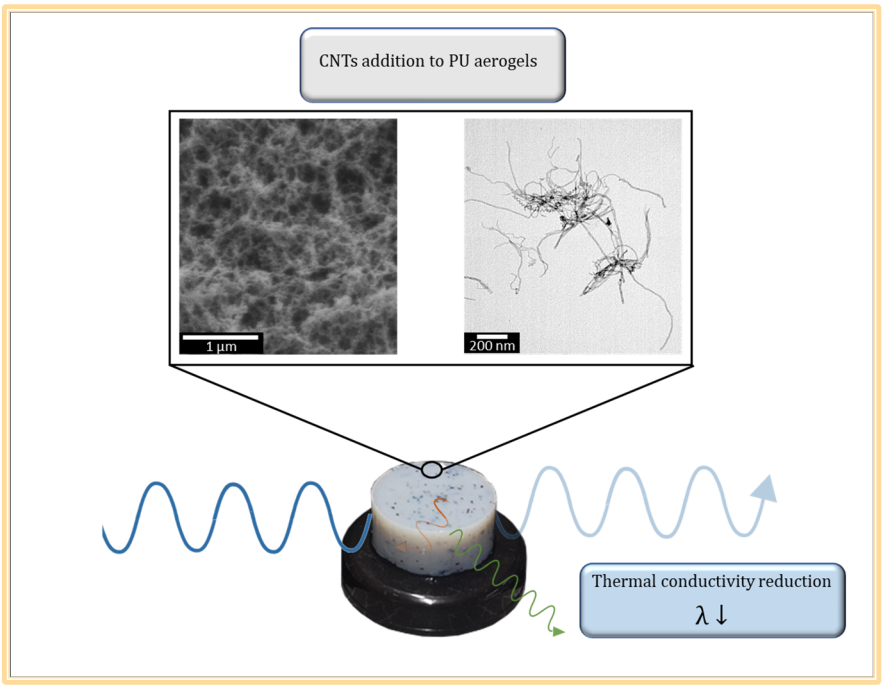

Figure 5.2. Graphical abstract of "Effect of the addition of carbon nanotubes on the final properties of polyurethane-polyisocyanurate aerogels".

Effect of the addition of carbon nanotubes on the final properties of polyurethane-polyisocyanurate aerogels

Beatriz Merillas[1*], Fernando Villafañe[2], and Miguel Ángel Rodríguez-Pérez[1,3*]

1 Cellular Materials Laboratory (CellMat), Condensed Matter Physics Department, Faculty of Science, University of Valladolid, Campus Miguel Delibes, Paseo de Belén 7, 47011 Valladolid, Spain

2 GIR MIOMeT-IU Cinquima-Química Inorgánica. Faculty of Science, University of Valladolid, Campus Miguel Delibes, Paseo de Belén 7, 47011 Valladolid, Spain

3 BioEcoUVA Research Institute on Bioeconomy, University of Valladolid, Spain

**Correspondence: Authors Email: b.merillas@fmc.uva.es, Tlf: +34 983 42 31 94, ORCID: 0000-0003-2995-6412,*

Submitted, 2022

Abstract: This article studies the effect of adding different contents of surface-modified carbon nanotubes on the structure and final properties of polyisocianurate-polyurethane aerogels. The produced samples were characterized in terms of their density, porosity, shrinkage, textural properties, mechanical behavior, and thermal conductivity. Low-weight aerogels were obtained with densities between 89 and 95 kg/m3. The inclusion of homogeneously dispersed carbon nanotubes protected the aerogel structure during supercritical drying decreasing the final shrinkage of these samples and, therefore, increasing their porosity. The porous structure of the aerogels containing CNTs was modified, and slightly larger pores were formed. The structural modifications contribute to decrease the stiffness of the samples while improving their resilience and elasticity. Finally, their thermal conductivity was measured finding a significant enhancement on the insulating performance of the aerogels when CNTs were added reaching values as low as 12 mW/mK. These fillers may be constraining the phonon transmission and acting as opacifiers blocking the infrared radiation, thus reducing the solid and radiative contributions. In fact, the radiation contribution was strongly reduced when the content of CNTs reached 3% by weight.

Keywords: carbon nanotubes; polyurethane aerogels; thermal insulation; radiative contribution; mechanical properties.

CHAPTER 6

IMPROVING THE THERMAL INSULATION OF POLYURETHANE FOAMS BY AEROGEL INCLUSION IN THE POROUS STRUCTURE

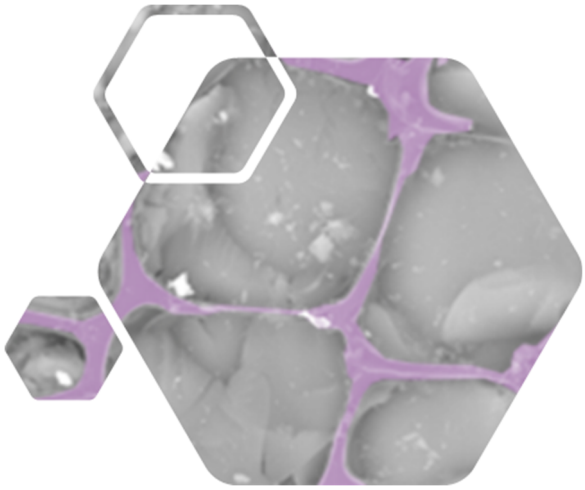

Chapter 6. Improving the thermal insulation of Polyurethane foams by aerogel inclusion in the porous structure

6.1 Introduction

Polyurethane foams are porous materials with a widespread use as thermal insulators. Nevertheless, the European Commission has strengthened the Energy Performance of Buildings Directive (EPBD) in the recent years, aiming to improve the energy efficiency performance of buildings. This document establishes that a 36 % of the total energy consumption should be reduced by 2030 [1]. In order to achieve this goal, the employment of advanced thermal insulating materials plays a key role in the renovation scenario.

For this reason, novel materials with improved thermal insulation should be developed. Polyurethane foams present thermal conductivity values between 25 and 33 mW/mK [2], thus there is a large room for improvement, and a great improvement could be achieved by the use of aerogels. Therefore, a novel strategy is herein presented, which consists of including polyurethane aerogels with a really low thermal conductivity (ca. 14 mW/mK) inside the pores of the PU foams. The final purpose is sharply reducing the gas conduction contribution to the total thermal conductivity of these composites.

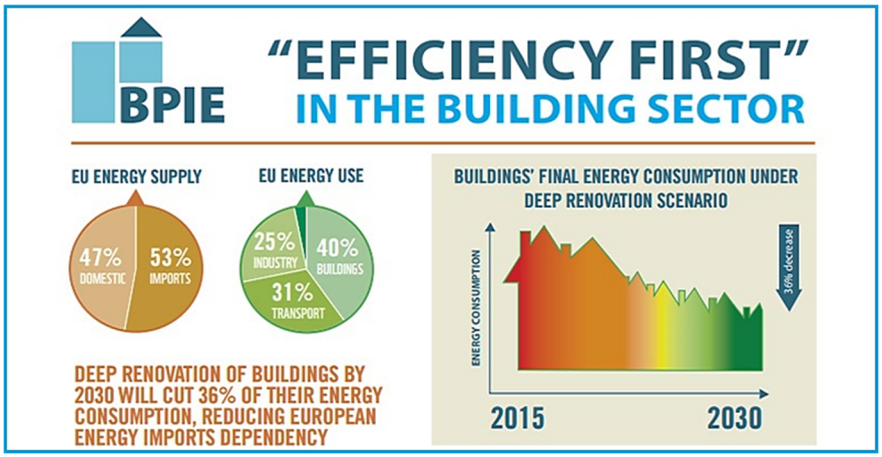

Figure 6.1. Future energy consumption reduction in the building sector. From Ref. [1].

In this chapter, a scientific paper is presented describing the synthesis and main properties of polyurethane foam-polyurethane aerogel composites. The characteristics of the employed polyurethane foams are gathered in **Figure 3.13** in Chapter 3. The synthesis of these composites is described in section 3.3.1.3 in Chapter 3. Additionally, the techniques and methods used for their characterization are included in the scientific publication.

Section 6.2 gathers relevant information concerning the synthesis, properties, and conclusions about the production of these PU_{foam} – $PU_{aerogel}$ composites.

6.2 Polyurethane aerogel inclusion in the porous structure of Polyurethane foams: improving their thermal insulation

The results based on the synthesis, characterization, thermal conductivity measurements and mechanical behavior are presented in the publication: **B. Merillas, F. Villafañe, and M. Á. Rodríguez-Pérez. Improving the Insulating Capacity of Polyurethane Foams through Polyurethane Aerogel Inclusion: From Insulation to Superinsulation. Nanomaterials, vol. 12, p. 2232, 2022, doi: 10.3390/nano12132232.**

The synthesis of polyurethane foam – polyurethane aerogel (PU_F–PU_A) composites, by a sol-gel method and by the subsequent supercritical drying, is herein described by using three different reticulated PU foams. These foams have similar densities of ca. 29 kg/m^3, and pore sizes of approximately 400, 1000 and 4000 μm (labeled as S, M and L, respectively) what allows to study the effect of the foam pore size on the final composite properties. Different parameters are analyzed, such as density, shrinkage, porous structure, mechanical properties, and thermal insulation at different temperatures.

This method constitutes an innovative solution to **enhance the polyurethane foams elastic modulus (from 0.03-0.08 to 0.85 MPa)** as well as significantly **reducing their thermal conductivities, until reaching values of ca. 16 mW/mK.** These insulating values are not achievable by using a polyurethane foam exclusively, since their large pores contributes to a high gas conduction and radiative contributions to the total thermal conductivity. In this work, the **inclusion of more than an 80 wt.% of aerogel inside the polyurethane foams** notably decreases these contributions, reaching super-insulation. The heat transfer mechanisms to the total thermal conductivity are herein analyzed through a theoretical model.

The effect of the foam pore size is also studied, obtaining that **larger pores reduce the final density by decreasing the final shrinkage during drying**. Additionally, the interaction between both materials is evaluated by scanning electron microscopy, showing small disconnections between them, and thus confirming a good cohesion.

Their mechanical behavior is also evaluated by uniaxial compression tests, concluding that the produced **composites show great flexibility and recovery ratios**. It should be noted that these **composites do not break at high deformations**, being densified when large forces were applied.

A **synergistic effect** is also present in the use of this strategy since the **density of the monolithic aerogel is reduced** (and porosity increased from 88 to 91 %) by the use of reticulated foams as skeleton. This reduction is possible through a decrease of shrinkage produced during the supercritical drying. The reason of this fact could be due to a possible **barrier-effect that the reticulated foams are producing on the polyurethane aerogel**, protecting its structure from a strong shrinkage of the porous structure.

Figure 6.2 shows the graphical abstract of the presented paper. The full publication is included in the next pages.

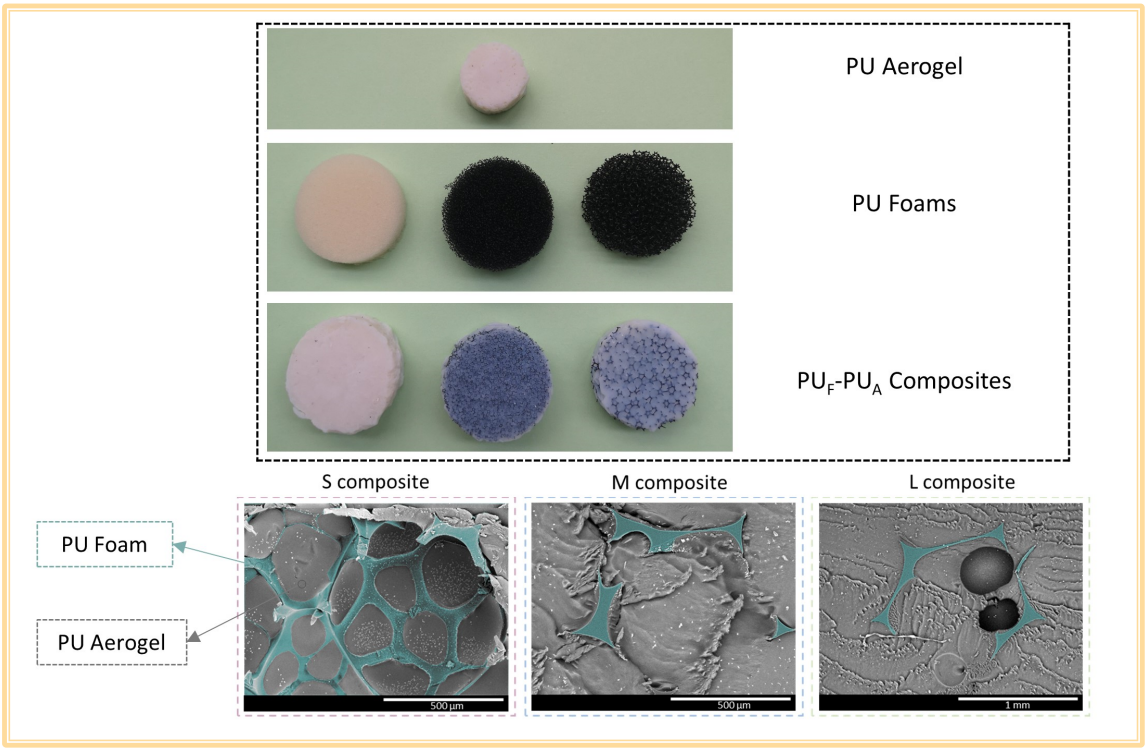

Figure 6.2. Graphical abstract of **"Improving the Insulating Capacity of Polyurethane Foams through Polyurethane Aerogel Inclusion: From Insulation to Superinsulation."**

Improving the Insulating Capacity of Polyurethane Foams through Polyurethane Aerogel Inclusion: From Insulation to Superinsulation

Beatriz Merillas[1*], Fernando Villafañe[2], and Miguel Ángel Rodríguez-Pérez[1,3*]

1 Cellular Materials Laboratory (CellMat), Condensed Matter Physics Department, Faculty of Science, University of Valladolid, Campus Miguel Delibes, Paseo de Belén 7, 47011 Valladolid, Spain

2 GIR MIOMeT-IU Cinquima-Química Inorgánica. Faculty of Science, University of Valladolid, Campus Miguel Delibes, Paseo de Belén 7, 47011 Valladolid, Spain

3 BioEcoUVA Research Institute on Bioeconomy, University of Valladolid, Spain

**Correspondence: Authors Email: b.merillas@fmc.uva.es, Tlf: +34 983 42 31 94, ORCID: 0000-0003-2995-6412,*

Email: marrod@fmc.uva.es, Tlf: +34 983 18 40 35, ORCID: 0000-0002-3607-690X

Nanomaterials, 12, 2232, 2022.

Abstract: A novel synthesis of polyurethane foam/polyurethane aerogel (PU_F–PU_A) composites is presented. Three different polyurethane reticulated foams which present the same density but different pore sizes (named S for small, M for medium, and L for large) have been used. After the characterization of the reference materials (either, foams, and pure aerogel), the obtained composites have been characterized in order to study the effect of the foam pore size on the final properties, so that density, shrinkage, porous structure, mechanical properties, and thermal conductivity are determined. A clear influence of the pore size on the density and shrinkage was found, and the lowest densities are those obtained from L composites (123 kg/m^3). Moreover, the aerogel density and shrinkage have been significantly reduced through the employment of the polyurethane (PU) foam skeleton. Due to the enhanced mechanical properties of polyurethane aerogels, the inclusion of polyurethane aerogel into the foam skeleton helps to increase the elastic modulus of the foams from 0.03 and 0.08 MPa to 0.85 MPa, while keeping great flexibility and recovery ratios. Moreover, the synthesized PU_F–PU_A composites show an excellent insulating performance, reducing the initial thermal conductivity values from 34.1, 40.3, and 50.6 mW/(m K) at 10 °C for the foams S, M, and L, to 15.8, 16.6, and 16.1 mW/(m K), respectively. Additionally, the effect of the different heat transfer mechanisms to the total thermal conductivity is herein analyzed by using a theoretical model as well as the influence of the measurement temperature.

Keywords: polyurethane foam; polyurethane aerogel; pore size; composites; mechanical properties; thermal superinsulation; Knudsen effect.

DOI: 10.3390/nano12132232

6.3 References

[1] Balkan Green Energy News, "https://balkangreenenergynews.com/new-eu-energy-performance-of-buildings-directive-an-opportunity-for-highly-efficient-healthy-and-comfortable-buildings/," 2018.

[2] M. Szycher, *Szycher's Handbook of Polyurethanes*, 2nd ed. Boca Raton, Florida, USA: CRC Press, 2012. doi: 10.1038/142853a0.

CHAPTER 7

MECHANICAL REINFORCEMENT OF SILICA AEROGELS WITH POLYURETHANE FOAMS AS SCAFFOLD

Chapter 7. Mechanical reinforcement of Silica Aerogels with Polyurethane foams as scaffold

7.1 Introduction

From the very beginning, silica aerogels became the main matrix employed for aerogel synthesis. Their interesting properties and wide chemical functionalization possibilities were some of the reasons for its excellence and versatility. The weak point of these aerogels is their poor mechanical strength when an extern force is applied, which, to a certain extent, limit their applications.

In this section, a novel reinforcing strategy for silica aerogels, consisting on the use of a reticulated polyurethane foam as skeleton for the silica aerogels, is developed. Two scientific papers are included in the following sections, which explain the effect of different parameters on the final density, porosity, specific surface area, shrinkage, thermal conductivity and mechanical properties of the synthesized composites.

In section 7.2, the first results using this strategy are gathered, which also prove its effectiveness.

Once the reinforcing strategy showed to be an effective and cost-efficient method for improving the mechanical properties of silica aerogels, an optimization of the methodology has been carried out. Therefore, in section 7.3, the influence of the foam pore size on the final properties of the silica aerogel-based composites is described.

7.2 Reinforcing silica aerogels by scaffolding with reticulated polyurethane foams

The initial study of the employment of reticulated polyurethane foams as scaffold for silica aerogels is included in the publication: **B. Merillas, A. Lamy-Mendes, F. Villafañe, L. Durães, M.Á. Rodríguez-Pérez. Silica-Based Aerogel Composites Reinforced with Reticulated Polyurethane Foams: Thermal and Mechanical Properties, Gels. 8 (2022) 392. doi:10.3390/gels8070392.**

The reinforcement of silica aerogels through reticulated PU foams showed to have an important effect on the aerogel density and porosity. The effect of the drying method (ambient pressure and supercritical conditions) is analyzed, as well as the influence of the surface modification caused by a silylating agent on the final properties of the composites.

It is concluded that the surface modification and supercritical drying improve the interaction between both matrixes forming the composites, and the mechanical and insulating properties thereof. The elastic modulus is improved from 130 kPa to 300 kPa for the SCD samples, while the elasticity that the foam provides to the aerogel avoids the aerogel breakage under compression. The thermal insulating performance is excellent, with a thermal conductivity value of 14 mW/mK when the modification is applied.

Figure 7.1 shows the graphical abstract of the presented paper. The full publication is included in the next pages.

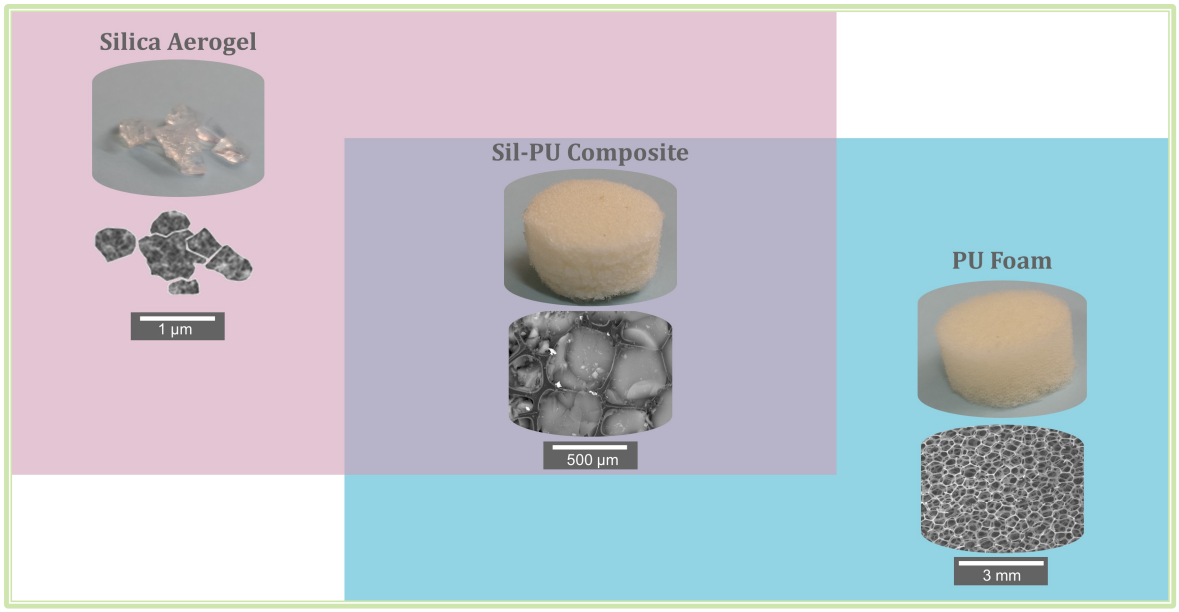

Figure 7.1. Graphical abstract of **"Silica-Based Aerogel Composites Reinforced with Reticulated Polyurethane Foams: Thermal and Mechanical Properties."**

Silica-Based Aerogel Composites Reinforced with Reticulated Polyurethane Foams: Thermal and Mechanical Properties

Beatriz Merillas[1*], Alyne Lamy-Mendes[2], Fernando Villafañe[3], Luisa Durães [2], and Miguel Ángel Rodríguez-Pérez[1,4*]

1 Cellular Materials Laboratory (CellMat), Condensed Matter Physics Department, Faculty of Science, University of Valladolid, Paseo de Belén 7, 47011 Valladolid, Spain; marrod@fmc.uva.es

2 University of Coimbra, CIEPQPF, Department of Chemical Engineering, University of Coimbra, CIEPQPF, Rua Sílvio Lima, 3030-790 Coimbra, Portugal; alyne@eq.uc.pt *(A.L.-M.);* luisa@eq.uc.pt *(L.D.)*

3 GIR MIOMeT-IU Cinquima-Química Inorgánica, Faculty of Science, University of Valladolid, Paseo de Belén 7, 47011 Valladolid, Spain; fernando.villafane@uva.es

4 BioEcoUVA Research Institute on Bioeconomy, University of Valladolid, 47011 Valladolid, Spain

** Correspondence*: b.merillas@fmc.uva.es

Abstract: In this work, silica aerogel composites reinforced with reticulated polyurethane (PU) foams have been manufactured having densities in the range from 117 to 266 kg/m^3 and porosities between 85.7 and 92.3%. Two different drying processes were employed (ambient pressure drying and supercritical drying) and a surface modification step was applied to some of the silica formulations. These composites, together with the reference PU foam and the monolithic silica aerogels, were fully characterized in terms of their textural properties, mechanical properties, and thermal conductivities. The surface modification with hexamethyldisilazane (HMDZ) proved to improve the cohesion between the reticulated foam and the silica aerogels, giving rise to a continuous network of aerogel reinforced by a polyurethane porous structure. The samples dried under supercritical conditions showed the best interaction between matrixes as well as mechanical and insulating properties. These samples present better mechanical properties than the monolithic aerogels having a higher elastic modulus (from 130 to 450 kPa), really exceptional flexibility and resilience, and the capacity of being deformed without breaking. Moreover, these silica aerogel-polyurethane foam (Sil-PU) composites showed an excellent insulating capacity, reaching thermal conductivities as low as 14 mW/(m·K).

Keywords: silica aerogel; polyurethane foam; composites; thermal insulation; reinforcement.

DOI: 10.3390/gels8070392

Gels, 8, 392, 2022.

7.3 Influence of the foam pore size in the reinforcement of silica aerogels with reticulated polyurethane foams

Based on the results obtained from the paper described in section 7.2 in which the improvements of the silica aerogel properties were attributed to the use of a reticulated PU foam, an optimization of the strategy is performed. The effect of the pore size of the polyurethane skeleton on the final properties of the produced composites is thoroughly analysed. The publication gathering the mentioned results is **B. Merillas, A. Lamy-Mendes, F. Villafañe, L. Durães, and M. Á. Rodríguez-Pérez. Polyurethane foam scaffold for silica aerogels : effect of cell size on the mechanical properties and thermal insulation, Mater. Today Chem., 26 (2022), 101257. doi: 10.1016/j.mtchem.2022.101257.**

This publication contains the study of the density, shrinkage, aerogel percentage, porous structure, mechanical properties, and thermal conductivity of the synthesized composites with and without a surface modification.

This contribution proves that the size of the foam pores in which the silica aerogel is scaffolded significantly affects the composite properties:

- The smallest pore size contributes to a better attachment between the PU skeleton and the silica aerogel, whereas the composite density decreases for larger pore sizes.
- The composites showing greater elasticity were the composites with the larger foam pores, reaching a smaller energy dissipation during the compression-decompression tests.
- All the foam pore size contributed to super-insulation, being the lowest thermal conductivity that with the largest pores (12.3 mW/mK).

All the produced composites show notably improved mechanical properties (stiffness, recovery ratios, no breakage) in comparison with the non-reinforced silica aerogels, and incredibly low thermal conductivities.

Figure 7.2 shows the graphical abstract of the presented paper. The full publication is included in the next pages.

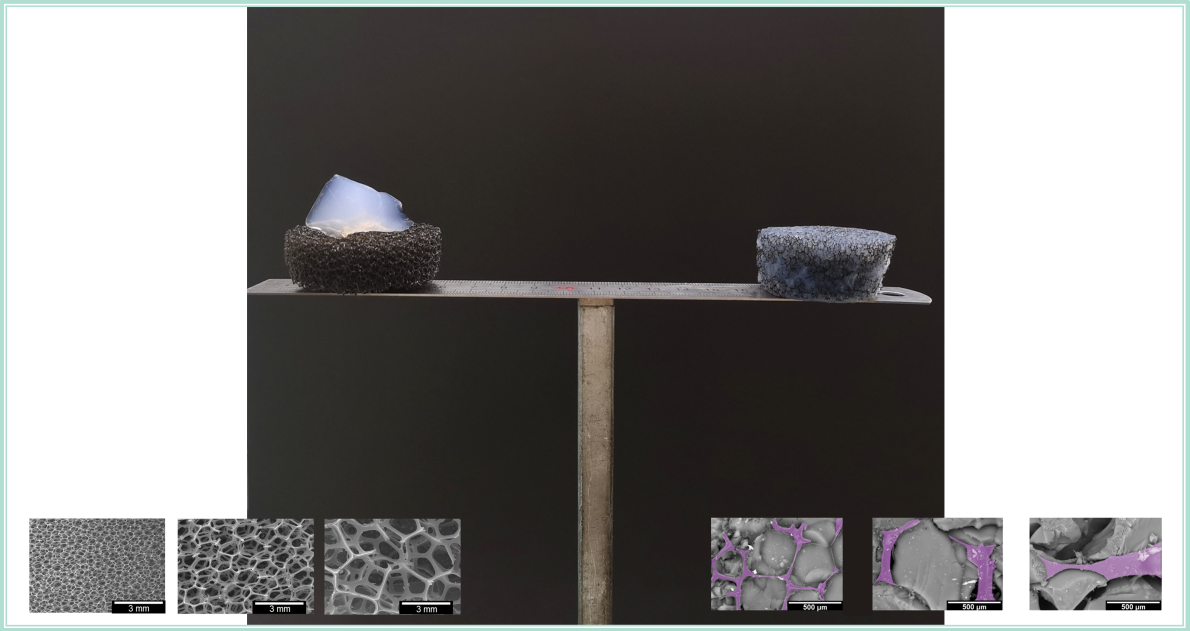

Figure 7.2. Graphical abstract of **"Polyurethane foam scaffold for silica aerogels: effect of the cell size on the mechanical properties and thermal insulation."**

Polyurethane foam scaffold for silica aerogels: effect of cell size on the mechanical properties and thermal insulation

Beatriz Merillas[1*], Alyne Lamy-Mendes[2], Fernando Villafañe[3], Luisa Durães [2], and Miguel Ángel Rodríguez-Pérez[1,4*]

1 Cellular Materials Laboratory (CellMat), Condensed Matter Physics Department, Faculty of Science, University of Valladolid, Paseo de Belén 7, 47011 Valladolid, Spain; b.merillas@fmc.uva.es; marrod@fmc.uva.es
2 University of Coimbra, CIEPQPF, Department of Chemical Engineering, University of Coimbra, CIEPQPF, Rua Sílvio Lima, 3030-790 Coimbra, Portugal; alyne@eq.uc.pt *(A.L.-M.);* luisa@eq.uc.pt *(L.D.)*
3 GIR MIOMeT-IU Cinquima-Química Inorgánica, Faculty of Science, University of Valladolid, Paseo de Belén 7, 47011 Valladolid, Spain; fernando.villafane@uva.es
4 BioEcoUVA Research Institute on Bioeconomy, University of Valladolid, 47011 Valladolid, Spain
** Correspondence*: b.merillas@fmc.uva.es

Abstract: Silica-based aerogels have been successfully reinforced by means of reticulated polymeric polyurethane (PU) foams with different cell sizes. The resultant silica aerogel-PU foam composites (Sil-PU composites) were fully characterized (density, shrinkage, aerogel percentage, and porous structure), and the mechanical properties and thermal conductivities were analyzed. Moreover, the effect of the application of a surface modification was assessed. A clear influence of the foam pore size on the final properties was found, and the mechanical properties of the aerogels have been notably improved reaching higher elastic modulus (from 130 to 307 kPa), excellent recovery ratios (above 95%), and significant deformations (more than 70%) without breaking. Therefore, the synthesized composites showed a great elasticity (high recovery ratios), tenacity, resilience, and stiffness in comparison with the non-reinforced aerogels. The obtained samples also showed excellent insulating capacities, reaching values between 14.0 and 12.3 mW/(m·K) for the surface-modified composites that were dried under supercritical conditions. Thus, using reticulated PU foams as a skeleton for aerogels is a promising strategy for a broad spectrum of applications in which silica aerogels are suitable candidates.

Keywords: Polyurethane foams; Nano-structures; Mechanical properties; silica composites; Aerogel.

Polymers, 13, 2952, 2021.

DOI: 10.1016/j.mtchem.2022.101257

CHAPTER 8

CONCLUSIONS AND FUTURE WORK

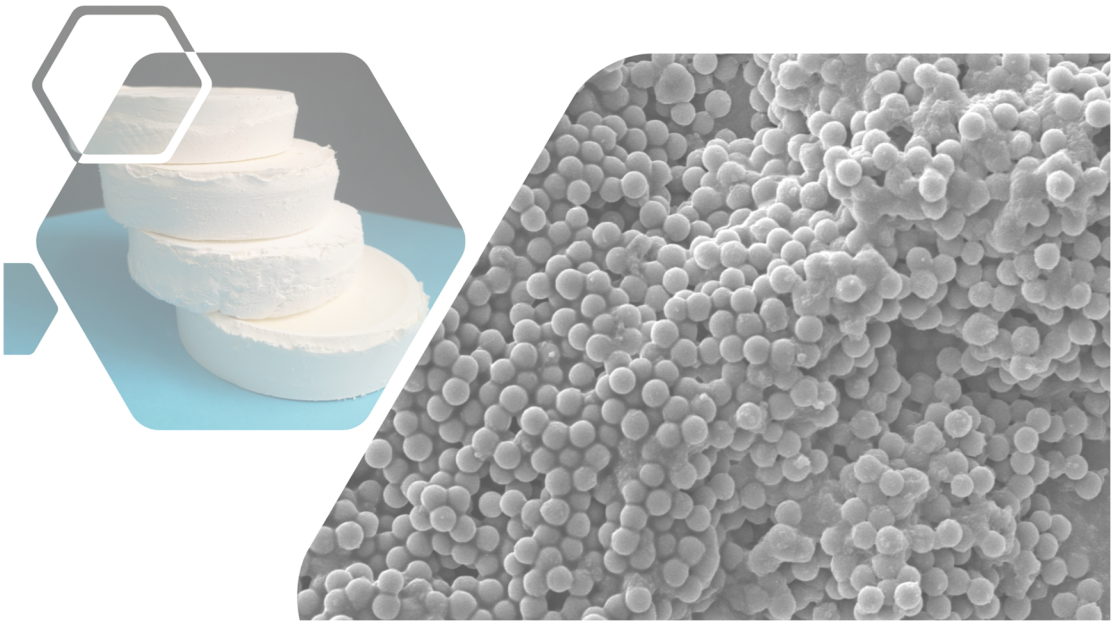

Chapter 8. Conclusions and Future Work

8.1 Conclusions

The results obtained along this thesis have been gathered in the previous chapters (from **Chapter 4** to **Chapter 7,** and **Annex**) and are included in a total of eleven scientific publications. These results have allowed to reach relevant conclusions in the field of aerogels and aerogel-based composites, fulfilling the key objectives set at the beginning of this thesis (**Chapter 1**). Thus, **section 8.1** of this chapter summarizes the main conclusions of each of the topics addressed in this thesis, that were divided into two different research lines (**Figure 8.1**). Additionally, the results obtained are compared with those found in the literature for each topic, thus aiming to summarize the main novelties of this research.

Afterwards, in **section 8.2**, some possible ideas that could be carried out as future work are included.

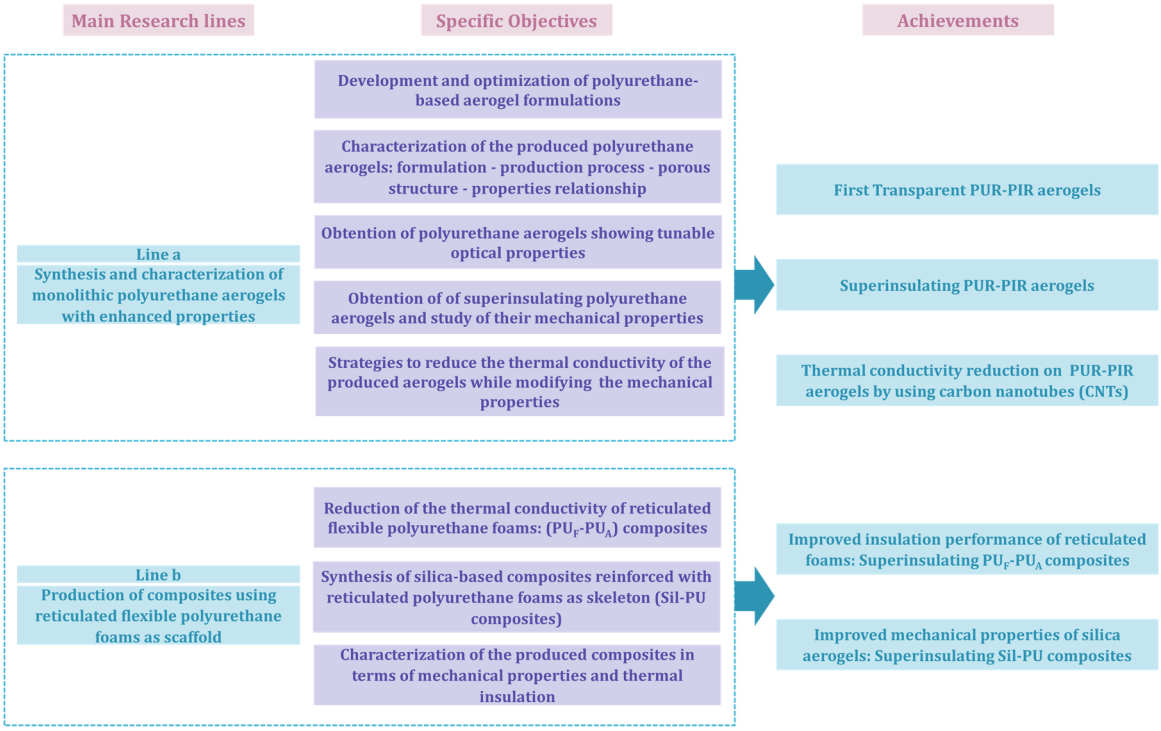

Figure 8.1. Main research lines, specific objectives, and summary of the achievements of this thesis.

Line a: Synthesis and characterization of monolithic polyurethane aerogels with enhanced properties

8.1.1 Thermal conductivity of nanoporous materials: techniques and heat transfer mechanisms

A scientific review has been written [1] gathering the research concerning the thermal conductivity of nanoporous materials and analyzing the main differences between nanocellular polymers and aerogels (**Chapter 2, section 2.3.3.1**).

Measuring techniques

- A detailed comparison between transient and steady-state methods for measuring the thermal conductivity of highly insulating porous materials has been developed theoretically and experimentally.
- The experimental results, based on aerogel composites produced for this study and on PMMA foams, demonstrate that the measuring differences between the transient plane source method (TPS) and the heat flow meter method (steady-state method) are higher when the insulating performance is greater (values below 20 mW/m K), being the steady-state method the most accurate and reliable technique.

Heat transfer mechanisms in nanoporous materials

- The main thermal insulating differences between nanocellular polymers and aerogels lies in their structural features: different pore size (larger for nanocellular polymers) and solid distribution (continuous in nanocellular polymers and with solid interruptions in aerogels).
- Thus, the key point for developing insulating materials with a further reduced thermal conductivity compared to the current ones is creating materials with high porosity and nanometric pores, as small as possible, to have a large Knudsen effect that strongly reduces the gas conduction contribution.
- In addition, an effective strategy to minimize the thermal conductivity is to create a solid phase with "solid interruptions" that restrict the phonon transfer.

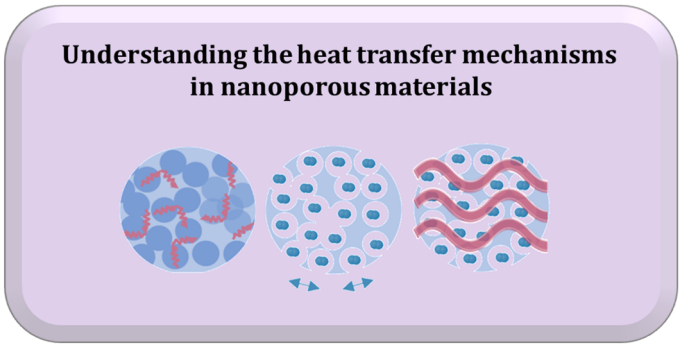

Figure 8.2. Main conclusion of section 8.1.1.

The production of low-density materials with cells or pores in the nanoscale as small as possible and presenting interruptions along the solid phase is the key point to develop super-insulating materials.

8.1.2 Synthesis of Polyisocyanurate-Polyurethane aerogels

Different parameters and properties have been studied in relation to the synthesis of polyisocyanurate-polyurethane aerogels [2]–[4]:

Reaction kinetics

- The modification of the reaction kinetics during the polymerization reaction and the gelation procedure produces a clear modification of the porous structure, including particle size, particle size distribution, particle packaging (i.e. bulk density), pore size, specific surface area and shrinkage. Modifying the catalyst concentration in polyurethane-based aerogel formulations becomes an effective strategy for obtaining tunable aerogel structures (**Chapter 4, section 4.2**).
- Reducing the catalyst amount leads to polyurethane aerogels with smaller particles and pores.
- Additionally, the bulk density of aerogels with low catalyst amounts is incremented through an effective particle-packaging and a larger shrinkage.

Transparency

- In relation to the previous section, decreasing the catalyst amount in the synthesis of the polyurethane aerogels produced in this thesis leads to a strong reduction of the particle and pore size, reaching particle sizes below 25 nm and average pore sizes below 90 nm. The significantly small features present in these aerogels allow to transmit visible light to a certain extent, reaching light transmittances above 76 % at 532 nm and above 85 % at 650 nm for aerogels of 1 mm thickness.
- This fact constitutes one of the main goals of this thesis, that is to produce **transparent polyisocyanurate-polyurethane-based aerogels for the first time (Chapter 4, section 4.2)**.
- In comparison with the data found in the bibliography for transparent aerogels produced with other organic matrixes (**Figure 8.3**), the following observations can be done:
  - Transmittance values (at 550 nm) obtained for aerogels of 1 mm thickness are comparable to that reached with cellulose aerogels and higher than those obtained with polyimide or chitosan matrixes.
  - When increasing the thickness of the polyurethane aerogels, light transmittance is progressively reduced, being lower than for other matrixes such as melamine-formaldehyde or hybrid aerogels.

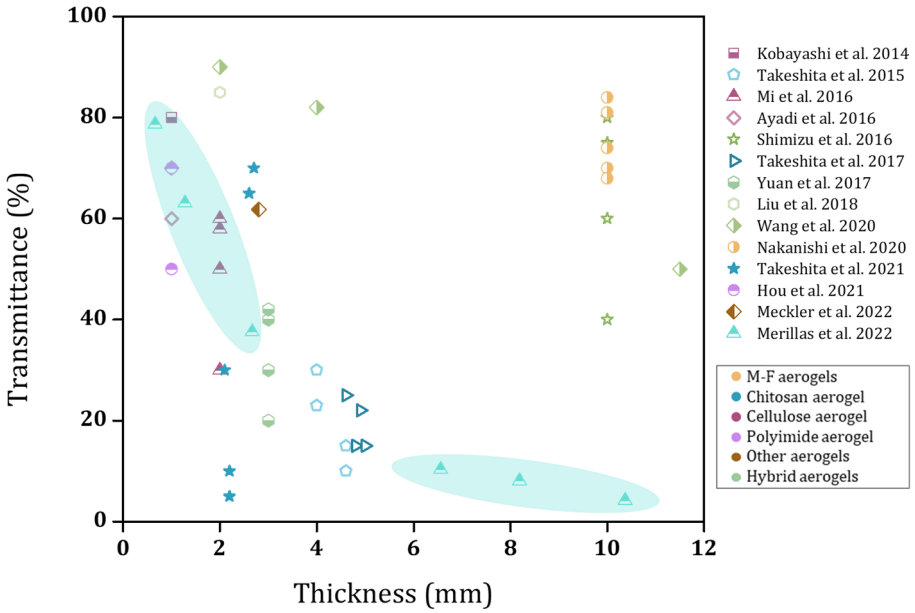

Figure 8.3. Light transmittance at 550 nm as a function of the sample thickness for different organic aerogels and the aerogels produced in this thesis.

Different factors affecting the final transmittance were studied, what allowed to conclude the following statements (**Chapter 4, section 4.3**):

- The highest transmittances were reached for aerogels with lower catalyst contents, that led to smaller particles and pores.
- The fulfillment of the Beer-Lambert law was demonstrated by the variation of samples thickness.
- The attenuation coefficient shows a direct relationship with the particle size and an inverse trend with the light wavelength.
- A strong correlation between particle size and particle size distribution with the transmitted light has been found. A sharp decrease in transparency is observed when particles are above 30 nm.

Scattering mechanisms

- The dependence of transmittance on the light wavelength allows to determine the scattering mechanism acting for each sample.
- A particle size variation from 23 to 78 nm allows to observe the transition from Rayleigh scattering (L/λ^4) to Mie scattering (L/λ), being the former the main mechanism acting for aerogels with particle sizes below 32 nm, whereas the latter is the main mechanism for aerogels with particles above this value.

Mechanical properties

- The produced polyisocyanurate-polyurethane aerogels show tailorable stiffness through tunable density and nanostructure (see Reaction Kinetics section) (**Chapter 5, section 5.2**).

- The obtained elastic moduli vary from 0.13 to 6.32 MPa, due to the different densities and particle connectivity of the aerogels when tuning their porous structure:
  - A power fitting with an exponent 10.2 for the elastic modulus versus the relative density is calculated.
  - Not only the density variation produces notable changes in the stiffness of the produced aerogels, but the particle connectivity and the interparticle necks are also important factors.
- The synthesized polyurethane aerogels do not break at high deformations, being densified for deformations above 40 %.
- The great elasticity of the polyurethane aerogels has been proved by compression-decompression tests at a deformation of 10 %, In addition, high recovery ratios have been observed.
- The obtained data can be compared with data found in the bibliography for polyurethane-based aerogels (**Figure 8.4** and **Figure 8.5**) reaching the following conclusions:
  - The elastic moduli of the produced polyisocyanurate-polyurethane aerogels are similar to those obtained for other with the same bulk density (between 0.1 and 0.2 g/cm^3).

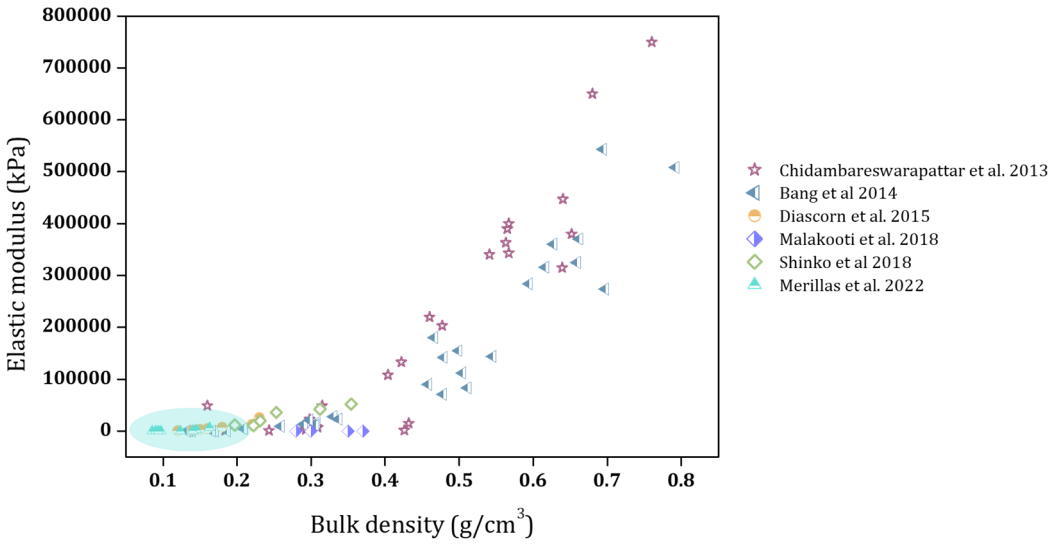

Figure 8.4. Elastic modulus as a function of bulk density for polyurethane-based aerogels from the literature and the aerogels produced in this thesis.

  - The stress needed to deform the polyurethane aerogels at a 50 % of strain follows the same tendency as that of other polyurethane-based aerogels from the literature, reaching values between 100 and 1000 kPa for densities between 0.1 and 0.2 g/cm^3.

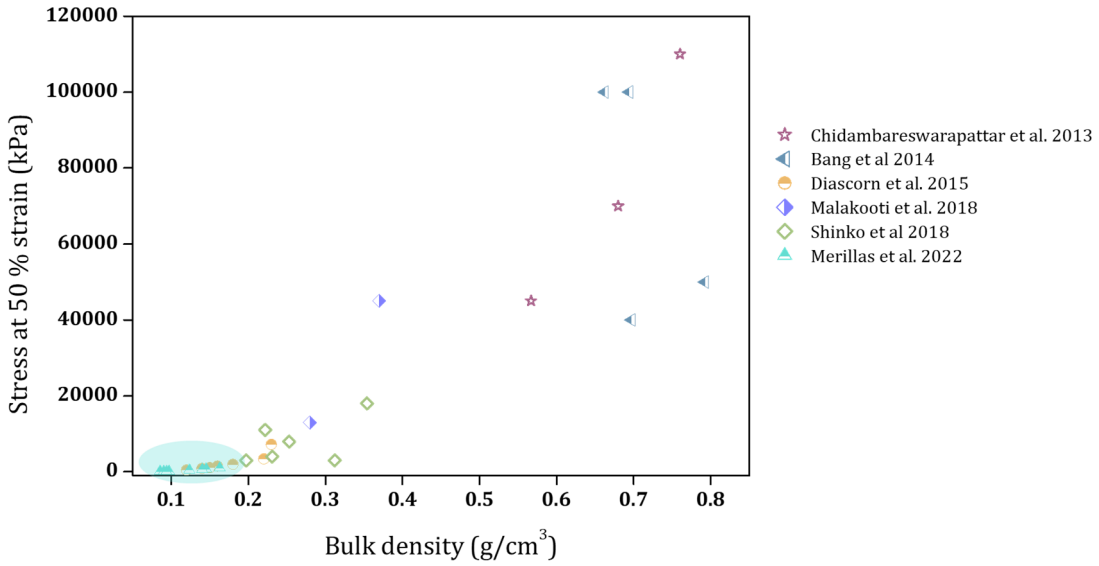

Figure 8.5. Stress at a 50 % strain as a function of bulk density for polyurethane-based aerogels from the literature and the aerogels produced in this thesis.

Thermal conductivity

- The produced polyurethane aerogels show super-insulating values of the thermal conductivity (from 12 to 24 mW/mK at 10 °C (**Chapter 5, section 5.2**)).
- Theoretical calculations of the heat transfer mechanisms acting in these samples suggest that the reduction of pores and particles occurring when the catalyst amount is reduced has a higher relevance than the increase in the bulk density experimented by these samples.
- Thus, the main difference of the insulating performance of the aerogels produced with a low amount of catalyst is due to the decrease in the pore and particle size, that significantly reduce the gaseous and solid contributions through the Knudsen and size effects, respectively.
- The radiative contribution of these samples reaches a value of around 1 mW/mK, whereas no significant differences between the specimens were detected.
- Comparing the obtained thermal conductivities to the data found in the literature for polyurethane-based aerogels, (**Figure 8.6**) we can conclude that:
  - The **value of 12 mW/mK is the lowest ever achieved with polyurethane matrixes** independently of the bulk density.
  - Trifu et al. [5] synthesized polyurethane-based aerogels with lower densities than those produced in this thesis, 0.04 g/cm^3 reaching a thermal conductivity of 18 mW/mK.

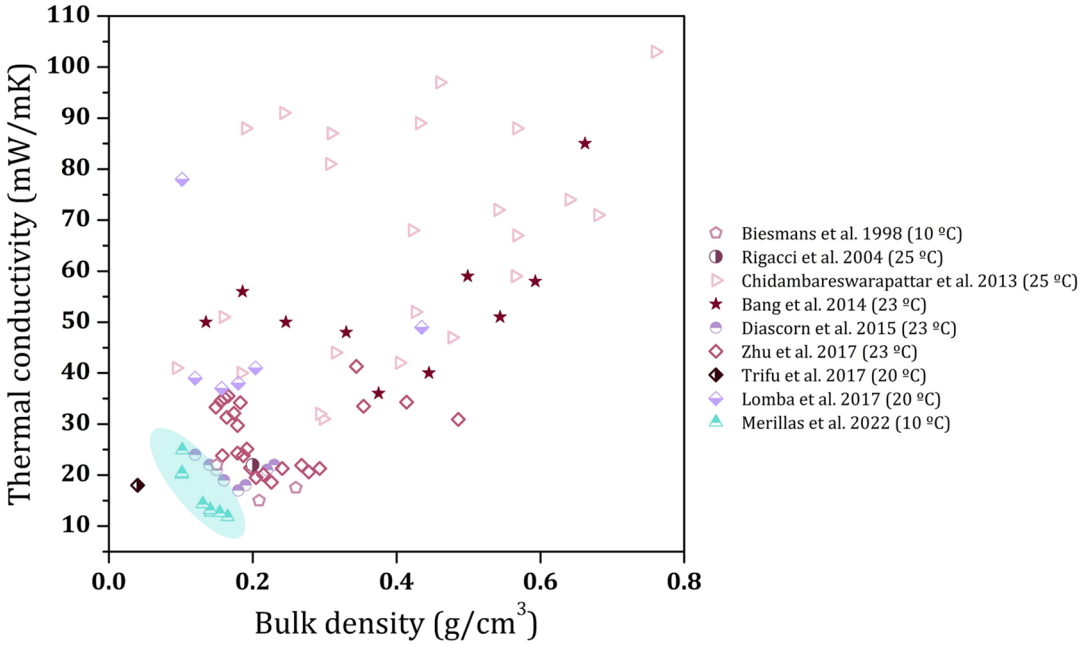

Figure 8.6. Thermal conductivity as a function of the bulk density of polyurethane and polyisocyanurate aerogels from literature data and the aerogels produced in this thesis.

CNTs addition

The incorporation and effective dispersion of different contents (0.5, 1.0 and 3.0 wt.%) of modified carbon nanotubes in polyurethane aerogel formulations led to interesting findings (**Chapter 5, section 5.3**):

- The gelation process is affected by the inclusion of these particles, modifying the reaction kinetics. Small amounts of CNTs increase the gelation rate whereas a further increase in the particles amount leads to a slight delay on the chemical reaction rates.
- When CNTs are added, slightly lower densities are reached. This fact is due to the lower shrinkage of aerogels when carbon nanotubes are dispersed along their structure, which contributes to a greater withstanding during the supercritical drying process and, therefore, to the increase of the final porosities.
- The structural modification produced by CNTs in polyurethane aerogels worsen the aerogel stiffness, reducing the elastic moduli. Despite this effect, these nanocomposites can be compressed until more than 80 % without breaking. On the contrary, elasticity is enhanced, and the energy loss coefficient of the produced nanocomposites is reduced.
- The thermal conductivity of samples containing CNTs is notably decreased, and this reduction is higher for larger amounts of particles. The highest reduction achieved in this work is from 15.07 mW/mK obtained for the reference aerogel produced with a 4 wt.% content of catalyst to 12.02 mW/mK for the aerogel with 3.0 wt.% of CNTs. This reduction was analyzed in detail taking into account the different heat transfer mechanisms:
  - Larger pores are formed since a smaller shrinkage takes place for the produced nanocomposites, leading to a slight increase in the gas conduction.
  - CNTs reduce the particle connectivity (which reduced the aerogel stiffness), restricting the phonon transfer and, thus, reducing the solid conduction.

- The scattering and absorption produced by CNTs block the infrared radiation increasing the extinction coefficient of samples containing these particles.

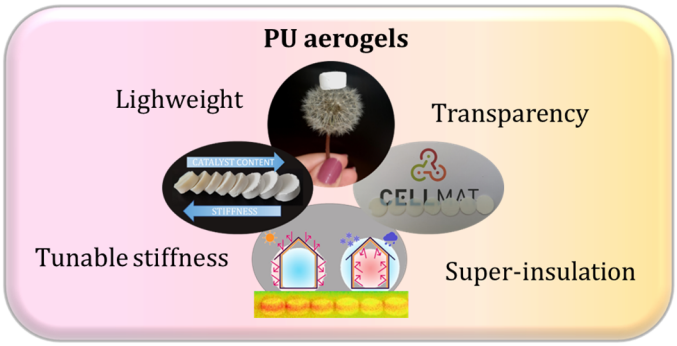

Figure 8.7. Main conclusion of section 8.1.2.

Polyisocyanurate-polyurethane aerogels showing transparency have been synthesized for the very first time. These materials also displayed the greatest insulating values found in the literature for this aerogel matrix, and tunable stiffness by tuning the reaction kinetics.
Additionally, the incorporation of infrared blockers such as carbon nanotubes led to a further enhancement of the insulating capacity.
Therefore, these aerogels are promising materials for applications in which low-density, high porosity, good mechanical properties, transparency, and thermal insulation are needed.

Line b: Production of composites using reticulated flexible polyurethane foams as scaffold

8.1.3 Synthesis of Polyurethane Foam-Polyurethane Aerogel (PU_F-PU_A) composites

- A new methodology for reducing the thermal conductivity of reticulated flexible polyurethane foams has been developed [6] (**Chapter 6, section 6.2**). It is based on reducing the contribution of the conduction of the gas phase of the initial materials by filling their whole open structure with a polyurethane aerogel that presents very low thermal conductivity.
- Composites with low densities (from 123 to 134 kg/m^3) and a high amount of aerogel (ca. 80 wt.%) have been obtained.

The main results obtained during the study of these novel materials are included in the following paragraphs.

Synergistic effects

- A synergistic effect between the employed flexible reticulated PU foams and aerogels is found. Not only the aerogels reduce the total thermal conductivity of the reticulated foams, but foams are also protecting the aerogel structure from collapsing.

In fact, the effect of the reticulated structure on the polyurethane aerogels is a scaffolding effect that reduces the shrinkage during drying, therefore reducing their bulk density and increasing the aerogels porosity (from 88 to 91 %).

Composite structure

- The produced composites present a good cohesion between both materials (PU foam and aerogels) being constituted by a continuous aerogel network attached to the struts of the reticulated foams.

Mechanical properties

- The inclusion of aerogel inside the flexible foams leads to a large increase of the elastic modulus and a 12-fold higher compressive stress needed for deforming at a 10 % of strain, respect to the initial foams.
- The PU_F-PU_A composites can be compressed until high deformations (more than 70 %) without breaking and experimenting a strong densification from 60 % strain on.
- Flexibility and elasticity are reached for the produced composites, recovering almost the initial height after a 10 % of compression.

Thermal conductivity

- Significantly greater insulating performance is reached by the produced PU_F-PU_A composites. Thermal conductivities of 16 mW/mK (at 10 °C) are reached, thus being framed in the super-insulating range, whereas the thermal conductivities of the initial foams were comprised between 34 and 50 mW/mK.
- The low thermal conductivity of the incorporated aerogels to the foam structure drastically reduces the gaseous contribution of the initial foams and the possible convective mechanism.
- Additionally, thermal conductivity measurements at different temperatures allow to conclude that the radiation contribution is notably reduced by the inclusion of aerogels, due to an increased extinction coefficient produced by the density rise.

Effect of foam pore size

The use of three foams having different pore sizes leads to the determination of the optimum cell size for the aerogel inclusion:

- Although the aerogel mass is almost the same for each composite, their bulk density is reduced when increasing the foam pore size (L size) since a smaller shrinkage in the aerogel takes place.
- The composite stiffness is lower for higher pore sizes (L size), being these samples those which present the highest elasticity, as occurs also for the initial foam. Therefore, some of the initial properties of the reticulated foams are transmitted to the final composites.

- Smaller pores lead to the greatest thermal insulating performance, reaching values of 15.79, 16.61, and 16.07 mW/mK for the S, M and L sizes, respectively. Nevertheless, it has to be noticed that, despite the significantly different initial values of thermal conductivity for the initial foams (34, 40 and 50 mW/mK), all the composites reached a similar insulating capacity of ca. 16 mW/mK.

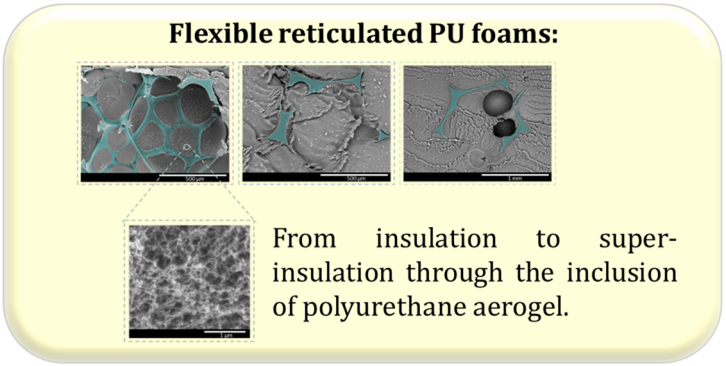

Figure 8.8. Main conclusion of section 8.1.3.

The inclusion of polyurethane aerogel into the pores of flexible reticulated polyurethane foams leads to an effective cohesion between both matrixes. It promotes a sharp reduction of the gas conduction through the pores, therefore decreasing their thermal conductivity, and thus allowing to reach values in the super-insulating region. In addition, the composites show excellent mechanical performance.

8.1.4 Synthesis of Silica Aerogel-Polyurethane Foam (Sil-PU) composites

- A novel strategy to effectively reinforce silica aerogels has been developed based on the use of flexible reticulated polyurethane foams as scaffold [7] (**Chapter 7, section 7.2**).
- A high aerogel mass percentage is included in the final composites, reaching values ca. 87 %.

The main results obtained during the study of these novel materials are included in the following paragraphs.

Mechanical properties

- The elastic moduli of the synthesized reinforced silica aerogels are significantly increased by the employment of this strategy, thus rising from 130 to 307 kPa.
- Whereas the silica aerogel monoliths broke into small pieces at a 12 % of deformation under compression, the herein reinforced aerogels could be deformed until more than 80 % without being broken, experimenting a strong densification.
- Despite the stiffness of the silica aerogels is strongly enhanced, their flexibility and elasticity at a strain of 10 % and 25 % is maintained.

- High recovery ratios of ca. 95 % are reached after performing compression-decompression tests to a strain of 25 %.

Thermal conductivity

- The thermal conductivity of the produced composites shows similar values to those of pure silica aerogels, not being worsen by the addition of the reticulated skeleton.

Effect of drying

- Higher densities are obtained for the composites dried under ambient pressure conditions, as a consequence of a stronger shrinkage, thus, reducing their porosity. On the contrary, composites dried under supercritical conditions reach smaller densities, shrinkages and a greater porosity in comparison to the APD composites.

Effect of surface modification

- A silylation agent (HMDZ) reduces the final density of the produced composites, reaching densities of 117 kg/m^3. This fact reveals that smaller shrinkages occur when modifying these composites and even, for some specific cases, negative shrinkages are achieved, since these foams make swelling during the gelation step.
- Additionally, the modified composites present an enhanced stability and cohesion between the polyurethane struts and the silica aerogel, thus obtaining lower disconnections and increasing the aerogel mass percentage in the final composite (from 76 to 82 % for the SCD composites and from 74 to 87 % for the APD composites).
- The combination of the surface modification with the SCD drying leads to a notably improvement on the stiffness of the pure aerogel (from 130 to 450 kPa), as well as a super-insulating value for the thermal conductivity of 14 mW/mK.

Effect of the foam pore size

- Foams with larger pore sizes diminish the final density of the Sil-PU composites (**Chapter 7, section 7.3**) [8].
- The progressive increase of the foam pore size contributes to the appearance of cracks and small voids between the foam and the silica aerogel. Therefore, the smallest pores lead to a more continuous aerogel network than the largest pores.
- Composites with smaller foam pore sizes reach greater stiffness, according to their higher density. Nevertheless, the composites fabricated with the largest pore size are those showing more elasticity.
- The optimum pore size for producing Sil-PU composites should be above 1000 microns, since smaller pores give rise to high densities, shrinkages and, therefore, high thermal conductivities. Foams with pore sizes of 1 and 4 mm allow the obtention of Sil-PU composites having a thermal conductivity of 13.0 and 12.3 mW/mK, respectively.

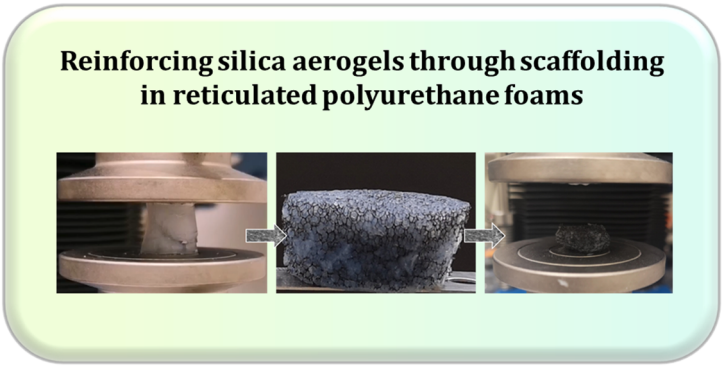

Figure 8.9. Main conclusion of section 8.1.4.

Flexible reticulated polyurethane foams provide an effective reinforcement for silica aerogels acting as scaffolds that improve their brittleness. Apart from producing composites with enhanced stiffness that support high compressive strengths with no breakage, their excellent insulating performance is maintained, not being altered by the inclusion of the foam matrix.

8.1.5 Annex

Three articles [9]–[11] included in the annex of this thesis gave rise to interesting conclusions in relation to polyurethane foams that are gathered in the following sections (**Annex section**).

8.1.5.1 Influence of nanoparticles on the cellular structure of polyurethane foams: study of the real mechanism behind the strategy

- The design of three different manufacturing procedures for producing rigid polyurethane foams containing nanoclays (types: Clay Na^+ and 30B, contents: 0.5 and 1.0 wt.%) allows to control the amount of air trapped during the mixing process. Thus, different levels of trapped-air are reached during the production of these foams (**Annex, section 2**).
- The manufacturing of foams containing clays under vacuum conditions leads to cellular structures having a similar cell size and nucleation density than the reference foam. Therefore, the possibility of a mechanism in which nanoclays reduce the cell size by a surface tension reduction is discarded.
- Nevertheless, the foams produced at atmospheric conditions indicate that the largest amount of air is included during the mixing process, the higher is the nucleation effect.
- A correlation between the increase of the polyol viscosity when nanoclays are added to the blend and the possibility of trapping air has been found, what allows to propose a mechanism acting under the addition of nanoclays to the reactive blend:
  - The nucleation effect and the subsequent reduction in cell size, due to the incorporation of nanoparticles to a rigid polyurethane formulation is promoted by the presence of a higher number of air bubbles, that act as nucleation sites. The presence of more air bubbles is a direct consequence of the increase in the polyol viscosity when nanoparticles are added, which allows to a more effective air-trapping.

The mechanism behind the reduction of cell size when nanoclays are added to rigid polyurethane foams consists of a larger amount of air trapped into the reactive blend that increases the nucleation density thus reducing the final cell size. This effect of trapping air bubbles in the blend is the direct consequence of the increase in the polyol viscosity when nanoparticles are added.

8.1.5.2 Description of novel structural parameters to evaluate the acoustic insulation of semirigid polyurethane foams

- Novel structural parameters to describe the cellular structure of semirigid PU foams have been defined to correlate them with the acoustic absorption (**Annex, section 3**). These are foams that are characterized by the presence of small holes in the cell walls.
- In order to develop an accurate methodology based exclusively on the cellular structure of polyurethane foams, changes in density, open cell content, and cell size have been avoided.
- The area of the holes (S_h), the number of holes per unit area (N_h) and the percentage of cell wall area occupied by these holes (*%HCW*) are the key parameters connecting the characteristic holes in the cell walls of these foams and their sound insulation performance.
- These novel parameters have been related to the acoustic absorption coefficient at different frequencies, and the results obtained allow to conclude that a structure containing a small number of holes with a large surface presents more effective sound absorption than one with a higher number of smaller holes.
- The key parameter describing the sound absorption behavior of these foams is the percentage of holes per cell wall (*%HCW*). The larger this parameter, the higher the absorption coefficient is. Thus, the optimum cellular structure for an effective absorption of sound consists of walls containing a small number of holes with a large surface.

The sound absorption properties of semirigid polyurethane foams can be predicted by the analysis of their cellular structure. The main parameter related to this property is the percentage of holes on the cell walls (*%HCW*), that promotes a higher sound absorption when it is higher. Thus, few holes with a large area should be present on the cell walls in order to obtain excellent sound absorbers.

8.1.5.3 Nitrates adsorption by flexible polyurethane foams containing sepiolites

- The incorporation of sepiolite functionalized with quaternary ammonium salts in the reactive blend of hydrophilic flexible polyurethane foams leads to a great nitrate adsorption capacity (about 23 mg/g) from water resources (**Annex, section 4**).
- Employing the proposed material (Se-PU) improves previous methodologies described in the literature, since there is no need of controlling the temperature or pH during the adsorption process, as well as a final filtration process is not required.

- The interaction between treated sepiolite and nitrates is described by the Langmuir model.
- The study of different sepiolite contents allows to conclude that the highest content leading to a non-damaged cellular structure is 8 wt.%.
- The combination of an open-cell hydrophilic foam with active sepiolite allows a proper interaction between polluted water and these particles by absorption of the polyurethane matrix and adsorption at the active sites of the sepiolite. Moreover, it has been demonstrated that no nitrates release occurs after the adsorption process.
- Actual nitrates-polluted water containing additional ions has been used to check the real effectiveness of the produced composites, achieving acceptable nitrates adsorption capacities ca. 11 mg/g

Hydrophilic polyurethane foams containing modified sepiolites are highly effective nitrate adsorbers from polluted waters. There exists a synergistic effect between the polyurethane matrix, that allows the water absorption, and the sepiolites, which act as nitrates adsorptive centers. This strategy is an alternative to other methods, and allows to improve their cost-effectiveness, safety, and handling, since no filtration, temperature, or pH control are necessary.

8.2 Future Work

The promising results obtained in this thesis regarding the production of aerogels and aerogel-based composites open new working paths that can be divided into three lines:

1. **Detailed study of the porous structure and additional properties of the materials developed along this thesis.**

a. Porous structure

- A **thorough analysis of the porous structure** of the synthesized PUR-PIR aerogels and composites could provide a deeper understanding of the structural features, comprising the bimodal porosity that aerogels commonly show. In order to fulfill this goal, X-ray nano-tomography will be employed as main resource. An application for beam time at the **European Synchrotron Radiation Facility (ESRF)** in Grenoble, France has been accepted for 2023. The use of synchrotron radiation-based phase-contrast hard cryo **X-ray nanoholotomography (XNH)** at the ID16A-NI nanoimaging beamline will provide relevant information about the aerogel structure and, therefore, about its influence on different properties [12].

- Based on the more detailed understanding of the porous structure of the aerogels developed in this thesis it would be important to develop more accurate **theoretical models for the thermal conductivity of these materials**. In these new models it would be necessary to take into account the **bimodal pore size** that aerogels show (ie. pores inside particles and pores surrounding them).

b. Phase separation

- Study of the **microphase separation** (formation of ordered hydrogen-bonded urea) between urethane and urea, and its influence on the cross-linking density and the final morphology of the PU matrix. This analysis can be carried out by deconvolution of the carbonyl region by FT-IR.

- Understanding of the **particle formation process** in PUR-PIR aerogels by evaluating their size distribution profile by **Dynamic Light Scattering (DLS)**. One possible collaboration with Prof. Dr. Lorenz Ratke from the German Aerospace Center (DLR), is being set to analyze the sedimentation versus aggregation mechanisms occurring in some polyurethane-based systems.

c. Study of additional properties

- The development of polyurethane aerogels with interesting properties, such as optical transparency, excellent heat insulation and a significant stiffness, drives to **explore additional properties**:

  - Thermal stability by Thermogravimetric Analysis (TGA) and Differential scanning calorimetry (DSC).
  - Thermal expansion by Dynamic Mechanical Analysis (DMA).

- Hydrophobicity and its possible modification through functionalization [13], [14], [15].
- Sound absorption.

2. Enhancement of the materials developed along this thesis.

a. Composition improvements

- The aerogel formulations developed along this thesis can be modified by **crosslinking with other polymers** or by the addition of different **surfactants and additives,** in order to study their influence on the final properties thereof.

- Exploring different **organic and biopolymeric matrixes** such as cellulose, lignin, alginate or chitosan for producing aerogels, and the possible combination with polyurethane aerogels to enhance their recyclability and biodegradability.

- Incorporation of different **infrared blockers,** in order to study their effectiveness on the reduction of the aerogel's thermal conductivity and the possible changes in their nanostructure.

- Analyzing the **cohesion between different reticulated foams and different aerogel** matrixes and the influence on their mechanical properties and thermal insulation.

- **PU foam functionalization** with the aim of improving the physical and chemical compatibility between foams and the scaffolded aerogels.

b. Process optimization

- **Optimization of the manufacturing process** by the exploration of different drying procedures, such as ambient pressure drying at different temperature conditions and freeze drying.

- The **scaling up of the sample size** would be an interesting topic for future research that would open a wide range of possible applications in the building, automotive, or energy management sectors.

3. Search of potential applications of the developed materials.

a. PIR-PUR aerogels

- Study of applicability of the synthesized PIR-PUR aerogels in the **construction, automotive and energy management sectors**: glazing windows, wall insulating systems, car engine insulation, among others.

- Incorporation of the polyurethane aerogels presenting the highest thermal insulating values into **Vacuum Insulation Panels (VIPS)** and the subsequent study of the thermal conductivity with pressure and time.

- **Functionalizing** silica and polyurethane aerogels with functional groups, to **tailor their surface properties** for specific applications as sensors, supercapacitors, catalysts, batteries, etc. [16], [17].

b. Foam-aerogel composites

- Study of the applicability of the produced composites as insulators in different sectors where mechanical stiffness should be increased.

8.3 References

[1] B. Merillas, J. P. Vareda, J. Martín-de León, M. Á. Rodríguez-Pérez, and L. Durães, "Thermal Conductivity of Nanoporous Materials : Where Is the Limit ?," *Polymers (Basel).*, vol. 14, **2022**.

[2] B. Merillas, J. Martín-de León, F. Villafañe, and M. A. Rodríguez-Pérez, "Transparent Polyisocyanurate-Polyurethane-Based Aerogels: Key Aspects on the Synthesis and Their Porous Structures," *ACS Appl. Polym. Mater.*, vol. 3, no. 9, pp. 4607–4615, **2021**, doi: 10.1021/acsapm.1c00712.

[3] B. Merillas, J. Martín-de León, F. Villafañe, and M. Á. Rodríguez-Pérez, "Optical Properties of Polyisocyanurate – Polyurethane Aerogels : Study of the Scattering Mechanisms," *Nanomaterials*, vol. 12, p. 1522, **2022**, doi: https://doi.org/10.3390/nano 12091522.

[4] B. Merillas, F. Villafañe, and M. Á. Rodríguez-Pérez, "Super-insulating transparent polyisocyanurate-polyurethane aerogels: Analysis of the thermal conductivity and mechanical properties," *Nanomaterials*, vol. 12, no. 14, p. 2409, **2022**, doi: 10.3390/ nano12142409.

[5] R. Trifu, G. Gould, and S. White, "Flexible Polyisocyanate Based Aerogels," *MRS Adv.*, vol. 357, **2017**, doi: 10.1557/adv.201.

[6] B. Merillas, F. Villafañe, and M. Á. Rodríguez-Pérez, "Improving the Insulating Capacity of Polyurethane Foams through Polyurethane Aerogel Inclusion: From Insulation to Superinsulation," *Nanomaterials*, vol. 12, p. 2232, **2022**, doi: 10.3390/nano12132232.

[7] B. Merillas, A. Lamy-Mendes, F. Villafañe, L. Durães, and M. Á. Rodríguez-Pérez, "Silica-Based Aerogel Composites Reinforced with Reticulated Polyurethane Foams: Thermal and Mechanical Properties," *Gels*, vol. 8, no. 7, p. 392, **2022**, doi: 10.3390/gels8070392.

[8] B. Merillas, A. Lamy-Mendes, F. Villafañe, L. Durães, and M. Á. Rodríguez-Pérez, "Polyurethane foam scaffold for silica aerogels : effect of cell size on the mechanical properties and thermal insulation," *Mater. Today Chem.*, vol. 26, p. 101257, **2022**, doi: 10.1016/j.mtchem.2022.101257.

[9] B. Merillas, F. Villafañe, and M. Á. Rodríguez-Pérez, "Nanoparticles addition in pu foams: The dramatic effect of trapped-air on nucleation," *Polymers (Basel).*, vol. 13, no. 17, pp. 1–11, **2021**, doi: 10.3390/polym13172952.

[10] B. Merillas, F. Villafañe, and M. Á. Rodríguez-Pérez, "A New Methodology Based on Cell-Wall Hole Analysis for the Structure-Acoustic Absorption Correlation on Polyurethane Foams," *Polymers (Basel).*, vol. 14, p. 1807., **2022**, doi: 10.3390/polym14091807.

[11] S. Barroso-Solares, B. Merillas, P. Cimavilla-Roman, M. A. Rodriguez-Perez, and J. Pinto, "Enhanced nitrates-polluted water remediation by polyurethane / sepiolite cellular nanocomposites," *J. Clean. Prod.*, vol. 254, p. 120038, **2020**, doi: 10.1016/j.jclepro.2020.120038.

[12] R. Tannert, M. Schwan, A. Rege, M. Eggeler, J. C. da Silva, M. Bartsch, B. Milow, M. Itskov, and L. Ratke, "The three-dimensional structure of flexible resorcinol-formaldehyde aerogels investigated by means of holotomography," *J. Sol-Gel Sci. Technol.*, vol. 84, no. 3, pp. 391–399, **2017**, doi: 10.1007/s10971-017-4363-6.

[13] L. M. Sanz-Moral, M. Rueda, A. Nieto, Z. Novak, Ž. Knez, and Á. Martín, "Gradual hydrophobic surface functionalization of dry silica aerogels by reaction with silane precursors dissolved in supercritical carbon dioxide," *J. Supercrit. Fluids*, vol. 84, pp. 74–79, **2013**, doi: 10.1016/j.supflu.2013.09.010.

[14] Z. Li, L. Zhong, T. Zhang, F. Qiu, X. Yue, and D. Yang, "Sustainable, Flexible, and Superhydrophobic Functionalized Cellulose Aerogel for Selective and Versatile Oil/Water Separation," *ACS Sustain. Chem. Eng.*, vol. 7, pp. 9984–9994, **2019**, doi: 10.1021/acssuschemeng.9b01122.

[15] Z. Li, S. Zhao, M. M. Koebel, and W. J. Malfait, "Silica aerogels with tailored chemical functionality," *Mater. Des.*, vol. 193, p. 108833, **2020**, doi: 10.1016/j.matdes.2020.108833.

[16] M. T. Noman, N. Amor, A. Ali, S. Petrik, R. Coufal, K. Adach, and M. Fijalkowski, "Aerogels for biomedical, energy and sensing applications," *Gels*, vol. 7, no. 264, **2021**, doi:

10.3390/gels7040264.

[17] M. Alnaief and I. Smirnova, "Effect of surface functionalization of silica aerogel on their adsorptive and release properties," *J. Non. Cryst. Solids*, vol. 356, pp. 1644–1649, **2010**, doi: 10.1016/j.jnoncrysol.2010.06.027.

ANNEX

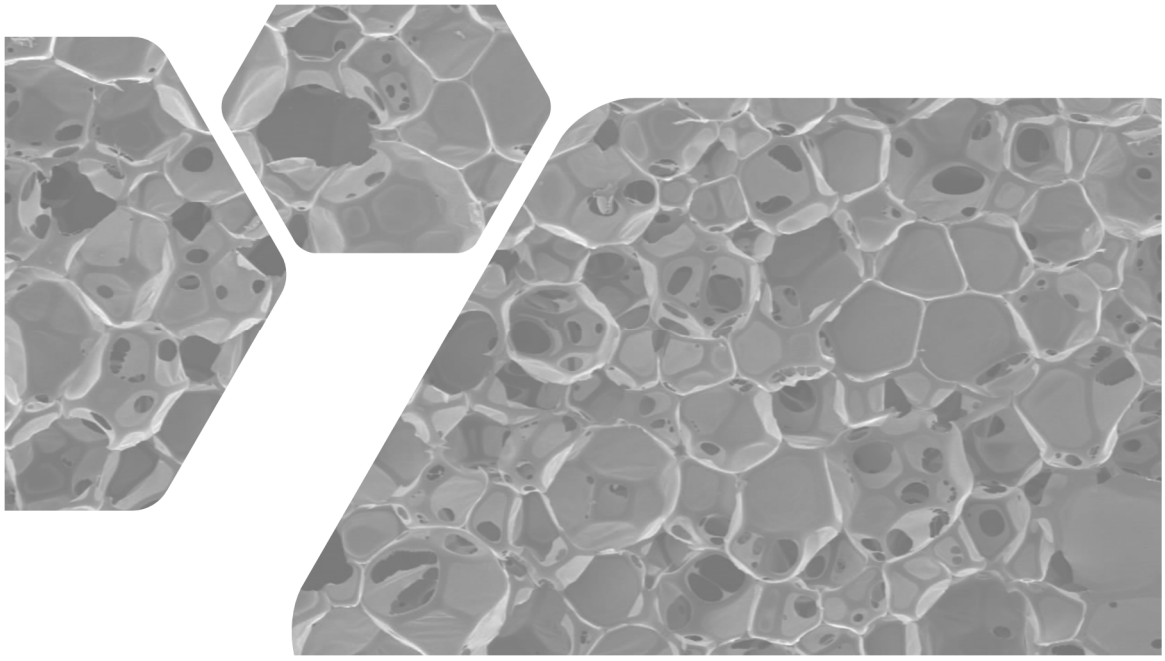

Annex

1. Introduction

Polyurethane foams are one of the most versatile materials and thus they are present in a wide variety of sectors. Owing to the expertise that CellMat Laboratory has developed on these polymeric foams, several works have been carried out regarding this topic during this thesis.

Several properties of polyurethane foams are yet aimed to be improved, and at the same time, the basis and fundamentals to reach these improvements must be understood. For instance, the reduction of the cell size of porous materials is highly important to modify and improve some of the final properties of these materials. One strategy to reduce the cell size is incorporating nucleating agents such as particles or nanoparticles. However, there is some lack of knowledge on the reasons why the size of the cells is reduced when certain particles are added. This aspect is studied in detail in section 2, which describes the results obtained when nanoparticles are added with this purpose. This paper analyzes the key mechanisms justifying the cell size reduction.

Secondly, the sound absorption properties of semirigid PU foams are analyzed in section 3, establishing new parameters to relate the cellular structure thereof with their acoustic performance. In this way, structural features, such as the holes present in the cell walls, are quantitatively analyzed, giving rise to the structure-sound absorption relationship which is necessary to develop optimum noise absorbers.

Afterwards, Section 4 describes flexible PU foams in which nanosepiolite have been introduced as fillers. These nanocomposites have been designed for water treatment through nitrates removal, what constitutes a novel strategy able to overcome some of the drawbacks of previously reported studies.

The similarities between foams and aerogels in regard to their porous structure and characterization, together with the similar polymerization chemical reaction for polyurethane foams and polyurethane aerogels, made working with polyurethane foams an interesting starting point for this thesis. Additionally, part of the knowledge developed during the research on PU foams could be extrapolated to polyurethane aerogels.

2. Studying the influence of nanoparticles and air trapping on cell nucleation in polyurethane foams.

Reducing the cell size of PU foams has become a pursued objective in order to improve some of the final properties of these materials. For instance, the insulating capacity of porous materials (**see Chapter 2, section 2.3.3**) can be enhanced by reducing the radiative contribution to the thermal conductivity through a reduction in the cell size of these materials. Additionally, other properties such as compressive strength or sound insulation could be affected by this parameter. Therefore, one commonly used strategy to reduce the cell size of PU foams is the addition of different nanoparticles in the reactive blend. Traditionally, for those systems showing a cell size reduction, this effect has been attributed to a decrease in the surface tension that would lead to a more effective nucleation and, consequently, to smaller cells. Nevertheless, the possibility that other factors could influence the aforementioned effect was the starting point of this research.

In this section, the results obtained regarding the study of the influence that nanoparticles present on the nucleation mechanisms in polyurethane foam formulations are gathered in the

following scientific publication: **B. Merillas, F. Villafañe, and M. Á. Rodríguez-Pérez, Nanoparticles addition in PU foams: The dramatic effect of trapped-air on nucleation. Polymers (Basel)., vol. 13, no. 17, pp. 1–11, 2021, doi: 10.3390/polym13172952.**

This work is focused on analyzing the cell nucleation density of polyurethane foams and how this parameter is affected by the inclusion of nanoparticles. The selected nanoparticles are natural (Clay Na^+) and organomodified (Clay 30B) nanoclays and different contents have been added (0.5 and 1 wt.%). In order to evaluate their effect, the manufacturing method has been carefully altered, giving rise to three different production procedures which led to different amounts of trapped-air in the polyol blend (**Figure A.1**):

A) Electric mixing at atmospheric conditions: high air-trapping level.
B) Magnetic mixing at atmospheric conditions: intermediate air-trapping level.
C) Magnetic mixing at vacuum conditions: low air-trapping level.

The results obtained indicate that the mixing step and the amount of air trapped into the reactive blend are key factors on the final cellular structures. The three different procedures described above lead to different levels of air are trapped into the mixture, thus allowing us to evaluate its effect on the cellular structure of the produced foams.

In order to carry out the analysis of these parameters, different properties have been studied. The **viscosity of the pristine polyol blend significantly increased when nanoparticles were added**, being more noticeable for the highest nanoparticles amount (1 wt.%). Then, the cellular structures of the PU foams were studied by measuring the cell size and cell nucleation density, reaching the following conclusion:

- **The more air is included into the reactive blend, the higher the nucleation effect.** Therefore, the previously mentioned production procedures promote a clear effect on the cell nucleation density, leading to 1.54, 1.25 and 1.09 times the cell nucleation density of the sample without particles (reference).

Since the C procedure does not produce a significant change in the cell nucleation despite nanoclays are added, it is proved that these particles are not acting as nucleants by reducing the surface tension. On the contrary, the mechanism involved in the observed cell size decrease (by increasing the cell nucleation) depends on the **trapped air included into the mixture,** which is **higher when the polyol viscosity increases due to the addition of the nanoclays.**

Therefore, this publication describes an innovative procedure which demonstrates the mechanism involved in the nucleation of PU foams when particles are added. It is the increase in the polyol blend viscosity when the particles are added, and the corresponding higher amount of gas trapped, the reason for the higher cell nucleation density in the final foam when nanoparticles are included in the composition.

Figure A.1. shows the graphical abstract of the presented paper. The full publication is included in the next pages.

Graphical abstract

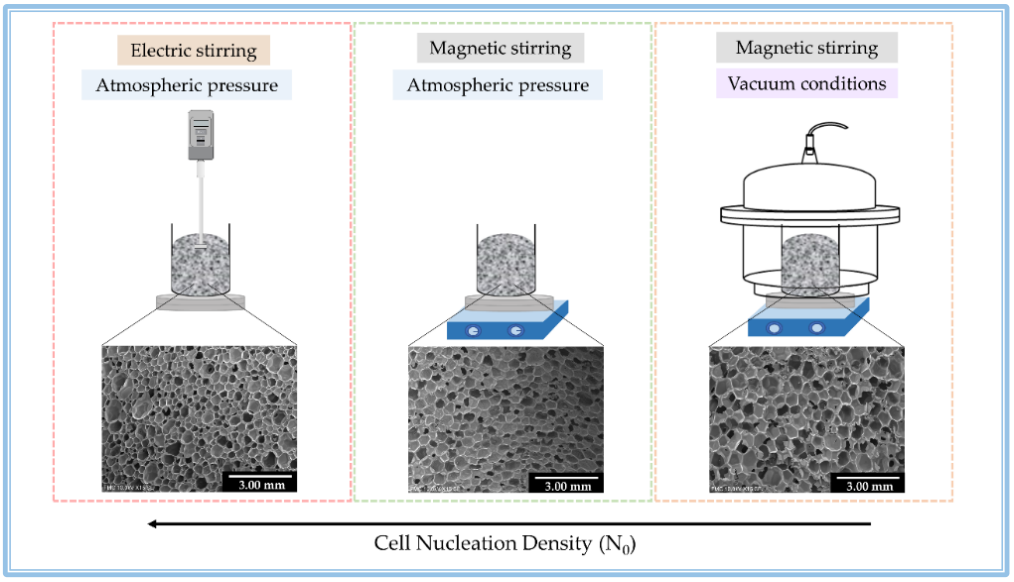

Figure A.1. Graphical abstract of **"Nanoparticles addition in PU foams: The dramatic effect of trapped-air on nucleation."**

Nanoparticles Addition in PU foams: The Dramatic Effect of Trapped-air on Nucleation

Beatriz Merillas[1*], Fernando Villafañe[2], and Miguel Ángel Rodríguez-Pérez[1,3]

1 Cellular Materials Laboratory (CellMat), Condensed Matter Physics Department, Faculty of Science, University of Valladolid, Paseo de Belén 7, 47011 Valladolid, Spain; b.merillas@fmc.uva.es; marrod@fmc.uva.es

2 GIR MIOMeT-IU Cinquima-Química Inorgánica, Faculty of Science, University of Valladolid, Paseo de Belén 7, 47011 Valladolid, Spain; fernando.villafane@uva.es

3 BioEcoUVA Research Institute on Bioeconomy, University of Valladolid, 47011 Valladolid, Spain

** Correspondence*: b.merillas@fmc.uva.es; ORCID 0000-0003-2995-6412

Abstract: To determine the effect of nanoclays and trapped air on the formation of rigid polyurethane foams, three different production procedures were used. To study the influence of mixing at atmospheric pressure, two approaches were carried out employing either an electric or a magnetic stirrer. The third approach was executed by mixing under vacuum conditions with a magnetic stirring. The samples thus obtained were characterized, and the effect of trapped air into the reactive mixtures was evaluated by analyzing the cellular structures. Different levels of trapped air were achieved when employing each manufacturing method. A correlation between the trapped air and the increase in the nucleation density when nanoclays were added was found: the cell nucleation density increased by 1.54 and 1.25 times at atmospheric conditions with electric and magnetic stirring, respectively. Nevertheless, samples fabricated without the presence of air did not show any nucleating effect despite the nanoclay addition (ratio of 1.09). This result suggests that the inclusion of air into the components is key for improving nucleation and that this effect is more pronounced when the polyol viscosity increases due to nanoclay addition. This is the most important feature determining the nucleating effect and, therefore, the corresponding cell size decreases.

Keywords: air nucleation; cell nucleation density; nanoclays; polyurethane foams; nucleation mechanisms; air trapping.

Polymers, 13, 2952, 2021.

DOI: 10.3390/polym13172952

3. Understanding the relationship between sound absorption and cellular structure of polyurethane foams.

Sound absorbing materials are currently being developed aiming to face noise-related problems such as noise pollution and the subsequent diseases that it may cause. For this reason, developing effective sound insulating materials is a major issue contributing to improve human's life-quality. One of the main requirements that allows the development of these materials is the understanding of the structural features that promote this property.

Despite several works describe some parameters affecting the noise absorption capacity of porous materials, a deeper study of their cellular structure was needed in order to understand the key features that contribute to absorb as much sound as possible. In particular, the sound absorption of semirigid PU foams is much less studied than that of flexible PU foams.

Therefore, in this section, an innovative methodology to characterize the porous structure of semirigid polyurethane foams and their relationship with their sound absorption capacity is described. The obtained results are found in the publication: **B. Merillas, F. Villafañe, and M. Á. Rodríguez-Pérez. A New Methodology Based on Cell-Wall Hole Analysis for the Structure-Acoustic Absorption Correlation on Polyurethane Foams. Polymers (Basel)., vol. 14, p. 1807., 2022, doi: 10.3390/polym14091807.**

Semirigid polyurethane foams usually present an intermediate cellular structure between rigid and flexible PU foams. They are materials with a high open cell content and the interconnections between cells are due to the presence of small holes in the cell walls. The methodology developed in this publication consists of **describing new parameters characterizing the holes present in the cell walls that could play a key role on the sound absorption capacity**: the number of holes (N_h), their surface (S_h), and the area percentage thereof (%HCW) (described in **Figure A.2**) are herein quantitatively measured for five different polyurethane foams. The produced foams present a similar density, cell size, and open cell content in order to focus the study on the structural differences among them.

These novel parameters have been related to the acoustic absorption coefficient at different frequencies, and the results obtained allow to conclude that **a structure containing a small number of holes with a large surface presents more effective sound absorption than one with a higher number of smaller holes.**

Figure A.2 shows the graphical abstract of the presented paper. The full publication is included in the next pages.

Graphical abstract

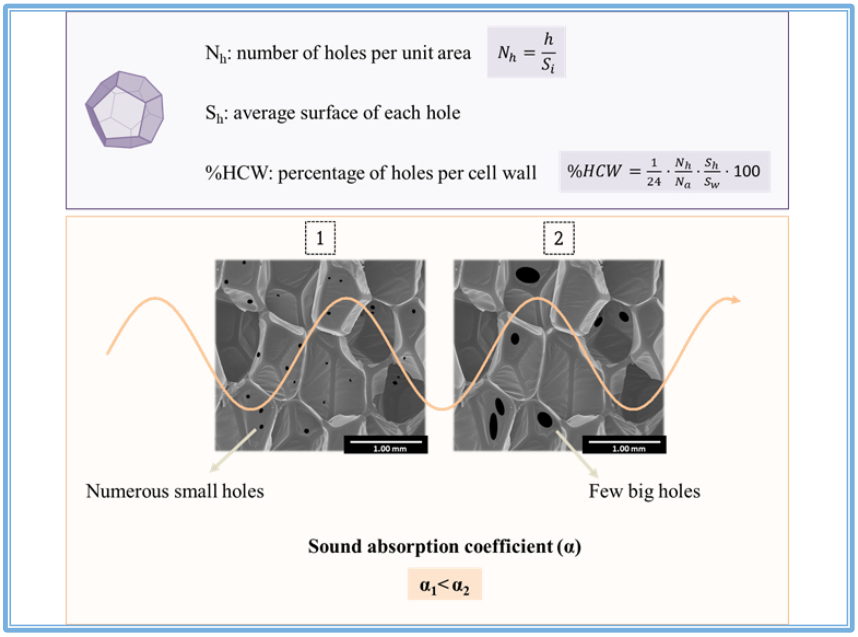

Figure A.2. Graphical abstract of **"A New Methodology Based on Cell-Wall Hole Analysis for the Structure-Acoustic Absorption Correlation on Polyurethane Foams."**

A New Methodology Based on Cell-Wall Hole Analysis for the Structure-Acoustic Absorption Correlation on Polyurethane Foams

Beatriz Merillas[1*], Fernando Villafañe[2], and Miguel Ángel Rodríguez-Pérez[1,3]

1 Cellular Materials Laboratory (CellMat), Condensed Matter Physics Department, Faculty of Science, University of Valladolid, Paseo de Belén 7, 47011 Valladolid, Spain; b.merillas@fmc.uva.es; marrod@fmc.uva.es

2 GIR MIOMeT-IU Cinquima-Química Inorgánica, Faculty of Science, University of Valladolid, Paseo de Belén 7, 47011 Valladolid, Spain; fernando.villafane@uva.es

3 BioEcoUVA Research Institute on Bioeconomy, University of Valladolid, 47011 Valladolid, Spain

** Correspondence*: b.merillas@fmc.uva.es; ORCID 0000-0003-2995-6412

Abstract: Polyurethane foams with a hybrid structure between closed cell and open cell were fabricated and fully characterized. Sound absorption measurements were carried out in order to assess their acoustic performance at different frequency ranges. The cellular structure of these systems was studied in detail by defining some novel structural parameters that characterize the cell wall openings such as the average surface of holes (S_h), the number of holes (h), and the area percentage thereof (%HCW). Therefore, these parameters allow to analyze quantitatively the effect of different structural factors on the acoustic absorption performance. It has been found that the parameters under study have a remarkable influence on the normalized acoustic absorption coefficient at different frequency ranges. In particular, it has been demonstrated that increasing the surface of the holes and the percentage of holes in the cell walls allows increasing the acoustic absorption of these types of foams, a promising statement for developing highly efficient acoustic insulators. Additionally, we could determine that a suitable minimum value of hole surface to reach the highest sound dissipation for these samples exists.

Keywords: acoustic absorption; cellular structure analysis; cell wall holes; polyurethane foams.

DOI: 10.3390/polym14091807

4. Polyurethane foams-sepiolite nanocomposites for an effective nitrate-removal from water resources.

This section contains the publication: **S. Barroso-Solares, B. Merillas, P. Cimavilla-Roman, M.A. Rodriguez-Perez, and J. Pinto. Enhanced nitrates-polluted water remediation by polyurethane/sepiolite cellular nanocomposites. J. Clean. Prod. 254 (2020) 120038. doi:10.1016/j.jclepro.2020.120038.**

Polluted water containing more than a certain limit of nitrates is not acceptable for human consumption, owing to the toxicity of these compounds. A great variety of strategies have been developed in order to solve this problem. Some of them have demonstrated the effectiveness of sepiolite for nitrate removal. However, the dispersion of these particles in water requires a subsequent tedious filtration step to remove them, thus increasing the final price of the treatment. It was this problem that spawned the idea of using hydrophilic polyurethane foams as support for these active particles.

In this paper, **flexible hydrophilic polyurethane foams with different amounts of natural and organomodified sepiolites as fillers (SePU)** are used to study the **nitrates adsorption capacity**. The organomodification of sepiolites with quaternary ammonium salts significantly improves the performance of the composites, reaching a maximum capacity of **23 mg/g, with no need of controlling the temperature or pH of the medium**. The optimum sepiolite amount is 8 wt.%, since higher amounts lead to collapse of the PU cellular structure. The hydrophilic PU foams allows a great contact between the embedded sepiolite and nitrates, since a swelling process is observed with water, thus favoring the removal.

Finally, Langmuir and Freundlich adsorption isotherm models are employed, finding that the **Langmuir model** is that which better **describes the interaction between the treated sepiolite and nitrates**.

Therefore, these nanocomposites constitute a safe and easy-handling solution for nitrates removal from polluted water, which has never been explored before.

Figure 3 shows the graphical abstract of the presented paper. The full publication is included in the next pages.

Graphical abstract

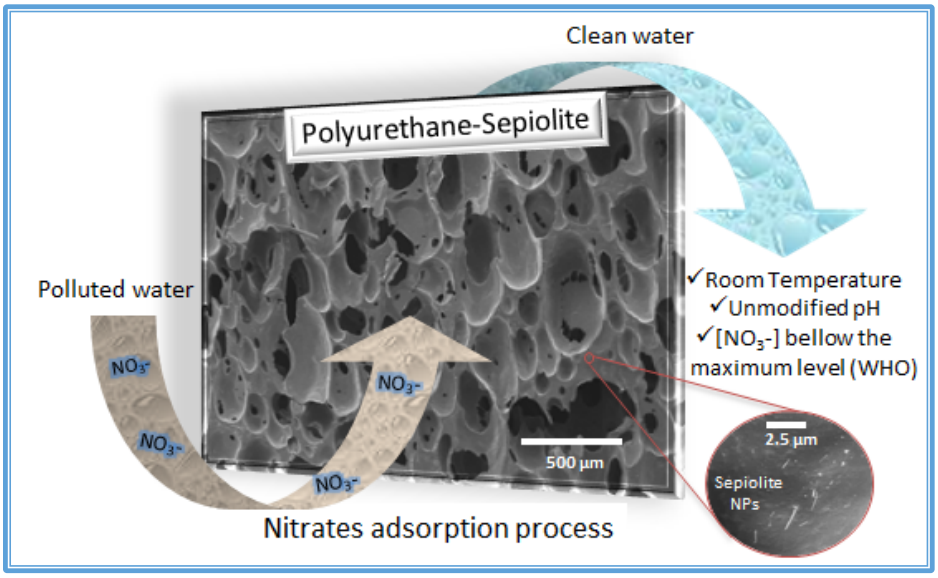

Figure 3. Graphical abstract of **"Enhanced nitrates-polluted water remediation by polyurethane/sepiolite cellular nanocomposites."**

Enhanced nitrates-polluted water remediation by polyurethane/sepiolite cellular nanocomposites

Suset Barroso-Solares[1,2], Beatriz Merillas[1], Paula Cimavilla-Román[1], Miguel Ángel Rodríguez-Pérez[1,2], and Javier Pinto[1,2]

1 Cellular Materials Laboratory (CellMat), Condensed Matter Physics Department, Faculty of Science, University of Valladolid, Paseo de Belén 7, 47011 Valladolid, Spain; +34 983423572

2 BioEcoUVA Research Institute on Bioeconomy, University of Valladolid, 47011 Valladolid, Spain

** Corresponding Authors*: sbarroso@fmc.uva.es, jpinto@fmc.uva.es

Abstract: Nanocomposite hydrophilic flexible polyurethane foams were prepared by in situ polymerization using an organomodified sepiolite as filler. The sepiolite affinity by nitrates dissolved in water was increased by treating them with quaternary ammonium salts (S-QAS), leading to remarkable nitrates maximum adsorption capacity (q_{max}= 23.30 mg/g). The Langmuir model well described the adsorption process of the nitrates by the modified sepiolite, and more remarkably, the sepiolite suffers no decrease of their nitrates removal capacity after being imbibed in the flexible polyurethane foam. The proper selection of the polyurethane chemistry allows significant contact between the polluted-water and the sepiolite, even when enclosed inside the cell walls. Accordingly, the as-prepared hydrophilic polyurethane/sepiolite foams provided a facile removal of nitrates-pollution from water, even actual nitrates-polluted water with a competitive adsorption environment, without the need to control or modify the pH and temperature of the polluted water neither to add further filtration steps to collect the active particles from the water.

Keywords: nitrate removal; adsorption; polyurethane; sepiolite; wastewater.

DOI: 10.1016/j.jclepro.2020.120038